1-1-2015

(i)chromatographic Methods For Solute Descriptor Determinations (ii)ruthenium Substrate-Catalyzed Growth Of Nickel Nitride Thin Films By Atomic Layer Deposition

Thiloka Chandima Ariyasena
Wayne State University,

(I) CHROMATOGRAPHIC METHODS FOR SOLUTE DESCRIPTOR DETERMINATIONS
(II) RUTHENIUM SUBSTRATE-CATALYZED GROWTH OF NICKEL NITRIDE THIN FILMS BY ATOMIC LAYER DEPOSITION

by

THILOKA CHANDIMA ARIYASENA

DISSERTATION

Submitted to the Graduate School

of Wayne State University,

Detroit, Michigan

in partial fulfillment of the requirements

for the degree of

DOCTOR OF PHILOSOPHY

2015

MAJOR: CHEMISTRY

Approved By:

_____
Advisor   Date

_____

_____

DEDICATION

To my parents M. A. Amara M. Ariyasena and J. A. Ariyasena, sister Iranya Ariyasena,

husband Priyanga Wijesinghe, and daughter Senuli Wijesinghe.

TABLE OF CONTENTS

LIST OF TABLES

LIST OF FIGURES

LIST OF CHARTS

LIST OF ABBREVIATIONS

Abbreviation	**Long Form**
A	Hydrogen Bond Acidity Descriptor
a	Hydrogen Bond Basicity System Constant
ALD	Atomic Layer Deposition
AFM	Atomic Force Microscopy
B	Hydrogen Bond Basicity Descriptor
b	Hydrogen Bond Acidity System Constant
CMOS	Complementary Metal Oxide Semiconductor
CVD	Chemical Vapor Deposition
DMSO	Dimethyl sulfoxide
DRAM	Dynamic Random Access Memory
E	Excess Molar Refraction
e	Excess Molar Refraction System Constant
EU	European Union
EC_{50}	Effect Concentration 50
EA	Ethanolamine
FA	Formamide
HEP	Heptane
IPE	Isopentyl Ether
ITRS	International Technology Roadmap for Semiconductors
K_{OC}	Soil Adsorption Co-efficient Normalized to the Total Organic Carbon Content
K_H	Henry's Law Constant

K_{OA}…………………………………….…...……Octanol-Air Partition Co-efficient

K_{OW}………………………………………….. Octanol-Water Partition Co-efficient

K_p……………………………………………………….…Partition Coefficient

L…………………………………..Gas-Hexadecane Partition Coefficient at 298 K

l……………………………….System Constant for Gas-Hexadecane Partition Coefficient at 298 K

LC_{50}…………………………… ....Lethal Concentration 50

LFER ……………………………………….…...Linear Free Energy Relationship

MEKC ……………………………….………..Micellar Electrokinetic Chromatography

MOCVD………………………………….…Metal Organic chemical Vapor Deposition

NMR…………………………………….…………….. Nuclear Magnetic Resonance

PNEC……………………………………...…......Predicted No-Effect Concentration

PEC……………………………………….…...Predicted Environmental Concentration

PAH…………………………………………...……..Polycyclic Aromatic Hydrocarbon

PVD……………………………………………….…Physical Vapor Deposition

QSPR………………………………………..Quantitative Structure Property Relationship

RMS……………………………………………………….Root Mean Square

S……………………………………………………….Dipolarity/Polarizability Descriptor

s………………………………………………...Dipolarity/Polarizability System Constant

S_W……………………………………………………...….Solubility in Water

SD…………………………………………………………...Standard Deviation

SEM………………………………………………….Scanning Electron Microscopy

TEA……………………………………………………….….Triethylamine

TSCA………………………………………...………………Toxic Substance Control Act

U. S. EPA …………………………………………United States Environmental Protection Agency

UV/Vis……………………………………………………………..... Ultraviolet/Visible

V……………………………………...………….McGowan's Characteristic Volume

v……………………………...……………..McGowan's Characteristic Volume System Constant

XRD…………………………………………………………...…X-Ray Diffraction

XPS……………………………………………………….…X-ray Photoelectron Spectroscopy

CHAPTER 1

INTRODUCTION TO APPLICATIONS OF SOLVATION PARAMETER MODEL

1.1 Determination of Concentration Levels in Environmental Compartments

Determination of the concentration levels of chemicals in various environmental compartments is considered an important procedure in many industries. For example, it plays a significant role in environmental risk assessment procedures, food and drug production, the perfumery industry, and in pharmaceutical and medicinal chemistry, to name only a few.[1] Out of these, it plays a vital role in environmental risk assessment procedures, as many chemicals are released into the environment everyday due to human activities, and their possible risk to human health and to the ecosystem should be determined.

1.2 Environmental Risk Assessment

The environmental risk assessment procedure established by the United States Environmental Protection Agency (U.S. EPA) and European Union (EU) consists of four major steps, which are, hazard identification, dose-response or effect assessment, exposure or fate assessment, and risk characterization, respectively (Figure 1).[1a]

Hazard identification evaluates whether a particular chemical stressor has the ability to cause an increase in adverse health effects in humans. A hazard identification procedure is carried out by monitoring the negative health effects in humans and gathering evidence whether the subjects under study are exposed to a particular chemical for a prolonged time, or to a certain dose of the chemical. Dose-response assessment is the evaluation of the extent of the severity of the damage caused to human health, with respect to the amount of the chemical stressor provided. For dose-response assessment, a critical effect such as weight loss, disease, tumor, or death is considered

as the response. The experimental subjects are animals when detecting a severe effect such as death, and can be humans when detecting non-severe effects such as skin irritations. Test subjects are fed or exposed to definite amounts of chemical stressors and the extent of the response is observed. Since there can be variations in age, gender, species, etc. of the subject, an average value for the minimum concentration required to manifest the effect is determined.
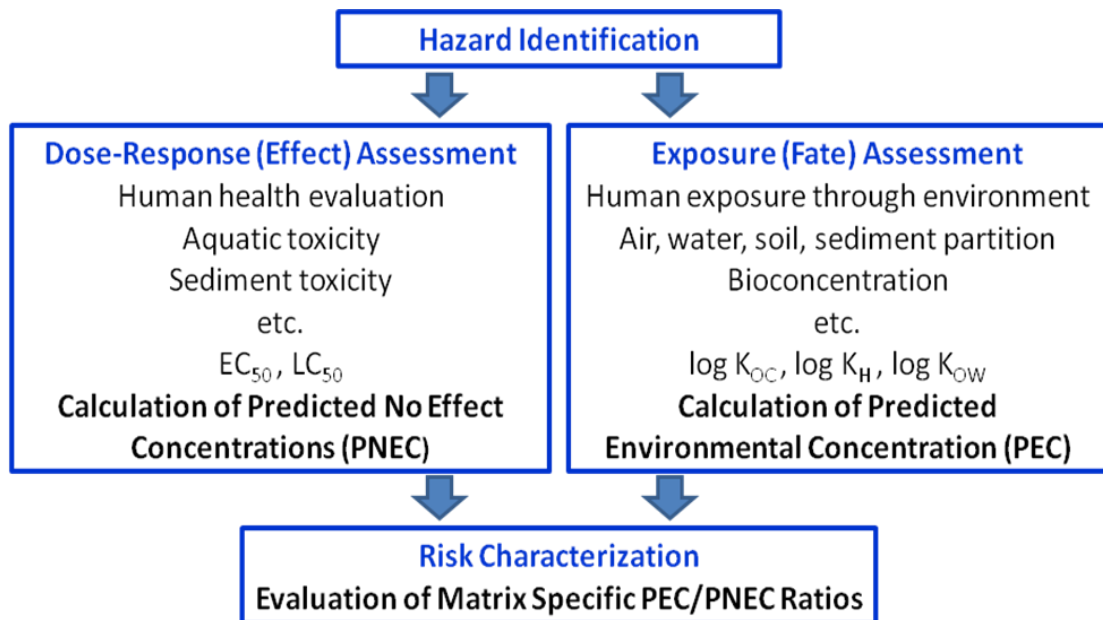
Figure 1. Selected Steps in U. S. EPA Environmental Risk Assessment Procedure[1a]

The two common parameters used to evaluate dose-response assessments are the EC_{50} value, which is the concentration of the substance needed to manifest a certain effect in 50% of the test population, and the LC_{50} value, which is the concentration of the substance needed to kill 50% of the test population, within an observed time period, under a previously defined set of conditions. In the final step of the procedure, a predicted no-effect concentration (PNEC) is calculated.

PNEC value is considered as the highest concentration that the test subject can be administered or exposed to, without observing statistically significant increase in frequency of occurrence, or severity of adverse effects with respect to a control population. Exposure or fate assessment evaluates the concentration, frequency, and duration of the chemical which comes in contact with the subject.[1a, 2] Humans and animals can be exposed to a chemical through different routes, and the specific parameters for exposure assessment are defined according to the route that the chemical uptake has taken place. For example, the bio-concentration defines the accumulation of a chemical in an aquatic organism due to the transfer of a chemical from surrounding water to the organism, whereas the bio-accumulation defines the accumulation of a chemical in an organism as a result of uptake from all exposure routes including water, soil, sediment, and air.[3] Often, due to the difficulties of accessibility of the natural environment, surrogate physicochemical parameters are used to determine the exposure levels. Commonly used physicochemical parameters are solubility in water (S_W), soil adsorption coefficient normalized to the total organic carbon content (K_{OC}), Henry's law constant or water-air partition coefficient (K_H), octanol-air partition coefficient (K_{OA}), and the octanol-water partition coefficient (K_{OW}).[1d, 4] As the last step of the exposure assessment, predicted environmental concentration (PEC), which is the concentration level of the chemical in each environmental compartment, is determined.[1a] A PEC value indicates the magnitude of the exposure of the test subject to the chemical stressor. In the fourth step, the extent of the risk is characterized based on PEC:PNEC ratios which depend on the particular matrix and the environment considered.

1.3 Exposure Assessment of Organic Chemicals

Each year, large amounts of discrete organic chemicals are released into the environment from industry. The toxic substance control act (TSCA) listing contains more than 12,000 discrete

mass produced organic chemicals which do not have any effect or exposure data or for which there is only limited amount of data.[3] Both effect and exposure assessment of these large inventories of chemicals is an almost impossible task due to the limitation of human, technical, and economical resources required to determine their concentration levels in various environmental compartments. As a solution to this problem, quantitative structure property relationships (QSPR) are used to estimate environmental and physicochemical endpoint values.

1.4 Use of Quantitative Structure Property Relationships to Determine Endpoint Values

In QSPRs, a chemical property of a compound is modeled as the response variable, as a function of physicochemical and structural properties. Environmental endpoints such as air-particulate matter distribution, soil-water distribution, nonspecific toxicity to fish, water-skin distribution, and eye-irritation levels can be estimated using QSPRs.[5] A global model, which is a QSPR built considering all global factors such as age, sex, health, stress levels, genetic factors, dietary factors etc. for the test population, can provide an accurate estimation of the endpoint for the global population considered. A local model, which is a QSPR constructed using only the specific parameters relevant to the local population under study, will provide an accurate estimation of endpoints relevant to the specific population and matrix considered for the study. QSPRs can be used to determine the concentration levels of organic chemicals in environmental compartments. For static systems, several assumptions are taken into consideration in the procedure for determining concentration levels.[6] The first assumption is that chemical transformations are negligible. Secondly, it is assumed that the driving force for chemical accumulation in one medium is the partitioning of the chemical between the exposure media and receiving phase. Thirdly, it is assumed that the chemical has reached equilibrium between the two phases. For dynamic systems such as flow systems, a steady state hypothesis is considered

during the application of QSPRs. However, this is beyond our focus, as the research reported herein takes only static systems into consideration. Despite the fact that the organic compounds may exist as mixtures in nature, and the physical conditions such as temperature, pH, and composition may vary between matrices, QSPR models based on static systems have been applied to estimate many environmental endpoints, thereby economizing on the cost needed for complex experimental procedures. Although an experimental procedure is essential to determine the endpoint values accurately, in the instances where limited sources are available to generate large amounts of experimental data, the use of QSPRs is important for an initial estimate of the range within which the true value can be found.

1.5 Development of Quantitative Structure Property Relationships

Mortimer Kamlet, Robert Taft, and Jose Abboud are recognized as the intellectual forefathers of linear free energy relationships (LFER), which are currently in use for the rationalization of solvation processes. Kamlet and co-workers developed the solvatochromic scale known as π^* scale.[7] The π^* scale was developed by selecting forty different probe solutes and measuring the frequency of maximum absorbance (υ_{max}) in their ultraviolet/visible (UV/Vis) spectra with different solvents for each solute. The probe compounds used in the π^* scale were neither good hydrogen bond acids, nor good hydrogen bond bases. Therefore, the data obtained from the measurements accounted for solvent dipolarity. The plots of υ_{max} of solvent versus υ_{max} of the probe solute showed good linearity. Also, for specific probe compounds, such as 1-ethyl-4-nitrobenzene, N,N-diethyl-3-nitrobenzene, 4-methoxy-β-styrene, plots of υ_{max} of one indicator versus υ_{max} of second indicator were linear over a wide solvent dipolarity range. A particular π^* value for a specific solvent is assigned by calculating the average of the π^* values for different

probe solutes. Later, Abboud and co-workers developed the π^* scale for a large number of solvents.[8]

One of the earliest developed linear free energy relationships is given by Equation 1.[9]

$$SP = c + s\,(\pi^* + d\delta) + a\alpha + b\beta \qquad (1)$$

In equation 1, SP is a solvent dependent property such as the rate of a chemical reaction or the solvatochromic shift of a probe solute. Term 'c' is a system constant or an intercept term which is independent of the probe solute. Terms π^*, δ, α, and β are measures of solvent polarity, polarizability, hydrogen bond acidity, and hydrogen bond basicity, respectively. The coefficients s, d, a, and b are system constants.

The basis of the solvatochromic model is the assumption that the solvent parameters can provide an estimate of solute properties. However, since a solute molecule in a solvent is surrounded by other solvent molecules, and therefore can have widely different interactions compared to a solvent molecule surrounded by the bulk solvent, solvatochromic models are not really suitable to describe the solvation process of a solute.

1.6 Solvation Parameter Model

Among the variety of QSPRs or LFERs available to estimate solute properties, the most accepted relationship to describe the solvation of a solute in a medium, is the solvation parameter model founded by Michael H. Abraham.[10] The solvation parameter model is based on a parameterization of the cavity model of solvation. The cavity model considers transfer of a solute from one phase to another as a three-step process (Figure 2).[6a] In the first step, a cavity is formed in the receiving phase, which is of a suitable size to accommodate the solute molecules. Cavity formation occurs by disrupting the solvent-solvent interactions and therefore is an endothermic process. The free energy associated with the solute transfer is favorable when the

donating phase has weaker solvent-solvent interactions than the receiving phase. In the second step, solvent molecules reorganize around the cavity. The reorganization minimizes the disruption that occurs when the cavity is created, and results in a more favorable orientation for solute-solvent interactions. The free energy change involved in this step is minimal due to the compensation of entropy and enthalpy.
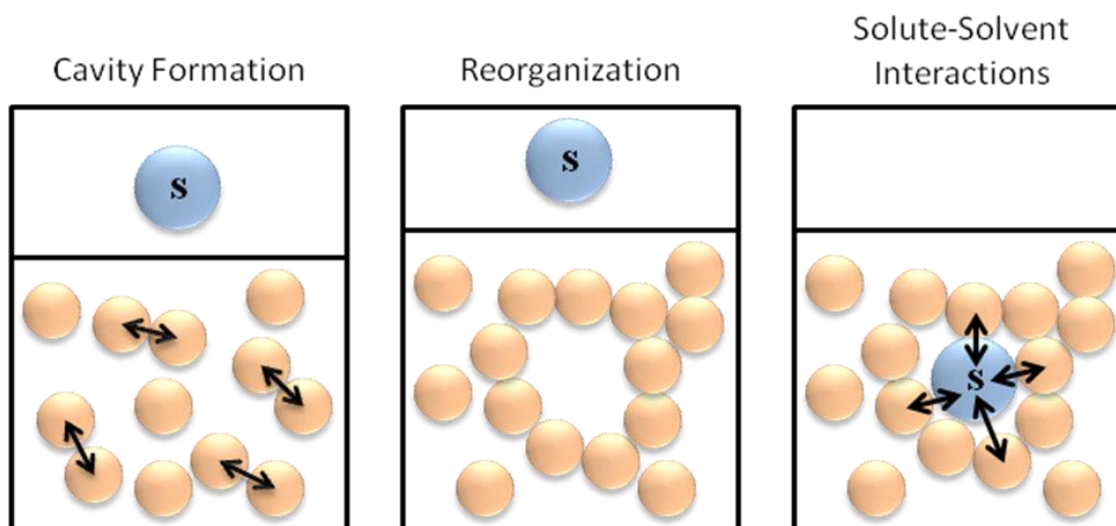
Figure 2. Major Steps of the Cavity Model of Solvation.

In the third step, the solute is inserted into the cavity and solute-solvent interactions are established. If there are same interactions in the donor phase, they will be collapsed. Energy is released in the solute insertion step and therefore, solute insertion is exothermic.

The solvation parameter model for transfer of a neutral compound between two phases takes two forms. For transfer of the solute from gas phase to condensed phase the model is,

$$\log \text{SP} = c + e\text{E} + s\text{S} + a\text{A} + b\text{B} + l\text{L} \qquad (2)$$

and for transfer of solute between two condensed phases the model is,

$$\log \text{SP} = c + e\text{E} + s\text{S} + a\text{A} + b\text{B} + v\text{V} \qquad (3)$$

SP is a free energy related solute property, and c is a system constant independent of the solute property. Lower case letters are the system constants, which describe complementary interactions of the system with the solute, and the upper case letters are the solute descriptors, which describe the complementary interactions of the solute with the system. Upper case letters E, S, A, B, L, and V stand for the excess molar refraction, dipolarity/polarizability, hydrogen-bond acidity, hydrogen-bond basicity, gas-hexadecane partition co-efficient, and McGowan's characteristic volume, respectively. Lower case letters e, s, a, b, l, and v represent excess molar refraction, dipolarity/polarizability, hydrogen-bond basicity, hydrogen-bond acidity, and cavity formation/dispersion interactions of the system for solute transfer from a gas phase to a condensed phase, and the difference in cavity formation and residual dispersion interactions of a biphasic system for solute transfer between two condensed phases, respectively.

Another form of solvation parameter model contains both L and V descriptors, but not the excess molar refraction (E) descriptor (Equation 4).[11]

$$\log \text{SP} = c + s\text{S} + a\text{A} + b\text{B} + l\text{L} + v\text{V} \qquad (4)$$

The model in Equation 4 is called the Goss-modified Abraham solvation parameter model and performs similar to equations 2 and 3. However, in the instances where the determination of the gas-liquid partition coefficient in hexadecane at 298 K (L descriptor) is difficult due to the compound's high molecular weight or less thermal stability, using equation 4 can be problematic. For ionic compounds, a separate free energy relationship is considered.

$$\log \text{SP} = c + e\text{E} + s\text{S} + a\text{A} + b\text{B} + l\text{L} + j^{+}\text{J}^{+} \qquad (5)$$

$$\log \text{SP} = c + e\text{E} + s\text{S} + a\text{A} + b\text{B} + l\text{L} + j^{-}\text{J}^{-} \qquad (6)$$

Equation 5 is used when the solute is a cation where the J^+ descriptor defines the properties of a cation, and Equation 6 when the solute is an anion, where the J^- descriptor defines the properties of an anion.

1.7 Solute Descriptors in the Solvation Parameter Model

1.7.1 McGowan's Characteristic Volume (V)

McGowan's characteristic volume is the volume of one mole of a compound when the molecules are at a stationary position, and is calculated using the following equation.

$$V = \frac{[\ \Sigma\ (\text{contribution to volume from all atoms}) - 6.56\ (N - 1 + R_g)\ ]}{100} \qquad (7)$$

In Equation 7, V is the McGowan's characteristic volume, N is the total number of atoms, and R_g is the total number of ring structures in the molecule. Usually the McGowan's characteristic volume is scaled to the other descriptors by division by 100 and has units of $cm^3\ mol^{-1}/100$. For isomers, McGowan's characteristic volume have the same values, although inclusion of a boiling point term for the two isomers can be used for their distinction.[12]

McGowan's characteristic volume is a measure of the cavity effect and mainly accounts for dispersion interactions.

1.7.2 Excess Molar Refraction (E)

Excess molar refraction is defined as the difference between the excess molar refraction of a solute and the excess molar refraction of a hypothetical n-alkane which has the same volume as the solute. The excess molar refraction is calculated using the following equation.

$$E = 10V\ [\eta^2 - 1/\eta^2 + 2] - 2.832\ V + 0.526 \qquad (8)$$

In Equation 8, E is the excess molar refraction, V is the McGowan's characteristic volume, η is the refractive index. The excess molar refraction has units of cm^3 $mol^{-1}/10$. For liquids, the excess molar refraction is calculated using the refractive index at 20 °C for the sodium D-line. For solids, refractive index values are estimated by either using software, such as ChemSketch or Absolv, or by summation of assigned fragment values. However, both methods contribute to the uncertainty of the excess molar refraction value. Therefore, determining the excess molar refraction experimentally is preferred for solids, to minimize the error involved in using estimated refractive index values.

Excess molar refraction accounts for the additional contribution to dispersion interactions beyond what has been already accounted for by cavity formation using the vV and lL terms. In the initial scales of excess molar refraction the n-alkanes were assigned a value of zero. The excess molar refraction values for other compounds are assigned using the n-alkanes as reference values. Therefore, compounds such as fluorocarbons and organosilicon compounds, which are less polarizable than n-alkanes, can have negative values for excess molar refraction.

1.7.3 The L Descriptor

The L descriptor is defined as the gas-liquid partition coefficient for the solute in n-hexadecane at 298 K. For volatile compounds this can be determined by gas chromatography using n-hexadecane as the stationary phase.[13] Normal hexadecane is a readily available, non polar liquid having a well defined structure, and is widely used to determine water-hexadecane partition coefficients in pharmaceutical and medicinal chemistry. Therefore, n-hexadecane is used as the reference compound to determine the L descriptor. For compounds of low volatility the L descriptor is determined by back calculation on a low polarity phase at higher temperatures.

The L descriptor accounts for dispersion interactions when the solute is transferred from the gas phase to a condensed phase.

1.7.4 Dipolarity/Polarizability (S)

The dipolarity/polarizability descriptor accounts for both stable and induced dipoles. In the original scales for the dipolarity/polarizability descriptor, the n-alkanes were assigned a value of zero. Hence, the values of other compounds are normalized with respect to the n-alkanes. Certain flourocarbons and organosiloxanes can have negative values for dipolarity/polarizability values, as they are less polarizable than n-alkanes. The original scales for dipolarity/polarizability were built by determining the dipolarity/polarizability descriptor for compounds with known E and L descriptors.[14] For these compounds, gas chromatography on polar stationary phases, where hydrogen bonding interactions are negligible, can be used to calculate the S descriptor.

1.7.5 Hydrogen Bonding Descriptors (A and B)

As the name implies, A and B descriptors account for the hydrogen bond acidity and hydrogen bond basicity interactions of the solute, respectively. Initial scales for hydrogen bond acidity and basicity were developed based on the complexation equilibria of monomeric hydrogen bond acids and hydrogen bond bases. These reactions were carried out in an inert solvent such as tetrachloromethane at 298 K.[15]

$$A-H + B \longrightarrow A-H^{..}B \qquad (9)$$

When the initial scales were constructed, a set of equilibrium constants for hydrogen bond complex formation (log K) were obtained for a group of acids against a reference base.[16] It was found that these log K values show a linear relationship with the log K values of the acids with any other reference base. Based on this observation, initial scales were constructed such that the

log K values of acids against any given base are linearly related to the hydrogen bond acidity of the solute (log $K_A{}^H$).

Log K (of a series of acids, with reference to a base B) = L_B. log $K_A{}^H$ + D_B (10)

In the initial work, forty five acids were studied to yield forty five values for L_B and forty five values for D_B. It was found that these equations intersected at (−1.1, −1.1) when K is expressed on the molar concentration scale. Therefore, the hydrogen-bond acidity descriptor can be obtained using the relationship,

$$\alpha_2{}^H = (\log K_A{}^H + 1.1)/4.636 \qquad (11)$$

In Equation 11, $\alpha_2{}^H$ is the hydrogen-bond acidity descriptor and 4.636 is a scaling factor. All non hydrogen-bond acids have a $\alpha_2{}^H$ value of zero and solute hydrogen bond acidity (log $K_A{}^H$) of −1.1 units.

In a similar manner, equilibrium constants for a series of monomeric bases against reference monomeric acids were used to obtain a scale for the hydrogen-bond basicity descriptor ($\beta_2{}^H$). Hydrogen-bond basicity descriptor can be obtained from the relationship,

$$\beta_2{}^H = (\log K_B{}^H + 1.1)/4.636 \qquad (12)$$

In Equation 12, log $K_B{}^H$ is the solute hydrogen-bond basicity. However, in practice solute molecules are surrounded by many solvent molecules and it was necessary to broaden the initial scales to take multiple hydrogen-bond acidity and hydrogen-bond basicity interactions into account. Therefore, the original scales were expanded to give effective hydrogen-bond acidity scales which are identified by the symbols A and B. Effective hydrogen bond acidity scales were obtained by solving a series of equations for solutes with no hydrogen bond acidity or using monomeric hydrogen bond acids, and finding the effective value through back calculations.[6a]

Alkylamines, alkyl pyridines, sulfoxides, anilines, and heterocyclic nitrogen compounds exhibit variable hydrogen-bond basicity values, in aqueous biphasic systems where water is miscible to a significant extent in the other phase. Examples for such biphasic systems are octanol-water, ethyl acetate-water, reversed-phase liquid chromatography, and micelles. For these systems, a new hydrogen bond basicity descriptor B^0 is required to account for the variation of hydrogen bond-basicity resulting from the hydration of solute in the non-aqueous phase.

1.8 Interpretation of the Solvation Parameter Model

In the solvation parameter model, the difference in solvent interactions in the two phases are indicated by the magnitude of the system constants.[9] Therefore, the system constants also indicate in which phase the solute will retain preferentially, during chromatographic measurements. Since the coefficients reflect the solvent properties, they are specific for all solutes under study. Multiple linear regression analysis is suitable to evaluate the sign and magnitude of the coefficients. For a particular interaction the sign of the coefficients indicates which phase has the more dominant ability to interact with the solute.

1.9 Versatility of Solvation Parameter Model Over Other Models for Descriptor Determinations

Models based on quantitative structure property relationships can be constructed either theoretically or experimentally.[6a] In theoretical methods, models are created by generating a large number of molecular descriptors using structure-based computational methods, and subsequently reducing the number of descriptors to a smaller number using statistical tools. Theoretical models can be used to determine descriptors for compounds which are not available, or which have not been synthesized yet. On the other hand, the main disadvantage of the theoretical approach is that the selected descriptors might not express the chemical significance of the compound, and of the

system accurately. In experimental methods, few descriptors are defined prior to the experiments and these descriptors are used to characterize the processes under study. Experimental models require that the solute is available for the study. Fragmentation methods combine both theoretical and experimental methods by assigning descriptor values to each fragment of a molecule, and afterwards combining them to give the total descriptor value for the compound. However, in fragment methods, the training set used for model validation is generally quite large, containing a large number of experimental solute property values for different compounds. For compounds with a variety of functional groups, fragment methods may be inaccurate as they cannot account for intramolecular interactions.

While solvatochromic models were developed by considering solvent effects, the solvation parameter model was developed taking both solute and solvent effects into consideration. In the solvation parameter model, the solute property is determined experimentally. Therefore, the descriptors will reflect the chemical significance of the solute. Due to its ability to accurately reflect the chemical properties of the solute and the surrounding system, the solvation parameter model is applicable to many free energy related solvation processes.

1.10 Surrogate Solute Property Estimation Methods

When the environmental system is inaccessible, or when the experimental procedure is expensive, time consuming, and if there are any ethical concerns which prevent obtaining reliable data from the environmental system, traditional emulation and correlation processes are used to estimate the solute property.[10] In emulation models, the intermolecular interactions that cause the distribution of the solute in the two phases are quantitatively similar in both the environmental and emulated system, although the two systems may not be chemically identical. Therefore,

emulation systems are rare. If they exist, their system constants will be identical for the compared systems, indicating an identical distribution processes for the two systems. In correlation models, the chromatographic systems, which are highly correlated to the environmental system, are identified. To accomplish this task, chromatographic databases are searched and systems which have close system constant ratios to that of the environmental system are identified.[17] Mainly two methods are carried out to identify the best correlation system. In the first method, the system constants in the correlation and environmental systems are assumed as points in five-dimensional space. Then the Euclidean distance between the environmental system and the correlation system (D-parameter) are calculated using the five points in each system. Since systems which have similar chemical properties will exhibit small D-parameters, the system having the smallest D-parameter value is selected as the best correlation system. In the second method, the system constants are considered as vectors in five-dimensional space. When the angle between the vectors in the environmental model and the correlation model (θ) has a Cos θ value close to unity, the system constants in the two systems are similar, and therefore the chemical properties of the correlation system are close to that of the environmental system.

Both emulation and correlation models have their own disadvantages. Emulation processes are uncommon in general. Correlation models have a large uncertainty associated with the measurements. The overall uncertainty in the correlation model is given by Equation 13.[17]

$$SD_{cor}^2 = SD_{env}^2 + (p\ SD_{chr})^2 + SD_d^2 \qquad (13)$$

In equation 13, SD_{cor} is the total expected error in the two correlated systems. Uncertainty in the environmental model is given by SD_{env}, and uncertainty in the chromatography model is given by SD_{chr}. Dissimilarity of the chromatographic and environmental models are given by SD_d. The slope of the correlation model is indicated by 'p'. The best correlation model will possess a

minimum value for SD_{cor}. In order to obtain a minimum value for SD_{cor}, the error in the environmental model, the error in the chromatography model, and the dissimilarity in the two correlated models should be minimal. Ideally, the slope of the correlation system should be equal to one, which indicates a good correlation. A slope other than one indicates that the current measurements were obtained for a system which is different to the environmental model for which the original measurements were obtained.[10] On the other hand, a shallow slope limits the range of environmental endpoint values that can be predicted using the data obtained from the chromatography model.

In correlation methods, uncertainty involved in the solute property determinations can be a problem in situations where expensive or a limited amount of resources are available. Therefore, having an estimation of the value which the solute property can take will facilitate economical measurements.

1.11 Direct Estimation of Solute Properties using Chromatographic Methods

Direct estimation methods can be used for both environmental systems and for correlated systems to identify an accurate or approximate value for the endpoint before the experiments are conducted. Therefore, direct estimation methods play an important role in the instances where the environmental system is inaccessible, or when there is a necessity to conduct solute property estimations with limited resources to hand, using surrogate emulation and correlation methods.

The solvation parameter model can be used to determine a free-energy related solute property for a system previously characterized, when the descriptors for the solutes are known.[6a] Hence, the extent of partition of the solute in any physicochemical and environmental system can be directly estimated after a proper descriptor assignment for the solute is carried out.

Partition coefficient for a solute at equilibrium in a biphasic system can be determined with ultraviolet/visible (UV/Vis), fluorescence, nuclear magnetic resonance (NMR), chromatographic methods etc. Of the many available methods, chromatographic methods are preferred for several reasons. First, in chromatographic methods, retention factors can be accurately determined resulting in accurate models which helps to determine an exact endpoint value. Secondly, chromatographic methods are fast and more economical than most other methods. Thirdly, large sample amounts are not necessary for chromatographic methods. Also, impurities if present in the sample matrices, can be removed easily using chromatographic methods.

1.12 Methods for the Determination of Descriptors

1.12.1 Gas-Solvent Partition Systems

Gas-solvent partition systems are suitable to determine the gas-hexadecane partition coefficient (L), hydrogen bond acidity (A), dipolarity/polarizability (S), and hydrogen bond basicity (B) descriptors. Headspace methods are used to determine gas-solvent partition coefficients.[18] However, compounds need to be sufficiently volatile to be analyzed by headspace methods. If the volatile compounds have low solubility in the solvent, measurement error can be quite high. Literature values for gas-solvent partition coefficients often demonstrate several values for the same compound and extreme values often have to be rejected to calculate an average value.

It is common practice to relate gas-solvent partition coefficients with solvent-solvent partition coefficients to generate additional equations to increase the accuracy of the determined descriptor value.[6a, 19] For example, hexadecane-water (log P_{Hexd-W}) partition coefficient and gas-

water partition coefficient (log K_W) at 25 °C can be used to obtain the gas-hexadecane partition

coefficient (L) as shown by Equation 14.

$$\log P_{Hexd-W} = L - \log K_W \qquad (14)$$

Similarly, gas-solvent partition coefficients (log K_S) and gas-water partition coefficients (log K_W)

can be used to estimate solvent-water partition coefficients (log P_{S-W}) as shown by Equation 15.

$$\log P_{S-W} = \log K_S - \log K_W \qquad (15)$$

When calculating the solvent-water partition coefficients, log P_{S-W} refers to the partition

coefficient of the water-dry organic solvent systems. Water-saturated systems can possess

different properties to the hypothetical dry solvent systems. Therefore, in order to calculate

descriptor values using the models built considering the dry solvent systems, the log P_{S-W} values

should be determined using similar experimental protocols.

1.12.2 Aqueous Biphasic Systems

Water-organic solvent systems can be used to determine mainly the hydrogen bond

acidity (A), hydrogen bond basicity (B) descriptor values for compounds which have sufficient

water solubility and which are stable in water. Although not to a great extent, water-solvent

systems can be used to determine the dipolarity/polarizability (S) descriptor.[20] Abraham and

coworkers have characterized more than fifty aqueous biphasic solvent systems.[21] The range of

system constants for a selected group of characterized aqueous biphasic systems are shown in

Figure 3.[22]

The system constant values in Figure 3 demonstrates that the variation of system

properties for aqueous biphasic systems are generally small. Cohesivity (v) and hydrogen bond

acidity (b) of the systems take numerical values which are greater than four (v > 4, b > −4).

Hydrogen bond basicity (a) values vary approximately around −4. The higher cohesivity of water

compared to the organic solvents cause high molecular weight solutes to migrate to the counter solvent in aqueous biphasic systems. Hydrogen bond acidity and hydrogen bond basicity of water cause the solute to prefer the aqueous phase. Figure 3 indicates that counter solvents in aqueous biphasic systems can be classified into mainly two types based on dipolarity and polarizability. One category includes counter solvents that have similar polarity to water. Systems in this category have a dipolarity/polarizability (*s*) system constants around zero. The second category has a dipolarity/polarizability (*s*) system constant value of approximately −2 and consists of relatively non polar counter solvents that fail to compete with water.
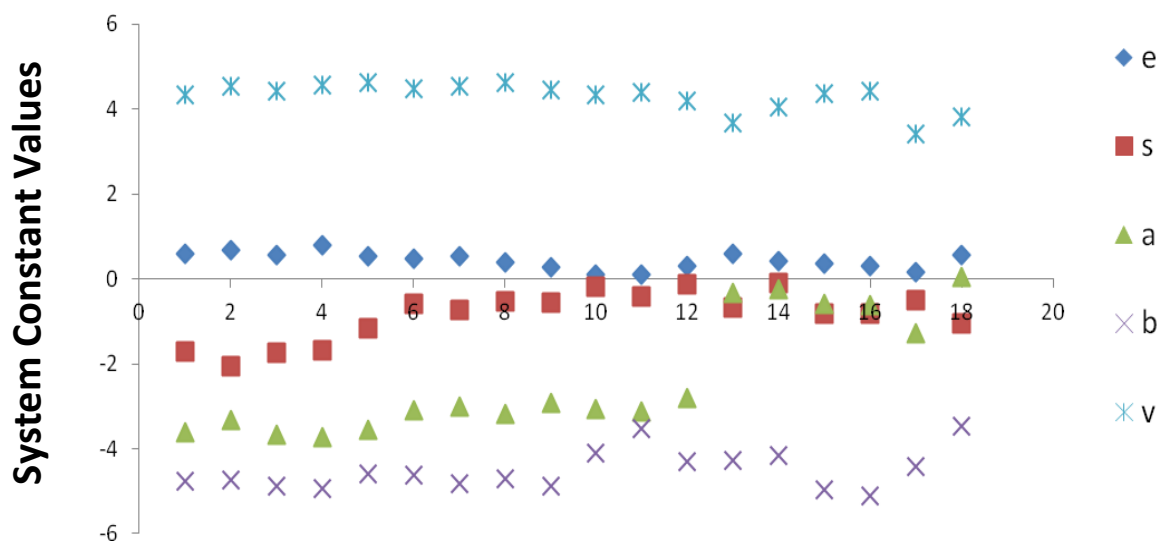
Figure 3. Variation of System Constant Values for a Selected Group of Aqueous Biphasic Systems.
(Figure 3 is Reused from Reference 22 with Permission.)

There are also two categories of aqueous biphasic systems when the hydrogen bond basicity (*a*) system constant is considered. The first category consists of systems with counter solvents which are competitive with water and have small *a* system constant values which are close to zero. The second category consists of systems that compete to a lessser extent with water and have an *a*

system constant value around −4. The charactristic feature of Figure 3 is that there is not much variation of the system constants although there is a variety of aqueous biphasic systems with different counter solvents. The full range of selectivity for the aqueous biphasic systems can be summarized using only the five biphasic systems indicated in Table 1.

Table 1. Aqueous Biphasic Systems Representing the Total Selectivity Range for Available System Constant Values.
(Table 1 is Reused from Reference 22 with Permission.)

Counter Solvent	*c*	*e*	*s*	*a*	*b*	*v*
n-Heptane	0.325	0.678	−2.061	−3.317	−4.733	4.543
Dichloromethane	0.319	0.102	−0.187	−3.058	−4.090	4.324
Diethyl ether	0.248	0.561	−1.016	−0.226	−4.553	4.075
Ethyl Acetate	0.441	0.591	−0.699	−0.325	−4.261	3.666
Octanol	0.088	0.562	−1.054	0.034	−3.460	3.814

1.12.3 Totally Organic Biphasic Partition Systems

(Portions of Text under This Sub Topic are Reused from Reference 22 with Permission)

Variation of system constant values for totally organic biphasic partition systems are demonstrated in Figure 4.[22] Figure 4 indicates that the system constant values for totally organic biphasic partition systems are unique for each system and have a wide range of selectivity. At the same time, each system constant shows a continuous variation of values, quite different to aqueous biphasic systems. Organic solvent systems are less cohesive and less hydrogen bond acidic than water. Therefore, *v* and *b* system constants take values which are less than 2. Due to

the low cohesion and wide range of selectivity, totally organic biphasic systems are more useful for separating high molecular weight compounds, and in obtaining optimum biphasic systems to determine descriptor values. In descriptor determinations, totally organic biphasic systems are used to determine the dipoarity/polarizability (S), hydrogen bond acidity (A), and hydrogen bond basicity (B) descriptors. Also, for compounds of low water solubility and for compounds which are not stable in water, using totally organic biphasic systems is the most appropriate method as the solute property fall into a range that can be accurately determined by experiments.
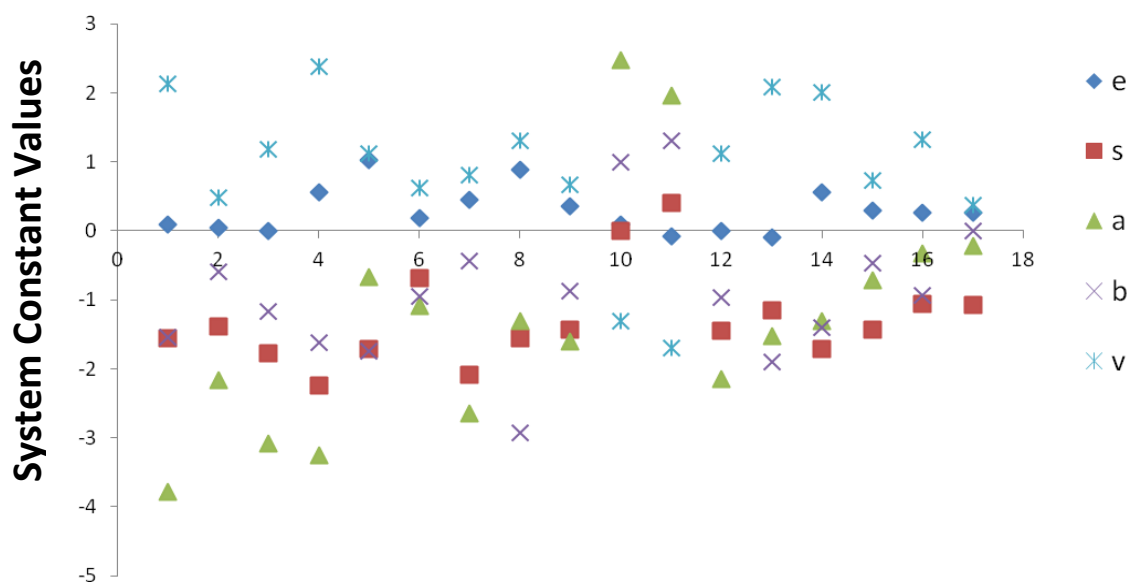
Figure 4. Variation of System Constant Values for a Selected Group of Totally Organic Biphasic Partition Systems.
(Figure 4 is Reused from Reference 22 with Permission.)

The octanol-water partition coefficient is commonly used as a surrogate system for lipophilicity. Poole and coworkers demonstrated that the descriptor values determined for some phthalate esters, polycyclic aromatic hydrocarbons, terpenes, and steroids could be used to predict the octanol-water partition coefficients. The correlation plot in Figure 5 shows the

correlation between the predicted octanol-water partition coefficients and the experimentally

determined octanol-water partition coefficients.[22]
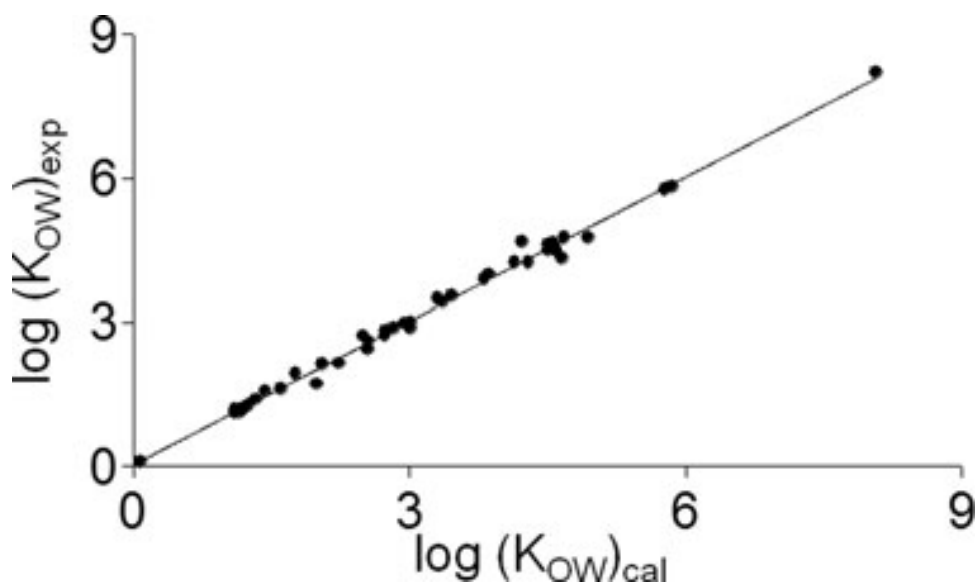
Figure 5: Correlation Plot for Experimental and Calculated Octanol-Water Partition Coefficients
for a Selected Group of Phthalate Esters, Polycyclic Aromatic Hydrocarbons, Terpenes,
and Steroids.
(Figure 5 is Reused from Reference 22 with Permission)

The correlation model for the data used in Figure 5 is given below.

$$\log (K_{OW})_{exp} = 0.010 \ (\pm 0.045) + 0.997 \ (\pm 0.012) \ \log(K_{OW})_{cal} \qquad (16)$$

$$r^2 = 0.993 \quad SE = 0.133 \quad F = 6155 \quad n = 42$$

In Equation 16, $(K_{OW})_{exp}$ is the experimentally determined octanol-water partition coefficient,

and $\log(K_{OW})_{cal}$ is the calculated octanol-water partition coefficient. The values for the octanol-

water partition coefficients cover about eight orders of magnitude. The intercept for the

correlation model includes zero and the slope includes 1 at 95% confidence interval, which

indicates that there is no bias in predicting the partition coefficients. Therefore, the use of

partition coefficients determined using the totally organic biphasic systems to predict partition coefficients for aqueous systems is a viable option when direct measurement is difficult.

1.12.4 Gas Chromatography Methods

Gas chromatography is preferred over other techniques for the determination of the gas-hexadecane partition coefficient at 298 K (L descriptor).[6a] Gas chromatography is also suitable to determine the dipolarity/polarizability (S) and hydrogen bond acidity (A) descriptors by selecting stationary phases capable of polar and hydrogen-bond interactions. The model standard error for the open tubular column stationary phases characterized to date is about 0.015-0.035.

The expected error in the descriptor value is proportional to the ratio of the model standard error and the system constant value. For this reason, when the characterized stationary phase has a large system constant value for a particular intermolecular interaction, the expected error in the determined descriptor value is minimized. Therefore, to determine the gas-hexadecane partition coefficient at 298 K (L) and excess molar refraction (E), poly(methyloctylsiloxane) is most suitable due to the significant contribution of L and E to retention on this stationary phase. To determine the L descriptor, the poly(dimethylsiloxane) stationary phase is less useful due to the significant values for the dipolarity/polarizability (*s*) and hydrogen bond basicity (*a*) system constants. For the estimation of dipolarity/polarizability (S) descriptors poly(methyltriflouropropylsiloxane) stationary phases are suitable due to their high *s*/*a* ratio. Poly(ethylene glycol) stationary phase can be used to determine the hydrogen bond acidity descriptor (A), due to their large value for the *a*/*s* ratio. Strong dipolarity/polarizability and hydrogen bond basicity simultaneously occur for cyanoalkylsiloxane stationary phases. Therefore, the S and A descriptors can be determined simultaneously using these stationary phases. Although the excess molar refraction (E) is determined by calculation for liquids, for

solids it can be determined using poly(ethyleneglycol) and poly(methyltriflouropropylsiloxane) stationary phases since these stationary phases have a relatively large *e* system constant value. The system map for a poly(phenylene dimethylsiloxane) stationary phase is given in Figure 6.[23]
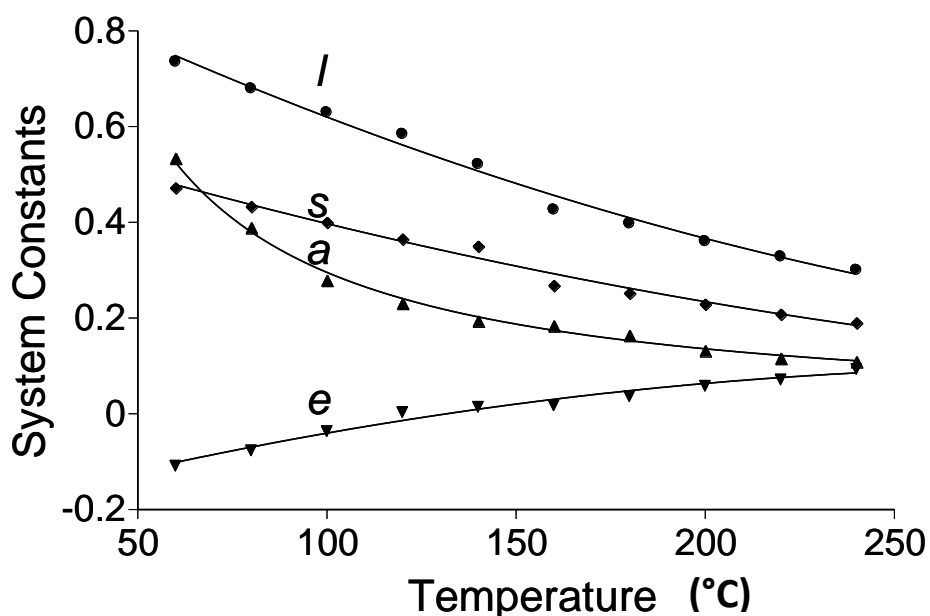
Figure 6: System Map for Rxi 5 Sil MS Column with Poly(phenylene dimethylsiloxane) Stationary Phase.
(Figure 6 is Reused from Reference 23 with Permission)

The variation of system constants as a function of temperature is illustrated by system maps. In Figure 6, a decrease in polar interactions and the cavity and dispersion interactions is observed with the increase in temperature. In contrast, an increase in electron lone pair interactions is observed at higher temperatures. Since large system constant values lead to more accurate descriptor estimates, theoretically the retention factors should be determined at low temperatures. However, the retention of a compound is affected significantly by the column phase ratio (ratio of the volume of mobile and stationary phases for the column) and volatility of the compounds.

Therefore, under practical conditions moderate to high temperatures are usually selected to obtain measurements, in order to obtain reasonable retention times. The gas chromatography retention models possess the lowest model standard errors compared to other techniques. The necessity to measure retention factors at high temperatures does not introduce a significant increase in the expected error for descriptor measurements.[24]

In gas chromatography it is assumed that the retention mechanism occurs exclusively through gas-liquid partitioning.[25] However, adsorption of the solute by the column wall or the stationary phase can occur, leading to incorrect retention factors. The most common possibility is the adsorption at the surface of the stationary phase, when the stationary phase and solute differ significantly in polarity. Interfacial adsorption is often observed for n-alkanes on poly(biscyanopropylsiloxane) and poly(ethylene glycol) stationary phases. The occurrence of interfacial adsorption can be identified by eluting the solute simultaneously in two columns containing the same stationary phase, but with different phase ratios. When the interfacial adsorption is significant, the correlation of retention factors with the phase ratio observed under normal conditions is lost. A disadvantage of gas chromatographic methods is that there are no commercial open tubular columns with significant hydrogen-bond acidity (b~0). Therefore, it is difficult to determine the hydrogen bond basicity (B) descriptor using gas chromatographic methods. As an alternative, liquid chromatography methods can be used to determine the hydrogen-bond basicity descriptor.

1.12.5 Liquid Chromatography Methods

Reversed-phase liquid chromatography is mainly used for the determination of the hydrogen-bond basicity (B) descriptor. It can also be used to determine the

dipolarity/polarizability (S) and hydrogen bond-acidity (A) descriptors. The retention mechanism

for a Sunfire C_{18} column is illustrated in Figure 7.[26]
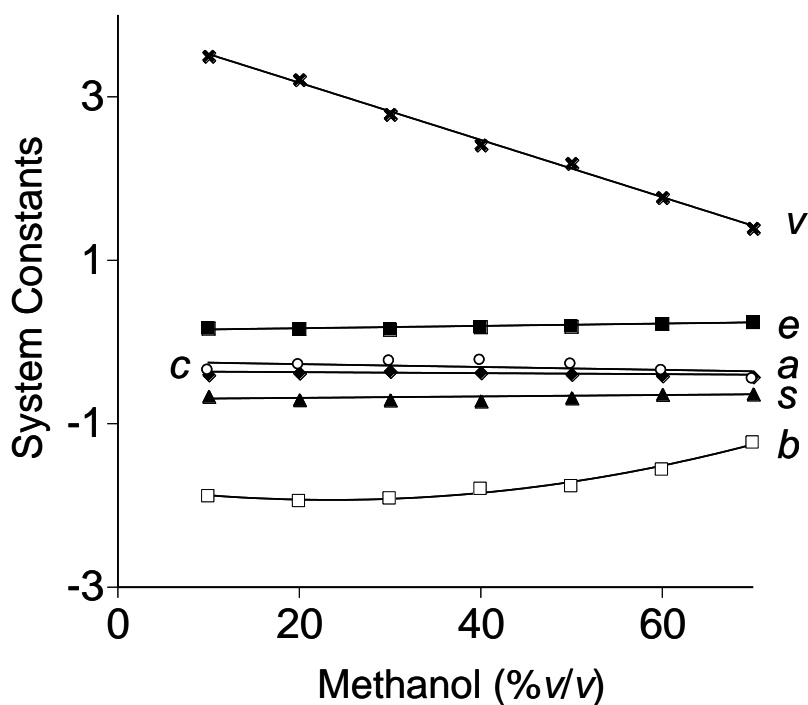
Figure 7. System Map for Sunfire C_{18} Octadecylsiloxane-Bonded Silica Stationary Phase for Methanol-Water Mobile Phase Compositions in Reversed-Phase Chromatography. (Figure 7 is Reused from Reference 26 with Permission)

Figure 7 indicates that the two dominating forces which govern solute retention in the stationary

phase are the hydrogen bond-acidity of the mobile phase (*b*) and cavity formation and dispersion

interactions (*v*). Model standard errors for liquid chromatography are about 0.02-0.07, which is

higher than for gas chromatography (~0.01-0.04).[27] For organic solvent compositions greater

than 50% (v/v), the system constants except *v* and *b* have smaller values. The high values of the *v*

and *b* system constants at low organic mobile phase compositions introduce less error to the

model, and low organic solvent compositions are preferred to determine descriptor values.

However, under practical experimental conditions, moderate to high organic solvent compositions result in reasonable retention times although the model error is larger. Regardless of this uncertainty, liquid chromatography is still the selected method for the determination of the hydrogen bond-basicity descriptor (B).

Normal-phase chromatography can be used to estimate the dipolarity/polarizability descriptor (S) using polar, chemically bonded stationary phases.[28] Reversed-phase chromatography is well suited to determine the hydrogen-bond basicity descriptor.

The dependent variable in liquid chromatography retention models is the retention factor (k). The retention factor is defined by Equation 18 in time units.[6a, 29]

$$k = t'_R/t_M = (t_R-t_M)/(t_M-t_{excol}) \qquad (18)$$

In Equation 18, t'_R is the adjusted retention time and t_M is the column hold up time. Extra column hold up time is given by $t_{excol.}$ The gross column hold up time is usually determined by the injection of a non retained solute such as $NaNO_3$ and KBr for reversed phase chromatography. The extra column hold up time is the time consumed when the solute is transferred to and from the column during injection and detection. The extra column hold up time is measured by replacing the column by a zero-dead-volume union and determining the retention time for a non retained solute to travel from the injector to detector.

Pore dewetting, steric resistance, and electrostatic interactions are the three major problems encountered in reversed-phase chromatography using porous chemically bonded stationary phases to determine descriptors. To enter the pores of the packing the surface tension of the mobile phase must be less than the local column pressure to fill the pores. This phenomenon is called pore dewetting. Pore dewetting causes retention loss of the sample due to the inaccessibility of the solute to the interior surface of the stationary phase. Pore dewetting can

occur for stationary phases with small pores, for stationary phases with a high bonding density and for mobile phases with a high water composition. Pore dewetting can be identified by a discontinuity in the system map and the pressure dependence of the retention factors.

When the solute size increases, the solutes tend not to insert fully into the stationary phase. This is called steric resistance. In chemically bonded phases with a high bonding density, only a part of the solute can insert itself into the solvated stationary phase and the other part resides in the mobile phase or in the interface region. Steric resistance results in two types of retention factors. First type arising from the fully solvated stationary phase is suitable for inclusion in the solvation parameter model. The second type, affected by the steric resistance is not suitable for modeling.[30] Compounds affected by steric resistance include angular compounds such as benzophenones, rigid planar compounds, such as polycyclic aromatic hydrocarbons, compounds having long alkyl chains such as n-alkyl phenones, and bulky compounds such as dialkyl phthalates.[27b, 31] Steric resistance is enhanced for mobile phases with a high water content. Steric resistance can be identified by the sharp discontinuity in plots of the retention factor ($\log k$) versus composition of mobile phase.

Electrostatic interactions between ionized silanol groups of the stationary phase and solute protonated bases result in anomalous retention properties. This is observed for silica-based, chemically bonded stationary phases. Protonated bases have higher retention factors than those predicted by the solvation parameter model.[27, 31a] To prevent electrostatic interactions, a suitable stationary phase should be selected with limited access to ionized silanol groups, and the pH of the mobile phase should be adjusted to suppress ionization. Electrostatic interactions are significant for highly-fluorinated siloxane-bonded stationary phases, such as Flourophase-RP.[26] Electrostatic interactions are more often observed for acetonitrile-water and tetrahydrofuran-

water mobile phases than for the methanol-water mobile phase. Electrostatic interactions are not important for neutral compounds.[6a]

1.12.6 Solubility Methods

Solubility measurements can be used to determine the gas-hexadecane partition coefficient at 298 K (L), dipolarity/polarizability (S), hydrogen-bond acidity (A), and hydrogen-bond basicity (B) descriptors. Partition coefficients in different solvents can be calculated for compounds if the aqueous solubility and vapor pressure at 25 °C are known.[19, 32] Partition coefficients for water solvent systems (P) can be determined, if the solubility (mol l^{-1}) of a solvent (C_S) and the aqueous solubility (C_W) is known (Equation 19).[6a]

$$\log P = \log C_S - \log C_W \qquad (19)$$

Similarly, the partition coefficient of a solute between the solvent and the gas phase (K_S) can be determined using Equation 20, by calculating the gas phase concentration (C_G) if the solid saturated vapor pressure at 25 °C is known.

$$\log K_S = \log C_S - \log C_G \qquad (20)$$

Using Equations 19 and 20, a series of equations can be obtained for different solvents to form a linear model. The accuracy of the calculated partition coefficients can be determined by comparison with the experimental values for dry solvents. The disadvantage of solubility methods is that they are applicable only when three conditions are met. First, the solute should be in the same physical and chemical form when in equilibrium between the two phases. Secondly, the secondary medium activity coefficient of the solute in the two phases should be near unity. That is, the infinite dilution situation is considered for the solute (solute should not be too soluble in the two phases). Thirdly, for solutes that can be ionized, the concentration of the neutral species is used to determine the concentration in the aqueous medium (C_W).

1.12.7 Micellar Electrokinetic Chromatography

Retention factors obtained by micellar electrokinetic chromatography (MEKC) can be used to estimate descriptors and to supplement descriptor values obtained by other methods.[6a] In MEKC systems, a charged separation carrier, such as micelles, migrate in a definite direction in a moving electrolyte solution. The migration velocity or directions of the micelles are different to that of the bulk electrolyte solution. Bulk electrolyte migrates at a constant velocity by electroosmosis. Neutral compounds are distributed between the micellar and electrolyte phases. Therefore, separation occurs within the window created by the electroosmotic flow and migration of the micellar phase. The unique feature of this method is that the start and the end of the separation is known and can be changed by varying the experimental conditions.

The MEKC systems are suitable to determine the hydrogen-bond basicity (B), dipoarity/polarizability (S), and hydrogen-bond acidity (A) descriptors in combination with other methods. MEKC systems have model standard errors between 0.05-0.10.[33] Within the pH range of 3-11 ionization of weak acids and bases can be suppressed and acceptable migration rates established for fused silica or sulfonic acid coated capillary columns. Electrolytes having up to 30% (v/v) organic solvent are used to determine retention properties for compounds with low water solubility. When the solute migration time is greater than 14% of the electroosmotic flow marker and 25% less than the migration time of the micellar phase retention factors can be obtained with less than 5% error. If the compounds have migration rates outside these boundaries, it can introduce significant error to the retention factors.

If a compound is partially ionized, it may have interactions with the electric field used to generate the electroosmotic flow, and the compound can also interact with the separation carrier by electrostatic forces. Therefore, partially ionized compounds cannot be analyzed by the

solvation parameter model, as the solute property cannot be accurately modeled due to the above additional interactions.

1.13 Required Properties of Models for Descriptor Determinations

Suitable systems which are capable of determining descriptor values should yield models which have high correlation between the solute property and the system constants. Rigorous models also should possess small standard errors. If the ratio between the model standard error and the system constant is small, the expected error associated with the determined descriptor value will be less. Therefore, appropriate models are expected to have one or more dominant system constant values in order to be suitable for descriptor determinations.

In order to build appropriate models, the solutes should satisfy certain requirements. Solutes should be distributed evenly within the largest possible descriptor range. The number of solutes should be sufficient to validate the model chemically and statistically. The solutes should also cover a reasonable descriptor space, so they can be separated easily into a training set and a test set. There should be minimal cross correlation between the descriptors. If cross correlation is present, it will lead to inaccurate solute property estimations. The dependent variable should possess a reasonable range of values without clustering. The expected value range for the dependent variable in totally organic biphasic systems is between -4 to $+4$ log units, whereas for gas and liquid chromatography it lies between -3 to $+3$ log units.

1.14 Thesis Problem for the Research Segment 'Chromatographic Methods for Solute Descriptor Determinations'

The direct determination of the concentration of compounds in environmental and physiological systems is important when the resources for the experimental procedures are limited. The solvation parameter model can be used to estimate solute properties directly in

environmental, physiological, and physicochemical systems. In order to estimate the distribution of compounds in environmental compartments, the descriptor values for the solutes should be accurately assigned. To accomplish this task, suitable solvent systems with dominant system constant values need to be identified and characterized. Therefore, the research work reported herein focuses on two different directions. In the first part, the focus will be on the identification and characterization of appropriate solvent systems suitable for descriptor determinations. In the second part, the focus will be on the determination of descriptor values for compounds of environmental interest.

Since the totally organic biphasic partition systems afford access to a wide selectivity space, solvent systems containing ethanolamine as a base solvent, and triethylamine as a counter solvent will be evaluated to identify biphasic systems with optimal system constants for accurate descriptor measurements. The purpose is to identify systems suitable for increasing the selectivity space for hydrogen-bond acidity and hydrogen-bond basicity system constants. These systems will then be explored for the determination of descriptors for polycyclic aromatic hydrocarbons and related compounds. The low solubility of these compounds in water renders conventional methods of limited use for these applications.

Use of gas and liquid chromatography methods will allow the determination of experimental solute properties rapidly and accurately with well defined experimental procedures. Models will be constructed using linear regression analysis and will be validated for accuracy and reliability using statistical tools. The validity of the descriptor values will be evaluated by assessing their performance using standard environmental models (octanol-water, octanol-air, and air-water partition coefficients) and by comparison with experimentally determined solute physicochemical properties.

CHAPTER 2

EVALUATION OF ETHANOLAMINE AS A POTENTIAL SOLVENT FOR DESCRIPTOR DETERMINATIONS

Text, figures, and tables of this chapter were reused or adapted with permission from Ariyasena, T. C.; Poole, C. F. *Chromatographia* **2013**, *76*, 157-164.[34]

2.1 Introduction

Recent developments in liquid phase microextraction methods for sample preparation have renewed interest in liquid-liquid partition systems. Liquid-liquid partition systems have low sample size utilization and facilitate system selection for chromatography techniques.[22, 35] Compared with sorbent-based methods liquid partition systems are more tolerant of matrix burden and afford a wider selectivity range. In addition, solvent properties are more reproducible than sorbents and compare favorably with adsorption methods in terms of equipment, operational requirements, and costs.[35c, 36]

Totally organic biphasic systems were shown to be suitable for the measurement of descriptors for organosiloxanes,[1c, 37] fragrance compounds,[38] plasticizers,[39] and steroids[40] overcoming the limitations of aqueous biphasic systems for these measurements. However, the number of systems available with suitable system constants for determining descriptors is still limited providing further impetus for the studies described here. Poole and coworkers demonstrated that ethylene glycol afforded several totally organic biphasic systems with a useful range of selectivity for liquid-liquid partition studies.[41] In the research work reported herein, our aim is to investigate the use of ethanolamine (2-aminoethanol) as a base solvent for liquid-liquid

partition employing different counter solvents to extend the selectivity range of totally organic biphasic systems currently available, and for descriptor determination purposes.

Ethanolamine has found many applications in industry as a polar solvent, particularly for processing biomass to useful materials and as a component of carbon dioxide storage systems.[42] Its solvatochromic parameters indicate that it is a highly structured polar liquid, strongly hydrogen-bond basic and moderately hydrogen-bond acidic.[42b, 42c, 43] Spectroscopic studies and theoretical calculations show that in the liquid state ethanolamine has significant internal hydrogen bonding which may reduce its capacity to hydrogen bond with solutes.[44] It is also suggested that in the liquid state ethanolamine exists predominantly as an equilibrium mixture of monomers and dimers with the later formed as hydrogen-bonded complexes between the hydroxyl terminus and amino terminus of adjacent molecules.[45]

To date there are no reports of liquid-liquid partition coefficients for ethanolamine, which could be used to quantify its solvent properties. Modeling of ethanolamine as a base solvent with counter solvents of different polarity using the solvation parameter model will facilitate the evaluation of ethanolamine as a potential solvent for descriptor determinations.

2.2 Experimental Section

2.2.1 Materials

Ethanolamine was obtained from Acros Organics (Morris Plains, NJ, USA) and n-heptane and isopentyl ether from Sigma-Aldrich (Milwaukee, WI, USA) and dried over molecular sieves before use. Common chemicals were of the highest purity available and obtained from several sources. The 30 m x 0.32 mm id HP-5 open-tubular column, 0.25 μm film thickness, was obtained from Agilent Technologies (Folsom, CA, USA).

2.2.2 Instrumentation

Gas chromatographic measurements were made with an Agilent Technologies (Palo Alto, CA, USA) HP 6890 gas chromatograph fitted with a split/splitless injector and flame ionization detector using ChemStation software (rev. B.04.01) for data acquisition. Nitrogen was used as carrier gas at a constant flow rate of 2.5 mL min^{-1} (velocity 47 cm s^{-1}). The split ratio was set to 30:1, septum purge 1 mL min^{-1}, inlet temperature 275 °C, and detector temperature 300 °C. Separations were performed using a temperature program with an initial temperature of 150 °C for 1 min and then raised to 280 °C at 25 °C min^{-1}. To handle co-elution of some solutes with either the internal standard or solvent peaks this program was modified slightly as needed.

2.2.3 Determination of Partition Coefficients

Partition coefficients were determined by a method previously published by the Poole group.[41] Screw-capped vials, 2.0 mL with PTFE-lined caps (Supelco, Bellefonte, PA, USA) were charged by syringe with 0.75 mL of ethanolamine saturated with counter solvent, 0.75 mL of counter solvent saturated with ethanolamine, 1-10 μL of liquid sample, and 1 μL (1.31 gml^{-1}) of internal standard. Solid samples were dissolved in either the ethanolamine or counter solvent (depending on solubility) at a concentration of about 0.5-1.5 mg mL^{-1} and added to the vial as described for the pure solvent. Smaller sample sizes were used in some cases to avoid saturation in one of the phases. The vials were shaken and allowed to stand overnight or longer to reach equilibrium at room temperature (22 ± 2 °C). Each vial was centrifuged at about 3,400 rpm for 15 min to facilitate phase separation. Sample volumes of 1 μL from each phase were taken for calculation of the partition coefficients using Equation 21.

$$K_p = (S_{cs} / S_{ea}) (I_{ea} / I_{cs}) K_p^{IS} \qquad (21)$$

In equation 21, K_p is the partition coefficient for compound S. The peak areas for compound S in the counter solvent and ethanolamine is given by S_{cs} and S_{ea}, respectively. The peak areas for the internal standard in the counter solvent and ethanolamine are given by I_{cs} and I_{ea}, respectively. Partition coefficient for the internal standard in the biphasic system is given by K_p^{IS}. The internal standard was 1-nitronaphthalene with $K_p = 0.776 \pm 0.017$ ($n = 10$) for n-heptane-ethanolamine and $K_p = 1.182 \pm 0.086$ ($n = 10$) for isopentyl ether-ethanolamine, where n is the number of measurements.

2.2.4 Calculations

Multiple linear regression analysis and statistical calculations were performed on a Dell Dimension 9200 computer (Austin, TX, USA) using the program PASW v18.0 (PASW, Chicago, IL, USA). The solute descriptors were taken from an in-house database, [6a, 40-41] and are summarized in Table 2 together with the experimental partition coefficients. The Kennard-Stone algorithm programmed in visual basic for use in Excel 2007 (Microsoft Corporation, Redmond, WA, USA) was used to split the data sets into training and test sets to estimate the predictive ability of the partition models.[46]

2.3 Results and Discussion

2.3.1 Characterization of n-Heptane-Ethanolamine Biphasic System

Fitting the partition coefficients ($\log K_p$) in Table 2 to the solvation parameter model for the n-heptane-ethanolamine biphasic system gave Equation 22.

$$\log K_p = -0.233(\pm 0.084) - 0.264(\pm 0.046)E - 1.086(\pm 0.070)S - 4.533(\pm 0.066)A$$

$$-1.299(\pm 0.063)B + 1.992(\pm 0.060)V \tag{22}$$

$$r = 0.997 \qquad r_{adj}^2 = 0.994 \qquad SE = 0.130 \qquad F = 2581 \qquad n = 76$$

In Equation 22, r is the multiple correlation coefficient, r_{adj}^2 is the coefficient of determination adjusted for the number of degrees of freedom, SE is the standard error of the estimate, F is the Fisher's statistic, n is the number of compounds with partition coefficients included in the model, and the coefficients in parenthesis are the standard deviation for the system constants.

The driving force for the transfer of solutes from the n-heptane layer to enthanolamine is indicated by the system constants with a negative sign. Polar interactions characterized by the dipolarity/polarizability (*s*), hydrogen bond basicity (*a*), and hydrogen bond acidity (*b*) system constants are primarily responsible for transfer to ethanolamine. The system constants support the assertion that ethanolamine is a cohesive solvent, reasonably dipolar/polarizable, strongly hydrogen-bond basic, and moderately hydrogen-bond acidic. Electron lone pair interactions, represented by the *e* system constant, are weak but also favor transfer to the ethanolamine layer. Since n-heptane is a solvent of low cohesion the large positive *v* system constant suggests that ethanolamine is a cohesive solvent. For perspective it is about as cohesive as formamide and ethylene glycol, significantly more cohesive than dimethyl sulfoxide and 2,2,2-trifluoroethanol, and slightly less than half as cohesive as water, as measured by the *v* system constant in n-heptane-organic solvent (or water) biphasic systems.[21-22, 47] In particular the relatively large value for the *a* system constant indicates that ethanolamine is a strong hydrogen-bond base, significantly stronger than water, ethylene glycol, formamide, and dimethyl sulfoxide as measured by the *a* system constant in n-heptane-organic solvent (or water) biphasic systems.

Table 2. Descriptor Values and Partition Coefficients for Compounds Used in the Solvation Parameter Model to Characterize the n-Heptane-Ethanolamine (HEP-EA) and Isopentyl Ether-Ethanolamine (IPE-EA) Biphasic Systems.

Compound	E	S	A	B	V	HEP-EA log K_p	IPE-EA log K_p
Acenaphthene	1.350	0.910	0	0.226	1.2586	0.855	0.288
Acenaphthylene	1.570	1.120	0	0.218	1.215	0.329	0.170
Acetanilide	0.962	1.162	0.548	0.704	1.1137	−2.851	−1.687
Aniline	0.956	1.012	0.237	0.432	0.8162	−1.727	
Anisole	0.712	0.762	0	0.312	0.9160	0.416	0.168
Anthracene	1.980	1.278	0	0.270	1.4544	0.524	
Benzamide	1.257	1.365	0.660	0.657	0.9728	−3.791	−2.469
Benzyl alcohol	0.803	0.868	0.410	0.558	0.9160	−2.148	−1.201
Biphenyl	1.372	0.978	0	0.156	1.2604		0.351
Borneol	0.763	0.704	0.166	0.650	1.3591	−0.213	0.006
1-Bromonaphthalene	1.594	1.014	0	0.156	1.2604	0.534	0.160
3-Bromophenol	1.081	0.760	0.942	0.209	0.9501	−4.039	−3.051

Table 2. Continued.

Compound	E	S	A	B	V	HEP-EA log K_p	IPE-EA log K_p
Carbazole	2.051	1.553	0.388	0.229	1.3154	−2.009	−1.434
2-Chloroaniline	1.026	1.006	0.238	0.317	0.9386	−0.902	−0.807
4-Chloroaniline	0.998	1.177	0.342	0.295	0.9386	−1.798	−1.319
4-Chloro-3-methylphenol	0.571	0.677	0.799	0.300	1.0384		−2.316
1-Chloronaphthalene	1.419	0.941	0	0.137	1.2078		0.526
2-Chlorophenol	0.874	0.683	0.516	0.344	0.8975	−2.293	−1.572
4-Chlorophenol	1.006	0.786	0.862	0.211	0.8975	−3.613	−2.733
Chrysene	2.647	1.667	0	0.302	1.8234	0.527	0.230
Cinnamyl alcohol	1.095	0.984	0.480	0.597	1.1548	−2.186	−1.709
n-Decanol	0.191	0.417	0.347	0.536	1.5763	0.329	0.130
Dibenzofuran	1.598	1.092	0	0.123	1.2087	0.448	0.386
Dibenzylamine	1.340	1.013	0.101	0.926	1.7058	0.110	0.296

Table 2. Continued.

Compound	E	S	A	B	V	HEP-EA log K_p	IPE-EA log K_p
Dibenzyl ether	1.212	1.113	0	0.719	1.6647	0.474	0.250
3,4-Dichloroaniline	1.362	1.290	0.412	0.247	1.0610	−1.954	−1.258
2,6-Dichloro-4-nitrophenol	1.263	1.494	0.369	0.319	1.2352	−1.724	−1.150
Dicyclohexylamine	0.585	0.423	0.015	0.560	1.8132	2.067	1.125
N,*N*-Diethylcarbanilide	1.692	1.295	0	1.304	2.2440	0.652	0.320
N,*N*-Diethyldodecanamide	0.331	0.936	0	0.948	2.2635	1.846	1.356
N,*N*-Dimethylaniline	0.956	0.815	0	0.445	1.0980	0.110	0.371
N,*N*-Dimethyldodecylamine	0.080	0.199	0	1.467	2.1810	1.897	1.374
3,5-Dimethylphenol	0.762	0.755	0.688	0.347	1.0569	−2.659	−1.766
1,3-Dinitrobenzene	1.056	1.760	0	0.416	1.0648	−0.961	−0.481
Diphenylamine	1.704	1.278	0.149	0.532	1.4240	−0.609	−0.299
Diphenyl ether	1.221	0.979	0	0.267	1.3829	0.765	0.316

Table 2. Continued.

Compound	E	S	A	B	V	HEP-EA log K_p	IPE-EA log K_p
N,N-Diphenyl-p-phenylenediamine	2.715	2.090	0.312	0.981	2.1316	−1.456	−1.110
1,5-Divinyl-1,1,3,3,5,5-hexamethyltrisiloxane	−0.238	0.008	0	0.525	2.2861	3.870	
Dodecane	0	0	0	0	1.7994	3.209	2.279
1,12-Dodecanediol	0.455	0.805	0.819	1.219	1.9168	−2.636	
Fluoranthene	2.310	1.470	0	0.286	1.5846	0.233	0.264
Fluorene	1.669	1.105	0	0.257	1.3565	0.448	0.297
Geraniol	0.493	0.640	0.270	0.603	1.4903	−0.074	−0.113
Hexachlorobenzene	1.374	0.876	0	0	1.4508	1.304	0.959
n-Hexadecylamine	0.170	0.280	0.235	0.610	2.4680		1.700
n-Hexanol	0.210	0.432	0.350	0.535	1.0127	−0.908	
Indole	1.071	1.240	0.417	0.228	0.9464	−2.363	−1.253
Iodobenzene	1.182	0.790	0	0.134	0.9747	0.375	−0.034

42

Table 2. Continued.

Compound	E	S	A	B	V	HEP-EA log K_p	IPE-EA log K_p
Limonene	0.497	0.337	0	0.167	1.3230	1.742	1.175
Linalool	0.391	0.536	0.198	0.733	1.4903	0.272	0.292
2-Methoxynaphthalene	1.451	1.151	0	0.355	1.2850	0.159	0.342
1-Methylnaphthalene	1.337	0.903	0	0.206	1.2263	0.596	
2-Methylnaphthalene	1.304	0.888	0	0.206	1.2263	0.623	0.342
2-Methylphenol	0.775	0.740	0.614	0.356	0.9160	−2.824	−1.912
3-Methylphenol	0.810	0.767	0.678	0.350	0.9160	−3.066	−2.175
Naphthalene	1.230	0.905	0	0.191	1.0854		0.129
2-Naphthylethanol	1.592	1.233	0.440	0.745	1.4259	−2.340	−1.417
Nicotinamide	1.191	1.798	0.431	0.773	0.9317		−2.018
Nicotine	0.861	0.958	0	1.082	1.3710	−0.405	0.051
2-Nitroaniline	1.228	1.473	0.343	0.352	0.9904	−2.285	−1.269

Table 2. Continued.

Compound	E	S	A	B	V	HEP-EA log K_p	IPE-EA log K_p
3-Nitroaniline	1.252	1.564	0.496	0.420	0.9904	−3.168	−2.073
Nitrobenzene	0.846	1.143	0	0.268	0.8906	−0.271	−0.275
4-Nitrobenzyl alcohol	1.008	1.358	0.509	0.583	1.0902	−2.939	−1.881
1-Nitronaphthalene	1.381	1.478	0	0.287	1.2596	−0.110	0.072
2-Nitrotoluene	0.866	1.154	0	0.225	1.0315	0.062	−0.118
3-Nitrotoluene	0.874	1.138	0	0.211	1.0315	0.075	−0.063
4-Nitrotoluene	0.879	1.171	0	0.265	1.0315	−0.030	0.165
n-Nonanol	0.199	0.368	0.370	0.555	1.4354		-0.058
Octan-2-ol	0.176	0.414	0.273	0.525	1.2945	0.187	
Pentachlorophenol	1.745	0.956	0.665	0.061	1.3871	−1.616	
Perylene	2.697	1.835	0	0.411	1.9536	0.634	−0.021
Phenanthrene	1.934	1.284	0	0.284	1.4544	0.491	0.379

Table 2. Continued.

Compound	E	S	A	B	V	HEP-EA log K_p	IPE-EA log K_p
2-Phenylethanol	0.787	0.815	0.415	0.620	1.0569	−1.924	−1.440
4-Phenylphenol	1.517	1.179	0.817	0.445	1.3829	−3.609	−2.496
3-Phenylpropan-1-ol	0.819	0.888	0.359	0.670	1.1978	−1.694	−1.137
Pyrene	2.296	1.463	0	0.293	1.5846	0.409	0.072
trans-Stilbene	1.619	1.216	0	0.286	1.5630	0.610	0.641
Quinoline	1.265	1.091	0	0.619	1.0443	−0.254	−0.325
Terpinen-4-ol	0.553	0.557	0.173	0.652	1.4247	0.115	0.133
1,2,4,5-Tetrachlorobenzene	1.070	0.714	0	0.024	1.2060	0.942	0.682
Tribenzylamine	1.821	1.270	0	0.631	2.4545		1.004
1,2,4-Trichlorobenzene	1.022	0.746	0	0.024	1.0836	0.839	0.614
1,3,5-Triethylbenzene	0.672	0.500	0	0.190	1.5618	1.118	
Trisopropanolamine	0.629	1.335	0.412	1.499	1.6526		−1.228

Table 2. Continued.

Compound	E	S	A	B	V	HEP-EA log K_p	IPE-EA log K_p
Trimethoprim	1.760	1.947	0.075	2.081	2.1813	−1.507	
Triphenylamine	2.439	0.983	0	0.755	2.0318	0.942	0.786
Triphenylmethane	1.865	1.152	0	0.549	2.0729	0.757	
Undecane	0	0	0	0	1.6585	2.878	2.035
Vanillin	1.120	1.385	0.385	0.673	1.1313		−1.390
m-Xylene	0.625	0.505	0	0.184	0.9982		0.649

To evaluate the predictive ability of the model the data set in Table 2 was split into a training set of 51 compounds and a test set of 25 compounds using the Kennard-Stone algorithm.[46] This approach ensures that the training set and test set are selected to occupy a similar descriptor space. The model for the training set in Equation 23 is similar to the model in Equation 22.

$$\log K_p = -\,0.267(\pm0.089) - 0.232(\pm0.060)E - 1.100(\pm0.085)S - 4.477(\pm0.077)A$$

$$- 1.284(\pm0.069)B + 1.978(\pm0.065)V \tag{23}$$

$$r = 0.998 \qquad r_{adj}^{2} = 0.995 \quad SE = 0.123 \quad F = 1{,}880 \qquad n = 51$$

Equation 23 was then used to predict the partition coefficients ($\log K_p$) for the compounds in the test set. The average error, average absolute error, and root mean square error of the difference between the experimental and model predicted partition coefficients are used to assess the ability of Equation 23 to estimate further values of $\log K_p$ within the same descriptor space. The average error is an indication of bias and at 0.021 is not a concern for equation 23. The absolute average error (0.155) and root mean square error (0.154) are an indication of the likely error in predicting further partition coefficients based on equation 23. Since Equation 23 is similar to Equation 22, which is preferred because it is based on a larger number of compounds, it is reasonable to conclude that Equation 22 should be able to predict partition coefficients to about ±0.15 log units for further compounds that lie within or close to the descriptor space (E = −0.24 to 2.72, S = 0 to 2.09, A = 0 to 0.92, B = 0 to 2.08, and V = 0.816 to 2.286) used to define the model.

The system constants for the biphasic system n-heptane-ethylene glycol ($e = 0.095$, $s = -1.486$, $a = -3.797$, $b = -1.536$, and $v = 2.075$) have been reported previously and can be used to

assess differences in solvation properties for n-heptane-ethylene glycol and n-heptane-ethanolamine biphasic systems.[40-41] Ethylene glycol and ethanolamine have similar cohesion (v system constant about the same) but ethylene glycol is significantly more polar/polarizable than ethanolamine (s ethylene glycol > s ethanolamine). Electron lone pair interactions are virtually insignificant for ethylene glycol but not so for ethanolamine and contribute to the transfer of compounds to the polar solvent from n-heptane. Ethylene glycol is considerably more hydrogen-bond acidic than ethanolamine (b ethylene glycol > b ethanolamine) but a significantly weaker hydrogen-bond base. The 'a' system constant for the n-heptane-ethanolamine biphasic system is the largest recorded for a liquid-liquid partition system and is considerably larger than n-alkane-water biphasic systems.[19, 21] Biphasic systems with a large single dominant system constant are useful for estimating descriptor values and this is foreseen as a major application of this system. For sample preparation purpose the n-heptane-ethanolamine system should be useful for the selective extraction of hydrogen-bond acids from matrices soluble in n-heptane.

Ethanolamine was observed to be unsuitable for handling certain samples due to chemical reactions either in solution or the injection port of the gas chromatograph. Ketones, aldehydes, and aromatic esters (e.g., phthalate esters) showed additional products in the chromatogram most likely due to nucleophilic carbonyl addition reactions involving Schiff base formation. Alkoxysilanes are unstable in ethanolamine forming silyl derivatives of the amine and hydroxyl groups. Similar reactions were not observed with ethylene glycol indicating the participation of the amine group as a base in promoting these reactions. Using cryoscopic measurements Baliah and Ramakrishnan suggested that phenols react with ethanolamine forming ion pairs which dissociate only partially in ethanolamine.[48] There are seven phenols in the data set used to

construct Equation 22. Removing these from the data set gave Equation 24 which is virtually

identical to Equation 22.

$$\log K_p = -\, 0.225(\pm 0.087) - 0.245(\pm 0.050)E - 1.116(\pm 0.075)S - 4.452(\pm 0.091)A$$
$$-\, 1.305(\pm 0.064)B + 1.990(\pm 0.061)V \tag{24}$$

$r = 0.997 \qquad r_{adj}{}^2 = 0.993 \quad SE = 0.130 \quad F = 1883 \qquad n = 69$

In addition the model residuals for the phenols show alternating signs and the average

error for the phenol residuals of -0.052 does not indicate a significant bias in the prediction of

their solvation properties. Thus, it is reasonable to conclude that phenols are unlikely to form ion

pairs in ethanolamine since their experimental partition coefficients can be described by the

general model. This was confirmed for the isopentyl ether-ethanolamine data set, discussed

below, which contains eleven phenols for which the average error for the model residuals was

-0.036.

2.3.2 Characterization of Isopentyl Ether-Ethanolamine Biphasic System

Fitting the partition coefficients ($\log K_p$) for the isopentyl ether-ethanolamine system in

Table 2 to the solvation parameter model gave Equation 25.

$$\log K_p = -\, 0.091(\pm 0.087) - 0.302(\pm 0.051)E - 0.564(\pm 0.073)S - 3.212(\pm 0.071)A$$
$$-\, 0.701(\pm 0.071)B + 1.231(\pm 0.060)V \tag{25}$$

$r = 0.993 \qquad r_{adj}{}^2 = 0.985 \quad SE = 0.144 \quad F = 1045 \qquad n = 81$

The higher cohesion of the ethanolamine layer favors transfer of the solutes to the

isopentyl ether layer (positive *v* system constant) while polar interactions have a negative sign (*e*,

s, *a*, and *b*) and favor solubility in the ethanolamine layer. Isopentyl ether is more cohesive, dipolar/polarizable, and hydrogen-bond basic than n-heptane and this is reflected in the smaller values for the *v*, *s* and *a* system constants compared with the n-heptane-ethanolamine system. The Kennard-Stone algorithm was used to split the data set into a training set of 54 compounds and a test set of 27 compounds. The model for the training set is given in Equation 26.

$$\log K_p = -0.068(\pm0.100) - 0.282(\pm0.059)E - 0.584(\pm0.087)S - 3.139(\pm0.096)A$$
$$- 0.623(\pm0.106)B + 1.179(\pm0.072)V \tag{26}$$

$r = 0.992 \qquad r_{adj}^2 = 0.982 \quad SE = 0.145 \quad F = 578 \qquad n = 54$

Equation 26 is quite similar to the Equation 25. For the test set, the average error was −0.024, the average absolute error was 0.164, and the root mean square error was 0.163. Thus Equation 25 should be able to predict further values of the partition coefficient to about 0.16 log units for compounds with descriptor values that lie within or close to the descriptor space (E = 0 to 2.71, S = 0 to 2.09, A = 0 to 0.94, B = 0 to 1.49, and V = 0.891 to 2.468) used to define the model.

The system constants for the biphasic system isopentyl ether-ethylene glycol (*e* = −0.130, *s* = −1.093, *a* = −1.537, *b* = −1.919, and *v* = 2.093) indicate that the isopentyl ether-ethanolamine system has complementary separation properties.[40-41] The ethanolamine biphasic system is not as cohesive, dipolar/polarizable or as hydrogen-bond acidic (smaller *v*, *s*, and *b* system constants) as the ethylene glycol system. On the other hand, the ethanolamine biphasic system is considerably more hydrogen-bond basic (larger *a* system constant). Isopentyl ether competes to some extent with ethanolamine as a hydrogen-bond acid but the significant '*a*' system constant suggests that it would be useful for determining the hydrogen bond acidity (A) descriptor for compounds with

limited solubility in n-heptane. The solubility of isopentyl ether in ethanolamine is about 1.19 %

(*v/v*) and ethanolamine in isopentyl ether 0.73% (*v/v*) at equilibrium and room temperature. With

the exception of aromatic solvents, such as toluene, ethanolamine does not form biphasic systems

with moderately dipolar solvents, such as 1,2-dichloroethane (unlike ethylene glycol), or more

polar organic solvents. Thus, there are limited options for the choice of further counter solvents

that might be used with ethanolamine to adjust selectivity.

Hierarchical cluster analysis using the average linkage between groups agglomeration

algorithm and the system constants as variables was used to obtain a global view of the

extraction properties of the nineteen totally organic biphasic systems characterized using the

solvation parameter model.[22, 40, 47a] The dendrogram in Figure 8 demonstrates that these totally

organic biphasic systems encompass a wide range of selectivity with little clustering.

Both the n-heptane-ethanolamine and isopentyl ether-ethanolamine systems are indicated

as behaving independently and do not duplicate the separation properties of any of the other

biphasic systems in the database. n-Heptane-ethanolamine is loosely connected with the group

containing n-heptane-ethylene glycol[41] and n-heptane-formamide[47b]. These three systems have

the largest value for the '*a*' and '*v*' system constants and are suitable candidates for determining

the hydrogen bond acidity (A) descriptor. They are somewhat different in their other solvation

properties and thus do not form a tight cluster with n-heptane-ethanolamine standing out by its

significantly larger value for the '*a*' system constant. The isopentyl-ether-ethanolamine biphasic

system is loosely connected with the ethylene glycol-1,2-dichloroethane[41] and formamide-1,2-

dichloroethane[47b] biphasic systems. These systems have a reasonably large '*a*' system constant,

small '*s*' system constant, and intermediate '*v*' system constant. They provide an alternative to

the biphasic systems like n-heptane-ethanolamine for the determination of the hydrogen bond

acidity (A) descriptor for compounds with limited solubility in n-heptane. The analysis of the solvation characteristics of the biphasic systems in Figure 8 confirm that the two ethanolamine systems add to the diversity of the liquid-liquid partition systems available for sample preparation and descriptor measurements without duplicating the properties of those systems.
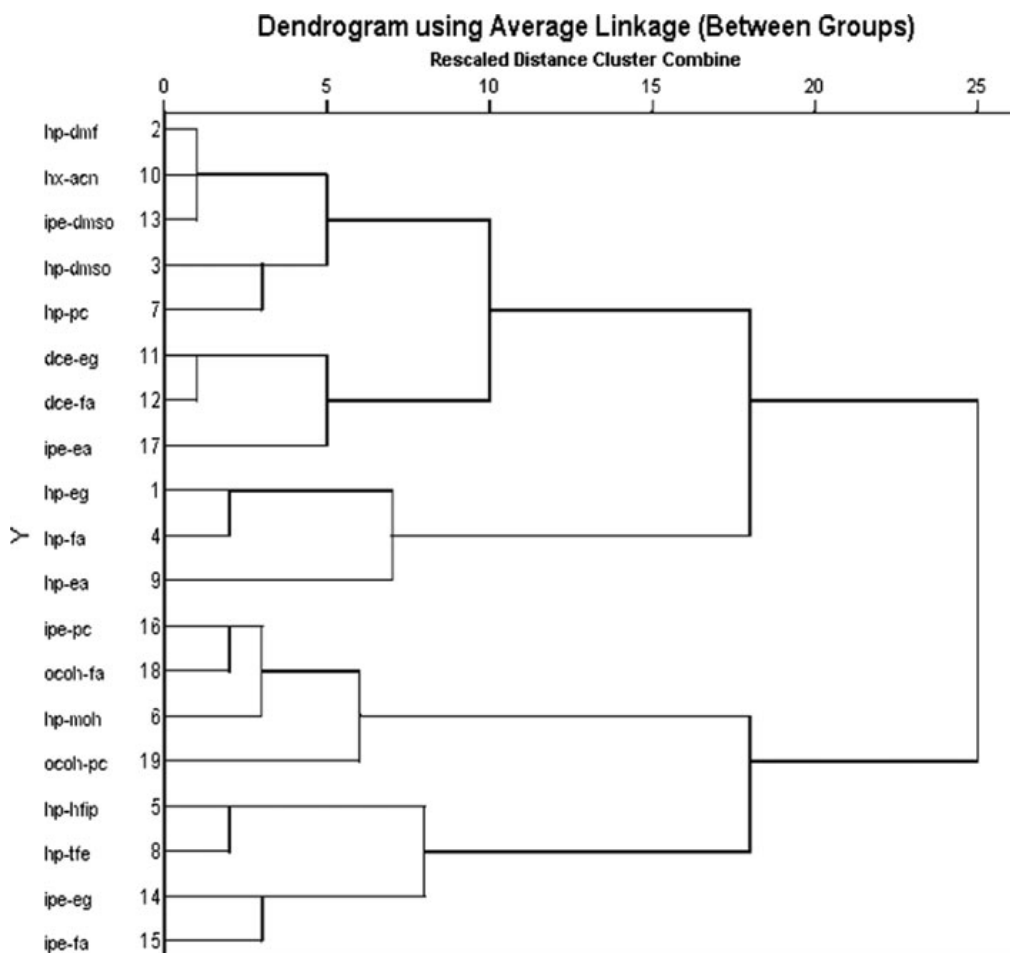
Figure 8. Dendrogram for Totally Organic Biphasic Systems with the System Constants as Variables Using the Average Linkage Between Groups Agglomeration Algorithm.

(Solvents: hp = n-heptane, ipe = isopentyl ether, dce = 1,2-dichloro ethane, ocoh = 1-octanol dmf = N,N-dimethylformamide, acn = acetonitrile, dmso = dimethylsulfoxide, pc = propylene carbonate, eg = ethylene glycol, fa = formamide, moh = methanol, hfip = hexaflouroisopropanol, tfe = 2,2,2-triflouroethanol)

2.4. Conclusions

Ethanolamine is shown to be a useful solvent for liquid-liquid partition forming complementary biphasic systems with organic counter solvents with potential applications for sample preparation and descriptor measurements. Ethanolamine is a relatively cohesive solvent, moderately dipolar/polarizable and hydrogen-bond acidic, and strongly hydrogen-bond basic. It is its capability as a strong hydrogen-bond base which sets it apart from other organic solvents studied so far as well as water. The two models for the characterized ethanolamine systems demonstrate that the ethanolamine-based systems are suitable for descriptor determinations, as well as the two systems contributed to increase the selectivity space for totally organic biphasic systems. We have used ethanolamine systems to determine descriptors for a group of amine and amide compounds.

CHAPTER 3

EVALUATION OF TRIETHYLAMINE AS A POTENTIAL SOLVENT FOR DESCRIPTOR DETERMINATIONS

Text, figures, and tables of this chapter were reused or adapted with permission from Ariyasena, T. C.; Poole, C. F. *Chromatographia* **2013**, *76*, 1031-1039.[49]

3.1 Introduction

Poole and coworkers have reported the characterization of n-heptane, 1,2-dichloroethane, isopentyl ether, and octan-1-ol as counter solvents in totally organic biphasic systems (Figure 9).[22] Due to mutual solubility, it is difficult to extend the coverage of these biphasic systems by identifying further polar solvents which demonstrate different selectivity properties than those reported so far. Characterization of systems with counter solvents which exhibit diverse chemical properties is important to enhance the selectivity space for totally organic biphasic partition systems. To this end, triethylamine was explored as a counter solvent with solvation properties different to those of n-heptane, 1,2-dichloroethane, isopentyl ether, and 1-octanol. Triethylamine is a weakly cohesive and dipolar/polarizable solvent that is strongly hydrogen-bond basic, but lacks any hydrogen-bond acidity.[50] It forms biphasic systems with dimethyl sulfoxide and formamide of the polar solvents indicated in Figure 9. We could find no reports of liquid-liquid partition coefficients for totally organic biphasic systems formed with triethylamine, which could be used to facilitate an understanding of its solvent properties, and set about determining these values to identify its selectivity properties and its potential ability for descriptor determinations.

Polar Solvent	Counter Solvent				
	Heptane	1,2-DCE	IPE	OcOH	TEA
Acetonitrile	▨				
Dimethylformamide	▨		▨		
Dimethyl sulfoxide	▨				▨
Ethylene glycol	▨	▨	▨		
Ethanolamine	▨		▨		▨
Formamide	▨	▨	▨	▨	▨
Hexafluoroisopropanol	▨				
Propylene carbonate	▨		▨	▨	▨
Methanol	▨				
Trifluoroethanol	▨				

Figure 9. Currently Explored Counter Solvents in Totally Organic Biphasic Partition Systems. Shaded Areas Indicate Solvent Pairs Having Less Solubility which Form Suitable Systems for Characterization.
(Solvents: 1,2-DCE = 1,2-Dichloroethane, IPE = Isopentyl ether OcOH = Octanol, TEA = Triethylamine)

3.2 Experimental

3.2.1 Materials

Triethylamine, ethanolamine, dimethyl sulfoxide, and formamide were obtained from Acros Organics (Morris Plains, NJ, USA) and dried over molecular sieves before use. Common chemicals were of the highest purity available and obtained from several sources. The 30 m x 0.32 mm id HP-5 open-tubular column, 0.25 μm film thickness, was obtained from Agilent Technologies (Folsom, CA, USA).

3.2.2 Instrumentation

Gas chromatographic measurements were made with an Agilent Technologies (Palo Alto, CA, USA) HP 6890 gas chromatograph fitted with a split/splitless injector and flame ionization detector using ChemStation software (rev. B.04.01) for data acquisition. Nitrogen was used as carrier gas at a constant flow rate of 2.5 mL min^{-1} (velocity 47 cm s^{-1}). The split ratio was set to 30:1, septum purge 1 mL min^{-1}, inlet temperature 275 °C, and detector temperature 300 °C. For the triethylamine-dimethyl sulfoxide and triethylamine-ethanolamine systems, separations were performed using a temperature program with an initial temperature of 100 °C for 1 min and then raised to 280 °C at 15 °C min^{-1} with a hold at the final temperature of 4 min. For the triethylamine-formamide system separations were performed using a temperature program with an initial temperature of 115 °C for 3 min and then raised to 128 °C at 2 °C/min, held at 128 °C for 1 min, then programmed to 280 °C at 15 °C/min and held at the final temperature for 4 min. The program conditions were optimized in this way to handle a broad decomposition peak that results from the decomposition of formamide on gas chromatography.[47b] To handle co-elution of some solutes with either the internal standard or solvent peaks both programs were modified slightly as needed.

3.2.3 Determination of Partition Coefficients

Partition coefficients were determined following a literature method.[41] Screw-capped vials, 2.0 mL with PTFE-lined caps (Supelco, Bellefonte, PA, USA) were charged by syringe with 0.75 mL of triethylamine saturated with polar solvent, 0.75 mL of polar solvent saturated with triethylamine, 1-10 μL of liquid sample, and 1 μL of internal standard. Solid samples were dissolved in either the triethylamine or polar solvent (depending on solubility) at a concentration of about 0.5-1.5 mg mL^{-1} and added to the vial as described for the pure solvent. Smaller sample

sizes were used in some cases to avoid saturation in one of the phases. The vials were shaken and allowed to stand overnight or longer to reach equilibrium at room temperature (22 ± 2 °C). Each vial was centrifuged at about 3,400 rpm for 15 min to facilitate phase separation. Sample volumes of 1 μL from each phase were taken for calculation of the partition coefficients using the relationship

$$K_p = (S_{tea} / S_{ps}) (I_{ps}/ I_{tea}) K_p^{IS} \qquad (27)$$

K_p is the partition coefficient for compound S, S_{tea} and S_{ps} the peak area for compound S in the triethylamine and polar solvent layers, respectively, I_{tea} and I_{ps} the peak area for the internal standard in the triethylamine and polar solvent layers, respectively, and K_p^{IS} is the partition coefficient for the internal standard in the biphasic system. The internal standard was dibenzyl ether with $K_p = 0.918 \pm 0.052$ (n = 10) for triethylamine-dimethyl sulfoxide and nitrobenzene with $K_p = 1.683 \pm 0.037$ (n = 10) for triethylamine-formamide and 0.971 ± 0.057 (n = 10) for triethylamine-ethanolamine.

3.2.4 Calculations

Multiple linear regression analysis and statistical calculations were performed on a Dell Dimension 9200 computer (Austin, TX, USA) using the program PASW v 21.0 (PASW, Chicago, IL, USA). The solute descriptors were taken from an in-house database[6a, 40-41] and are summarized in Table 3 together with the experimental partition coefficients. The Kennard-Stone algorithm programmed in visual basic for use in Excel 2007 (Microsoft Corporation, Redmond, WA, USA) was used to split the data sets into training and test sets to estimate the predictive ability of the partition models.[46]

3.3 Results and Discussion

Triethylamine forms biphasic systems with the polar solvents ethanolamine, dimethyl sulfoxide, formamide and propylene carbonate. The equilibrium solubility of propylene carbonate in triethylamine is 0.54% (*v/v*) and triethylamine in propylene carbonate 89.7% (*v/v*). The high solubility of triethylamine in propylene carbonate would make this biphasic system an unlikely candidate for practical applications in sample preparation and for descriptor measurements. The mutual solubility of the triethylamine-ethanolamine system is more favorable with the solubility of ethanolamine in triethylamine determined as 0.43% (*v/v*) and estimated as 5% (*v/v*) for triethylamine in ethanolamine. The solubility of triethylamine in dimethyl sulfoxide was 1.09% (*v/v*) and dimethyl sulfoxide in triethylamine 0.98% (*v/v*). Formamide is unstable to gas chromatography,[47b] and its mutual solubility was indicated as low based on the imperceptible change in volume of the two layers on mixing.

3.3.1 Characterization of Triethylamine-Dimethyl sulfoxide Biphasic System

Fitting the partition coefficients ($\log K_p$) in Table 3 to the solvation parameter model for the triethylamine-dimethyl sulfoxide biphasic system gave equation 28.

$$\log K_p = -0.167(\pm 0.093) + 0.085(\pm 0.054)E - 1.325(\pm 0.084)S - 1.215(\pm 0.095)A$$

$$- 0.716(\pm 0.081)B + 1.046(\pm 0.052)V \tag{28}$$

$$r = 0.977 \qquad r_{adj}^2 = 0.951 \quad SE = 0.187 \quad F = 329 \qquad n = 86$$

In Equation 28, r is the multiple correlation coefficient, r_{adj}^2 is the coefficient of determination adjusted for the number of degrees of freedom, SE is the standard error of the estimate, F is the Fisher's statistic, n is the number of compounds with partition coefficients included in the model,

and the coefficients in parenthesis are the standard deviation for the system constants. The driving force for the transfer of solutes from the triethylamine layer to dimethyl sulfoxide is indicated by the system constants with a negative sign. Polar interactions characterized by the *s*, *a*, and *b* system constants are primarily responsible for transfer to dimethyl sulfoxide. The difference in cohesion for the two solvents is mainly responsible for retention in the triethylamine layer. Electron lone pair interactions, represented by the *e* system constant, are weak and favor transfer to the triethylamine layer. Consequently, compounds of low polarity are expected to reside predominantly in the triethylamine layer with small polar compounds being selectively extracted by dimethyl sulfoxide.

Table 3. Descriptor Values and Partition Coefficients for Compouds Used in the Solvation Parameter Model to Characterize the Triethylamine-Dimethyl sulfoxide (TEA-DMSO), Triethylamine-Formamide (TEA-FA), and Triethylamine-Ethanolamine (TEA-EA) Biphasic Systems.

Compound	E	S	A	B	V	TEA-DMSO log K_p	TEA-FA log K_p	TEA-EA log K_p
Acenaphthene	1.350	0.910	0	0.226	1.258	0.022	1.749	0.030
Acenaphthylene	1.570	1.120	0	0.218	1.215	−0.329	1.292	−0.080
Acetanilide	0.962	1.162	0.548	0.704	1.113	−1.722	−0.535	−1.172
1-Acetonaphthone	1.517	1.414	0	0.559	1.382		0.639	
2-Acetonaphthone	1.429	1.457	0	0.601	1.382		0.572	
Acetophenone	0.806	1.057	0	0.497	1.013		0.188	
Androsterone	1.331	1.697	0.396	1.590	2.425		0.288	
Aniline	0.955	1.012	0.237	0.432	0.816			−0.684
Anisole	0.712	0.762	0	0.312	0.916			0.243
Anthracene	1.980	1.278	0	0.270	1.454	−0.356	1.537	0.065

Table 3. Continued.

Compound	E	S	A	B	V	TEA-DMSO log K_p	TEA-FA log K_p	TEA-EA log K_p
Benzamide	1.257	1.365	0.660	0.657	0.972	−2.406		−1.875
Benzonitrile	0.742	1.128	0	0.332	0.871		0.138	
Benzophenone	1.209	1.293	0	0.581	1.480	-0.715	0.532	
Benzyl alcohol	0.803	0.868	0.410	0.558	0.916	−1.216		−0.401
Benzyl benzoate	1.248	1.304	0	0.584	1.680	−0.177	1.252	
Benzyl ether	1.210	1.114	0	0.723	1.664	−0.037	1.076	0.341
Biphenyl	1.372	0.978	0	0.156	1.260	−0.106	1.215	0.596
Bis(2-butoxyethyl) phthalate	0.641	1.582	0	1.492	2.955		1.283	
Bis(2-ethoxyethyl) phthalate	0.619	1.558	0	1.501	2.391		0.374	
Bis(2-methoxyethyl) phthalate	0.788	1.748	0	1.483	1.436	−1.449	−0.433	
Borneol	0.763	0.704	0.166	0.650	1.359	−0.457		0.173
1-Bromonaphthalene	1.594	0.978	0	0.281	1.260			0.456

Table 3. Continued.

Compound	E	S	A	B	V	TEA-DMSO log K_p	TEA-FA log K_p	TEA-EA log K_p
3-Bromophenol	1.081	0.760	0.942	0.209	0.950	−1.148		
Butyl benzyl phthalate	1.296	1.728	0	1.010	2.459	−0.750	1.685	
Caffeine	1.568	1.684	0.044	1.249	1.363	−1.497		
Carbazole	2.051	1.553	0.388	0.229	1.315	−1.492	1.358	−0.310
2-Chloroaniline	1.026	1.006	0.238	0.317	0.938		0.413	−0.422
4-Chloroaniline	0.998	1.177	0.342	0.295	0.938	−1.179	0.226	−0.323
4-Chloro-3-methylphenol	0.571	0.677	0.799	0.300	1.038	−0.910		−1.017
1-Chloro naphthalene	1.419	0.941	0	0.137	1.207	−0.151	1.631	0.304
2-Chlorophenol	0.874	0.683	0.516	0.344	0.897	−1.190		
Cholesterol	1.353	1.087	0.212	0.558	3.494	1.482		
Chrysene	2.647	1.667	0	0.302	1.823	−0.375	1.890	−0.075
Cinnamyl alcohol	1.095	0.984	0.480	0.597	1.154	−1.005		−0.559

Table 3. Continued.

Compound	E	S	A	B	V	TEA-DMSO log K_p	TEA-FA log K_p	TEA-EA log K_p
n-Decanol	0.191	0.417	0.347	0.536	1.576	0.399		0.529
Decamethyltetrasiloxane	−0.717	−0.167	0	0.559	2.676	2.410	3.405	
Dibenzofuran	1.598	1.092	0	0.123	1.208	−0.249	1.674	0.562
Dibenzylamine	1.340	1.013	0.101	0.926	1.705	−0.065		0.315
Dibutyl phthalate	0.694	1.299	0	0.938	2.274	−0.228	1.380	
Dibutyl succinate	0.091	0.935	0	0.968	1.948		0.787	
3,4-Dichloroaniline	1.362	1.290	0.412	0.247	1.061	−1.584	0.495	−0.980
2,6-Dichloro-4-nitroaniline	1.263	1.494	0.369	0.319	1.235		0.159	−0.536
Di(cyclohexyl)adipate	0.649	1.259	0	1.075	2.510		1.607	
Dicyclohexylamine	0.585	0.423	0.015	0.560	1.813	0.631		0.976
Dicyclohexyl phthalate	1.405	1.508	0	1.067	2.620		1.879	
Diethyl adipate	0.085	1.009	0	0.868	1.666	−0.299	0.590	
N,N-Diethylcarbanilide	1.692	1.295	0	1.304	2.244	−0.071	1.281	−0.072

Table 3. Continued.

Compound	E	S	A	B	V	TEA-DMSO log K_p	TEA-FA log K_p	TEA-EA log K_p
Diethyl diethylmalonate	1.692	1.295	0	1.304	2.244	-0.071	1.281	−0.072
N,N-Diethyldodecanamide	0.331	0.936	0	0.948	2.263			1.485
Di(2-ethylhexyl) phthalate	0.693	1.155	0	1.189	3.401		2.844	
Diethyl phthalate	0.725	1.394	0	0.887	1.710		0.406	
Diisobutyl phthalate	0.672	1.235	0	0.948			1.566	
N,N-Dimethylaniline	0.956	0.815	0	0.445	1.098	−0.459		
N,N-Dimethyldodecylamine	0.080	0.199	0	1.467	2.181	0.684		1.147
2,6-Dimethyl phenol	0.771	0.788	0.413	0.403	1.056			−0.033
3,5-Dimethylphenol	0.762	0.755	0.688	0.347	1.056			−0.480
Dimethyl phthalate	0.780	1.410	0	0.880	1.429	−0.906	−0.055	
1,3-Dinitrobenzene	1.056	1.760	0	0.416	1.064		−0.493	−0.405
Dioctyl phthalate	0.662	1.220	0	1.121	3.401		2.838	
Diphenylamine	1.704	1.278	0.149	0.532	1.424		0.921	−0.070

Table 3. Continued.

Compound	E	S	A	B	V	TEA-DMSO log K_p	TEA-FA log K_p	TEA-EA log K_p
N,N-Diphenyl-p-phenylenediamine	2.715	2.090	0.312	0.981	2.131	−1.286	1.157	−1.235
1,5-Divinyl-1,1,3,3,5,5-hexamethyltrisiloxane	−0.238	0.008	0	0.525	2.286			3.014
Dodecane	0	0	0	0	1.799			2.556
Ethyl benzoate	0.694	0.881	0	0.452	1.213		0.679	
Eugenol	0.946	0.865	0.353	0.540		−0.871	0.841	−0.333
Fluoranthene	2.330	1.475	0	0.289	1.584	−0.369	2.161	−0.112
Fluorene	1.669	1.105	0	0.257	1.356	−0.014	1.678	0.458
Geraniol	0.493	0.640	0.270	0.603	1.490	−0.326		0.382
Hexachlorobenzene	1.374	0.876	0	0	1.450	0.453	2.208	0.722
n-Hexanol	0.210	0.432	0.350	0.535	1.012			0.210
Hexanophenone	0.790	0.951	0	0.510	1.577	0.110	1.362	
Indole	1.071	1.240	0.417	0.228	0.946	−1.338	0.476	
Iodobenzene	1.182	0.790	0	0.134	0.974	−0.471	1.076	−0.011

Table 3. Continued.

Compound	E	S	A	B	V	TEA-DMSO log K_p	TEA-FA log K_p	TEA-EA log K_p
Limonene	0.497	0.337	0	0.167	1.323	0.505		
Linalool	0.391	0.536	0.198	0.733	1.490	−0.147		0.245
2-Methylaniline	0.964	1.079	0.172	0.486	0.957	−1.257	0.048	
Methyl benzoate	0.738	0.918	0	0.440	1.072	−0.421		
Methyl decanoate	0.057	0.564	0	0.456	1.733	0.763	1.559	
2-Methoxynaphthalene	1.451	1.151	0	0.355	1.285	−0.572	1.264	−0.247
2-Methylnaphthalene	1.304	0.888	0	0.206	1.226	−0.170	1.582	0.259
Methyl octanoate	0.069	0.557	0	0.448	1.451	0.226	0.928	
2-Methylphenol	0.775	0.740	0.614	0.356	0.916	−1.256		−0.625
3-Methylphenol	0.810	0.767	0.678	0.350	0.916	−1.523		
Naphthalene	1.230	0.905	0	0.191	1.085	−0.514	1.048	0.534
2-Naphthol	1.453	1.174	0.783	0.347	1.144			−1.235
Nicotinamide	1.191	1.798	0.431	0.773	0.931	−2.259		−2.101

Table 3. Continued.

Compound	E	S	A	B	V	TEA-DMSO log K_p	TEA-FA log K_p	TEA-EA log K_p
Nicotine	0.861	0.958	0	1.082	1.371	−0.425	0.132	−0.102
2-Nitroaniline	1.228	1.473	0.343	0.352	0.990	−1.441	0.076	−0.615
3-Nitroaniline	1.252	1.564	0.496	0.420	0.990	−2.000	−0.740	−1.021
Nitrobenzene	0.846	1.143	0	0.268	0.890	−1.039		−0.013
4-Nitrobenzyl alcohol	1.008	1.358	0.509	0.583	1.090	−1.738		
1-Nitronaphthalene	1.381	1.478	0	0.287	1.259		0.590	−0.301
2-Nitrotoluene	0.866	1.154	0	0.225	1.031	−0.830	0.517	0.058
3-Nitrotoluene	0.874	1.138	0	0.211	1.031	−0.604	0.507	0.117
4-Nitrotoluene	0.879	1.171	0	0.265	1.031		0.445	−0.133
Nonan-1-ol	0.199	0.368	0.370	0.555	1.435			0.508
Octan-1-ol	0.199	0.440	0.344	0.520	1.294			0.272
Octan-2-ol	0.176	0.414	0.273	0.525	1.294	−0.025	1.067	0.435
Octanophenone	0.779	0.992	0	0.500	1.859	0.453	1.778	

Table 3. Continued.

Compound	E	S	A	B	V	TEA-DMSO log K_p	TEA-FA log K_p	TEA-EA log K_p
Pentachlorophenol	1.740	0.962	0.659	0.060	1.387			−0.316
Perylene	2.697	1.835	0	0.441	1.953	−0.924		
Phenanthrene	1.934	1.284	0	0.284	1.454	−0.217	1.475	0.427
2-Phenyl acetamide	1.818	2.060	0.279	0.784	1.113	−2.671		
Phenyl benzoate	1.624	1.464	0	0.364	1.539		1.402	
1-Phenyl ethanol	0.823	0.763	0.411	0.696	1.056	−0.848		
2-Phenylethanol	0.787	0.815	0.415	0.620	1.056	−1.044		−0.408
Phenyl ether	1.220	0.986	0	0.264	1.382	−0.108	1.452	0.451
4-Phenylphenol	1.517	1.179	0.817	0.445	1.382	−1.197		−1.091
3-Phenylpropan-1-ol	0.819	0.888	0.359	0.670	1.197	−0.938		−0.245
Phthalimide	1.169	1.700	0.250	0.602	1.020		−0.685	
Phthalonitrile	0.749	1.954	0	0.377	1.025		−0.790	
Pyrene	2.296	1.463	0	0.293	1.584	−0.651	2.110	0.436

Table 3. Continued.

Compound	E	S	A	B	V	TEA-DMSO log K_p	TEA-FA log K_p	TEA-EA log K_p
trans-Stilbene	1.619	1.216	0	0.286	1.563	−0.195	2.004	0.843
Quinoline	1.265	1.091	0	0.619	1.044	−0.865	0.156	−0.172
Terpinen-4-ol	0.553	0.557	0.173	0.652	1.424	−0.244		0.207
1,2,4,5-Tetrachlorobenzene	1.070	0.714	0	0.024	1.206	0.308	1.823	0.579
n-Tetradecane	0	0	0	0	2.081		3.208	
1,2,4-Trichloro benzene	1.022	0.744	0	0.023	1.083		1.297	0.708
p-Tolualdehyde	0.862	1.000	0	0.420	1.014	−0.709		
Tribenzylamine	1.821	1.270	0	0.631	2.454	0.116	2.840	1.423
Tri-*n*-butyrin	0.118	1.220	0	1.343	2.445		1.052	
1,3,5-Triethylbenzene	0.672	0.500	0	0.190	1.561			1.349
Trisopropanolamine	0.608	1.361	0.392	1.481	1.652			−1.288
Trimethoprim	1.760	1.947	0.075	2.081	2.181	−2.234	−1.152	−1.871

Table 3. Continued.

Compound	E	S	A	B	V	TEA-DMSO log K_p	TEA-FA log K_p	TEA-EA log K_p
Triphenylamine	2.439	0.983	0	0.755	2.031	0.400	2.426	0.238
Triphenylmethane	1.819	1.172	0	0.549	2.072	0.056	2.208	1.036
Undecane	0	0	0	0	1.658			2.558

To evaluate the predictive ability of the model, the data set in Table 3 was split into a training set of 57 compounds and a test set of 29 compounds using the Kennard-Stone algorithm.[46] This approach ensures that the training set and test set are selected to occupy a similar descriptor space. The model for the training set in Equation 29 is similar to the model in test set in Equation 28.

$$\log K_p = -0.136(\pm 0.134) + 0.065(\pm 0.067)E - 1.286(\pm 0.084)S - 1.300(\pm 0.134)A$$
$$- 0.729(\pm 0.108)B + 1.039(\pm 0.087)V \tag{29}$$

$$r = 0.977 \qquad r_{adj}^2 = 0.951 \qquad SE = 0.190 \qquad F = 218 \qquad n = 57$$

Equation 29 was then used to predict the partition coefficients ($\log K_p$) for the compounds in the test set and the average error, average absolute error, and root mean square error of the difference between the experimental and model predicted partition coefficients were used to assess the ability of Equation 29 to estimate further values of $\log K_p$ within the same descriptor space. The average error is an indication of bias and at 0.055 is not a concern for Equation 29. The absolute average error (0.183) and root mean square error (0.188) are an indication of the likely error in predicting further partition coefficients based on Equation 29. Since Equation 29 is similar to Equation 28, which is preferred because it is based on a larger number of compounds, it is reasonable to conclude that Equation 28 should be able to predict partition coefficients to about ±0.19 log units for further compounds that lie within or close to the descriptor space (E = −0.72 to 2.72, S = −0.17 to 2.09, A = 0 to 0.94, B = 0 to 2.08, and V = 0.898 to 3.494) used to define the model.

The system constants for the biphasic system n-heptane-dimethyl sulfoxide ($e = 0$, $s = -1.769$, $a = -3.277$, $b = -1.112$, and $v = 1.146$) have been reported previously,[22, 51] and can be used to assess differences in solvation properties for n-heptane and triethylamine. Since n-

heptane is a non polar solvent of low cohesive energy the differences in system constants should reflect the main difference in selectivity for the two solvents. For this to be true, it is necessary to assume that the difference in mutual solubility for the two biphasic systems does not significantly affect the interpretation of the system constants. This is likely the case as the difference in mutual solubility is small.[22] In which case, then n-heptane and triethylamine have similar cohesive energy ('*v*' system constants are nearly equal), triethylamine is weakly dipolar/polarizable ('*s*' system constant is negative and smaller than for n-heptane-dimethyl sulfoxide), and a reasonably strong hydrogen-bond base ('*a*' system constant much smaller than n-heptane-dimethyl sulfoxide but not as strong a hydrogen-bond base as dimethyl sulfoxide, since the '*a*' system constant is negative). Neither n-heptane nor triethylamine is expected to be a hydrogen-bond acid and the small difference in the '*b*' system constants is likely due to small differences in mutual solubility.

3.3.2 Characterization of Triethylamine-Formamide Biphasic System

Fitting the partition coefficients (log K_p) for the triethylamine-formamide system in Table 3 to the solvation parameter model gave equation 30.

$$\log K_p = -0.089(\pm0.093) + 0.561(\pm0.043)E - 1.100(\pm0.079)S - 0.377(\pm0.142)A$$
$$- 1.601(\pm0.084)B + 1.733(\pm0.052)V \tag{30}$$

$r = 0.984 \qquad r_{adj}^2 = 0.965 \quad SE = 0.171 \quad F = 448 \qquad n = 81$

The higher cohesion of the formamide layer favors transfer of the solutes to the triethylamine layer (positive '*v*' system constant) while polar interactions have a negative sign (*s*, *a*, and *b*) and favor solubility in the formamide layer. Electron lone pair interactions favor transfer to the triethylamine layer, probably as a result of electron lone pair repulsion in the formamide layer rather than attractive interactions with triethylamine. The Kennard-Stone algorithm was used to

split the data set into a training set of 54 compounds and a test set of 27 compounds. The model

for the training set is given in equation 31.

$$\log K_p = -0.108(\pm 0.128) + 0.517(\pm 0.056)E - 1.008(\pm 0.121)S - 0.569(\pm 0.207)A$$
$$- 1.650(\pm 0.107)B + 1.728(\pm 0.070)V \qquad (31)$$

$r = 0.982 \qquad r_{adj}^2 = 0.960 \quad SE = 0.179 \quad F = 578 \qquad n = 54$

Equation 31 is quite similar to equation 30. For the test set, the average error was 0.024, the

average absolute error 0.167 and the root mean square error 0.166. Thus equation 30 should be

able to predict further values of the partition coefficient to about 0.17 log units for compounds

with descriptor values that lie within or close to the descriptor space (E = −0.72 to 2.72, S =

−0.17 to 2.90, A = 0 to 0.60, B = 0 to 2.08, and V = 0.877 to 3.401) used to define the model.

Primary alcohols and phenols were observed to produce secondary peaks in the

triethylamine-formamide system. These compounds likely react with formamide in the presence

of triethylamine to form formyl esters. This reaction may occur in solution or at the point of

injection at the higher temperature of the injector. In the absence of triethylamine there was no

reaction observed between alcohols and phenols with formamide. The reactions resulted in

unreliable results for the partition coefficients of primary alcohols and phenols in the

triethylamine-formamide biphasic system which were removed from the model in equation 30.

The system constants for the biphasic system n-heptane-formamide ($e = -0.554$, $s =$

-2.169, $a = -3.356$, $b = -1.671$, and $v = 2.267$)[22, 47b] can be compared with the system constants

in equation 30 to confirm the observations made for the triethylamine-dimethyl sulfoxide

biphasic system with regard to the solvation properties of triethylamine. There is good agreement

with the assessment that triethylamine is a weak cohesive solvent, is weak to moderately strong

dipolar/polarizable, non-hydrogen-bond acidic, and a moderately strong hydrogen-bond base.

3.3.3 Characterization of Triethylamine-Ethanolamine Biphasic System

Fitting the partition coefficients (log K_P) for the triethylamine-ethanolamine system in

Table 3 to the solvation parameter model gave equation 32.

$$\log K_p = 0.067(\pm0.145) - 0.394(\pm0.083)E - 0.640(\pm0.123)S - 1.340(\pm0.119)A$$

$$- 1.282(\pm0.108)B + 1.406(\pm0.101)V \tag{32}$$

$r = 0.968 \qquad r_{adj}^2 = 0.933 \quad SE = 0.230 \quad F = 228 \qquad n = 82$

The higher cohesive energy of the ethanolamine layer favors transfer of the solutes to the

triethylamine layer (positive 'v' system constant) while polar interactions have a negative sign (e,

s, a, and b) and favor solubility in the ethanolamine layer. The Kennard-Stone algorithm was

used to split the data into a training set of 55 compounds and a test set of 27 compounds. The

model for the training set is given by equation 33.

$$\log K_p = - 0.116(\pm0.189) - 0.338(\pm0.124)E - 0.707(\pm0.177)S - 1.175(\pm0.159)A$$

$$- 1.312(\pm0.127)B + 1.540(\pm0.128)V \tag{33}$$

$r = 0.973 \qquad r_{adj}^2 = 0.942 \quad SE = 0.235 \quad F = 176 \qquad n = 55$

Equation 33 is quite similar to Equation 32. For the test set, the average error was 0.018,

the average absolute error 0.259 and the root mean square error 0.255. Thus Equation 32 should

be able to predict further values of the partition coefficient to about 0.26 log units for compounds

with descriptor values that lie within or close to the descriptor space (E = −0.24 to 2.72, S = 0 to 2.09, A = 0 to 0.82, B = 0 to 2.08, and V = 0.816 to 2.455) used to define the model.

Ketones, aldehydes, and some aromatic esters were observed to produce secondary peaks in the triethylamine-ethanolamine system. These reactions are most likely due to nucleophilic carbonyl addition reactions involving Schiff base formation. The same compounds formed secondary products in the n-heptane-ethanolamine biphasic system,[34] and the reactions are a property of ethanolamine and are not related to triethylamine. These secondary reactions resulted in unreliable results for the partition coefficients of aldehydes, ketones and aromatic esters in the triethylamine-ethanolamine biphasic system, which were removed from the model in equation 32.

The system constants for the biphasic system n-heptane-ethanolamine (e = −0.264, s = −1.086, a = −4.533, b = −1.299, and v = 1.992)[34] can be compared with the system constants in equation 32 to confirm the observations made for the triethylamine-dimethyl sulfoxide and triethylamine-formamide biphasic systems with regard to the solvation properties of triethylamine. There is good agreement with the assessment that triethylamine is a weak cohesive solvent, weak to moderately strong dipolar/polarizable, non-hydrogen-bond acidic, and a moderately strong hydrogen-bond base.

Hierarchical cluster analysis using the average linkage between groups agglomeration algorithm and the system constants as variables was used to obtain a global view of the extraction properties of the twenty-two totally organic biphasic systems characterized using the solvation parameter model.[22, 47a, 49] The dendrogram (Figure 10) demonstrates that characterized totally organic biphasic systems encompass a wide range of selectivity with little clustering.
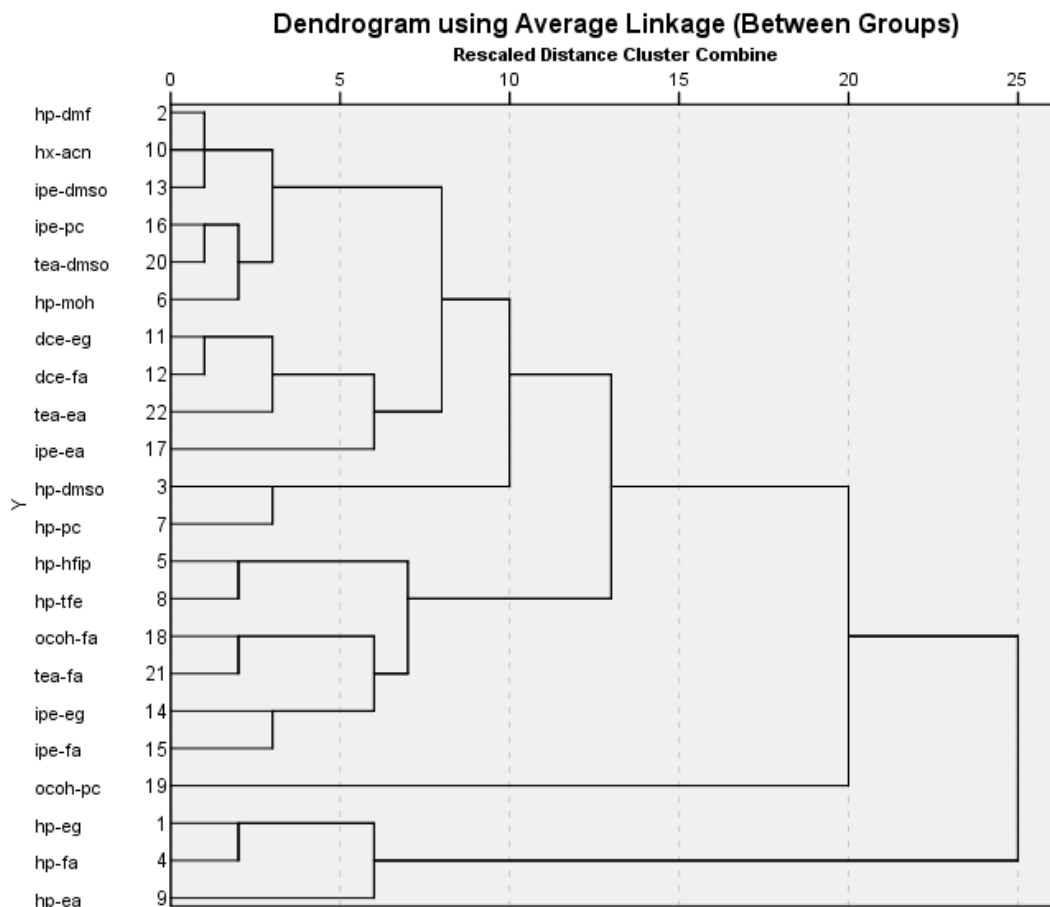
Figure 10. Dendogram for Totally Organic Biphasic Systems (Including Triethylamine Containing Systems) with the System Constants as Variables Using the Average Linkage Between Groups Agglomeration Algorithm.

(Solvents: hp = n-heptane, ipe = isopentyl ether, dce = 1,2-dichloroethane, ocoh = 1-octanol, dmf = N,N-dimethylformamide, acn = acetonitrile, dmso = dimethylsulfoxide, pc = propylene carbonate, eg = ethylene glycol, fa = formamide, moh = methanol, hfip = hexaflouroisopropanol, tea = triethylamine, tfe = 2,2,2-triflouroethanol)

The nearest neighbor for the triethylamine-dimethyl sulfoxide biphasic system is isopentyl ether-propylene carbonate ($e = 0.262$, $s = -1.514$, $a = -0.764$, $b = -0.593$, and $v = 0.691$) [22, 51] and for triethylamine-formamide biphasic system, octan-1-ol-formamide ($e = 0.285$, $s = -1.059$, $a = -0.306$, $b = -0.813$, and $v = 1.280$).[22, 47b] Neither pairs of biphasic systems are

selectivity equivalent. The significant difference in cohesive properties favors the distribution of larger solutes to the triethylamine layer and the greater hydrogen-bond basicity of dimethyl sulfoxide favors the selective extraction of hydrogen-bond acids by the dimethyl sulfoxide layer. For the triethylamine-formamide system, larger molecules have a slight preference for transfer to the triethylamine layer compared with octan-1-ol, and hydrogen-bond bases will be selectively extracted to the formamide layer, since triethylamine is not competitive with octan-1-ol as a hydrogen-bond acid solvent. The triethylamine-ethanolamine biphasic system has no partners and is loosely associated with the 1,2-dichloroethane-formamide and 1,2-dichloroethane-ethylene glycol biphasic systems. The three biphasic systems have similar cohesive energy and hydrogen-bond acidity but are quite different in their dipolarity/polarizability and hydrogen-bond basicity. For compounds of low polarity partition coefficients would be similar but significant differences are expected for polar compounds. The triethylamine-ethanolamine biphasic system has a significantly different *s*/*a* system constant ratio to the other two biphasic systems. Knowledge of the system properties facilitates the selection of the optimum biphasic system for specific applications.

The system constants in Equations 28, 30, and 32 are relatively small, except for the '*b*' system constant for triethylamine-formamide. Given the limited number of totally organic biphasic systems with moderate to large '*b*' system constants,[22, 47a] the triethylamine-formamide biphasic system could be used together with the other biphasic systems with similar '*b*' system constants to facilitate estimating the hydrogen bond basicity (B) descriptor for compounds of low water solubility or stability. [10, 22]

3.4 Conclusions

Triethylamine is shown to be a useful counter solvent for liquid-liquid partition forming complementary biphasic systems with polar organic solvents with potential applications for sample preparation and descriptor measurements. Triethylamine is a relatively weak cohesive solvent, weak to moderately dipolar/polarizable, non-hydrogen-bond acidic, and a reasonably strong hydrogen-bond base. Triethylamine-dimethyl sulfoxide, triethylamine-formamide, and triethylamine-ethanolamine have useful separation properties that are not duplicated in a data base of nineteen totally organic biphasic systems. The triethylamine-formamide system has useful properties for estimating the hydrogen bond basicity (B) descriptor when used together with other totally organic biphasic systems.

CHAPTER 4

DETERMINATION OF DESCRIPTORS FOR POLYCYCLIC AROMATIC HYDROCARBONS AND RELATED COMPOUNDS

Text, figures, and tables of this chapter were reused or adapted with permission from Ariyasena, T. C.; Poole, C. F. *Journal of Chromatography A* **2014**, *1361*, 240-254.[52]

4.1 Introduction

Polycyclic aromatic hydrocarbons (PAHs) are ubiquitous environmental contaminants usually found as complex mixtures with related compounds containing mainly ring hetero atoms and alkyl ring substituents. The United States Environmental Protection Agency has designated 16 of the common PAHs as priority pollutants, and along with other regulatory authorities worldwide, has established safe levels for individual PAHs and PAHs as a group in the environment, in food, in air, in water, in the workplace, and in industrial products.[53] A number of PAHs are known human carcinogens and considered genotoxic and mutagenic.[53a, 53b] Their low vapor pressure, poor water solubility, and reasonable stability favors their bioaccumulation in terrestrial and marine animals and long range transport in the atmosphere by sorption to particle matter. They have been actively studied for over a century and a large number of analytical methods have been described, and continue to be described, for their determination in a variety of different matrices.[53a, 54]

The large number of PAHs and their general distribution throughout the environment render comprehensive studies of their fate and distribution prohibitively expensive. Physicochemical properties are unknown or unreliably determined for many compounds, which limits the possibility of using more readily determined physicochemical properties to estimate

environmentally important properties using predictive models.[55] The physicochemical properties considered of most interest are vapor pressure, solubility in water, Henry's law constant (or water-air partition coefficient), octanol-air partition coefficient, and the octanol-water partition coefficient. For PAHs the determination of these properties is not straightforward due to their low vapor pressure and low water solubility. Experimental measurements are time consuming, expensive and often show poor agreement between different methods and research groups due to the non-trivial experimental problems of the measurements.[55-56]

Herein, we describe an alternative method that uses chromatographic data obtained from gas and liquid chromatography and liquid-liquid partition coefficients for totally organic biphasic systems for the determination of a set of descriptors suitable for the prediction of the physicochemical properties of PAHs and related compounds as well as the estimation of environmental properties through a set of models that use the descriptor values directly for property estimates. The approach to determine descriptors is based on Abraham's solvation parameter model.[10]

The procedure which is used to determine the descriptor values is illustrated in Figure 11. First, each chromatography and liquid-liquid partition system needs to be characterized using the solvation parameter model. The characterization of gas chromatographic systems is carried out by the measurement of retention factors (log k) for selected solutes on each stationary phase at several temperatures. In order to characterize the biphasic partition systems, partition coefficients (log K_p) for the solutes need to be determined. Then the coefficients of the solvation parameter model are determined using multiple linear regression analysis. These characterized systems are used to determine the descriptor values. To determine descriptor values for the polycyclic aromatic compounds retention factors for these compounds are measured at several temperatures

on different stationary phases, and partition coefficients for the compounds are determined in various biphasic systems. Then the descriptor values for the compounds are assigned using the Solver algorithm in Excel. The solver algorithm obtains the descriptor values which minimize the standard deviation between the calculated and experimentally determined solute property.
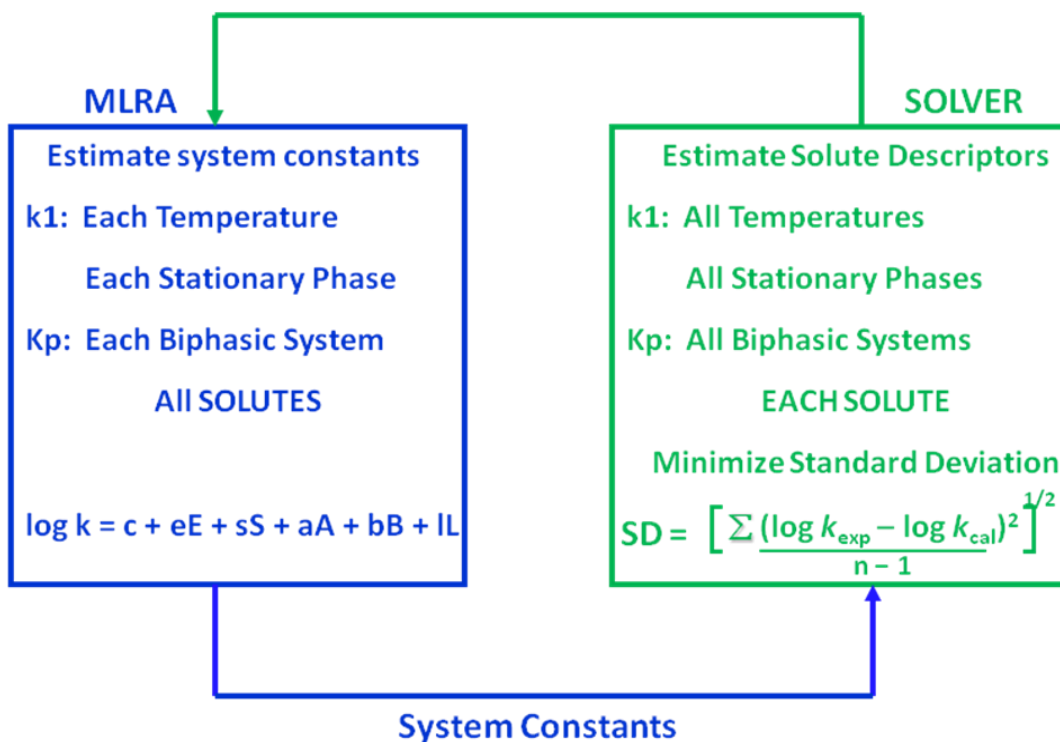
Figure 11. Diagram Illustrating the Procedure for Determination of Solute Descriptors.

In order to determine descriptor values retention measurements in different chromatographic systems are combined with water-organic solvent liquid-liquid partition coefficients.[6a, 10, 19] For compounds of low water solubility or reactivity, such as organosiloxanes,[1c, 57] some fragrance compounds,[38] and plasticizers like phthalate esters,[39] experimental aqueous biphasic partition coefficients are difficult to determine because of the very low concentration of the compounds in the aqueous phase. The same compounds in totally

organic biphasic systems generally afford partition coefficients that fall into a favorable range for experimental measurements and possess sufficiently large system constants to facilitate descriptor measurements (the main advantage of aqueous biphasic systems).[22, 47a] In addition, descriptor values for water insoluble compounds can be inferred from solubility measurements in organic solvents by setting up a series of equations for real and hypothetical partition systems.[19] The calculation requires either an experimental value for the saturated vapor pressure at 25 °C and solubility of the compounds in water, or the set of equations can be solved by including the gas-water partition coefficient as an additional unknown descriptor. This method was used to determine descriptor values for anthracene and phenanthrene,[58] acenaphthene, pyrene and fluoranthene,[59] fluorene,[60] and 1-nitronaphthalene.[61]

4.2 Experimental

4.2.1 Materials

n-Heptane, 2,2,2-trifluoroethanol, diisopentyl ether, N,N-dimethylformamide, azulene, naphthalene, 1-methylnaphthalene, acenaphthylene, anthracene, 9,10-dimethylanthracene, triphenylene, benzo[*e*]pyrene, pyrene, perylene, benzo[*g,h,i*]perylene, dibenzo[*a,i*]pyrene, 8-hydroxyquinoline, 3,3'-dichlorobenzidine, 1-nitropyrene, 9,10-anthraquinone, quinoline and quinine were obtained from Sigma-Aldrich (Milwaukee, WI, USA). Formamide, propylene carbonate, ethylene glycol, 1,2-dichloroethane, dimethyl sulfoxide (containing < 0.2% [v/v] water), chrysene, and benzo[*a*]anthracene were obtained from Across organics (Morris Plains, NJ, USA). 2-Methylnaphthalene, acenaphthene, biphenyl, fluorene, phenanthrene, fluoranthene, p-terphenyl, benzo[*a*]pyrene, dibenzo[*a,h*]anthracene, quinoline, 1-nitronaphthalene, 1-naphthol, 2-naphthol, carbazole, 1-acetonaphthone, 2-acetonaphthone, benzidine, benzothiazole, 2-methylbenzothiazole, 4,4'-dibromobiphenyl, 4-dimethylaminoazobenzene, 1-

hydroxyanthraquinone, and quinine were obtained from Chem Services (West Chester, PA, USA). n-Hexane, methanol and acetonitrile were OmniSolv grade from EMD Chemicals (Gibbstown, NJ, USA). The open-tubular columns used for gas chromatography and their sources are summarized in Table 4. The 50 mm x 4.6 mm I.D. SunFire C_{18} column packed with 4.5 μm particles of an average pore diameter of 10 nm with endcapping was obtained from Waters (Milford, MA, USA).

4.2.2 Instrumentation

Gas chromatographic retention factors were determined with an Agilent Technologies (Palo Alto, CA, USA) gas chromatograph fitted with a split/splitless injector and flame ionization detector using Chemstation software (rev. 8.04.01) for data acquisition. Nitrogen was used as the carrier gas at a constant velocity of 47 cm/s. The split ratio was set to 30:1, septum purge 1 ml/min, and injector and detector temperature 300 °C. Isothermal retention factors were determined at 20 °C temperature intervals in the range 160-320 °C as dictated by the retention characteristics of the compound and the thermal stability of the columns. Typically, three retention factor values were obtained for each column (column thermal stability allowing). The column hold-up time was determined by a separate injection of methane. For the measurement of liquid-liquid partition coefficients a temperature program starting at 150 °C for 1 min and then raised to 320 °C at 25 °C/min on the HP-5 column in Table 4 was used. The temperature program was modified as required to handle co-elution of some solutes with the internal standard or solvent peaks and to elute large-ring PAHs of low volatility.

Table 4. Open-Tubular Columns Used for Descriptor Measurements by Gas Chromatography.

Column	Stationary Phase	Manufacturer*	Dimensions
SPB-Octyl	Poly(methyloctylsiloxane)	Supelco	30m x 0.25 mm x 1 μm
HP-5	Poly(dimethyldiphenylsiloxane)	Agilent	30m x 0.32 mm x 0.25 μm
Rxi-5Sil MS	Silphenylene-dimethylsiloxane copolymer	Restek	30m x 0.25 mm x 0.5 μm
Stx-500	Carborane-siloxane copolymer	Restek	30m x 0.25 mm x 0.15 μm
Rxi-17	Poly(dimethyldiphenylsiloxane)	Restek	30m x 0.25 mm x 0.5 μm
Rtx-440	Proprietary structure	Restek	30m x 0.25 mm x 0.5 μm
Rtx-OPP	Poly(dimethylmethyltriflouropropylsiloxane)	Restek	30m x 0.32 mm x 0.15 μm
DB-1701	Poly(cyanopropylphenyldimethylsiloxane)	Agilent	15m x 0.32 mm x 0.25 μm
DB-225	Poly(cyanopropylphenyldimethylsiloxane)	Agilent	15m x 0.32 mm x 0.25 μm

*Supelco(Bellefonte, PA, USA), Restek(Bellefonte, PA, USA), and Agilent(Folsom, CA, USA)

Liquid chromatographic retention factors were determined with a Hitachi D-7000 liquid chromatograph (San Jose, CA, USA) fitted with a photodiode array detector and column oven set to 45 °C. All measurements were made with a column flow rate between 1-2 ml/min. The column hold-up time was determined by injection of an aqueous solution of sodium nitrate (26 mg/ml). The extra column hold-up volume was determined by replacing the column with a zero-volume connector and used to correct all retention factors.[25] Retention factors were measured at 10% (v/v) increments of organic solvent within the composition range 50-70% (v/v) methanol, 40-70% (v/v) acetonitrile, and 30-70% (v/v) tetrahydrofuran in water.

4.2.3 Determination of Liquid-Liquid Partition Coefficients

Partition coefficients were determined according to a literature method.[1c, 37-38] The 2.0 mL screw-capped sample vials (Supelco, Bellefonte. PA, USA) were charged by syringe with 0.75 mL of polar solvent saturated with counter solvent, 0.75 mL of low-polarity solvent saturated with counter solvent, and 1 μL of internal standard. Solid samples were dissolved in either solvent (depending on solubility) at a concentration of 0.5-1.0 mg/mL (less for the large-ring PAHs due to limited solubility) and added to the vials as described for solvents. For compounds giving nearly saturated solutions dilutions were performed to ensure the measured partition coefficients were independent of concentration. The vials were shaken by hand for 30 s and allowed to stand for several hours (usually overnight) at room temperature (22 ± 2 °C) and then centrifuged. Sample volumes of about 1 μL from each phase were taken for calculation of the partition coefficients. The biphasic solvent systems and their system constants are summarized in Table 5.[1c, 41, 47b, 51, 62] The identification of the internal standards is given in the citations. The system constants in Table 5 are up-dated compared with those in the original citations and were

recalculated after adding additional compounds to the data sets and re-determining descriptor values for some compounds.

Table 5. System Constants for Totally Organic Biphasic Solvent Systems Used for Descriptor Determinations.

Liquid-Liquid Partition System	*e*	*s*	*a*	*b*	*v*	*c*	r*	SE*	F*	n*
n-Heptane-Ethylene glycol[41]	0.097	-1.478	-3.778	-1.562	2.090	0.309	0.999	0.075	13556	157
n-Heptane-N,N-Dimethylformamide[62b]	0.036	-1.392	-2.054	-0.579	0.487	0.259	0.998	0.072	6492	124
n-Heptane-Dimethylformamide[51]	0	-1.768	-3.314	-1.109	1.141	0.377	0.997	0.113	5460	138
n-Heptane-Formamide[47b]	0.542	-2.167	-3.353	-1.669	2.264	0.163	0.998	0.104	5959	157
n-Heptane-Methanol[62b]	0.204	-0.723	-1.145	-0.920	0.593	-0.130	0.994	0.068	1265	86
n-Heptane-Proplylene Carbonate[62c]	0.439	-2.090	-2.685	-0.443	0.796	0.541	0.998	0.068	10134	162
n-Heptane-Triflouroethanol[62a]	0.917	-1.585	-1.269	-2.856	1.311	-0.026	0.998	0.072	12923	206
n-Hexane-Acetonitrile[62d]	0.388	-1.482	-1.677	-0.847	0.671	0.153	0.997	0.080	6220	184
Isopentyl ether-Ethylene glycol[41]	-0.130	-1.093	-1.537	-1.919	2.093	0.388	0.996	0.098	3838	143
Isopentyl ether-Formamide[47b]	0.577	-1.717	-1.321	-1.408	1.987	0.143	0.996	0.101	2927	114
Isopentyl ether-Dimethyl sulfoxide[51]	0	-1.465	-2.175	-0.958	1.111	0.183	0.997	0.094	4284	97
Formamide-1,2-Dichloroethane[47b]	-0.089	0.423	2.028	1.263	-1.642	-0.297	0.995	0.089	2244	111

* r = Overall correlation coefficient; SE = Standard error of the estimate; F = Fisher statistic;
n = Number of partition coefficients included as the dependent variable

4.2.4 Calculations

All calculations were performed on a Dell Dimension 9200 computer (Austin, TX, USA) using either the Solver add-in module in Excel 2007 (Microsoft Corporation, Redmond, WA) or IBM SPSS statistics v. 22 (IBM Corporation, Chicago, IL, USA). The McGowan's characteristic volume (V) descriptor was calculated from the molecular formula by summing atom constants and correcting for the number of bonds with units of cm^3 $mol^{-1}/100$.[63] The excess molar refraction (E) descriptor for liquids with units of cm^3 $mol^{-1}/10$ was calculated using equation 8.[64] The refractive index for solids was estimated using ChemSketch v12 (ACD Labs, Toronto, Canada) or the excess molar refraction (E) descriptor was determined simultaneously with the other descriptors. The descriptor values were optimized using the Solver algorithm.[6a, 10, 19] Solver is an optimization package that adjust selected changing cells (descriptors) to minimize the value in a target cell (standard deviation) as illustrated by Equation 34.

$$\text{Standard Deviation} = [\ \Sigma(\log k_{exp} - \log k_{cal})^2 / (n - 1) \ ]^{1/2} \qquad (34)$$

In Equation 34, $\log k_{exp}$ is the experimental retention factor (or partition coefficient), $\log k_{cal}$ is the model predicted retention factor (or partition coefficient). Descriptor values were thus assigned using solvation parameter model (using equation 2 or 3 as suitable). System constants were used for various characterized systems including gas chromatography columns in Table 4 for 60-140 °C,[24, 65] 160-240 °C,[23, 66] and 260-320 °C,[40] for the SunFire C_{18} reversed-phase liquid chromatography column with methanol, acetonitrile, and tetrahydrofuran as organic modifiers,[26] and for the liquid-liquid partition coefficients in Table 5.

4.3 Results and discussion

The 23 polycyclic aromatic hydrocarbons and 18 related compounds and their descriptor values determined in this study are summarized in Table 6. None of the PAHs contain hydrogen atoms expected to function as hydrogen-bond acids and the hydrogen bond acidity descriptor (A) was set to zero. There are several examples of compounds in the related compounds group expected to exhibit hydrogen-bond acidity, and in this case, a value for the A descriptor was determined simultaneously with the other descriptors. For some amines two hydrogen-bond basicity descriptors are indicated as B and B^0. The B^0 descriptor is required to explain the properties of these compounds in biphasic systems in which the organic phase contains an appreciable amount of water. Examples for such systems are water saturated-octanol in the octanol-water partition system, and reversed-phase liquid chromatography.[67] For the PAHs and related compounds other than the amines, the hydrogen bond basicity (B) descriptor is independent of system properties and the assigned value is used for all circumstances. By combining chromatographic retention factors and liquid-liquid partition coefficients for the systems described in the experimental section it was possible to obtain 40-60 experimental retention factors and partition coefficients for each compound. For some compounds a larger number of experimental values (indicated in Table 6) were used to calculate the descriptors. These additional values consisted of further retention factors for gas, liquid, and micellar electrokinetic chromatography and partition coefficients in totally organic and aqueous biphasic systems carried forward from previous studies and supplemented by new values determined here.[6a, 10] In this way we have maximized the data used for descriptor calculations while maintaining the common experimental protocols used for the measurements.

Table 6. Experimental Descriptors for Polycyclic Aromatic Hydrocarbons and Related Compounds.
(SD = Standard Deviation of the Residuals n = Number of Experimental Values for the Dependent Variable)

Compound	Composition	E	S	A	B	B^0	L	V	SD	n
Azulene	$C_{10}H_8$	1.393	1.058	0	0.211		5.776	1.0854	0.039	63
Naphthalene	$C_{10}H_8$	1.230	0.906	0	0.191		5.157	1.0854	0.036	410
1-Methylnaphthalene	$C_{11}H_{10}$	1.332	0.906	0	0.202		5.706	1.2263	0.046	95
2-Methylnaphthalene	$C_{11}H_{10}$	1.218	0.895	0	0.202		5.743	1.2263	0.027	61
Acenaphthylene	$C_{12}H_8$	1.553	1.125	0	0.214		6.395	1.2156	0.038	102
Acenaphthene	$C_{12}H_{10}$	1.453	0.951	0	0.221		6.709	1.2586	0.051	42
Biphenyl	$C_{12}H_{10}$	1.380	0.981	0	0.280		6.029	1.3242	0.035	177
Fluorene	$C_{13}H_{10}$	1.660	1.104	0	0.256		6.948	1.3565	0.029	220
Anthracene	$C_{14}H_{10}$	1.981	1.284	0	0.269		7.735	1.4544	0.039	107
Phenanthrene	$C_{14}H_{10}$	1.917	1.275	0	0.285		7.712	1.4544	0.032	214
Fluoranthene	$C_{16}H_{10}$	2.348	1.479	0	0.300		8.733	1.5846	0.041	84
Pyrene	$C_{16}H_{10}$	2.241	1.475	0	0.283		8.974	1.5846	0.042	70

Table 6. Continued.

Compound	Composition	E	S	A	B	B⁰	L	V	SD	n
9,10-Dimethylanthracene	$C_{16}H_{14}$	2.104	1.275	0	0.383		9.256	1.7362	0.043	52
Triphenylene	$C_{18}H_{12}$	2.919	1.757	0	0.426		9.933	1.8234	0.049	49
Chrysene	$C_{18}H_{12}$	2.593	1.660	0	0.294		10.142	1.8234	0.039	55
Benz[*a*]anthracene	$C_{18}H_{12}$	2.735	1.678	0	0.368		10.124	1.8234	0.039	53
p-Terphenyl	$C_{18}H_{14}$	1.495	1.164	0	0.729		9.680	2.3031	0.048	53
Benzo[*a*]pyrene	$C_{20}H_{12}$	3.023	1.846	0	0.418		11.540	1.9536	0.041	47
Benzo[*e*]pyrene	$C_{20}H_{12}$	3.095	1.881	0	0.408		11.431	1.9536	0.041	44
Perylene	$C_{20}H_{12}$	2.896	1.853	0	0.431		11.652	1.9536	0.037	39
Benzo[*g*,*h*,*i*]perylene	$C_{22}H_{12}$	3.612	2.110	0	0.436		12.707	2.0838	0.053	45
Dibenz[*a*,*h*]anthracene	$C_{22}H_{14}$	3.827	2.261	0	0.549		12.552	2.1924	0.049	28
Dibenzo[*a*,*i*]pyrene	$C_{24}H_{14}$	4.442	2.485	0	0.495		13.495	2.3226	0.055	33
Quinoline	C_9H_7N	1.268	1.092	0	0.622	0.559	5.367	1.0443	0.040	144

Table 6. Continued.

Compound	Composition	E	S	A	B	B^0	L	V	SD	n
8-Hydroxyquinoline	C$_9$H$_7$NO	1.088	1.072	0.243	0.373	0.550	5.969	1.1030	0.038	56
1-Nitronaphthalene	C$_{10}$H$_7$NO$_2$	1.389	1.480	0	0.289		6.844	1.2596	0.037	98
1-Naphthol	C$_{10}$H$_8$O	1.457	1.123	0.755	0.333		6.163	1.1441	0.036	229
2-Naphthol	C$_{10}$H$_8$O	1.453	1.174	0.783	0.347		6.148	1.1441	0.042	273
Carbazole	C$_{12}$H$_9$N	2.183	1.596	0.400	0.178	0.230	7.438	1.3154	0.038	90
3,3'-Dichlorobenzidine	C$_{12}$H$_{10}$Cl$_2$N$_2$	1.600	1.904	0.763	0.402	0.654	10.085	1.7686	0.043	51
1-Acetonaphthone	C$_{12}$H$_{10}$O	1.517	1.414	0	0.561		6.671	1.3829	0.033	101
2-Acetonaphthone	C$_{12}$H$_{10}$O	1.442	1.452	0	0.600		6.798	1.3829	0.034	100
Benzidine	C$_{12}$H$_{12}$N$_2$	1.116	1.567	0.228	1.018	0.989	9.166	1.5238	0.049	45
1-Nitropyrene	C$_{16}$H$_9$NO$_2$	2.809	2.074	0	0.325		10.456	1.7588	0.048	46
Benzothiazole	C$_7$H$_5$NS	1.298	1.212	0	0.473		5.209	0.9690	0.046	54
2-Methylbenzothiazole	C$_8$H$_7$NS	1.111	0.989	0	0.549		5.767	1.1099	0.042	54

Table 6. Continued.

Compound	Composition	E	S	A	B	B^0	L	V	SD	n
4,4'-Dibromobiphenyl	$C_{12}H_8Br_2$	2.149	1.183	0	0.245		8.659	1.6742	0.043	52
4-Dimethylaminoazobenzene	$C_{14}H_{15}N_3$	1.366	1.597	0	1.392	1.058	8.906	1.8624	0.050	52
9,10-Anthraquinone	$C_{14}H_8O_2$	1.653	1.443	0	0.576		8.644	1.5288	0.045	54
1-Hydroxyanthraquinone	$C_{14}H_8O_3$	1.504	1.491	0.050	0.539		9.075	1.5875	0.047	53
Quinine	$C_{20}H_{24}N_2O_2$	1.832	1.272	0.808	1.270	1.358	12.025	2.5512	0.054	42

Only two of the compounds in Table 6 are liquids (1-acetonaphthone and quinoline) for which the excess molar refraction (E) descriptor can be calculated from the experimental refractive indices using Equation 8. For the remaining compounds, estimated refractive index values can be obtained from several software packages. Estimated refractive indices using ChemSketch v.12 and the excess molar refraction descriptors (E) calculated from them are summarized in Table 7 together with a second collection of estimated E descriptors from the UCL descriptor database.[19]

Table 7. Comparison of Methods Used to Determine the Excess Molar Refraction (E) Descriptor for Solid Compounds.

Compound	Refractive Index Estimated Using ChemSketch	E value Calculated from Estimated Refractive Index (ChemSketch)	E Value from UCL Database*	Experimental E Value
Azulene	1.632	1.323	1.340	1.393
Naphthalene	1.632	1.323	1.340	1.230
1-Methylnaphthalene	1.617	1.344	1.344	1.332
2-Methylnaphthalene	1.617	1.344	1.304	1.218
Acenaphthylene	1.732	1.945	1.750	1.553
Acenaphthene	1.692	1.783	1.604	1.453
Biphenyl	1.571	1.126	1.360	1.380
Fluorene	1.645	1.602	1.588	1.660
Anthracene	1.715	2.121	2.290	1.981
Phenanthrene	1.715	2.121	2.055	1.917
Fluoranthene	1.652	3.129	2.377	2.348

* Database of Descriptors Developed by Prof. M. H. Abraham at University College London (UK)

Table 7. Continued.

Compound	Refractive Index Estimated Using ChemSketch	E value Calculated from Estimated Refractive Index (ChemSketch)	E Value from UCL Database*	Experimental E Value
Pyrene	1.852	3.129	2.808	2.241
9,10-Dimethylanthracene	1.675	2.140		2.104
Triphenylene	1.771	2.946		2.919
Chrysene	1.771	2.946	3.027	2.593
Benz[a]anthracene	1.771	2.946	2.992	2.735
p-Terphenyl	1.602	1.682		1.495
Benzo[a]pyrene	1.887	3.990	3.625	3.023
Benzo[e]pyrene	1.887	3.990	3.625	3.095
Perylene	1.887	3.990	3.256	2.896
Benzo[g,h,i]perylene	2.009	5.106	4.073	3.612
Dibenz[a,h]anthracene	1.812	3.792		3.827
Dibenzo[a,i]pyrene	1.903	4.863		4.442

Table 7. Continued.

Compound	Refractive Index Estimated Using ChemSketch	E value Calculated from Estimated Refractive Index (ChemSketch)	E Value from UCL Database*	Experimental E Value
8-Hydroxyquinoline	1.691	1.623		1.088
1-Nitronaphthalene	1.671	1.669	1.600	1.389
1-Naphthol	1.678	1.599	1.520	1.457
2-Naphthol	1.678	1.599	1.520	1.453
Carbazole	1.768	1.827	1.787	2.183
3,3'-Dichlorobenzidine	1.679	2.193		1.600
2-Acetonaphthone	1.615	1.435		1.442
Benzidine	1.667	1.882		1.116
1-Nitropyrene	1.871	3.540		2.809
Benzothiazole	1.642	1.281	1.330	1.298
2-Methylbenzothiazole	1.663	1.261		1.111
4,4'-Dibromobiphenyl	1.626	1.711		2.149

Table 7. Continued.

Compound	Refractive Index Estimated Using ChemSketch	E value Calculated from Estimated Refractive Index (ChemSketch)	E Value from UCL Database*	Experimental E Value
4-Dimethylaminoazobenzene	1.567	1.335		1.366
9,10-Anthraquinone	1.659	1.833		1.653
1-Hydroxyanthraquinone	1.695	2.132		1.504
Quinine	1.688	2.469		1.832

Estimated excess molar refraction (E) descriptor values are compared with the experimental values from this study obtained using the Solver method. (Table 7) For the two liquids there is a good agreement between the calculated and the experimental values (for 1-acetonaphthone calculated E value = 1.517, and E value determined by Solver method = 1.430, for quinoline calculated E value = 1.268, and E value determined by Solver method = 1.313). Since there is some uncertainty in the experimental refractive indices (values from the manufacturers catalog for compounds > 98% purity) and in the values obtained by the Solver method, the two sets of values for the E descriptor are not considered significantly different. For these compounds the E descriptor was set equal to the value calculated from the experimental refractive indices. There is also a good agreement with the estimated values from ChemSketch for these two compounds (1-acetonaphthone E = 1.435 and quinoline E = 1.340).

For the solid compounds the E descriptor estimated using ChemSketch tend to be larger than the experimental values (30 compounds larger and 9 compounds smaller). For 12 compounds (fluoranthene, pyrene, benzo[a]pyrene, benzo[e]pyrene, perylene, benzo(g,h,i)perylene, 8-hydroxyquinoline, 3,3'-dichlorobenzidine, benzidine, 1-nitropyrene, 1-hydroxyanthraquinone, and quinine) the difference in the E descriptor values is > 0.5. However, there is no obvious trend, just poor agreement for most compounds. For the E descriptors from the UCL database there is reasonable agreement for the small ring compounds but increasingly poorer agreement for the higher-ring number PAHs. The E descriptors for the higher ring number PAHs in the UCL database are generally larger than the experimental values determined in this work. The values in the UCL database are estimated values using a group contribution approach, and in some cases, subjected to further experimental optimization.[67-68] Unfortunately, most estimation methods result in different values for the E descriptor (and other descriptors) and there

is no particular reason to accept the values from one method over another.[38, 40, 69] Experimental values are subject to measurement uncertainty and for reliable measurements should be based on a sufficient number of models in which the E descriptor has a reasonably sharp descriptor well, as shown in Figure 12 for benzo[*a*]pyrene and pyrene.
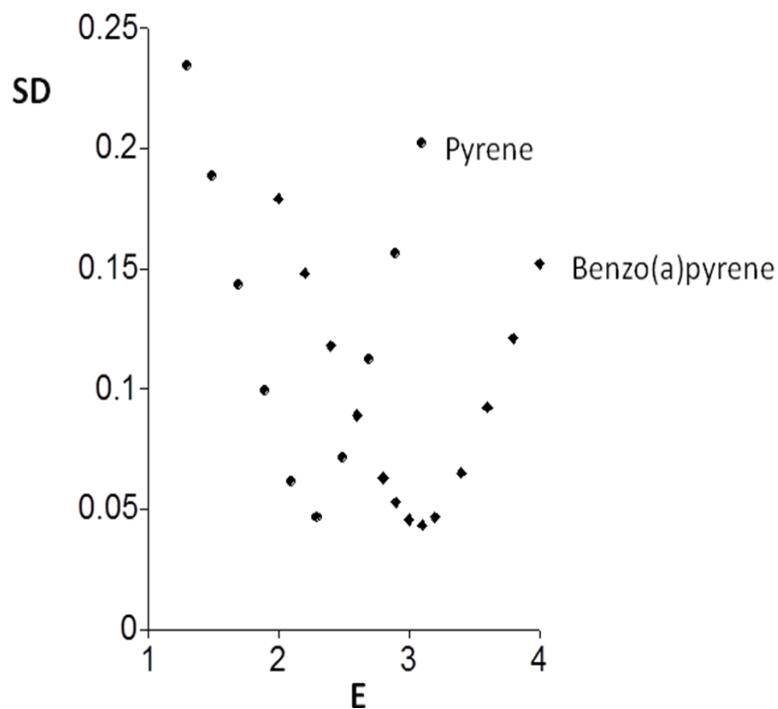
Figure 12. Descriptor Wells Using the Solver Method for the Estimation of the E (Excess Molar Refraction) Descriptor for Pyrene and Benzo[*a*]pyrene.

In Figure 12, SD is the standard deviation of the residuals (ordinate axis) and E is the excess molar refraction. SD is calculated by entering the calculated value for McGowan's characteristic volume V, setting hydrogen bond acidity equal to zero (A = 0) as neither PAH is a hydrogen-bond acid, selecting different test values for excess molar refraction (E) (x-coordinate), and allowing dipolarity/polarizability (S), hydrogen bond basicity (B) descriptors to assume any value that minimizes the standard deviation.[6a]

Descriptor wells with a sharp bottom allow identification of the best value for excess molar refraction (E) while wells with a shallow bottom only allow an indication of the range of values that can fit the system of equations with little change in the minimum value of the standard deviation of the residuals for the model predicted and experimental values. If one considers the alternative values for the E descriptor estimated by ChemSketch (pyrene = 3.129 and benzo[a]pyrene = 3.990) and from the UCL database (pyrene = 2.808 and benzo[a]pyrene = 3.625) the standard deviation for the models (when A is set to 0, and S, B, and L allowed to vary) are considerably higher than the observed minimum for the E descriptor when E is allowed to adopt any value. The E descriptor reported in these studies is the value that results in a minimum in the standard deviation of the residuals when all descriptors are determined simultaneously by the Solver method (where appropriate V is set to its calculated value).

Descriptors for some of the compounds in Table 6 have been determined previously as a group or individually. These values are summarized in Table 8.[5c, 14, 58-61, 69a, 70] Literature values for the gas-hexadecane partition coefficient at 298 K (L descriptor) were retrieved for 28 compounds.

Table 8. Descriptors for Polycyclic Aromatic Compounds Cited in the Literature.

Compound	E	S	A	B	B⁰	L
Azulene	1.340	1.17	0	0.16		
	1.340	1.17	0			5.707
Naphthalene	1.340	0.92	0	0.20		5.161
		0.92	0			5.152
						5.162
						5.277
1-Methylnaphthalene	1.337	0.94	0	0.22		5.802
	1.344	0.92	0	0.20		
		0.90	0			5.834
2-Methylnaphthalene	1.304	0.91	0	0.25		5.617
						5.768
						5.772
						5.771
Acenaphthylene	1.750	1.14	0	0.24		
	1.750	1.14	0			6.175
Acenaphthene	1.604	1.05	0	0.22		6.469
	1.604	1.04	0	0.20		
						6.539
Biphenyl	1.360	0.990	0	0.26		6.014
						6.07
		0.90	0			6.177

Table 8. Continued.

Compound	E	S	A	B	B⁰	L
Fluorene	1.588	1.06	0	0.25		6.922 7.061 6.936
Anthracene	2.290	1.34	0	0.28		7.568 7.598 7.721
Phenanthrene	2.055	1.29	0	0.26		7.632 7.723 7.638 7.670
Fluoranthene	2.377 2.377	1.55 1.53	0 0	0.24 0.20		8.827 8.721 8.764
Pyrene	2.808	1.71	0	0.28		8.833 8.764 8.949
9,10-Dimethylanthracene	2.290					9.283
Triphenylene	3.000	1.71				10.355 10.494
Chrysene	3.027	1.73	0	0.33		10.334
Benz[a]anthracene	2.992 2.992	1.70 1.70	 0	 0.33		10.291 10.494
p-Terphenyl	2.040	1.48	0			9.689

Table 8. Continued.

Compound	E	S	A	B	B⁰	L
Benzo[*a*]pyrene	3.625	1.98	0	0.44		11.736 12.000
Benzo[*e*]pyrene	3.625 3.625	1.99 1.99	0	0.44		 11.656
Perylene	3.256	1.76	0	0.40		12.053 12.000
Benzo[*g,h,i*]perylene	4.073 4.073 4.073	1.90 1.90 1.90	0 0 0	0.48 0.40		 13.264
Dibenz[*a,h*]anthracene	4.000 4.000	2.04 2.04	0	0.44		 12.960 12.996
Quinoline	1.268 1.268 	0.97 0.97 1.00	0 0 0.03	0.54	0.51	 5.457 5.28 5.422
1-Nitronaphthalene	1.600	1.59	0	0.29		7.056 6.80
1-Naphthol	1.520	1.10	0.66	0.34		6.284 6.23
2-Naphthol	1.520	1.08	0.61	0.40		6.200
Carbazole	1.787 1.787 1.790 	1.42 1.42 2.12 	0.47 0.09 	 0.10 	0.26 0.10 	 7.982 7.68
Benzothiazole	1.330	1.10	0	0.40		

Where multiple values are indicated in Table 8, an average was used for comparison with the experimental values determined in this study except for fluoranthene,[59] quinoline,[69a] 1-nitronaphthalene,[61] and carbazole,[70a] which resulted in a poor fit with the regression model. There is a good fit for a linear model for the plot of the experimental against literature L descriptors (Figure 13).
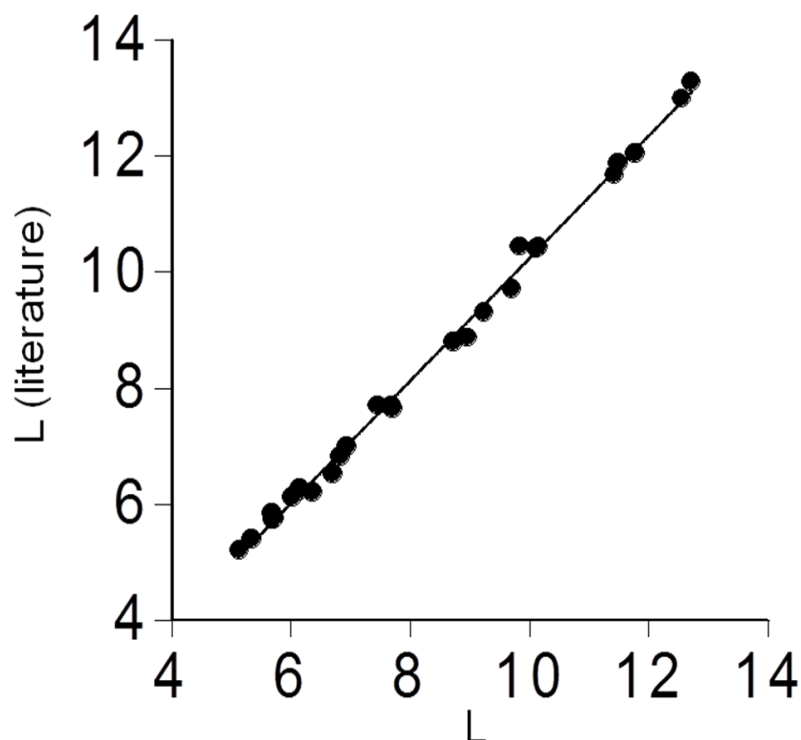
Figure 13. Correlation Between the Experimental L (Gas-Hexadecane Partition Coefficient at 298 K) Descriptor Values and the Average of the Available L Descriptor Values Reported in Literature.

The regression model shown in Equation 35 has an intercept that is statistically different to 0 (95% confidence interval 0.21 to 0.59) and a slope that does not include 1 (95% confidence interval 0.92 to 0.96).

$$L = 0.940 \, (\pm \, 0.010) \, L_{lit} + 0.398 \, (\pm \, 0.091) \tag{35}$$

$r^2 = 0.997$ $SE = 0.135$ $F = 8049$ $n = 27$

In Equation 35, r^2 is the coefficient of determination, SE is the standard error of the estimate, F is the Fisher statistic, and n is the number of compounds with descriptor values included in the model. For perspective, the average error for the two sets of L descriptors is 0.16 log units but there is a trend with the small-ring PAHs and related compounds having smaller differences than for the large-ring PAHs. In this context, the experimental L descriptors determined here have slightly smaller values than those extracted from the literature.

Literature values for the dipolarity/polarizability (S) descriptor were obtained for 28 compounds, most of which are single values with only a few average values taken for comparison. One of the literature S values for carbazole[5c] is considerably larger than the others and was omitted as a likely outlier. There is a modest fit for a linear model for the plot of the experimental against literature S descriptors (Figure 14).
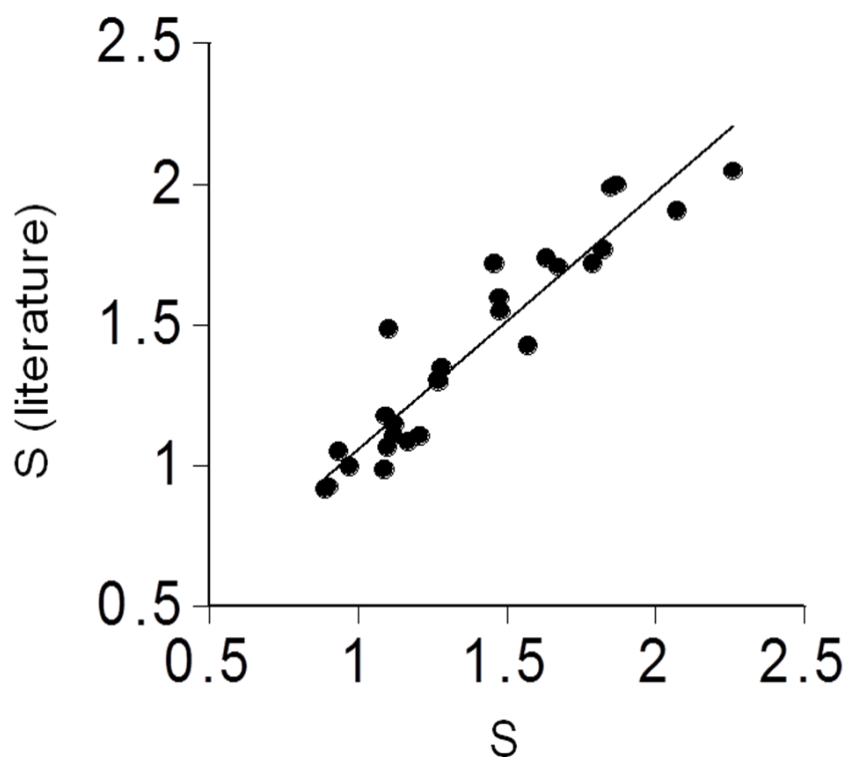

Figure 14. Correlation Between the Experimental S (Dipolarity/Polarizability) Descriptor Values and the Average of the Available S Descriptor Values Reported in Literature.

There is poor agreement for the S descriptors for pyrene and p-terphenyl. Removing these two compounds resulted in the regression model given in Equation 36.

$$S = 1.012 \, (\pm 0.052) \, S_{lit} - 0.007 \, (\pm 0.074) \qquad\qquad (36)$$

$$r^2 = 0.941 \qquad SE = 0.097 \qquad F = 380 \qquad n = 26$$

In the regression model the intercept is not statistically different from 0 (95% confidence interval −0.16 to 0.15) and the slope from 1 (95% confidence interval 0.91 to 1.12). Apart from pyrene and p-terphenyl, the general scatter in the plot shown in Figure 14 suggests that there are small differences in the S descriptor for the two data sets but these are largely random.

Literature values for the hydrogen bond basicity (B and B^0) descriptors were obtained for 23 compounds (two compounds with both B and B^0 descriptors). The B values for 1-methylnaphthalene,[70e] acenaphthene,[5c] benzo[g,h,i]perylene,[68] were not included as average values since two distinct and different values were indicated in the literature, which makes them unsuitable to average. The B^0 value for carbazole[5c] was omitted as an unlikely value. There is a poor fit for a linear model for the plot of experimental against literature combined B and B^0 descriptors (indicated as B descriptors below) in Figure 15.
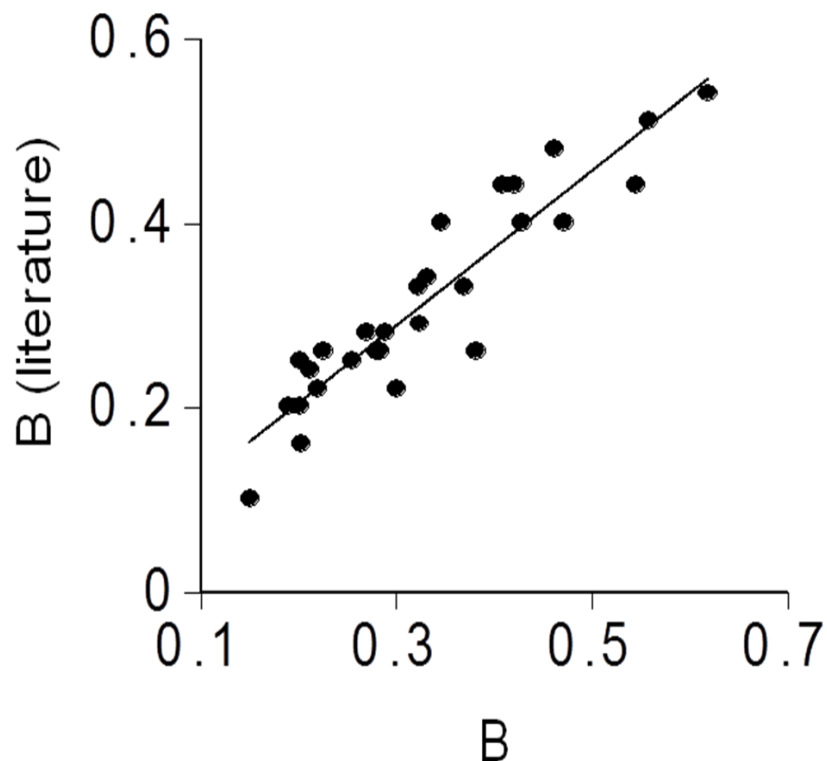
Figure 15. Correlation Between the Experimental B (Hydrogen Bond Basicity) Descriptor Values and the Average of the Available B Descriptor Values Reported in Literature.

There is poor agreement for the B descriptor for 9,10-dimethylanthracene, dibenzo[*a,h*]anthracene, 2-naphthol, 2-methylnaphthalene, and fluoranthene. Removing these five compounds resulted in the regression model given in Equation 37.

$$B = 1.0196 \, (\pm 0.068) \, B_{\text{lit}} + 0.005 \, (\pm 0.022) \tag{37}$$

$r^2 = 0.916$ SE $= 0.036$ F $= 228$ n $= 23$

In the regression model, intercept is not statistically different from 0 (95% confidence interval −0.042 to 0.052) and the slope from 1 (0.879 to 1.160). Apart from the five compounds indicated

above the general scatter shown in Figure 15 suggests that the modest differences in the B descriptor are largely random.

There are only three compounds (1-naphthol, 2-naphthol, and carbazole) with literature values for the A descriptor in Table 6. There are differences in the assigned values for the literature and experimental hydrogen bond acidity (A) descriptors determined here but the number of compounds is too small to draw any general conclusions.

Overall, the collection of descriptors in Table 6 differs from those in the literature by small but significant amounts. The excess molar refraction (E) and gas-hexadecane partition coefficient at 298 K (L) descriptors are generally smaller with greater differences for the PAHs of a large-ring number. Differences for the dipolarity/polarizability (S) and hydrogen bond basicity (B) descriptors are significant but for most compounds there is no trend. Such an analysis as this does not indicate that the descriptors determined in this study are more reliable than those that can be found in the literature, but they are more consistent as a homogeneous and verifiable experimental design is used for their measurements. In subsequent sections their usefulness for predicting experimental properties to support this statement is demonstrated.

4.4 A Fragment Model for Predicting Descriptors for Polycyclic Aromatic Hydrocarbons

Platts and coworkers have demonstrated the use of a fragment model for estimating descriptors.[67-68] In a simpler form we have adapted the same approach to obtain atom fragment constants for predicting descriptors for the fused ring polycyclic aromatic hydrocarbons. For the relevant compounds in Table 6 the atom fragment constants were obtained by deconstructing the compounds into four fragments (ring $-CH=$, ring fused carbon $>C<$, ring $-CH_2-$, and methyl substituent on a ring $-CH_3$). Appropriate descriptor values for each fragment were then obtained by setting up a series of equations containing the fragment count for each compound and the

experimental descriptor values from Table 6 using the Solver method to obtain the fragment descriptor values. The results are summarized in Table 9.

Table 9. Atom Fragment Descriptor Values for Polycyclic Aromatic Hydrocarbons.
(A = 0 for All Compounds)

Descriptor	Atom Fragment Constants				Statistics		
	ring -CH=	ring >C<	ring-CH$_2$-	-CH$_3$	n	SD	Descriptor Range
L	0.469	0.726	0.474	0.458	20	0.172	5-14
E	0.084	0.274	−0.115	−0.080	20	0.203	1.2-4.5
S	0.086	0.114	−0.041	0.011	22	0.078	0.9-2.5
B	0.020	0.022	0.030	0.008	22	0.037	0.19-0.55

The ability of the atom fragment constants to reproduce the descriptor values is quite good with a few exceptions. In general, atom fragment models do not account for the difference in descriptor values for isomers as they have the same atom counts. This seems to be most significant for the gas-hexadecane partition coefficient at 298 K (L descriptor), where the cavity formation component of the descriptor is not completely independent of the shape of the compound. Molecules interact at their surfaces and the shape and accessibility of the cavity surface could affect the contribution from dispersion. The PAHs with a fused four atom ring (azulene and fluoranthene) were not as well described by the atom fragment constants as the PAHs containing fused benzene rings. Azulene contains a seven membered ring fused to a four membered ring and shows the largest difference for the predicted L descriptor based on the summation of atom fragment constants ($L_{predicted}$ = 5.212 and $L_{experimental}$ = 5.776). For

fluoranthene the difference is not as great ($L_{predicted} = 9.066$ and $L_{experimental} = 8.733$). These values

were removed in the calculation of the atom fragment constants for the L descriptor in Table 9. It

is quite likely a better model could be found by including additional variables to account for

shape differences but this would require further data for PAHs with different ring sizes and is

outside the scope of this study. For the excess molar refraction (E) descriptor, the atom fragment

model adequately predicts the experimental values except for triphenylene ($E_{predicted} = 2.619$ and

$E_{experimental} = 2.919$). The experimental E descriptor for triphenylene is in good agreement with a

literature value,[70a] and is close to the value predicted by ChemSketch (Table 7). We do not

believe that the experimental E value is poorly determined. It is more likely that the simple

model employed here lacks some of the subtleties that would be required for more accurate

predictions. The dipolarity/polarizability (S) and hydrogen bond basicity (B) descriptors seem

more amenable to estimation with a simple atom fragment constant model as illustrated by the

data in Table 9. Overall, the atom fragment constant models can provide a reasonable estimate of

descriptor values for fused benzene ring compounds, with or without attached methyl groups,

which should be suitable for estimating descriptor values for further PAHs that currently lack

experimental values. For PAHs with different ring sizes there may be some deficiencies in the

estimation of the L and E descriptor. This analysis by atom fragment constants also supports the

hypothesis that the experimental descriptors are reasonably homogeneous as a group and do not

contain unexplainable values.

4.5 Estimation of the Octanol-Water Partition Coefficient for Polycyclic Aromatic Hydrocarbons and Related Compounds.

The octanol-water partition coefficient (as log K_{OW}) is widely used as an estimate of

lipophilicity and as a variable in numerous models to estimate a range of environmental

properties.[54b, 55-56] For compounds of low water (or octanol) solubility experimental measurement

can be tedious, difficult, and uncertain.[22, 56b] Poole and coworkers recently demonstrated the possibility of estimating the octanol-water partition coefficient for compounds of low water solubility from sets of descriptors derived from more convenient measurements of partition coefficients in totally organic biphasic systems and retention factors obtained by gas chromatography (e.g., organosiloxanes,[37] fragrance compounds,[38] and phthalate esters[39]). The same approach can be applied to estimate a number of water-based properties for compounds of environmental importance from descriptors summarized in Table 7 and to assist in the validation of descriptor quality.

The octanol-water partition coefficients for the polycyclic aromatic hydrocarbons and related compounds extracted from the literature are summarized in Table 10.[4e, 56b, 71] For some compounds only a single experimental value is available, while in other cases, for example the small-ring polycyclic aromatic hydrocarbons, there are numerous values but with poor agreement only, reflecting the difficulties of making such measurements for compounds with overwhelming solubility in a single phase. In general, the data cited in Table 10 refer to carefully considered average values that are assumed to better represent the true value and from which extreme values have been removed or adjusted in a thermodynamic cycle across a range of properties to obtain consistency, and indicated as LDV or FAV values, respectively.[56b] They are as close to consensus values as it is possible to identify. As well as a number of average or "consensus" values, the value taken for comparison with the predicted values is also indicated together with the estimated values for all compounds in Table 6 (with or without an experimental literature value) for comparison. Footnotes to Table 10 provide some additional information on how the literature values were selected in the cited sources and the model for the estimation of the octanol-water partition coefficient.

The general agreement between the selected experimental values and the model predicted values using the descriptors in Table 6 are very good with a few exceptions. The experimental octanol-water partition coefficient for quinine and the predicted value are significantly different (3.44 and 4.745, respectively). We removed this compound from the statistical summary of the data, but can offer no obvious reason beyond experimental uncertainty in either value for this observation. The differences for 9,10-dimethylanthracene and quinoline are more extreme than for the other compounds but were retained. The average error of 0.045 and average absolute error of 0.081 for the agreement between the experimental and predicted log K_{OW} values for the 37 compounds is an indication that there is no significant bias in the estimation method using the descriptors in Table 6 and that the descriptors provide an accurate prediction of the experimental octanol-water partition coefficients.

Table 10. Sources for Octanol-Water Partition Coefficients (log K_{OW}) and their Model Predicted Values.

Compound	Literature source[1]	Literature log K_{OW} Value	Calculated[2] log K_{OW} Value Using Descriptors Assigned in this Study
Azulene	3.20 [71c]	3.20	3.273
Naphthalene	LDV = 3.39 and FAV=3.40,[56b] 3.37,[71a] 3.35 [71d]	3.40	3.368
2-Methylnaphthalene	4.11, [71b] 3.86 [4]	3.86	3.867
Acenaphthylene	LDV=3.80 and FAV=3.85,[56b] 4.00,[71a] 4.70[71b]	3.80	3.758
Acenaphthene	LDV=-3.97 and FAV=3.95,[56b] 3.92,[71a] 4.00 [71b]	3.95	4.019
Biphenyl	3.90, [71a] 4.01[71c]	4.01	3.978

[1] LDV is the arithmetic mean of all reliable values at 25 °C or from linear regression equations between log property and 1/T when experiments had been carried out at different temperatures.

FAV values are obtained by adjusting the average value by an algorithm to obtain thermodynamic consistency across a range of properties, according to a literature method described in reference 56b.[56b]

[2] Model used for calculation log $K_{OW} = 0.123 + 0.680E - 1.169S - 0.207A - 3.412B + 3.788$ V

$$r = 0.998 \qquad SE = 0.118 \qquad F = 7631 \qquad n = 192$$

Table 10. Continued.

Compound	Literature source[1]	Literature log K_{OW} Value	Calculated[2] log K_{OW} Value Using Descriptors Assigned in this Study
Fluorene	LDV=4.14 and FAV=4.11,[56b] 4.18,[71a] 4.18 [71d]	4.16	4.233
Anthracene	LDV=4.63 and FAV=4.57,[56b] 4.54, [71a] 4.45, [71b] 4.53 [71d]	4.57	4.562
Phenanthrene	LDV=4.49 and FAV= 4.47,[56b] 3.24,[71a] 4.46[71b]	4.47	4.475
Fluoranthene	LDV=4.98 and FAV=4.97,[56b] 5.22, [71a] 4.90, [71b] 5.22[71d]	4.97	4.966
Pyrene	LDV=5.06 and FAV=5.01,[56b] 5.18, [71a] 4.88, [71b] 5.22 [71d]	5.01	4.962
9,10-Dimethylanthracene	5.69 [71c]	5.69	5.334
Triphenylene	5.49 [71a]	5.49	5.465
Chrysene	LDV=5.67 and FAV=5.67,[56b] 5.65,[71a] 5.61,[71b] 5.91 [71d]	5.67	5.763
Benz[*a*]anthracene	LDV=5.83 and FAV=5.83,[56b] 5.91,[71a] 5.60[71b]	5.83	5.656
p-Terphenyl	6.03[71a]	6.03	6.024

Table 10. Continued.

Compound	Literature source[1]	Literature log K_{OW} Value	Calculated[2] log K_{OW} Value Using Descriptors Assigned in this Study
Benzo[*a*]pyrene	LDV=5.99 and FAV=6.05,[56b] 6.02,[71a] 6.06, [71b] 6.50[71d]	6.05	6.040
Benzo[*e*]pyrene	6.44 [71c]	6.44	6.027
Perylene	6.25,[71a] 6.25,[71c] 5.82 [71e]	6.25	6.129
Benzo[*g,h,i*]perylene	LDV=6.60 and FAV=6.63,[56b] 6.50,[71a] 6.51, [71b] 7.10[71d]	6.63	6.518
Dibenz[a,h]anthracene	6.80,[71b] 6.75, 7.11,[71c] 6.50 [4e]	6.50	6.514
Dibenzo[*a,i*]pyrene	7.28 [71e]	7.28	7.348
Quinoline	2.03, [71c] 2.10 [71d]	2.03	1.769
8-Hydroxyquinoline	1.85 [71c]	1.85	1.868
1-Nitronaphthalene	3.19 [71e]	3.19	3.127
1-Naphthol	2.85[71c]	2.85	2.852

Table 10. Continued.

Compound	Literature source[1]	Literature log K_{OW} Value	Calculated[2] log K_{OW} Value Using Descriptors Assigned in this Study
2-Naphthol	2.70 [71c]	2.70	2.735
Carbazole	3.84 [71d]	3.84	3.844
3,3'-Dichlorobenzidine	1.75 [71c]	1.75	1.673
1-Acetonaphthone	2.86 [71e]	2.86	2.832
Benzothiazole	2.01 [71b]	2.01	1.655
Benzidine	1.34 [71c]	1.34	1.408
1-Nitropyrene	5.06 [71c]	5.06	5.152
4,4'-Dibromobiphenyl	5.72 [71c]	5.72	5.708
9,10-Anthraquinone	3.39 [71c]	3.39	3.396
1-Hydroxyanthraquinone	3.52 [71c]	3.52	3.570
Quinine	3.44 [71c]	3.44	4.772

4.6 Estimation of Octanol-Air Partition Coefficients for Polycyclic Aromatic Hydrocarbons and Related Compounds.

The octanol-air partition coefficient (as log K_{OA}) is widely used to estimate the atmospheric distribution of organic compounds between air and the organic matter of aerosols and as a variable in models used to estimate environmental distribution and fate of volatile organic compounds.[53b, 53c] Its measurement for compounds of low vapor pressure, such as PAHs, is challenging and estimation methods are widely used as a surrogate for experimentally determined values.[55a, 56c] The octanol-air partition coefficients for the polycyclic aromatic hydrocarbons and carbazole extracted from the literature are summarized in Table 11.[4d, 56b, 56c, 72] For compounds with multiple values, the selected value for comparison with the predicted value was an average with due regard to the general quality of the experimental results. In most cases the recommended values reported by Ma and coworkers and Ha and coworkers were adopted.[56b, 56c] In the case of dibenz(a,h)anthracene the two experimental values of log K_{OA} differ by 1.4 log units and neither value, nor their average, was used in calculations. Table 11 also summarizes the predicted values for all compounds in Table 6 using the experimental descriptors. The general agreement between the experimental and the predicted values for the octanol-air partition coefficient is very good with the exception of carbazole, which has an experimental log K_{OA} of 8.03[72a] and a predicted log K_{OA} of 8.864. The experimental log K_{OA} for carbazole is a single value and we have no method to estimate its experimental uncertainty and elected to remove it from the statistical summary of the remaining data in Table 11. For these compounds the average error is 0.075 and average absolute error 0.096 for the agreement between the experimental and predicted log K_{OA} for 16 compounds. This is an indication that there is no significant bias in the estimation method and that the experimental descriptors in Table 6 for the PAHs are suitable for

the prediction of octanol-air partition coefficients. This confirms reasonable expectations for descriptor quality. Table 12 summarizes the estimated log K_{OA} values for compounds without experimental values.

Table 11. Sources for Octanol-Air Partition Coefficients (log K_{OA}) for Polycyclic Aromatic Hydrocarbons and Related Compounds and their Model Predicted Values.

Compound	Literature source[1]	Literature log K_{OA} Value	Calculated[2] log K_{OA} Value Using Descriptors Assigned in this Study
Naphthalene	FAV = 5.19 and LAV=5.19,[56b] 5.37, 5.27, 5.46, 5.13,[56c] 5.19 [72b]	5.19	5.114
Acenaphthylene	FAV=6.46 and LAV=6.25 [56b]	6.46	6.350
Acenaphthene	FAV=6.44 and LDV=6.42[56b], 6.52, 6.43, 6.33,[56c] 6.31[72b]	6.44	6.572
Biphenyl	6.15 [71c]	6.15	6.007
Fluorene	FAV=6.85 and LDV=6.81,[56b] 6.84, 6.79,[73] 6.90, 7.45, 7.57[56c] 6.83 [72b]	6.85	6.865
Anthracene	FAV=7.70 and LDV=7.64,[56b] 7.71, 7.34,[56c] 7.55[72b]	7.70	7.649

[1] LDV is the arithmetic mean of all reliable values at 25 °C or from linear regression equations between log property and 1/T when experiments had been carried out at different temperatures.

FDV values are obtained by adjusting the average value by an algorithm to obtain thermodynamic consistency across a range of properties, according to a literature method described in reference 56b.[56b]

[2] Model used for calculation $\log K_{OA} = -0.120 - 0.203E + 0.560S + 3.560A + 0.702B + 0.939 L$[72b]

Table 11. Continued.

Compound	Literature source[1]	Literature log K_{OW} Value	Calculated[2] log K_{OW} Value Using Descriptors Assigned in this Study
Phenanthrene	FAV=7.64 and LDV=7.61,[56b] 7.62, 7.68, [56c] 7.68,[72a] 7.57,[73] 7.52[72a]	7.64	7.646
Fluoranthene	FAV=8.81 and LDV=8.80,[56b] 8.61, 8.48, 8.76, 8.76,[56c] 8.88,[73] 8.61[72b]	8.81	8.642
Pyrene	FAV= 8.86 and LAV=8.79,[56b] 8.86, 8.75, 8.65, 8.43[56c] 8.80 [73]	8.86	8.876
Chrysene	FAV=10.30 and LDV=10.30,[56b] 9.85, 10.44 [56c]	10.30	9.997
Benz[a]anthracene	FAV = 10.28 and LDV=10.28,[56b] 8.69,10.80[56c]	10.28	10.029
p-Terphenyl	9.87 [73]	9.87	9.830
Benzo[a]pyrene	FAV=11.48 and LDV=11.56,[56b] 10.7, 10.48 [56c]	11.48	11.430
Benzo[e]pyrene	11.35 [73]	11.35	11.325
Perylene	11.70 [56c]	11.70	11.574

Table 11. Continued.

Compound	Literature source[1]	Literature log K_{OW} Value	Calculated[2] log K_{OW} Value Using Descriptors Assigned in this Study
Benzo[*g,h,i*]perylene	FAV =12.55 and LDV=12.55[56b]	12.55	12.556
Dibenz[*a,h*]anthracene	12.59, 13.9 [56c]		12.541
Carbazole	8.03 [72a]	8.03	8.864

[1] LDV is the arithmetic mean of all reliable values at 25 °C or from linear regression equations between log property and 1/T when experiments had been carried out at different temperatures.

FDV values are obtained by adjusting the average value by an algorithm to obtain thermodynamic consistency across a range of properties, according to a literature method described in reference 56b.[56b]

[2] Model used for calculation log $K_{OA} = -0.120 - 0.203E + 0.560S + 3.560A$

$$+ 0.702B + 0.939 L[72b]$$

Table 12. Estimated Octanol-Air Partition Coefficients (log K_{OA}) Values for Compounds without Experimental Values.

Compound	Calculated[1] log K_{OA} Value Using Descriptors Assigned in this Study
Azulene	5.761
1-Methylnaphthalene	5.617
2-Methylnaphthalene	5.668
9,10-Dimethylanthracene	9.127
Triphenylene	9.898
Dibenzo[*a,i*]pyrene	13.389
Quinoline	5.710
8-Hydroxyquinoline	6.991
1-Nitronaphthalene	7.056
1-Naphthol	8.922
2-Naphthol	9.047
3,3'-Dichlorobenzidine	13.089
1-Acetonaphthone	7.022
2-Acetonaphthone	7.204
Benzidine	10.664
1-Nitropyrene	10.518
Benzothiazole	5.519
2-Methylbenzothiazole	6.009
4,4'-Dibromobiphenyl	8.409
4-Dimethylaminoazobenzene	9.837
9,10-Anthraquinone	8.874
1-Hydroxyanthraquinone	9.487
Quinine	15.280

[1]Model used for calculation of log K_{OA} = − 0.120 − 0.203E + 0.560S + 3.560A + 0.702B + 0.939L[72b]

4.7. Estimation of the Air-Water Partition Coefficient for Polycyclic Aromatic Hydrocarbons and Related Compounds

The air-water partition coefficient (the inverse of Henry's law constant with due regard to units) describes a compounds ability to partition between air and water. It is a key property for the assessment of a compounds environmental behavior and for fate modeling.[55a, 56d, 74] For compounds of low vapor pressure and/or low water solubility its measurement is challenging and only a small number of experimental values are available for compounds of environmental interest. The air-water partition coefficients (log K_{AW}) for nineteen polycyclic aromatic hydrocarbons and seven related compounds are summarized in Table 13.[55a, 56b, 56d, 70e, 71a, 72a, 75] For most compounds with multiple experimental values an average was taken for comparison purposes. For anthracene, phenanthrene and benz[a]anthracene we chose the values from Abraham and coworkers[75] as we have validated these internally in numerous calculations, and with the exception of anthracene, there is good agreement with the suggested reference values reported by Ma and coworkers.[56b] For benzo[a]pyrene there is considerable scatter in the experimental values and we chose an experimental value similar to benzo[e]pyrene and perylene, which all have the same ring number, and a clustering of values is anticipated. Table 13 also summarizes the predicted values for all compounds in Table 6 using the experimental descriptors for the calculation. The general agreement between the experimental and the predicted values for the air-water partition coefficient is good with the exception of 9,10-anthraquinone, and 1-hydroxyanthraquinone, which have an experimental log K_{AW} of 6.02 and 6.53,[71b] respectively, and predicted log K_{AW} of 4.433 and 4.422, respectively. The experimental log K_{AW} for anthraquinone and 1-hydroxyanthraquinone seem unusually large for compounds of this type, but as single determinations, we have no method to estimate their experimental uncertainty. We elected to remove them from the statistical summary of the remaining data in Table 13. For the

24 compounds the average error is −0.077 and average absolute error 0.188 for the agreement between the experimental and predicted log K_{AW} values. Thus, there is no significant bias in the estimation method and the experimental descriptors in Table 6 are suitable for the prediction of the air-water partition coefficients. Estimated log K_{AW} values for compounds without experimental values are given in Table 14.

Table 13. Sources for Air-Water Partition Coefficients (log K_{AW}) for Polycyclic Aromatic Hydrocarbons and Related Compounds and their Model Predicted Values.

Compound	Literature source[1]	Literature log K_{AW} Value	Calculated[2] log K_{AW} Value Using Descriptors Assigned in this Study
Naphthalene	Fav = 1.73 and LDV= 1.72,[56b] 1.638[56d]	1.73	1.810
1-Methylnaphthalene	1.75, 1.97, 1.67, [70e] 1.62, [71c] 1.62 [56d]	1.73	1.758
2-Methylnaphthalene	1.67, 1.77, 1.78, [70e] 1.47, [71c] 1.60 [56d]	1.66	1.660
Acenaphthylene	Fav = 2.41 and LDV= 2.31,[56b]	2.41	2.398
Acenaphthene	Fav = 2.24 and LDV= 2.25,[56b] 2.24, [53d] 2.31 [75]	2.24	1.765
Biphenyl	1.95, [75] 1.90 [71c]	1.95	2.272

[1] LDV is the arithmetic mean of all reliable values at 25 °C or from linear regression equations between log property and 1/T when experiments had been carried out at different temperatures.

FDV values are obtained by adjusting the average value by an algorithm to obtain thermodynamic consistency across a range of properties, according to a literature method described in reference 56b.[56b]

[2] Model used for calculation log $K_{AW} = -0.996 + 0.470E + 3.058S + 3.905A + 4.496B - 0.272L$

$$r = 0.996 \qquad SE = 0.175 \qquad F = 2112 \qquad n = 98$$

Table 13. Continued.

Compound	Literature source[1]	Literature log K_{AW} Value	Calculated[2] log K_{AW} Value Using Descriptors Assigned in this Study
Fluorene	Fav = 2.44 and LDV= 2.42,[56b] 2.46 [75]	2.44	2.422
Anthracene	Fav = 2.69 and LDV= 2.69, [56b] 2.90 [75]	2.90	2.968
Phenanthrene	Fav = 2.76 and LDV= 2.75,[56b] 2.85[75]	2.85	2.989
Fluoranthene	Fav = 3.27 and LDV= 3.23, [56b] 3.44, [53d] 3.61 [71a]	3.44	3.605
Pyrene	Fav = 3.27 and LDV= 3.27,[56b] 3.32,[74a] 3.54 [56d]	3.27	3.401
Triphenylene	5.20 [71c]	5.20	4.964
Chrysene	Fav = 3.82 and LDV= 3.75 [56b]	3.82	3.863
Benz[a]anthracene	Fav = 3.59 and LDV= 3.55,[56b] 3.31, [53d] 3.61 [75]	3.59	4.323
p-Terphenyl	3.84 [71c]	3.84	3.912
Benzo[a]pyrene	Fav = 4.51 and LDV= 4.69,[56b] 4.84, [53d] 4.70 [56d]	4.84	4.812

Table 13. Continued.

Compound	Literature source[1]	Literature log K_{AW} Value	Calculated[2] log K_{AW} Value Using Descriptors Assigned in this Study
Benzo[e]pyrene	4.91 [71c]	4.91	4.938
Perylene	4.83 [71c]	4.83	4.802
Benzo[g,h,i]perylene	Fav = 4.77 and LDV= 4.87,[56b] 4.94[71c]	4.91	5.660
Quinoline	4.20, [74a] 4.17 [71c]	4.19	4.277
1-Nitronaphthalene	4.14, [56d] 4.09 [71c]	4.09	3.622
1-Naphthol	5.63 [75]	5.63	5.893
2-Naphthol	5.95 [75]	5.95	6.224
Carbazole	5.32 [72a]	5.32	5.251
9,10-Anthraquinone	6.02 [71c]	6.02	4.434
1-Hydroxyanthraquinone	6.53 [71c]	6.53	4.422

Table 14. Estimated Air-Water Partition Coefficient (log K_{AW}) Values for Compounds without Experimental Values.

Compound	Calculated[1] log K_{AW} Value Using Descriptors Assigned in this Study
Azulene	2.273
9,10-Dimethylanthracene	3.097
Dibenz[*a,h*]anthracene	6.773
Dibenzo[*a,i*]pyrene	7.248
8-Hydroxyquinoline	3.797
3,3'-Dichlorobenzidine	7.624
1-Acetonaphthone	4.750
2-Acetonaphthone	4.972
Benzidine	7.296
1-Nitropyrene	5.286
Benzothiazole	4.031
2-Methylbenzothiazole	3.451
4,4'-Dibromobiphenyl	2.379
4-Dimethylaminoazobenzene	8.367
Quinine	9.350

[1]Model used for calculation of log $K_{AW} = -0.996 + 0.470E + 3.058S + 3.905A$

$$+ 4.496B - 0.272L$$

$$r = 0.996 \qquad SE = 0.175 \qquad F = 2112 \qquad n = 98$$

4.8. Comparison of Descriptors for the Prediction of Partition Coefficients

The descriptors determined in this study for polycyclic aromatic hydrocarbons and related compounds (Table 6) can be compared with literature values (Table 9) together with their associated calibration equations for their ability to predict the experimental octanol-water (Table

10), octanol-air (Table 11), and air-water (Table 13) partition coefficients.[6a, 10, 21] The average error and average absolute error for these predictions are summarized in Table 15 where m indicates the number of compounds with descriptor values in common from Tables 6 and 8 for which experimental partition coefficients are available.

Table 15. Comparison of Descriptors from this Study (Table 6) and the Literature (Table 8) for the Prediction of Partition Coefficients (log K).

Partition Coefficient (log K)	Descriptor Source*	Average Error	Average Absolute Error	Number of Compounds (m)
Octanol-water	This study	0.060	0.085	22
	Literature	0.019	0.112	22
Octanol-air	This study	0.081	0.105	17
	Literature	0.083	0.138	17
Air-Water	This study	−0.069	0.177	19
	Literature	−0.813	0.850	19

* Calibration models for calculations using literature descriptors[21]

$$\log K_{OW} = 0.088 + 0.562E - 1.054S + 0.044A - 3.460B + 3.814V$$

$$\log K_{OA} = -0.147 - 0.214E + 0.561S + 3.502A + 0.749B + 0.913L$$

$$\log K_{AW} = -1.271 + 0.822E + 2.743S + 3.964A + 4.814B - 0.213L$$

These are predominantly polycyclic aromatic hydrocarbons with quinoline, 1-nitronaphthalene, 1-naphthol and 2-naphthol included in the calculations for the octanol-water and air-water partition coefficients. Both sets of descriptors predict the octanol-water and octanol-air partition coefficients without obvious bias, as indicated by the average error, but the descriptors determined in this study improve the accuracy of the prediction as indicated by the smaller absolute average error. For the air-water partition coefficient the literature descriptors result in a biased estimation for the polycyclic aromatic hydrocarbons (the predicted values are systematically larger than the experimental values), which is not the case for the predictions using the descriptors determined in this study. Abraham and Acree have made similar observations and resorted to the use of an indicator variable for polycyclic aromatic hydrocarbons to define a general model that included some polycyclic aromatic hydrocarbons.[76]

To shed some light on why the two sets of descriptors provide different predictive ability for the air-water partition coefficients a breakdown of the contributions from the predicted intermolecular interactions to the partition coefficients for some representative polycyclic aromatic hydrocarbons and 1-naphthol is shown in Table 16. Since the calibration models associated with the two groups of descriptors have significantly different intercepts the use of either model alone with both groups of descriptors would bias the resulting comparison.

Table 16. Contribution of Different Intermolecular Interactions to the Air-Water Partition Coefficient (log K_{AW}) for the Descriptors Determined in this Study (Table 7) and Literature Descriptors (Table 9).

Polycyclic Aromatic Hydrocarbon	Descriptor	eE	sS	aA	bB	lL	Model Intercept
Naphthalene	This study	0.58	2.77	0	0.86	−1.40	−0.996
	Literature	1.10	2.52	0	0.96	−1.10	−1.271
Phenanthrene	This study	0.90	3.91	0	1.28	−2.10	−0.996
	Literature	1.69	3.54	0	1.25	−1.63	−1.271
Pyrene	This study	1.07	4.49	0	1.30	−2.44	−0.996
	Literature	2.31	4.69	0	1.35	−1.88	−1.271
Chrysene	This study	1.21	5.01	0	1.46	−2.77	−0.996
	Literature	2.49	4.75	0	1.59	−2.20	−1.271
Benzo[a]pyrene	This study	1.45	5.67	0	1.90	−3.13	−0.996
	Literature	2.98	5.43	0	2.12	−2.50	−1.271
1-Naphthol	This study	1.20	3.43	2.95	1.50	−1.31	−0.996
	Literature	0.71	3.02	2.58	1.53	−1.34	−1.271

From Table 16 it is clear that there is a large difference in the contribution from electron-lone pair interactions for the two calibration models (eE), which accounts for most of the observed differences, and a smaller but significant contribution from cavity formation/dispersion interactions (lL). Differences in the contributions from dipole-type interactions (sS) and hydrogen bonding (bB) are generally smaller and less important. As a reference point data is included for 1-naphthol, for which both models provide a reasonable prediction of the air-water partition coefficient, and is representative of the results for the four related polycyclic aromatic compounds included in the comparison. This is too small a data set to make global comparisons, but the contrast with the data for the polycyclic aromatic compounds is interesting, since it indicates reasonably close agreement for the contribution of the cavity/dispersion and hydrogen bond contributions (lL and bB) and small differences for dipole-type, electron-lone pair interactions, and hydrogen bond contributions (sS, eE, aA) to the predicted air-water partition coefficients. These differences usually off-set the difference in model intercepts and results in unbiased and similar prediction ability for the air-water partition coefficients. For the polycyclic aromatic hydrocarbons significant bias in the predictions is a combination of both differences in the values for the two sets of solute descriptors and the differences in their associated calibration models, especially the intercept term. The excess molar refraction (E) and gas-hexadecane partition coefficient at 298 K (L) descriptors found in Table 6 tend to be systematically smaller than the literature values, as discussed earlier, but the system constants for the calibration models are also systematically different for e and l. Thus, the bias in the prediction of the air-water partition coefficients cannot be as simple as poor descriptor quality for the literature descriptors alone.

For clarity, we emphasize that the significant anomaly in the prediction of the air-water partition coefficients is for the polycyclic aromatic hydrocarbons alone and not for the polar aromatic compounds included in this study, nor is it apparent in the predictions of the other partition systems studied here. Its origins, however, are complex involving both the descriptor set and the calibration model. The descriptors determined in this study together with their associated calibration model provide a bias-free prediction, as indicated in Table 16. The use of the literature descriptors with literature calibration model results in a significant bias in the prediction of the air-water partition coefficient that is generally larger than when the literature descriptors are combined with the calibration model associated with the descriptor database for the polycyclic aromatic hydrocarbons determined here. The largest bias in the prediction of the air-water partition coefficients for the polycyclic aromatic hydrocarbons is always for the literature descriptors and their associated calibration model.

4.8. Estimation of the Water Solubility for Polycyclic Aromatic Hydrocarbons and Related Compounds.

The solubility of compounds in water is an important property that provides an indication of the likely mobility and environmental fate of a compound. Indirectly it provides an indication of the likelihood of their uptake and accumulation in living organisms. The solvation parameter model was developed to model transfer properties but an amended model containing a cross-product term (AB) was proposed by Abraham and Le[77] and updated[61] to estimate the molar solubility of compounds in water. The cross-product term was introduced to allow for intermolecular interactions in the solid form, which are of course absent in transfer properties, where it is assumed that solute molecules interact only with solvent molecules. The water solubility for twenty-one polycyclic aromatic hydrocarbons and fifteen related compounds are

summarized in Table 17. [53b, 56a, 71a, 71c, 77-78] As mentioned earlier, the values taken for comparison are generally averages except for those compounds with only a single experimental value. The general agreement between the experimental and estimated values is good except for anthracene, 4-dimethylaminoazobenzene, and quinine, which have experimental values ($-\log S_W$) of 6.49, 5.96 and 3.36, respectively, and predicted values using the descriptors in Table 6 of 5.057, 2.073, and 5.156, respectively. The experimental solubility values for anthracene are reasonably consistent from several studies but are significantly different to phenanthrene, which is not typical of the isomeric PAHs in Table 17. In addition, the experimental descriptors for anthracene provided a reasonable estimate of the octanol-water, air-octanol, and air-water partition coefficients and so the problem may lie in how the model accounts for the contribution of the dissociation of the solid phase for this compound since the cross-product term is 0 (As is the case for all PAHs, but it does not seem to be a significant problem for most of the other PAHs). 4-Dimethylaminoazobenzene and quinine have only single solubility values and their experimental uncertainty is unknown. We removed these three compounds from the comparison of experimental and predicted solubility to give a more typical assessment of the capability of the descriptors to estimate solubility. It cannot be stated, however, that these three compounds are outliers because of poor experimental values, since the model used to predict solubility contains an approximate representation of interactions in the solid form. For the remaining compounds in Table 17 the average error is 0.412 and the average absolute error is 0.612 for the agreement between the experimental and predicted $-\log S_W$ for 33 compounds. The results would suggest the possibility of a small bias in the predictions (the calculated values in general suggesting higher solubility). The average absolute error for the prediction of solubility is similar to

observations for a larger and more diverse group of compounds at about 0.5 log units.[77]

Estimated water solubility of compounds without experimental values are given in Table 18.

Table 17. Sources for Solubility in Water ($-\log S_W$, mol/L) for Polycyclic Aromatic Hydrocarbons and Related Compounds and their Model Predicted Values.

Compound	Literature source	Literature $-\log S_W$ Value	Calculated[1] $-\log S_W$ Value Using Descriptors Assigned in this Study
Naphthalene	3.62, [71a] 3.60, [77] 3.61, [56a] 3.62[78a]	3.61	3.486
1-Methylnaphthalene	3.75, [71c] 3.70, [77] 3.69 [56a]	3.71	4.016
2-Methylnaphthalene	4.75, [71b] 3.76, [71c] 3.77, [77] 3.74[56a]	3.76	3.911
Acenaphthylene	3.48, [71c] 3.98, [71a] 4.59, [71b] 3.96[77]	3.97	4.083
Acenaphthene	4.61, [71a] 4.65, [71b] 4.63, [77] 4.59, [56a] 4.58 [78a]	4.61	4.163
Biphenyl	4.34, [71a] 4.35, [71c] 4.35, [77] 4.35 [78a]	4.35	4.110
Fluorene	4.94, [71a] 5.00, [77] 4.92 [56a], 4.96 [78a]	4.96	4.524
Anthracene	6.60, [71a] 6.60, [71b] 6.35, [77] 6.39, [56a] 6.49 [78a]	6.49	5.057

[1] Model used for calculation $\log S_W = 0.391 - 0.954E + 0.318S + 1.157A + 3.255B$

$$- 0.786AB - 3.329V \text{ [33]}$$

Table 17. Continued.

Compound	Literature source	Literature -log S_W Value	Calculated[1] -log S_W Value Using Descriptors Assigned in this Study
Phenanthrene	4.58, [71a] 5.25, [71b] 5.19 [75] 5.26, [77] 5.14, [56a] 5.21, [78a]	5.21	4.946
Fluoranthene	5.89, [71a] 5.99, [71b] 6.00, [77] 5.89, [56a] 5.96 [78a]	5.95	5.677
Pyrene	6.19, [71a] 6.19, [71b] 6.18, [77] 6.18, [56a] 6.19 [78a]	6.19	5.632
9,10-Dimethylanthracene	6.57, [71c] 6.57, [77] 6.57, [56a] 6.57 [78a]	6.57	5.744
Triphenylene	6.73, [71a] 6.66, [71c] 6.73 [56a]	6.70	6.518
Chrysene	8.10, [71b] 8.06, [77] 8.06, [56a] 8.09[78a]	8.08	6.668
Benz[a]anthracene	7.32, [53b] 7.69, [71b] 7.39, [71c] 7.21,[56a] 7.28 [78a]	7.38	6.557
p-Terphenyl	7.11 [71a]	7.11	5.959

Table 17. Continued.

Compound	Literature source	Literature -log S_W Value	Calculated[1] -log S_W Value Using Descriptors Assigned in this Study
Benzo[a]pyrene	7.82, [71a] 8.32, [71b] 8.70, [77] 7.82,[56a] 8.21 [78a]	8.17	7.049
Benzo[e]pyrene	7.80, [71a] 7.56, [71c] 7.65, [71b] 7.800, [77] 7.65 [78a]	7.69	7.139
Perylene	8.23,[71a] 7.80,[71c] 8.60 [77] 7.80, [56a] 8.80 [78a]	8.25	6.883
Benzo[g,h,i]perylene	9.03, [71a] 8.60, [71b] 9.02, [77] 9.03,[56a] 9.29 [78a]	9.09	7.902
Dibenz[a,h]anthracene	8.67, [71a] 8.74, [71b] 8.95[71c]	8.79	8.052
Quinoline	1.33, [71c] 1.30 [77]	1.32	1.793
8-Hydroxyquinoline	2.22 [71c]	2.22	2.552
1-Nitronaphthalene	4.28 [78b]	4.28	3.716
1-Naphthol	2.22, [71c] 2.22 [77]	2.22	2.684

Table 17. Continued.

Compound	Literature source	Literature -log S_W Value	Calculated[1] -log S_W Value Using Descriptors Assigned in this Study
2-Naphthol	2.28, [55b] 2.28 [77]	2.28	2.602
Carbazole	5.27 [77]	5.27	4.575
3,3'-Dichlorobenzidine	4.91 [71c]	4.91	4.459
2-Acetonaphthone	2.80 [71c]	2.80	3.174
Benzidine	2.76 [71c]	2.76	1.851
1-Nitropyrene	7.62 [78b]	7.62	6.426
Benzothiazole	1.50 [71c]	1.50	2.148
4-Dimethylaminoazobenzene	5.96 [71c]	5.96	2.073
9,10-Anthraquinone	5.19, [71c] 5.190 [77]	5.19	3.942
1-Hydroxyanthraquinone	4.42 [71c]	4.42	4.063
Quinine	3.36 [71c]	3.36	5.156

Table 18. Estimated Water Solubility ($-\log S_W$) of Compounds without Experimental Values.

Compound	Calculated[1] $-\log S_W$ Value Using Descriptors Assigned in this Study
Azulene	3.525
Dibenzo[*a,i*]pyrene	9.177
1-Acetonaphthone	3.384
2-Methylbenzothiazole	2.262
4,4'-Dibromobiphenyl	6.059

None of the PAHs are hydrogen-bond acids (A = 0) and therefore, the cross-product term (AB) added to the general model to correct for contribution of intermolecular interactions in the solid phase is zero for these compounds. This suggested that it might be possible to develop a simpler model to estimate their solubility as a separate group. The model obtained by multiple linear regression analysis is

$$\log S_W = 3.885\ (\pm\ 0.434) + 11.3680\ (\pm\ 1.323)B - 8.469\ (\pm\ 0.486)V \qquad (38)$$

$$r = 0.990 \qquad SE = 0.302 \qquad F = 303 \qquad n = 20$$

Equation 38 contains only the McGowan's characterisctic volume (V) and hydrogen bond basicity (B) descriptors. Anthracene was an outlier and was removed as observed for the general model used to calculate the results in Table 17. Equation 38 is quite a useful model for estimating the solubility of PAHs and is more accurate than the general model (average absolute error 0.229). Given that V is always available via calculation, and that B can be estimated

reasonably well from atom fragment constants (Table 10), then the aqueous solubility of PAHs could be estimated directly from structure using Equation 38.

4.9. Estimation of the Sub-cooled Liquid Vapor Pressure for Polycyclic Aromatic Hydrocarbons

The sub-cooled liquid vapor pressure plays an important role in establishing the vapor phase concentration in equilibrium with organic matter in environmental systems. Experimental values are available for the PAHs in Table 6 except for azulene and 9,10-dimethylanthracene.[79] Quina and coworkers have proposed a model for the estimation of the vapor pressure for organic compounds using a modified form of the solvation parameter model.[80] This model includes a fitting factor to modify the dipolarity/polarizability (S) descriptor for different compound types and a cross-product term (AB) to take into account differences in hydrogen-bonding in the liquid state for different compound types. Before exploring this complex relationship we looked for a simpler model that could be applied to PAHs without seeking a general model for all compound types. There is a simple relationship between the sub-cooled liquid vapor pressure log VP (Pa, 25 °C) and the gas-hexadecane partition coefficient at 298 K (L descriptor).

$$\log VP = 7.110 \ (\pm 0.092) - 1.063 \ (\pm 0.010)L \qquad (39)$$

$$r = 0.999 \qquad SE = 0.107 \qquad F = 11092 \qquad n = 20$$

Equation 39 is suitable for estimating the vapor pressure for PAHs. Although L is not predicted accurately it is estimated reasonably well from structure for PAHs containing fused benzene rings (Table 9). Equation 39 would facilitate a general estimate of the sub-cooled vapor pressure for

PAHs where some additional uncertainty can be tolerated due to using estimated L descriptor values. There is a less useful relationship containing the V descriptor

$$\log VP = 9.111 \ (\pm 0.497) - 2.904 \ (\pm 0.371)S + 4.533 \ (1.739)B - 5.333 \ (\pm 0.902)V \qquad (40)$$

$$r = 0.996 \qquad SE = 0.264 \qquad F = 608 \qquad n = 20$$

Equation 40 requires an additional knowledge of the dipolarity/polarizability (S) and hydrogen bond basicity (B) descriptors to predict vapor pressures. Equation 39 is more accurate and precise as well as simpler to use.

4.10 Conclusions

Chromatographic retention factors combined with liquid-liquid partition coefficients afford a flexible approach for the calculation of descriptors for compounds with a wide range of solubility characteristics.[6a, 10, 19] The use of totally organic biphasic systems overcomes the difficulty of using aqueous based systems for compounds of low water solubility. The descriptors calculated for the polycyclic aromatic hydrocarbons and related compounds were shown to be suitable for the accurate estimation of their physicochemical properties as well as demonstrating the reliability of the descriptors for additional applications using the large number of existing models formulated on the basis of the solvation parameter model for chromatographic, environmental and biological transport and distribution properties.[10]

CHAPTER 5

CONCLUSIONS ON SOLVENT SYSTEM CHARACTERIZATION AND DESCRIPTOR DETERMINATIONS

The determination of descriptor values for organic compounds will facilitate the estimation of their properties in environmental systems. The characterization of totally organic liquid-liquid partition systems contributes to this goal by providing appropriate systems for the experimental determination of descriptors with high accuracy.

In Chapter 2, ethanolamine was characterized as a base solvent with heptane and isopentyl ether as counter solvents. Two models were developed with high statistical quality. Both systems are suitable for the determination of the hydrogen bond acidity (A) descriptor and both models increase the selectivity space for determining descriptor values. The value of 4.533 for the hydrogen-bond basicity system constant for the ethanolamine-heptane biphasic system is the highest reported so far for a two-phase liquid-liquid partition system. The ethanolamine systems were used to facilitate the determination of descriptor values for a group of polycyclic aromatic hydrocarbons and related compounds.

In Chapter 3, triethylamine was characterized as a counter solvent with dimethyl sulfoxide, ethanolamine, and formamide as base solvents. A model with high statistical quality was developed for each system. The triethylamine-formamide system is suitable for the determination of the hydrogen bond-basicity (B) descriptor as it has a moderate hydrogen-bond acidity system constant value of 1.601.

In Chapter 4, descriptor values were determined for a group of polycyclic aromatic hydrocarbons and related compounds. The descriptor values were used to estimate partition coefficients for octanol-water, air-octanol, air-water systems and also for estimating the aqueous

solubility and sub cooled liquid vapor pressure of these compounds. When the determined descriptor values are applied in the environmental models, the average absolute error for the difference between calculated and experimental partition coefficients for octanol-water, octanol-air, and air-water partition coefficients are 0.085, 0.105, and 0.177, respectively. The small absolute average error indicates that the determined descriptor values are accurate and homogeneous as a group. A theoretical atom fragment constant model was also built to estimate descriptor values directly from the molecular formula. Two local models for solubility in water and sub-cooled liquid vapor pressure were constructed which are suitable for the prediction of solute property values.

The environmental properties were estimated without bias using the newly determined descriptor values. Since the selected group of polycyclic aromatic hydrocarbons possesses different solubility in environmental systems, the determination of reliable descriptor values is a significant contribution to accurately estimate their solute properties in environmental systems.

CHAPTER 6

INTRODUCTION TO ATOMIC LAYER DEPOSITION

6.1 Applications of Atomic Layer Deposition in Microelectronics Industry and Other Areas

The rapid development in the microelectronics industry during the last five decades was mainly a result of scaling down of microelectronic devices and integrated circuits following Moore's law, which stated that for integrated circuits, the number of transistors per unit area approximately doubles every two years.[81] Miniaturization of microelectronic devices increased the packing density of electronic memories, increased the speed and performance of microprocessors, and decreased the cost of microelectronic devices.[82] According to the predictions of the International Technology Roadmap for Semiconductors (ITRS), which defines the requirements and advances in the future semiconductor technology, the microelectronic device sizes will reach the 7 nm node in 2018 and 5 nm node in 2020.[83] Past technology nodes indicate that for both dynamic random access memory (DRAM) half-pitch (half of the distance between two adjacent metal pathways) and complementary metal oxide semiconductor (CMOS) field-effect transistor gate length (Figure 16), feature sizes have reduced faster than the values predicted by the corresponding technology node.

The downscaling of silicon dioxide, which is used as the capacitor dielectric in DRAMs, and as the transistor gate dielectric in CMOS logic devices leads to unacceptable levels of leakage currents.[81c, 84] Therefore, new materials having high dielectric constant values were introduced to replace silicon dioxide in memory and logic devices. The size reduction of devices also caused the metal cross section of interconnect structures to decrease.[85] The decrease in cross

section enhanced the interconnect resistance, resulting in signal propagation delays between transistors. Therefore, copper and materials having low dielectric constant values were introduced to replace aluminum alloy-silicon dioxide interconnects.
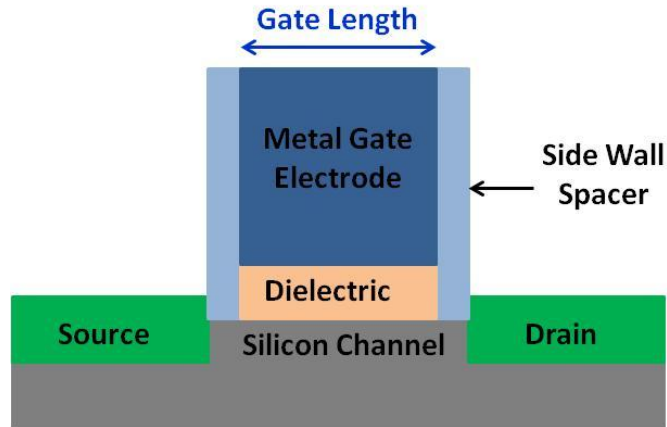

Figure 16. Cross-Section of a Basic Metal Gate in a Metal Oxide Semiconductor Field Effect (MOSFET) Transistor.[86]

When microelectronic device dimensions decreased, the complexity of the topography of integrated circuits increased.[87] It was necessary to deposit thin films of materials on three dimensional structures having a high aspect ratio (via holes having a high ratio between the depth and the diameter) features. To obtain the required level of performance of the microelectronic devices, a thin film deposition technique which produces highly uniform, conformal (having the same thickness on all exposed parts of a three dimensional structure) thin films with atomic scale thickness control was needed. To satisfy the above requirements, atomic layer deposition (ALD) was identified as the most suitable thin film deposition technique.

Other than microelectronic devices, currently ALD is used as a thin film deposition method in many application areas, including magnetic heads, thin film electroluminescent flat panel displays, protective and antireflective coatings, nanostructured solar cells, fuel cells, lithium batteries, metal oxide semiconductor gas sensors, photonic devices, nanomaterial

fabrications, and catalysts.[88] The ability of ALD to produce thin films with an excellent control of thickness, composition, mechanical and chemical properties on surfaces having nanoscale dimensions and intricate shapes and porosities resulted in its popularity as a major thin film deposition method.

6.2. Thin Film Deposition Techniques

Physical vapor deposition (PVD), chemical vapor deposition (CVD), and atomic layer deposition (ALD) are the three most commonly used gas phase methods to deposit thin films in microelectronic devices.[81a]

6.2.1 Physical Vapor Deposition (PVD)

In PVD, atoms or molecules of a solid or liquid source material are removed and transported in a vacuum chamber to a substrate.[89] The atoms or molecules which impinge on the substrate condense and form a film. The source materials have vapor pressures which are much lower than the working pressure of the deposition system. Atoms are removed from the source either by evaporation or sputtering (Figure 17).
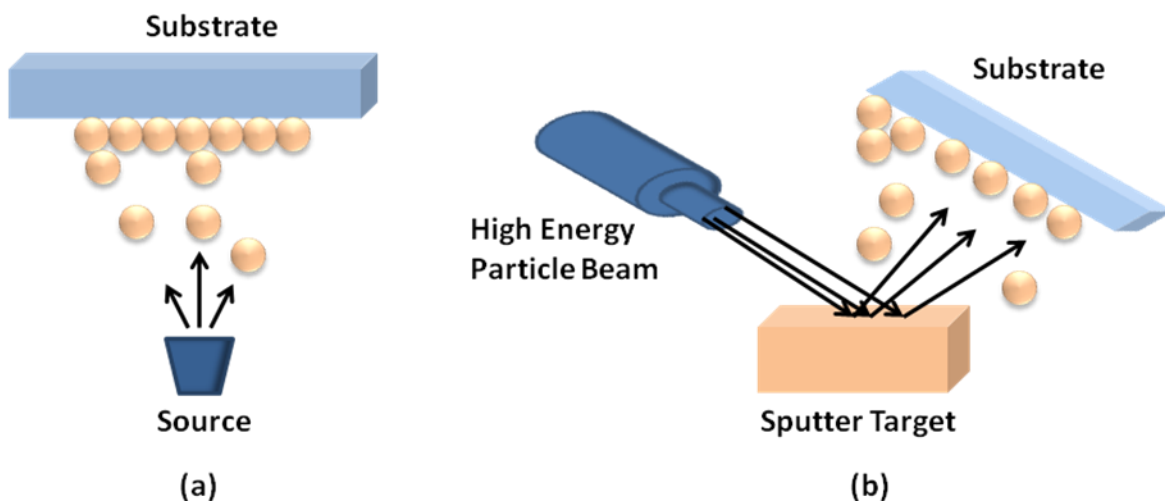
Figure 17. Physical Vapor Deposition Using (a) Evaporation and (b) Sputtering Methods.[89a, 90]

Evaporation methods can be classified into two main categories as quasi-equilibrium and non-equilibrium processes.[90] In quasi-equilibrium processes the source material is in a heated effusion cell, which has a large interior surface area compared to its orifice. The source material evaporates and escapes through the orifice. During the evaporation process, heated source material is in a nearly steady state equilibrium with the vapor. In non-equilibrium processes, source material is kept in an open container such as a boat or crucible. Therefore, when the source material evaporates, the vapor pressure above the source is lower than the equilibrium vapor pressure, and the evaporated atoms do not return to the source. In both processes, the source is heated to a temperature above its melting point. Resistive heating is used to heat the containers, while an electron beam is commonly used to heat the source in non-equilibrium processes. Unlike evaporative methods in which atoms are thermally emitted from the source by heating, sputter deposition removes surface atoms by bombarding the source or the target material with a high energy particle beam. The high energy beam consists of ions of an inert gas, but it can consist of any ion, molecule, atom, or photon having sufficient energy. The sputtered atoms are directed under vacuum to the substrate to be coated.

6.2.1.1 Physical Vapor Deposition of Alloy Films

Alloy films can be formed using evaporative methods, by keeping two adjacent sources with the required materials which are necessary to form the binary compounds, and adjusting the rate of emission of sources to the required level to get the correct composition of the alloy. Composition can also be adjusted by varying the distance between the sample and the source. Flash evaporation, in which a small amount of sample source is heated and evaporated to a temperature above the melting point very rapidly, and reactive evaporation, in which a second element is added to the vacuum chamber, are the other two methods for forming alloy films using

evaporative PVD. Nitrides are formed by using a variant of reactive evaporation in which a plasma or ionized beam of the second element is used as the reactive species. However, evaporative PVD is not widely used for the formation of alloy films, since sputter deposition, which utilizes a target having the accurate composition, is a more convenient method to form alloys. In situations where the sputter yield may change to varying degrees for two different elements, in order to obtain the accurate composition of the film the surface composition of the target is changed such that the surface composition is inversely proportional to the relative sputter yield of the two elements. Reactive sputter deposition is carried out in sputtering PVD by adding a second reactive gas species to the chamber.

6.2.1.2 Directional Nature of Physical Vapor Deposition Methods

For evaporative PVD, line-of-sight depositions are observed under vacuum conditions as a result of direct transport of source material to the substrate without undergoing collisions with background gas atoms. Sputter PVD is relatively non-directional compared to the evaporative PVD, due to the collisions occurring with the sputtered atoms in the gas phase. However, in high aspect ratio features, both evaporative and sputtering methods produce films with poor step coverage (ratio between the thickness of a film on a side wall or on the bottom of the step to the thickness of a film at the top of the step) arising from the directionality of the PVD methods and the low surface migration of the deposited atoms. Poor step coverage and non-conformal coating of thin films can severely affect the performance of the microelectronic devices as the electrical properties of these non-ideal films can deviate considerably from their bulk values for the considered thickness range.[81a] Therefore, despite the fact that PVD methods produce high purity films, and have a high production volume owing to high deposition rates, PVD is not a promising

thin film deposition method for the fabrication of high aspect ratio features in microelectronic devices.

6.2.2 Chemical Vapor Deposition (CVD)

Chemical vapor deposition employs gas phase chemical reactions to deposit a thin film of material on a heated substrate surface.[91] CVD precursors are delivered to the reaction chamber using an inert gas such as argon, nitrogen, or helium.[92] After being delivered to the surface, precursors diffuse and adsorb on the surface, and a chemical reaction takes place which produces the required material. The gaseous byproducts are carried out of the chamber using an inert gas stream to an exhaust system (Figure 18). CVD uses many types of reactions.[93] Thermal decomposition or pyrolysis, hydrogen reduction, co-reduction, hydrolysis, and disproportionation reactions are widely used in CVD. Oxygen, methane, and ammonia gases are used as the reactive species for the oxidation, carburization, and nitridation reactions.
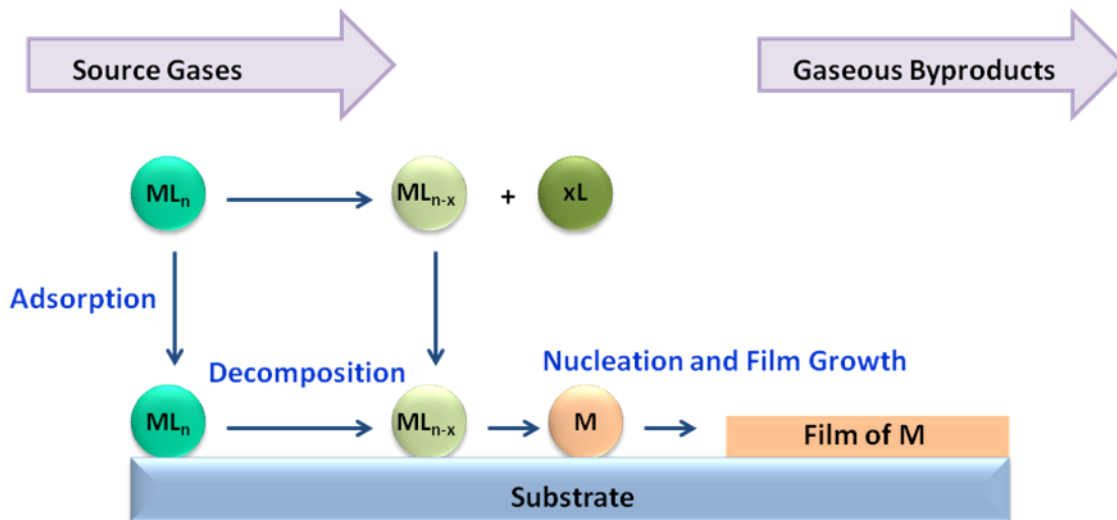
Figure 18. Sequence of Steps for the Formation of a Metal M, from the Precursor ML_n Using CVD.

CVD precursors should be sufficiently volatile to be efficiently delivered to the substrate, and should be able to produce in acceptable yields with a high degree of purity. Precursors also should be able to react without parasitic reactions or side reactions at the desired substrate temperature. If the temperature and the concentration of the precursors introduced to the reaction chamber are high, gas phase precipitation of particles can occur. The formed particles can incorporate into the thin film creating a non-uniform and a rough surface. To avoid gas phase precipitation, the gas pressures are usually kept below 10^{-4} Torr.[94] Factors such as temperature, surface area of the substrate, flow rates of the incoming source gases and outgoing gases affect the partial pressure of the precursor at the substrate.[95] Therefore, these factors should be monitored carefully in order to obtain uniform films. The growth rate of the film depends on the precursor fluxes at steady state and the reaction kinetics on the surface.[96] In CVD, the reactive sticking probability (S_R) indicates the fraction of the molecules which will stick on the surface when an incident flux hits the substrate.[92] The highest values S_R can get are near unity, which occurs in CVD for highly reactive precursors if they dissociate or chemisorb at the point of impact on the substrate, resulting in non-conformal film growth. Conformality can be achieved by the use of more thermally inert precursors. However, the reduced reactivity of precursors can cause low deposition rates.

6.2.3 Atomic Layer Deposition (ALD)

Line of sight delivery of highly reactive precursors in PVD, and the high sticking probability of CVD precursors at the initial point of contact of the substrate, cause the thin film material to accumulate near the top wall and on the bottom surface of the trenches with high aspect ratios, resulting in non-conformality of films (Figure 19 (a)). Atomic layer deposition,

which is a variant of chemical vapor deposition, produces highly conformal thin films due to its

inherently self-limiting surface reactions (Figure 19 (b)).[81a]
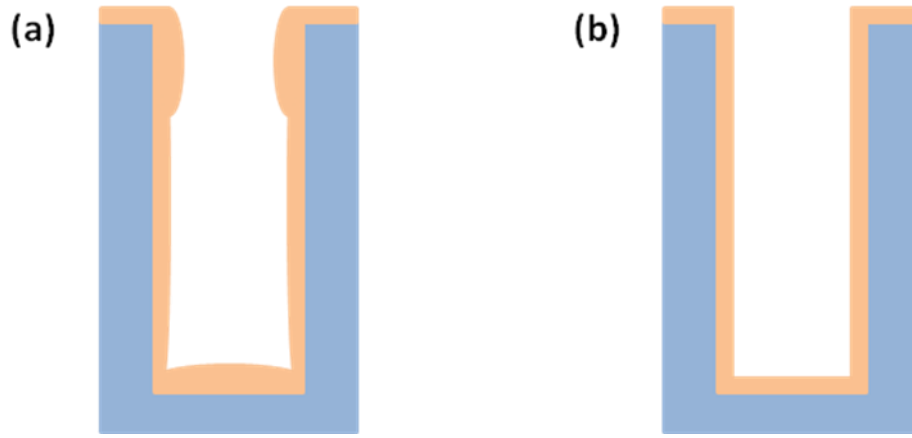
Figure 19. A Thin Film Deposited on Top, Side, and Bottom Walls of a Trench Demonstrating, (a) Non-conformal Coverage, and (b) Conformal Coverage.

The ALD principle, where the deposition proceeds through self-limiting sequential half

reactions was invented by Prof. S. I. Kol'tsov and Prof. V. B. Aleskovskii from Leningrad

Technological Institute under the concept of 'molecular layering' in the 1960s. The ALD

production technique was proposed by Dr. Tuomo Santola and co-workers in Finland in the

1970s gaining ALD a worldwide recognition as a useful thin film deposition technology.[97]

In ALD, film growth proceeds by exposing the substrate surface to alternate precursor

pulses in a cyclic manner.[98] The precursors are kept separate in the gas phase using inert gas

purges between pulses. Figure 20 illustrates the four major steps in an ALD cycle using the

growth process for Al_2O_3 thin films using trimethylaluminum and water, which is considered as a

model process in ALD.[99] In the first step, substrate surface is exposed to the pulse of the first

gaseous precursor trimethylaluminum, and the precursors are allowed to chemisorb on the

surface hydroxyl groups. The reaction of trimethylaluminum with surface hydroxyl groups

release methane as the byproduct. In the second step methane is removed from the deposition chamber together with excess trimethylaluminum precursor using an inert gas purge. In the third step, the surface is exposed to water. The reaction of water with the methyl groups of the chemisorbed trimethylaluminum precursor produces an Al_2O_3 thin-film material. In the final step, the methane byproduct formed in the third step is removed together with excess water using another inert gas purge. The ALD growth cycle is repeated to obtain the required film thickness.
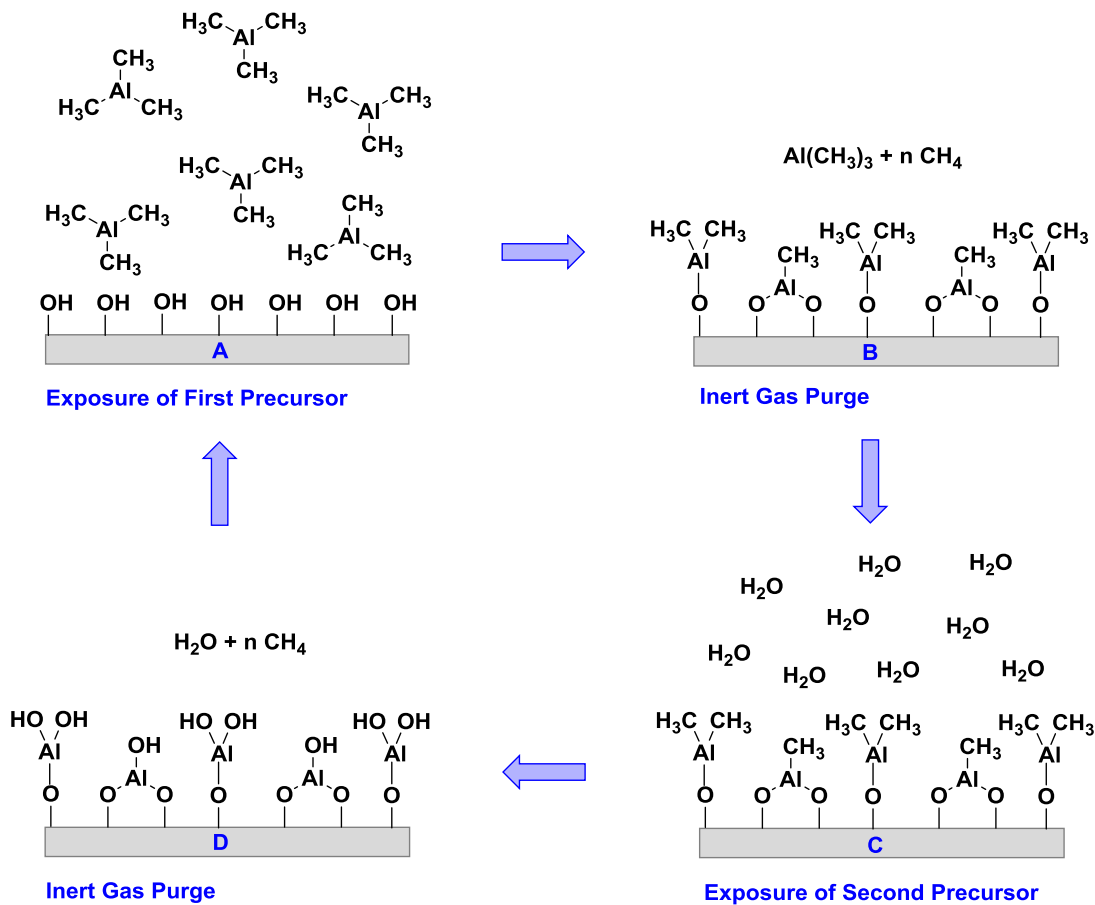
Figure 20. ALD Growth Cycle for the Growth of Al_2O_3 Thin Films from Trimethylaluminum and Water.

Precursors that lead to exothermic reactions with a negative free energy of reaction (ΔG) are preferred in ALD.[100] Ideally, when the precursor dose is high enough, and when there is sufficient energy for the reaction to proceed, precursors react with the surface saturatively.[101] After one chemisorbed layer is formed, the excess precursor molecules do not react or adsorb any further on the surface. This self-limiting growth mechanism results in deposition of a constant amount of thin-film material in each cycle. Therefore, in the ALD processes when the surface receives a sufficient concentration of precursors to achieve surface saturation, the growth rate stays constant with precursor pulse length (Figure 21).[102]
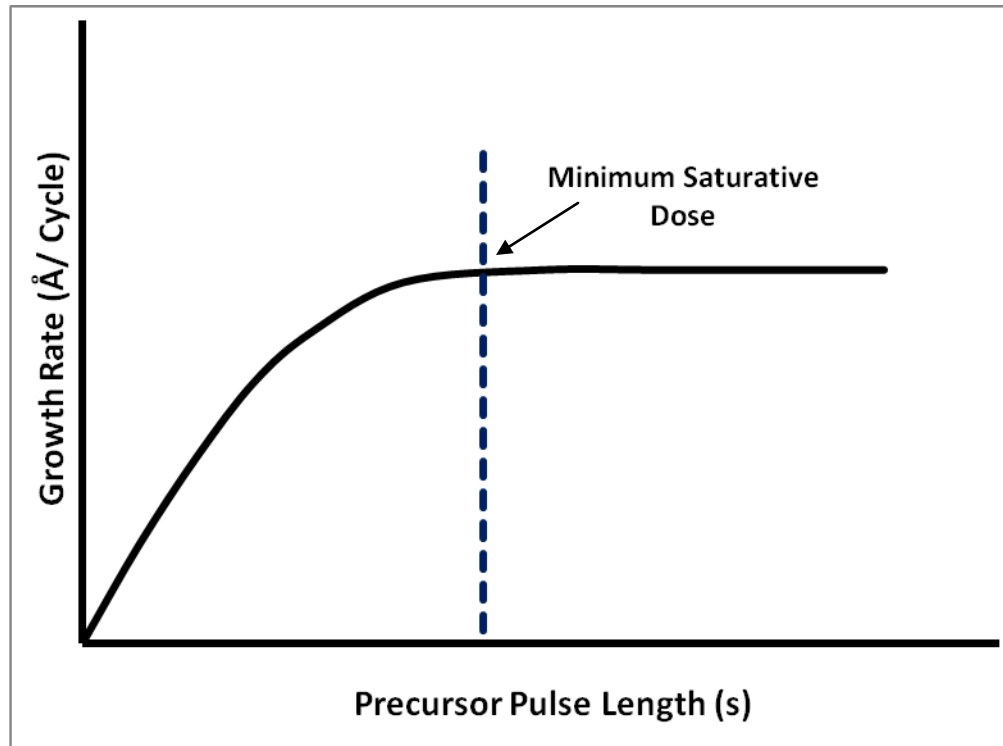
Figure 21. A Plot of Growth Rate Versus Precursor Pulse Length.

Although not a definite requirement, many ALD processes possess an ALD window, which is a temperature range where the film growth takes place by self-limited, surface controlled reactions and the growth rate remains constant (Figure 22).[98, 101c] Outside the limits of

the ALD window, at low deposition temperatures, film growth often decreases due to the lack of sufficient thermal energy for the reactions to attain completion. The growth rate can increase at low deposition temperatures due to the condensation of precursors on the substrate surface. At high deposition temperatures the growth rate often increases due to decomposition of the precursors. However, growth rate can decrease due to desorption of precursors from the substrate surface. If the substrate surface contains silanol groups, at high deposition temperatures, loss of water molecules and formation of bridging oxygen on the substrate surface can also lead to a reduced growth rate.
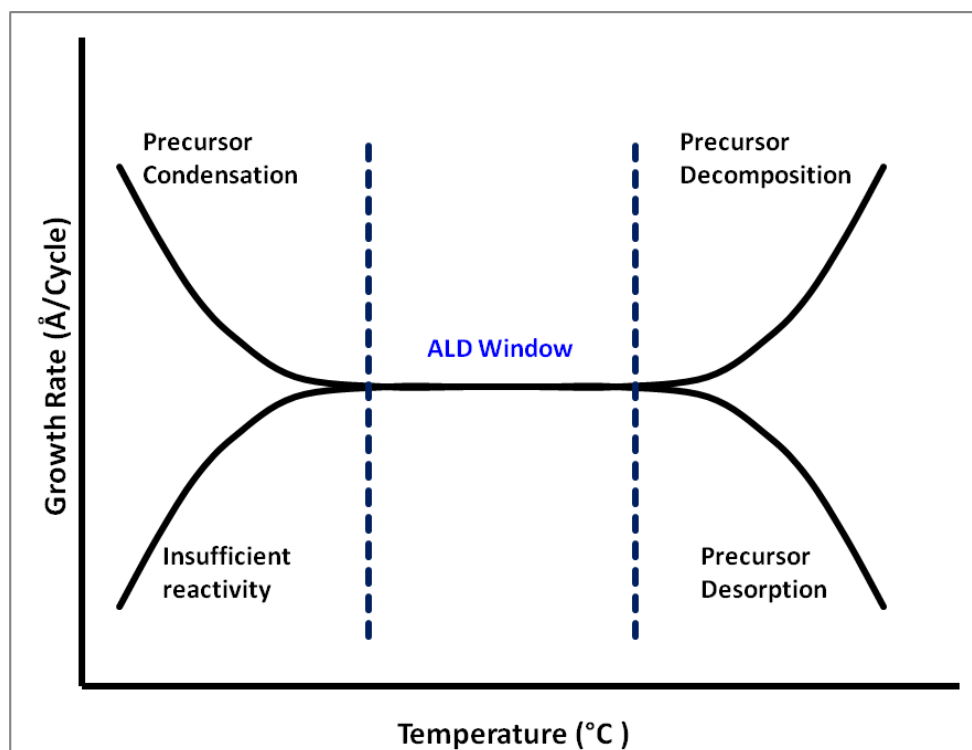
Figure 22. Schematic Illustration of an ALD Window.

Theoretically, one monolayer of thin film material should be deposited in one ALD cycle.[98, 103] However, under practical conditions, usually less than or equal to half a monolayer per cycle is formed due to steric hindrance of the precursors, which limits the number of

precursors reacting with or adsorbing on the surface. The limited number of reactive surface sites can also be a factor, which results in less than monolayer growth per cycle. Therefore, several ALD cycles may be needed to complete one monolayer. However, this is not considered a significant problem, as the film growth can still proceed layer-by-layer.

Due to the self-limited growth mechanism, ALD can be used to grow thin films with accurate thickness control and excellent conformality on complex topographies.[98, 101, 104] Uniform, dense, and pinhole-free films can be obtained over large areas with straightforward scale-up of films. In contrast to CVD, separation of precursor pulses using inert gas purges prevents the occurrence of gas phase reactions, and it is not necessary for the precursor flow to be homogeneous. The ability to generate precursor molecules in situ allows the usage of freshly prepared complexes, which are otherwise unstable. Within the ALD window, the film growth rate is reproducible regardless of small changes in temperature.

The main drawback of ALD is the low thickness increase of films per unit time, which results in low throughput.[98] Generally, a promising ALD process would exhibit approximately 100 nm h^{-1} deposition rate. To increase the production, batch processing can be used where the batch reactors are available with the facility of processing up to 150 wafers in a single load. The effective deposition rate can also be increased by the selection of proper precursor chemistry, which yields fast reaction kinetics and low cycle times.[98, 100] Another approach which is capable of increasing the throughput is spatial ALD, which operates under atmospheric pressure.[96-97, 105] In spatial ALD, precursors are confined to separate precursor zones, and the deposition is carried out by moving the substrate from one zone to the other sequentially. To prevent gas phase reactions, two precursor zones are separated by an inert gas flow. Spatial ALD eliminates the long purge times that conventional ALD need between the precursor pulses to purge the reactor.

As a result, the thickness of films produced by spatial ALD can reach the nanometers per second range. A modification of spatial ALD is the roll-to-roll ALD, which consists of a central drum that contains different precursor zones separated by inert gas flow zones.[105a] Depositions are carried out by moving a flexible substrate over the drum. The distance from the substrate to the outer surface of the drum is kept constant. Coating of substrates which are 300 mm wide and 1000 m long and up to 100 ALD cycles per pass are anticipated using this method in the future.

6.3 Precursors for Atomic Layer Deposition

Since ALD reactions occur only on the substrate surface in a self-limiting and saturative manner, and gas-phase reactions should be avoided, ALD precursors should have some specific properties.[98, 101b, 101c] Precursors must be sufficiently volatile at the deposition temperature. Gases and liquids having high vapor pressures can be efficiently transported to the reaction chamber with high fluxes. Solids which give appreciable vapor pressures at the deposition temperature can be used. Self-decomposing or self-reacting precursors should be avoided in the considered temperature limits, as they are likely to undergo side reactions in the gas phase or on the substrate surface.[100] Precursors must readily adsorb or chemisorb on the surface sites, and must readily react with the second precursor. Low deposition temperatures and low cycle times can be obtained using rapid and complete surface reactions. Precursors should not etch the substrate or the growing film. The byproducts must be volatile so that they can be easily removed from the deposition chamber. Byproducts must also be unreactive. Reactive byproducts can etch the film and the substrate, and can block the surface reactive sites by readsorption. Further, they can cause the corrosion of the reactor. The availability of precursors at a reasonable cost, and to be able to handle safely are two desirable properties.

Metal precursors for ALD consist of several categories, which include volatile metal halides,[106] metal alkoxides,[107] metal β-diketonates,[108] metal alkyls,[99, 109] metal cyclopentadienyls,[110] metal alkyl amides,[111] metal silyl amides,[112] metal amidinates and guanidinates,[113] pyrazolyl borates,[114] and metal alkylsilyl compounds.[115] Non-metal precursors can also be grouped into a few categories.[115a, 115b] Hydrogen has been used widely as a reducing agent. Metallic zinc vapor, boranes, and silanes have also been used successfully as reducing agents. Water, oxygen, ozone, nitrous oxide, and dinitrogen tetroxide are used as oxygen sources. To form nitride thin films, both a nitrogen source and a reducing agent are required. Ammonia is commonly used in the formation of metal nitrides. Other nitriding agents which have been used are hydrazine (N_2H_4), 1,1-dimethyl hydrazine ((CH_3)$_2$NNH$_2$), *tert*-butylamine ($^tBuNH_2$), and allyl amine ($CH_2CHCH_2NH_2$). Chalcogenide thin films can be deposited using elemental S, Se, and Te only in the situations where the other precursor is sufficiently volatile and reactive. In common use, H_2S, H_2Se, and H_2Te are employed to form the corresponding chalcogenide thin film material.

6.4. Thermal and Energy Enhanced ALD Processes

6.4.1 Thermal ALD

In ALD, precursor adsorption and ligand exchange reactions need to traverse the energy activation barrier in order for film growth to take place.[96, 116] ALD processes are classified mainly into two groups as thermal ALD and energy enhanced ALD, depending on how the energy is supplied to drive the ALD half-reactions.[117]

In thermal ALD processes, energy is supplied as heat to the precursors and to the substrate.[96, 116-117] Substrates are kept at elevated temperatures, typically between 150 and 350 °C. If the ALD half reactions have a negative change in free energy ($\Delta G < 0$) the activation

barrier can be overcome readily. Exothermic reactions with negative change in enthalpy ($\Delta H < 0$) are often used in ALD processes. However, when the reaction enthalpy change is positive ($\Delta H > 0$), a large positive entropy change can create a favorable thermodynamic driving force for the reaction. Efficiency in thermal ALD processes can be enhanced by using more reactive precursors or co-reagents. For example, fast reactions can be obtained by using hydrogen peroxide instead of water, and hydrazine instead of ammonia, for the growth of oxide and nitride films, respectively. The two major hindrances for thermal ALD processes are the lack of sufficient thermal energy at low deposition temperatures leading to lower growth per cycle and higher impurity contents, and the lower thermal stability of precursors at high deposition temperatures leading to parasitic CVD like reactions. Lack of thermal energy can limit the lower end of the ALD window, while precursor decomposition can limit the higher end of the ALD window.

6.4.2 Energy Enhanced ALD

Thin films with improved growth characteristics can be obtained by energy enhanced ALD methods at low deposition temperatures.[117] Highly thermally stable precursors, which have low reactivity in thermal ALD processes, can be used readily in energy enhanced processes, although at high deposition temperatures. In energy enhanced ALD, the co-reactant is a highly reactive species which has a short term stability, such as reactive neutral molecules, ions, and radicals. Generation of the reactive species is carried out by applying additional energy to gaseous co-reactants using a variety of methods such as electrical discharges, thermal cracking (hot-wire ALD), and UV photodissociation.

6.4.2.1 Plasma ALD

Plasma enhanced ALD is the most widely used energy enhanced ALD process, which is used as an alternative to thermal ALD.[118] A plasma is a mixture of gaseous mono and multinuclear ions, radicals, electrons, and meta-stable excited species which is on average, quasi-neutral.[117, 119] By adjusting the composition and properties, such as gas flow, pressure, plasma power, and exposure time, selective reactivity on the substrate surface can be obtained. The heat flux supplied to the substrate surface by plasma is low, although ion bombardment results in additional energy to the surface which is dissipated by the surface species. The dissipation of the extra energy can increase the reaction rates and surface diffusion of the deposited material. Due to the increased reactivity of the plasma, the thin films deposited by plasma processes can have high film density, a lower impurity content, and improved electrical properties. Chemically and thermally stable precursors, and substrate surfaces which have been found challenging in thermal processes, can be readily used to deposit thin-film materials using plasma processes. The ability to change the composition and operating parameters of the plasma allows the deposition of thin-film material with a good control of stoichiometry. Since a plasma can be turned on and off rapidly, purge times are reduced, which cause the growth rate to increase. Due to the high reactivity, the nucleation delay for the plasma processes can be lower than for the thermal ALD processes. Short cycle times and fast nucleation increases the throughput in the plasma processes.

However, plasma radicals can recombine on the walls of the reactor and on the substrate surface to form non-reactive molecules. The surface recombination probability (r), which can have a range of values from approximately 10^{-6} to 1, indicates the probability of the recombination reactions. In order to deposit materials in high aspect ratio structures and porous surfaces, plasma radicals have to undergo multiple collisions, which results in a higher

probability of radical recombinations and a reduced radical flux. Therefore, it is difficult to obtain conformal films with good step coverage on high aspect ratio features using plasma ALD. Good conformality can be achieved using long plasma exposure times. However, for aspect ratios ≥ 30, the duration of the plasma exposure times required are too long, and therefore impractical. A plasma contains a variety of gas phase and surface species, which can sometimes induce undesired reactions. Plasma-induced damage can result from the impact of high energy particles, which can create defects inside the material and on the surface. Further, a plasma requires the ALD reactors to have additional complex equipment when compared with thermal ALD. Due to the inherent disadvantages of the plasma processes mentioned above, in industrial applications, plasmas are used only in situations where they can provide significant benefits over thermal ALD. Thermal ALD, therefore, is still the mainstream ALD process.

6.5 Low Temperature ALD

The semiconductor industry, which is the key driver for ALD technology, demands low-temperature depositions in order to avoid inter-diffusion of materials at elevated temperatures, and to obtain smooth, high purity films with low resistivity.[117, 120] To prevent the films suffering from thermally induced stress and to obtain high quality films, deposition temperatures of ≤ 150 °C are preferred.

Plasma ALD can be used to carry out depositions at low temperatures, but the films deposited lack conformality, and suffer from plasma induced damage as mentioned in section 6.4.2.1. There are only a few thermal ALD processes carried out at low temperatures that demonstrate favorable thermochemistry to obtain high quality thin films. The main challenge in low temperature depositions is the lack of thermal energy to drive the surface reactions. There are significant nucleation delays observed at low temperatures, which leads to island-like film

growth and rough films. Due to the increased probability for precursors to condense on the surface and reactor walls, long purge times are required. Therefore, long processing times are needed at low temperatures, leading to low growth per cycle values. Trimethylaluminum used in the formation of Al_2O_3 thin films is generally known as an ideal precursor capable of reacting even at room temperature. Groner and coworkers reported that the average density of amorphous Al_2O_3 films are around 3.0 g cm^{-3} when deposited at 177 °C, and reduced to around 2.5 g cm^{-3} for depositions at 33 °C.[121] Due to incomplete reactions and the low vapor pressure of precursors and byproducts, the incorporation of impurities in films at low deposition temperatures can be high.

Apart from Al_2O_3 ALD, other ALD systems which were well developed for low-temperature depositions below 100 °C, owing to good precursor reactivity, include deposition of TiO_2 using $TiCl_4$ and water[122] or $Ti(OiPr)_4$ and water[123] and deposition of ZnO using $Zn(CH_2CH_3)_2$ and water,[124] and deposition of ZrO_2 using TDMAZr (tetrakis(dimethylamido)zirconium(IV)) and water.[125] Some of these low-temperature depositions have extended the application range of ALD by enabling the fabrication of polymers, organic materials, and biomaterials.[120b, 122a]

In addition to conventional two-step ALD processes, three-step processes which were originally developed by Niinistö and coworkers have been used to obtain thin-film materials via an additional intermediate step.[122a, 126] Winter and coworkers employed a copper alkoxide precursor, an acid, and a reducing co-reagent in a three-precursor sequence to produce copper metal thin films at low substrate temperatures.[127] In the three-step process, the copper precursor $Cu(OCHMeCH_2NMe_2)_2$ does not react with anhydrous hydrazine, which is a strong reducing co-reagent. Instead, the copper precursor was first converted to copper(II)formate by reacting with

formic acid, which is then reduced to copper metal using anhydrous hydrazine. This process afforded copper metal thin films within an ALD window between 100-160 °C on Si(100) substrates. Thin films consisting of high purity copper metal having low resistivity (9-16 µΩ cm) were obtained. The films were of an average surface roughness, which is approximately 3.5 nm for a 50 nm thick film deposited at 120 °C.

6.6 Chemically-Catalyzed Thermal ALD Processes for Low Temperature ALD

The quest to find optimum low-temperature depositions is stretching the limits of ALD process technology. A key factor for obtaining an efficient low-temperature ALD process is the high reactivity of precursors which leads to strong exothermic reactions. A major challenge that affects the field of ALD, and particularly low-temperature ALD, is the low reactivity of precursors, which makes surface reactions impossible or makes them possible only at higher temperatures. Use of a catalyst can drive the reaction at lower temperatures.

There are several examples for chemically-catalyzed ALD processes where a catalyst is mixed with a reactant and supplied to the surface together with the gas-phase reactant flow.[128] George and coworkers developed Lewis base catalyzed silicon dioxide ALD, using pyridine or ammonia as the catalyst (Chart 1).[120b, 128a, 128b]

$$\text{SiCl}_4 + 2\ \text{H}_2\text{O} \longrightarrow \text{SiO}_2 + 4\ \text{HCl} \quad \Delta H = -32\ \text{kcal} \quad (1)$$

ALD Half Reactions

$$\text{SiOH*} + \text{SiCl}_4 \longrightarrow \text{SiOSiCl}_3\text{*} + \text{HCl} \quad (2)$$

$$\text{SiCl*} + \text{H}_2\text{O} \longrightarrow \text{SiOH*} + \text{HCl} \quad (3)$$
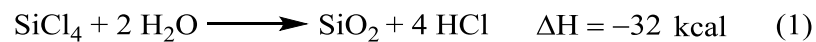
Asterik (*) indicates surface species, bonded to the surface by a silicon atom

Chart 1. Reaction Steps for the Silicon Dioxide ALD Process.

Although the reaction of SiCl$_4$ with water has a negative reaction enthalpy, the reaction is slow and occurs at temperatures > 325 °C on Si(100) substrates only with a large amount of reactant exposure. A Lewis base, like pyridine or ammonia can hydrogen bond with surface - SiOH during the first ALD half reaction with SiCl$_4$, weakening the SiO-H bond, and thereby, making the oxygen atom a stronger nucleophile. The increased nucleophilicity of the oxygen atoms facilitate the nucleophilic attack of oxygen on the silicon atom of SiCl$_4$. In a similar manner, the hydrogen bonding between the Lewis base and water in the second ALD half reaction facilitates the nucleophilic attack by the oxygen atom of water on the silicon atom of surface –SiCl. Although this method brings the reaction temperatures close to room temperature, a major drawback is the possibility that the Lewis base will react with the HCl byproduct, forming a salt which can accumulate over time and poison the surface. Use of tetraethoxysilane (Si(OCH$_2$CH$_3$)$_4$) instead of SiCl$_4$ prevents salt formation.[129] However, the reaction with tetraethoxysilane is much slower. Another disadvantage is that the Lewis bases can catalyze the surface reactions within a limited temperature range only. As the catalyst should have a sufficient vapor pressure in order to be efficiently delivered to the surface, the method of adding the catalyst extraneously, mixed with the reactant is limited to a narrow range of ALD reactions. A self catalytic SiO$_2$ process was reported using 3-aminopropyltriethoxysilane, water, and ozone.[130] However, precursor systems which exhibit self catalysis are rare.

Rapid SiO$_2$ ALD is another process which uses aluminum catalyst from a trimethyl aluminum precursor, which is initially chemisorbed on the substrate.[131] The process developed by Gordon and coworkers employed alternating exposure of trimethylaluminum and tris(*tert*-butoxy)silanol to the surface, resulting in deposition rates that are more than a hundred times greater (one silanol flux resulting in thickness up to ~120 Å SiO$_2$ layers) than rates obtained by

other conventional SiO_2 deposition processes. Growth of siloxane polymer chains occurs at aluminum catalytic sites.[131-132] Eventual cross linking of the polymer chains results in a dense SiO_2 film and self-terminates the growth, preserving the ALD characteristics. Therefore, a new ALD cycle can begin with another exposure to the trimethylaluminum vapor on newly formed silanol surface. However, initial depositions were carried out at higher substrate temperatures (>200 °C). George and coworkers developed a rapid SiO_2 process using trimethylaluminum and tris(*tert*-pentoxy)silanol precursors.[133] Nucleation and the cross-linking rate of the siloxane polymer were dependent on the temperature, and the flux and pressure of tris(*tert*-pentoxy)silanol. Therefore, low deposition temperatures were obtained in the process by varying the silanol pressure and exposure times and by adding tris(*tert*-pentoxy)silylpyridine as an impurity. The pyridine derivatives contribute to the lower deposition temperature by catalyzing the initial nucleation and cross linking reaction. Hafnium and zirconium have also been used as the catalyst for rapid SiO_2 ALD, although they were not as effective as the aluminum catalyst.[134] Thus far, this method is limited to the growth of SiO_2 films.

6.7 Noble Metal Catalysis in Atomic Layer Deposition

Noble metals consist of elements that have a high resistance to oxidation, corrosion, chemical action, and attack by acids.[135] Ruthenium, osmium, rhodium, iridium, palladium, platinum, silver, and gold are classified as noble metals. This class of elements is widely used in chemistry to catalyze oxidation, reduction, and hydrogenation reactions. Atomic layer deposition processes where the noble metal catalysis has been utilized, can be categorized mainly as two types. The first category includes the deposition of noble metal thin films where noble metal precursors are employed, and the film growth proceeds by a mechanism where the noble metal on the deposited thin-film surface catalyze the noble metal deposition itself. The second category

includes the use of a noble metal seed layer to initiate the film growth. After this initiation step, film growth proceeds by catalysis by the deposited metal on the surface of the thin film in the instances where catalytic metals are deposited, or by ligand exchange ALD reactions. The catalyzed ALD reactions demonstrate an increase in growth rates of thin films and a reduction of the lower limit of the deposition temperatures, in comparison to the thermal ALD processes where a catalyst is not used.

In the reported noble metal ALD processes, oxygen is used as the most common reactant to obtain noble metal thin films.[136] Higher deposition temperatures (≥ 275 °C) are needed when the film nucleation and onset of film growth take place on catalytically inactive substrate surfaces, such as amorphous aluminum oxide on silicon or glass substrates.[136a, 137] Several reactions are known to take place during the oxygen-based processes. First, the noble metal precursor adsorbs on the substrate. Then the already adsorbed noble metal precursor catalytically activates oxygen by dissociating molecular oxygen into atomic oxygen.[138] The adsorbed atomic oxygen combusts the ligands of the noble metal precursor, producing a noble metal thin film. The two main byproducts are water and CO_2, although some reactions may produce hydrogen and carbon monoxide as byproducts.[135, 139] After the noble metal nuclei are formed on the substrate, this freshly prepared metal layer further catalyzes the oxygen decomposition, thereby substantially increasing the growth rate of film formation. An example for a self-catalyzed noble metal ALD process is the deposition of ruthenium metal films using bis(cyclopentadienyl)ruthenium ($RuCp_2$) and oxygen. Only a fraction of the ligands are combusted during the $Ru(Cp_2)$ pulse (Chart 2. Reactions 4 and 5). During the next consecutive oxygen pulse, the reaction goes to completion with the combustion of the remaining ligands (Chart 2. Reactions 6 and 7).

$$Ru(C_5H_5)_{2\,(g)} \longrightarrow Ru(C_5H_5)_{2\,(ads)} \tag{4}$$

$$Ru(C_5H_5)_{2(ads)} + 25x\,O_{\,(ads)} \longrightarrow Ru(C_5H_5)_{2-2x\,(ads)} + 10x\,CO_{2\,(g)} + 5x\,H_2O_{\,(g)} \tag{5}$$

$$12.5\,O_{2\,(g)} \longrightarrow 25\,O_{\,(ads)} \tag{6}$$

$$Ru(C_5H_5)_{2-2x\,(ads)} + 25\,O_{\,(ads)} \longrightarrow Ru_{\,(s)} + 5(1\text{-}x)\,H_2O_{\,(g)} + 10(1\text{-}x)\,CO_{2\,(g)} + 25x\,O_{\,(ads)} \tag{7}$$
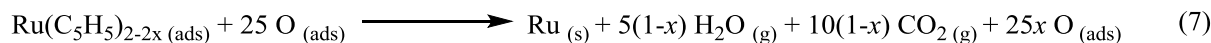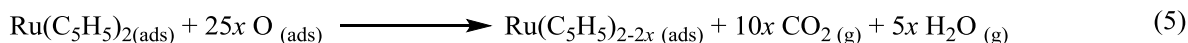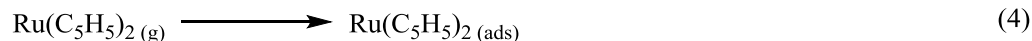
Chart 2. Reaction Steps for the Formation of Ruthenium Films from RuCp$_2$ and Oxygen.

Penetration of some dissociated atomic oxygen into the subsurface region of the deposited film was also observed during the depositions of ruthenium films at temperatures $\geq 280\ °C$.[98, 136a]

Nucleation delay periods were observed for noble metal ALD processes carried out on substrates which are not catalytically active. This problem was overcome by the use of a catalytically active seed layer in some noble metal ALD processes, which also enabled reduced deposition temperatures of around 200 °C.[140] For example, the low temperature limit of 275 °C to obtain ruthenium films from RuCp$_2$ and oxygen was brought down to 225 °C by using an as-deposited iridium seed layer. The deposition of copper metal using bis(2,2,6,6-tetramethyl-3,5-heptanedionato)Cu(II) and hydrogen on glass substrates using a platinum and palladium mixed seed layer between 190 and 260 °C had also been reported.[141] The film growth is initiated by the dissociation of molecular hydrogen to atomic hydrogen on a noble metal seed layer. The atomic hydrogen reduces the metal ion into metal atoms and cleaves the ligands. After the copper metal surface is formed, hydrogen dissociates on the freshly formed copper metal surface and the film growth continues. Deposition of palladium using palladium(II)hexaflouroacetylacetonate (Pd^{II}(hfac)$_2$) and hydrogen on an iridium surface between 60 and 230 °C was reported.[142] This process consists of an incubation period resulting from carbon contamination on the iridium

surface. The adventitious carbon is a result of high reactivity of hydrogen with $Pd^{II}(hfac)_2$. Although the onset of the film growth is initiated on an iridium substrate, the film formation proceeds through the catalysis of the reaction (dissociation of molecular hydrogen to atomic hydrogen), by palladium deposited on the surface of the thin film. The substrate reactivity effects of Ru and RuO_2 on growth of ALD aluminum oxide using trimethylaluminum and water had been studied previously.[143] The aluminum oxide deposition process was carried out on ruthenium and RuO_2 films deposited on a ZrO_2 substrate at 280 °C. In the reported ALD process, normal ligand-exchange type ALD growth takes place on Ru substrate. When the RuO_2 substrate is used, an increase in the Al_2O_3 growth rate was observed in the first few cycles due to the active participation of oxygen from RuO_2 on the reaction with trimethylaluminum. However, after the first few cycles, when the Al_2O_3 layer is formed on the surface, further ALD film growth proceeds by ligand-exchange type ALD reactions between trimethylaluminum and water.

The catalyzed ALD processes, which were carried out prior to the research work reported herein, are not solely substrate-dependent. In the noble metal atomic layer deposition processes, the film growth proceeds through the self-catalysis of the noble metal precursor by the freshly deposited elemental noble metal on the surface of the thin film. When a noble metal seed layer is used, the seed layer catalyzes the film nucleation, but the film growth proceeds through catalysis of the precursors either by freshly formed surface metal atoms in the instances where the catalytic metals are deposited, or by uncatalyzed normal ligand-exchange type reactions. Therefore, in the ALD processes carried out thus far, the film growth is independent of the catalytic activation by the substrate. This fact is evidenced by the continuous linearity of the thickness versus number of ALD cycles graphs demonstrated by all catalytic thermal ALD processes conducted prior to the research work reported herein.

6.8 Nickel Nitride Thin Films

Nickel nitride thin films are used in spintronic devices[144] and magnetic memory storage devices as a contact material.[145] Nickel silicide is a major constituent in source and drain contacts in microelectronic devices. Nickel metal films are used as protective and decorative coatings, as selective absorbers, as fuel cells, and as catalysts.[146] Nickel nitride serves as a starting material for the formation of both NiSi and Ni metal thin films.[147]

Nickel nitride thin films have been prepared by physical vapor deposition using ion beam implantation[148] and sputtering methods.[149] The reported CVD methods for nickel nitride thin films include deposition using bis(2,2,6,6-teramethyl-3,5-heptanedianato)nickel(II) and NH_3 as precursors at temperatures between 160 and 200 °C,[150] and using bis[*N,N'*-di(*tert*-butyl)acetamidinato]nickel(II) and NH_3 as precursors at temperatures between 160 and 200 °C.[146]

Nickel nitride ALD has been carried out using bis[*N,N'*-di(*tert*-butyl)acetamidinato]nickel(II) and NH_3 on glassy carbon.[151] Due to carbon incorporation in the films at deposition temperatures ≥ 240 °C, the ALD deposition temperature for this process was kept at 200 °C. Nickel nitride ALD has been carried out also using bis(1,4-di-*tert*-butyl-1,3-diazabutadienyl)nickel(II) and 1,1-dimethylhydrazine on thermal SiO_2.[152] The ALD window for the process is between 225-240 °C. However, since the decomposition of the nickel precursor occurs at 230 °C, it is probable that the film growth may proceed through a CVD type growth mechanism. Both the significant surface roughness of films (root mean square surface roughness of a film deposited at 225 °C was ~10.87 nm for a 70 nm thick film) and the significant amounts of carbon and hydrogen impurity incorporation in films may have resulted from the thermal decomposition of the nickel precursor.

A nickel nitride thermal ALD process which produces smooth, uniform, high purity films at low deposition temperatures is unprecedented.

6.9 Low Reactivity of Precursors-A Major Obstacle in Atomic Layer Deposition

A considerable problem in the growth of ALD metal thin films is the low reactivity of the metal precursors towards reducing co-reagents. In the copper ALD process reported by Winter and coworkers, a solution to this problem was obtained where the copper metal precursor was converted to a copper(II)formate species using formic acid followed by the subsequent reduction to metal using the reducing co-reagent (Chart 3).[127]

Cu(dmap)$_2$
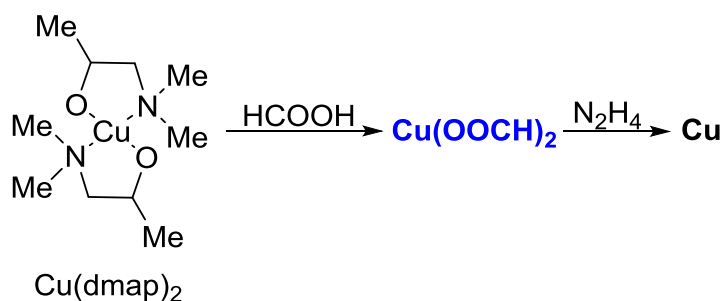
Chart 3. Scheme for the Growth of Copper Metal Thin Films.

However, many ALD precursors show low reactivity to an extent that neither the use of more reactive precursors or co-reagents, nor the carrying out of the reaction through multi-step ALD processes would produce the required thin-film material within an acceptable temperature range. Therefore, low reactivity of precursors is a central problem in growth of ALD thin films.

The lack of reactivity is caused by the higher activation energy barrier needed to overcome the reaction in order for the products to form. The enthalpy needed to overcome the activation energy barrier can be high, making the ALD reaction possible only at higher

temperatures where only poor quality films can be obtained or making the reaction impossible at all within the acceptable temperature limits. For this reason, developing a new ALD process which can address the problem of low reactivity of precursors, and which can make the low-temperature depositions possible, would be a significant improvement in the field of ALD.

Use of a heterogeneous catalyst in the ALD process will lower the activation energy of the ALD reaction and will facilitate the reaction to go to completion at lower temperatures (Figure 23). In ALD, the starting surface is known to influence the film nucleation and the start of film growth.[153] Therefore, using a catalytic substrate can produce better film growth and film properties in the ALD processes.
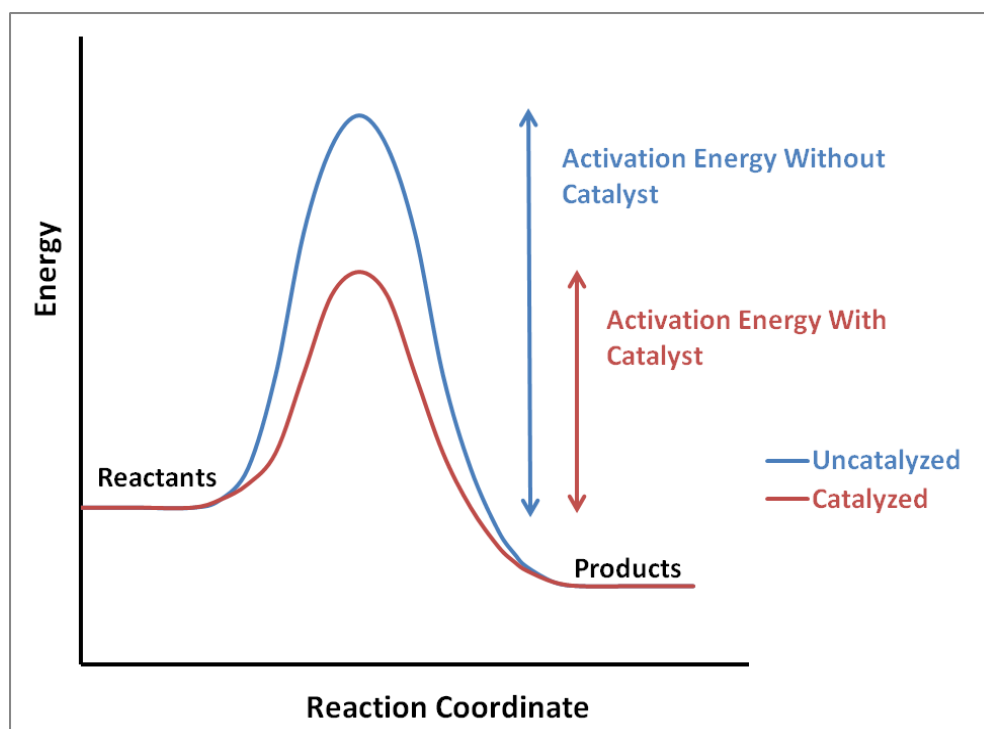
Figure 23. Lowering the Activation Energy of a Reaction Using a Catalyst.

6.10 Thesis Problem for the Research Segment 'Ruthenium-Substrate Catalyzed Growth of Nickel Nitride Thin Films by Atomic Layer Deposition'

A major problem in ALD is the low reactivity of precursors. The ALD research work documented in this thesis focuses on developing a new ALD process to address the problem of the low reactivity of precursors. To this end, substrate-dependent catalytic ALD film growth was explored.

Nickel nitride thermal ALD processes, which have been developed to date, are carried out at high deposition temperatures ($\geq$ 200 °C). The other disadvantages of existing nickel nitride ALD processes include a narrow ALD process window, high surface roughness of films, and significant amount of impurity incorporation. Therefore, the research work reported herein also focuses on developing a nickel nitride thermal ALD process at low temperatures. High purity, smooth, uniform, and conformal thin films are anticipated to meet the demands of the microelectronics industry.

A new substrate-dependent catalytic ALD technique will be introduced. The ALD growth studies of nickel nitride thin films will be performed by varying film growth parameters. Composition of the films and the surface morphology will be analyzed using X-ray diffraction (XRD), X-ray photoelectron spectroscopy (XPS), scanning electron microscopy (SEM), and atomic force microscopy (AFM) techniques.

CHAPTER 7

RUTHENIUM SUBSTRATE-CATALYZED GROWTH OF NICKEL NITRIDE THIN FILMS BY ATOMIC LAYER DEPOSITION

7.1 Introduction

In this chapter, the first example of the substrate-dependent catalytic ALD film growth is described. Two new low temperature nickel nitride ALD processes are developed using catalytic ruthenium substrates. The substrate dependent catalytic technique reduces the activation energy of the ALD reaction and allows depositions at low temperatures. Therefore, analogous substrate-dependent catalytic processes can be utilized to obtain a diverse range of thin-film materials using various precursors and co-reactants which can be catalytically activated.

7.2 Results and Discussion

Literature reports indicate that nickel aminoalkoxide complexes have been used as promising precursors in ALD and metal organic chemical vapor deposition (MOCVD) processes for the formation of nickel and nickel alloy thin films.[107e, 154] Therefore, $Ni(OCHMeCH_2NMe_2)_2$ $(Ni(dmap)_2)$ (**1**) (Chart 4) was selected as the nickel precursor to carry out the nickel nitride film growth studies reported herein.
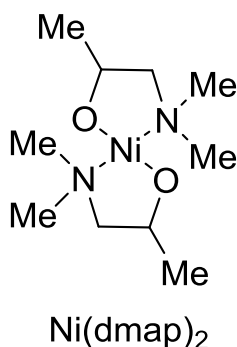
$Ni(dmap)_2$

Chart 4. Structure of (**1**), Bis(dimethylamino-2-propoxo)nickel(II) or $Ni(dmap)_2$ Precursor.

From preparative sublimation studies 95% sublimed recovery and 5% nonvolatile residue was observed for **1** (~0.70 g) at 60 °C/0.05 Torr within approximately 3 hours. The solid state decomposition temperature range for **1** is between 178 and 185 °C.

Hydrazine is used in ALD as a strong reducing co-reagent and also as a source of nitrogen for the formation of nitride thin films.[155] The enthalpy and free energy for dissociation of hydrazine are much smaller than the corresponding values for ammonia (Chart 5). Therefore, hydrazine demonstrates a higher reactivity than ammonia in nitridation reactions.

$$NH_{3\,(g)} \longrightarrow NH_{2\,(g)} + H_{(g)} \qquad \Delta H = 108.5 \text{ kcal}, \Delta G = 100.9 \text{ kcal} \qquad (8)$$

$$N_2H_{4\,(g)} \longrightarrow 2\,NH_{2\,(g)} \qquad \Delta H = 68.1 \text{ kcal}, \Delta G = 58.4 \text{ kcal} \qquad (9)$$

Chart 5. Decomposition Reactions of Ammonia and Hydrazine.

Due to the high reactivity of hydrazine, often the growth rates and film densities of nitride thin films deposited using hydrazine are higher than the corresponding values obtained for the films deposited using ammonia. However, even a strong reducing agent like hydrazine may not be effective for certain reactions due to the high activation energy needed for the reaction. From the preliminary ALD experiments, depositions using both **1** with anhydrous hydrazine and **1** with formic acid and anhydrous hydrazine did not afford films on hydrogen terminated silicon, silicon with native oxide, or thermal silicon dioxide substrates. Only island-like discontinuous films on Si(100) substrates were observed at temperatures ≥ 175 °C. Thermal reduction of nickel formate to nickel metal requires elevated temperatures ≥ 266 °C.[156] Therefore, the discontinuous films

obtained from these preliminary studies can be a result of CVD type film growth following the thermal decomposition of **1.**

Hydrazine is known to catalytically decompose on ruthenium surfaces.[157] Above 220 K, dissociation of hydrazine on ruthenium generates various surface species and desorption products including surface amino ($-NH_2$) and imide ($-NH$) groups, adsorbed atomic N and H, and gaseous NH_3, N_2, and H_2.

A ruthenium seed layer was used by Waechtler and coworkers to efficiently reduce ALD grown Cu_2O thin films on copper.[158] After the Cu_2O ALD process, the Cu_2O films were heat-treated at 115 °C in formic acid vapor on a ruthenium seed layer to obtain a copper film. Formic acid is known to dissociate on ruthenium by dehydrogenation, producing CO_2 and H_2, and dehydration, producing CO and H_2O. Formic acid is also known to dissociate on copper surfaces, producing CO_2 and H_2.[159]

Therefore, use of a catalytic ruthenium substrate would enable the nickel nitride film growth at reduced temperatures. Accordingly, two new low-temperature ruthenium substrate-catalyzed ALD processes were developed using **1** and anhydrous hydrazine in a two precursor sequence, and **1**, formic acid, and anhydrous hydrazine in a three precursor sequence (Chart 6).
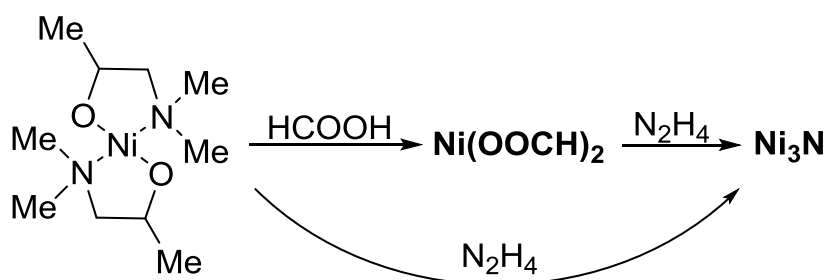
Chart 6. Scheme for the Growth of Nickel Nitride Thin Films.

Initial film growth studies were investigated on several substrates which can demonstrate catalytic activity. Non-uniform, island-like film growth was observed on Pt/Ti/SiO$_2$/Si and Pd/Ti/SiO$_2$/Si substrates, indicating poor nucleation. Continuous films were deposited on 5 nm sputtered ruthenium on 100 nm thermal SiO$_2$ (Ru/SiO$_2$/Si). RuO$_2$ species may be present on the surface of the ruthenium substrates.[108d] Nickel or nickel nitride film growth was not observed for the reaction of **1** with formic acid at temperatures < 175 °C.

Film growth studies were carried out for nickel nitride films obtained using both the three precursor sequence (three-step) process and the two precursor sequence (two-step) process on Ru/SiO$_2$/Si substrates.

7.2.1. New Low Temperature Ruthenium Substrate-Catalyzed Three-Step Ni$_x$N ALD Process

For the three-step process (Chart 7) the growth behavior was evaluated by varying the precursor pulse length, substrate temperature, and number of deposition cycles.
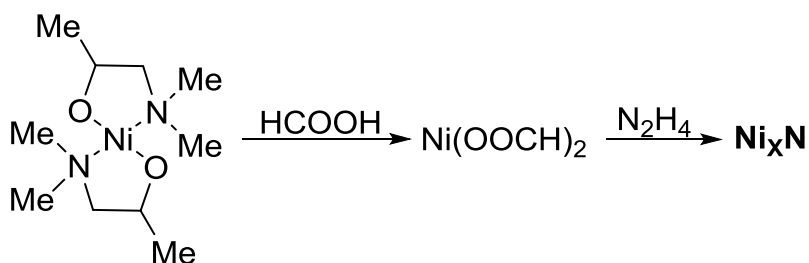
Chart 7. Scheme for the Growth of Ni$_x$N Thin Films by Three-Step Process.

The variation of the film growth rate on the pulse length of **1** was examined at 150 °C (Figure 24). The number of deposition cycles, the formic acid pulse length, the hydrazine pulse length,

and the length of the purge following the formic acid and hydrazine pulses were held constant at 1000, 0.2 s, 0.2 s, and 5.0 s, respectively. The growth rate was constant at about 0.35 Å/cycle with $\geq$ 1.0 s pulse lengths for **1.** This constant growth rate is indicative of self-limited growth.
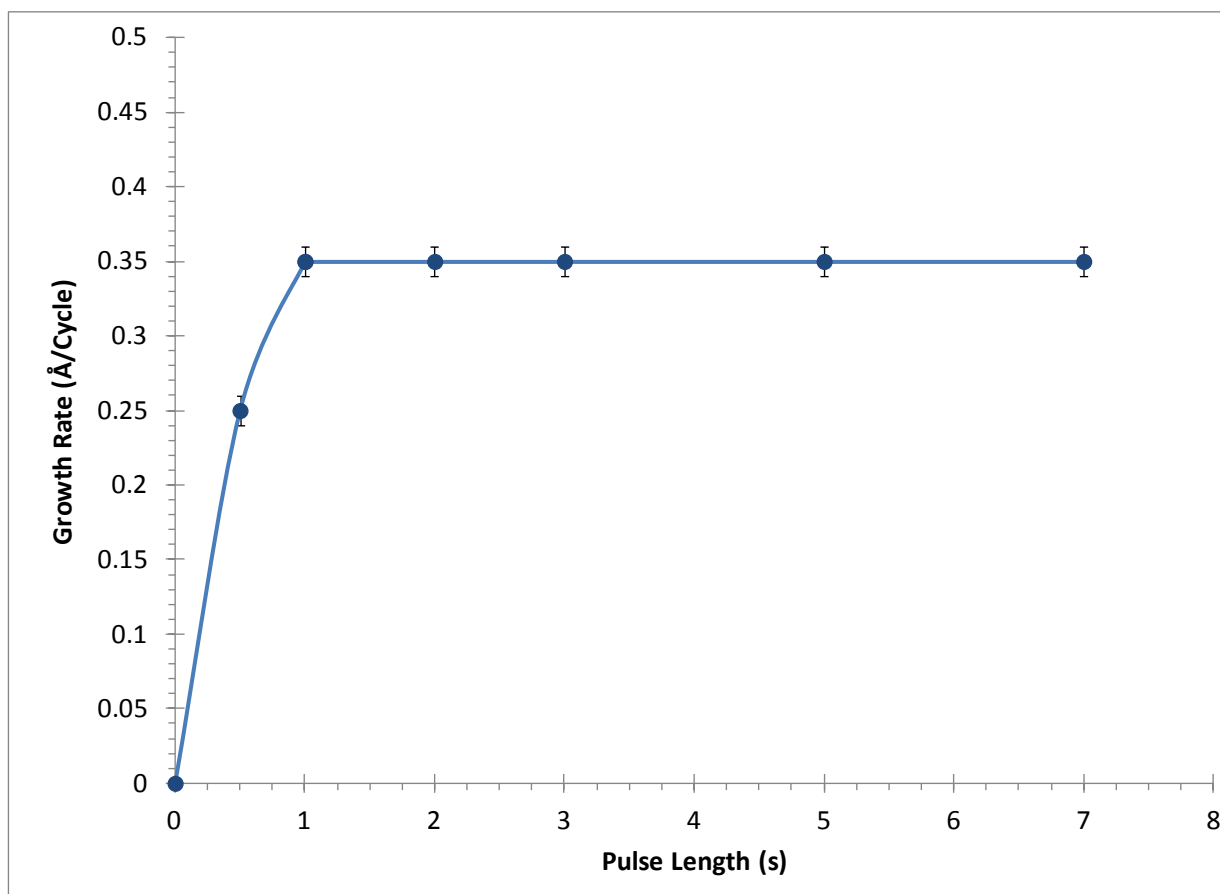
Figure 24. Plot of Growth Rate Versus Pulse Length of **1** at 150 °C for the Three-Step Ni_xN ALD Process.

The dependence of film growth rate on the pulse length of formic acid and anhydrous hydrazine was also investigated at a growth temperature of 150 °C. For the investigation of the growth behavior as a function of the formic acid pulse (Figure 25), the number of deposition cycles, pulse length of **1**, pulse length of anhydrous hydrazine, and the length of the purge

between precursor pulses were kept constant at 1000, 3.0 s, 0.2 s, and 5.0 s, respectively. In a similar manner, the growth behavior was investigated as a function of the pulse length of anhydrous hydrazine, keeping the number of deposition cycles, pulse length of **1**, pulse length of formic acid, and the length of the purge between precursor pulses constant at 1000, 3.0 s, 0.2 s, and 5.0 s, respectively (Figure 26). Saturative growth was observed for formic acid and hydrazine pulse lengths ≥ 0.1 s.
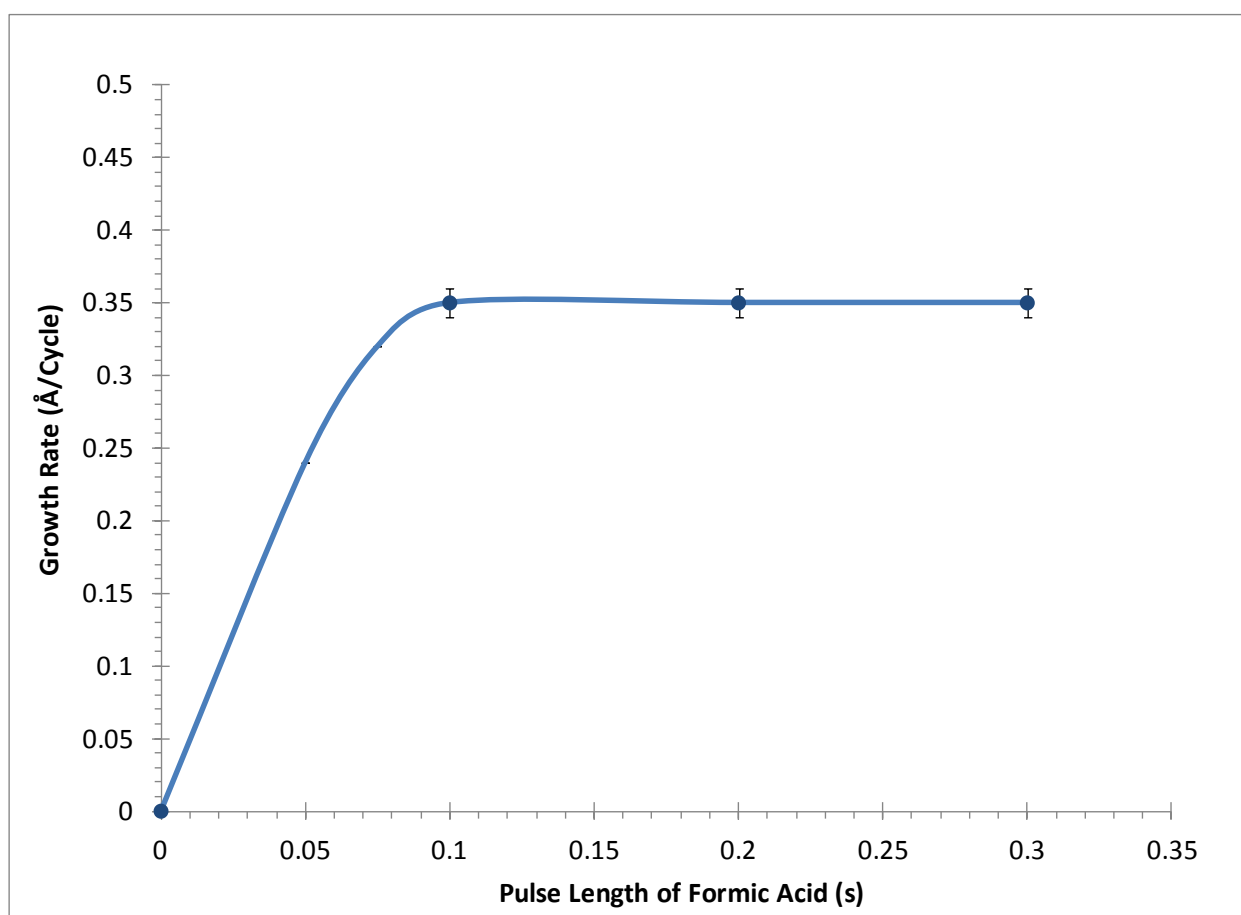
Figure 25. Plot of Growth Rate Versus Pulse Length of Formic Acid at 150 °C for the Three-Step Ni_xN ALD Process.
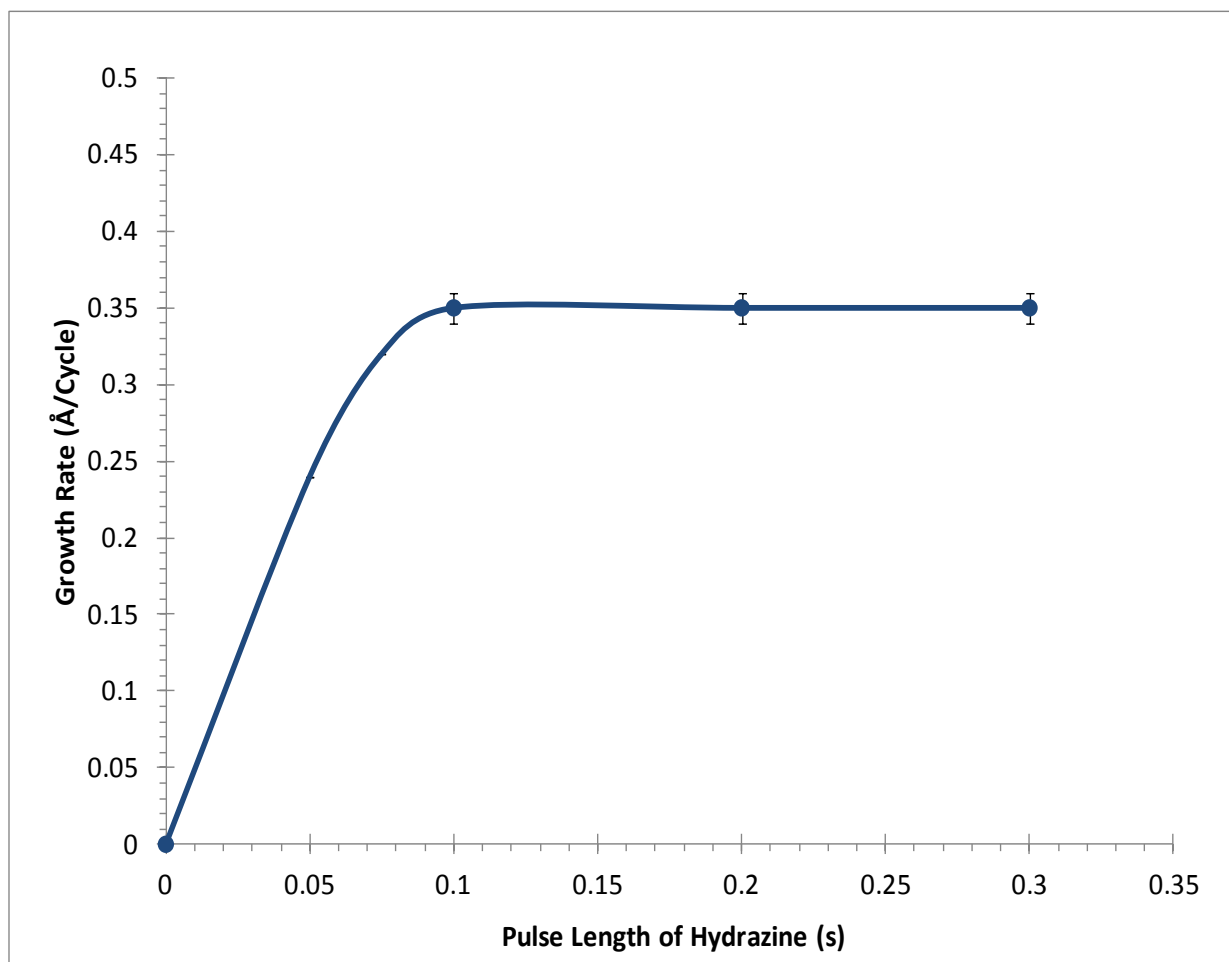
Figure 26. Plot of Growth Rate Versus Pulse Length of Anhydrous Hydrazine at 150 °C for the Three-Step Ni$_x$N ALD Process.

The film growth rate was investigated as a function of the deposition temperature (Figure 27). The depositions were carried out using 3.0 s pulse lengths of **1**, and formic acid, and anhydrous hydrazine pulse lengths of 0.2 s each, with a 5.0 s purge length between pulses, and 1000 deposition cycles. A constant growth rate of ~0.35 Å/cycle was observed for substrate temperatures between 120 and 180 °C (ALD window). Growth rates of 0.29 Å/cycle and 0.32 Å/cycle were observed at 100 and 200 °C, respectively, which are outside the ALD window. The lower growth rate below the ALD window was a result of the lack of thermal energy for the

reaction of the precursors. The reduced growth rate above 180 °C resulted from decomposition of the precursor in the gas phase followed by removal of the decomposition products from the reaction chamber by the purge.
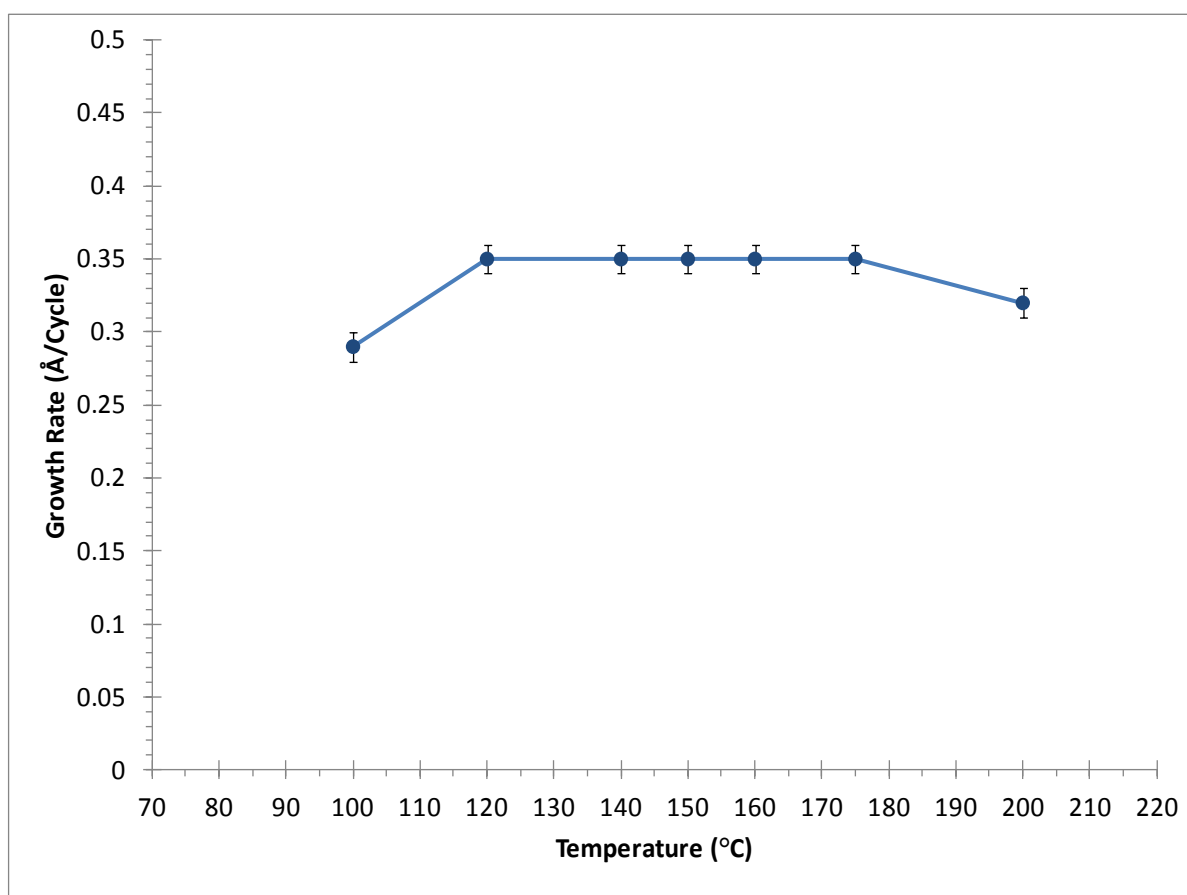
Figure 27. Plot of Growth Rate as a Function of the Deposition Temperature for the Three-Step Ni_xN ALD Process.

Cross sectional SEM view of a ~35 nm thick film is shown in Figure 28.
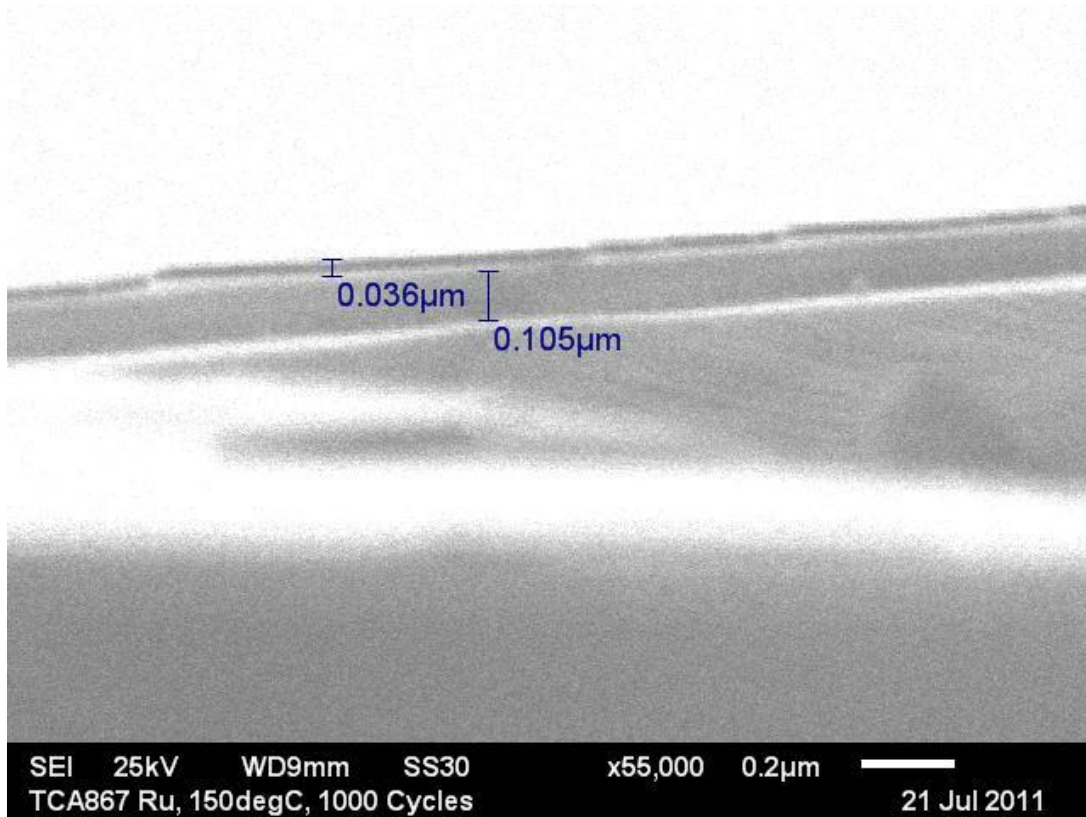
Figure 28. Cross Sectional Scanning Electron Micrograph Image of a Ni_xN Film Deposited by Three-Step Ni_xN ALD Process.

The variation of the film thickness on the number of deposition cycles was investigated (Figure 29). The deposition temperature was 150 °C with 2.0 s, 0.1 s, and 0.1 s pulse lengths of **1**, formic acid, and anhydrous hydrazine, respectively, with 5.0 s purges between pulses. A linear variation of film thickness was observed with the number of deposition cycles up to 1000 cycles. The slope of the line (0.348 Å/cycle) is similar to the saturative growth rate which is ~0.35 Å/cycle. From 1000 to 2000 deposition cycles the film thickness remained constant at ~35 nm.

This growth plateau in a film thickness versus number of deposition cycles graph is unprecedented in ALD processes carried out prior to the ALD processes documented herein.

Hydrazine is catalytically activated on ruthenium surfaces, followed by reduction of the nickel precursor and eventual nitridation. Further growth of the nickel nitride layer stops when the growing nickel nitride layer blocks hydrazine from reaching active substrate ruthenium sites, or when the already activated nitriding agent is completely consumed and not available anymore to permeate through the growing nickel nitride layer. Therefore, the constant film thickness observed beyond 1000 deposition cycles indicates substrate-dependent catalytic film growth. The intercept of −0.6, which is within experimental error, indicates a small nucleation delay period.
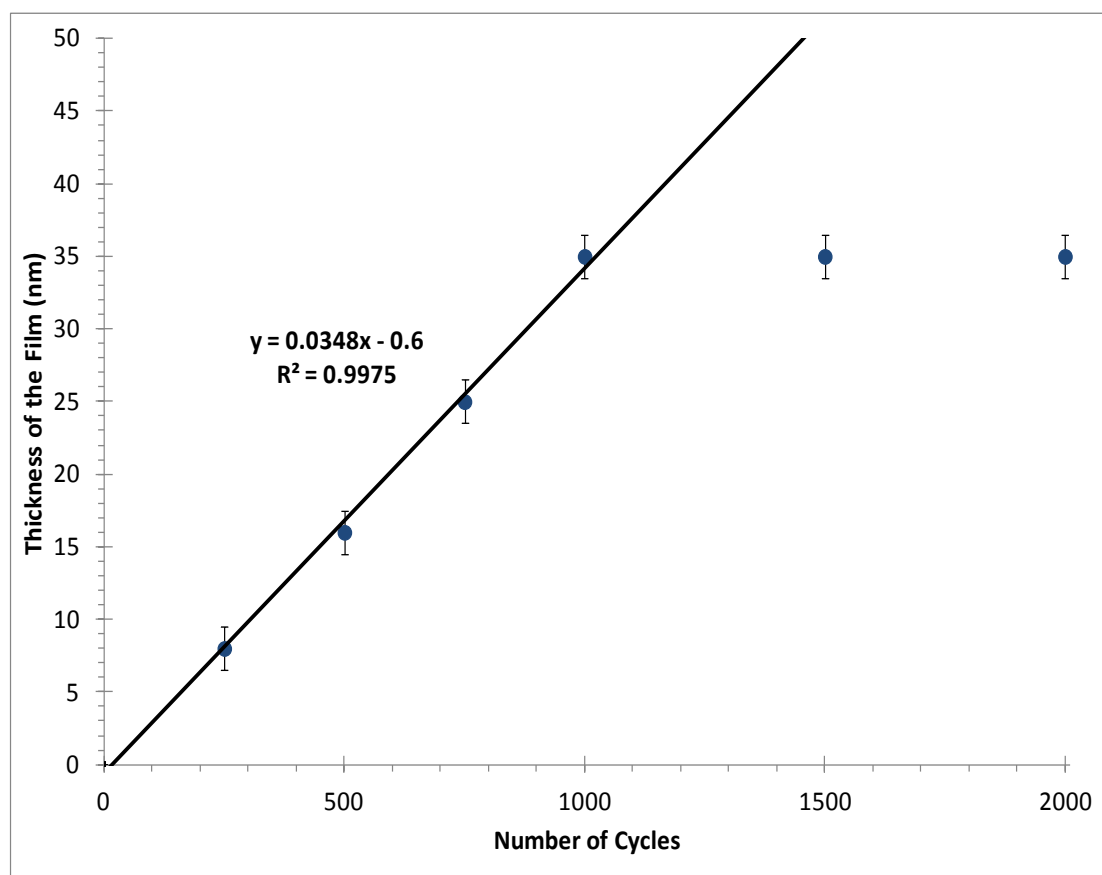
Figure 29. Plot of Film Thickness as a Function of Number of Deposition Cycles at 150 °C for the Three-Step Ni_xN ALD Process.

Powder X-ray diffraction experiments were carried out on the 35 nm thick films deposited at various temperatures (Figure 30). The X-ray diffraction pattern showed reflections arising from (110), (002), and (111) planes of the polycrystalline Ni_3N (JCPDS file number 10-0280).
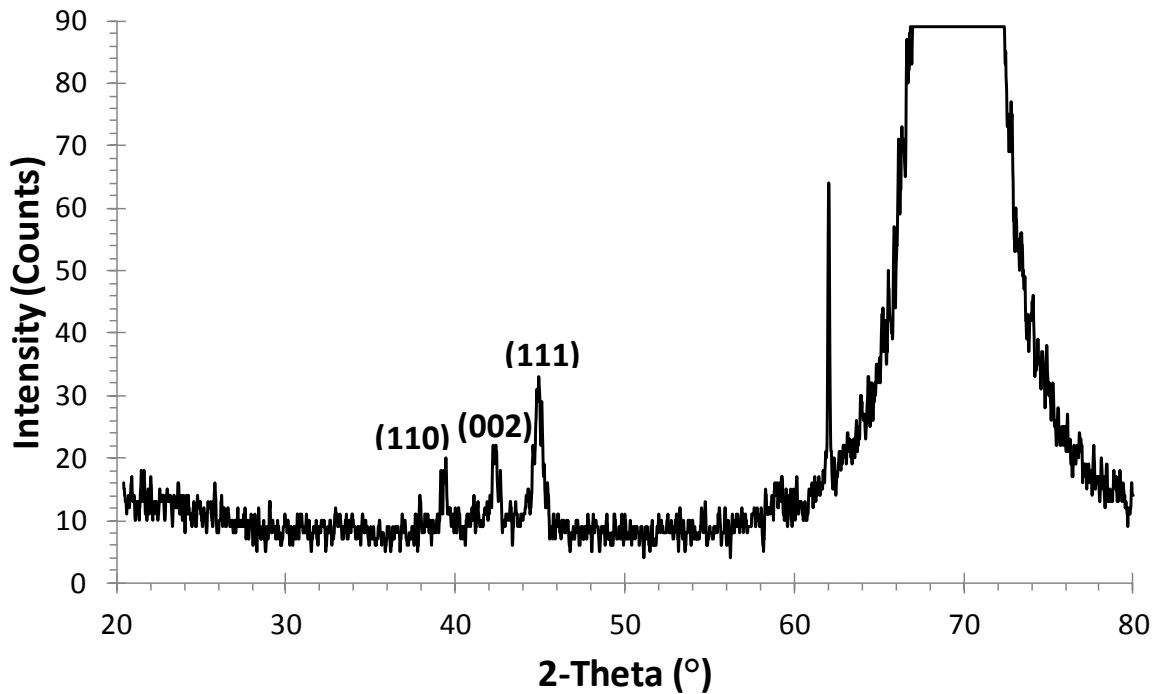

Figure 30. Powder X-Ray Diffraction Pattern of a 35 nm Thick Ni_xN Film Deposited at 120 °C Using the Three-Step Ni_xN ALD Process.

X-ray photoelectron spectroscopy (XPS) was performed on 35 nm thick films deposited at 150 °C (Figure 31). The spectrum of the film surface before argon ion sputtering showed nickel and nitrogen ionizations as well as ionizations arising from oxygen and carbon. The composition of the film after two argon ion sputters (60 s each) was 87.8 at % nickel, 8.0 at % nitrogen, 2.9 at % carbon, and 1.3 at % oxygen (Table 19). The Ni $2p^{1/2}$ and Ni $2p^{3/2}$ ionizations appeared at 869.65 and 852.55 eV corresponding to nickel metal (Figure 32).[160] The reduction of the nitrogen content of Ni_xN films when NH_3 and H_2 were used as co-reactants was previously

reported.[146] However, since the X-ray powder diffraction pattern indicates the formation of crystalline Ni_3N films, the reduced content of nitrogen in this work compared to the Ni_3N stoichiometry could be as a result of preferential sputtering of nitrogen by the argon ion beam.[150a] The high percentages of oxygen and carbon observed before argon ion sputtering changed to considerably smaller values after argon ion sputtering. Adventitious carbon and oxygen in the sample could result from the exposure of the sample to the ambient atmosphere before XPS analysis. The low percentages of carbon and oxygen impurity incorporation after argon ion sputtering indicate that the deposited films were of high purity.
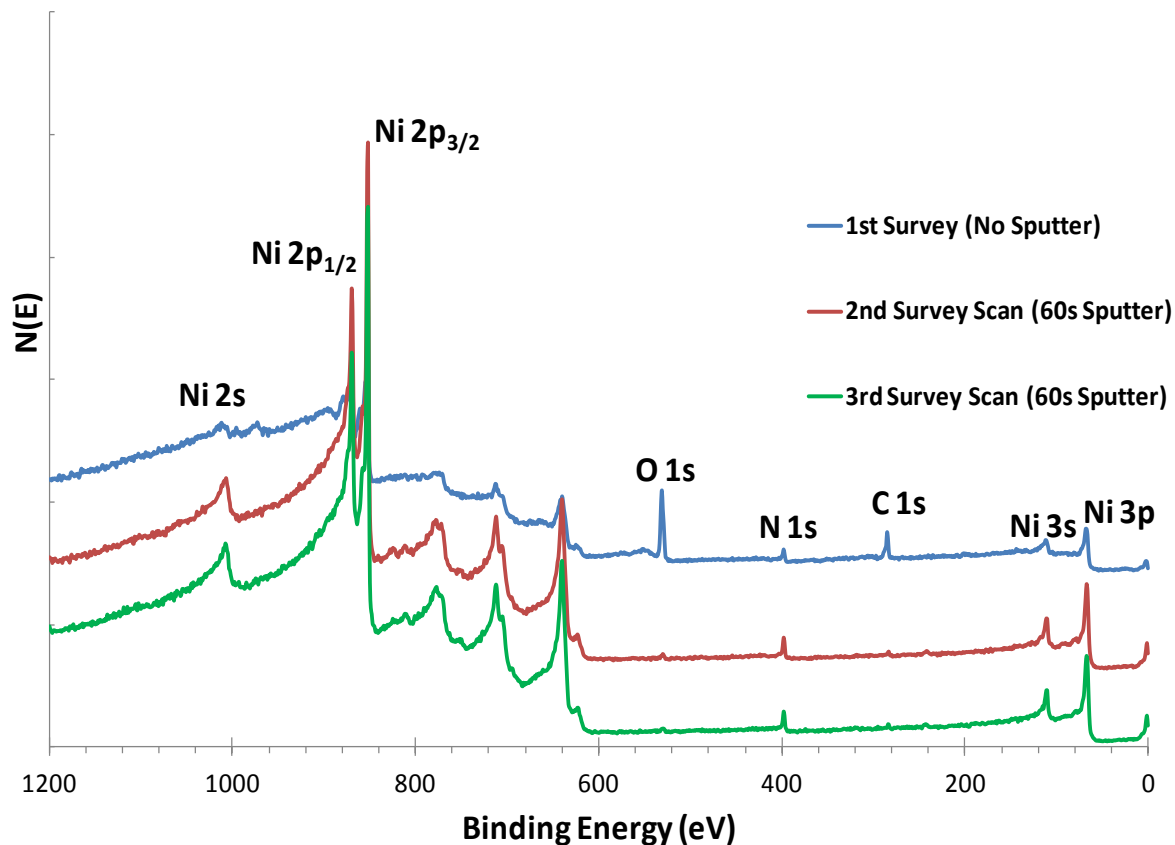
Figure 31. XPS Survey Spectrum for a 35nm Thick Ni_xN Film Deposited at 150 °C Using the Three-Step Ni_xN ALD Process.

Table 19. Elemental Compositions of Ni, N, C, and O in 35 nm Thick Ni_xN Films Determined by XPS.

|	**Initial Survey**	**Second Survey**	**Third Survey**
% Ni	40.5	87.7	87.8
% N	5.7	8.1	8.0
% C	24.4	2.2	2.9
% O	29.4	2.0	1.3
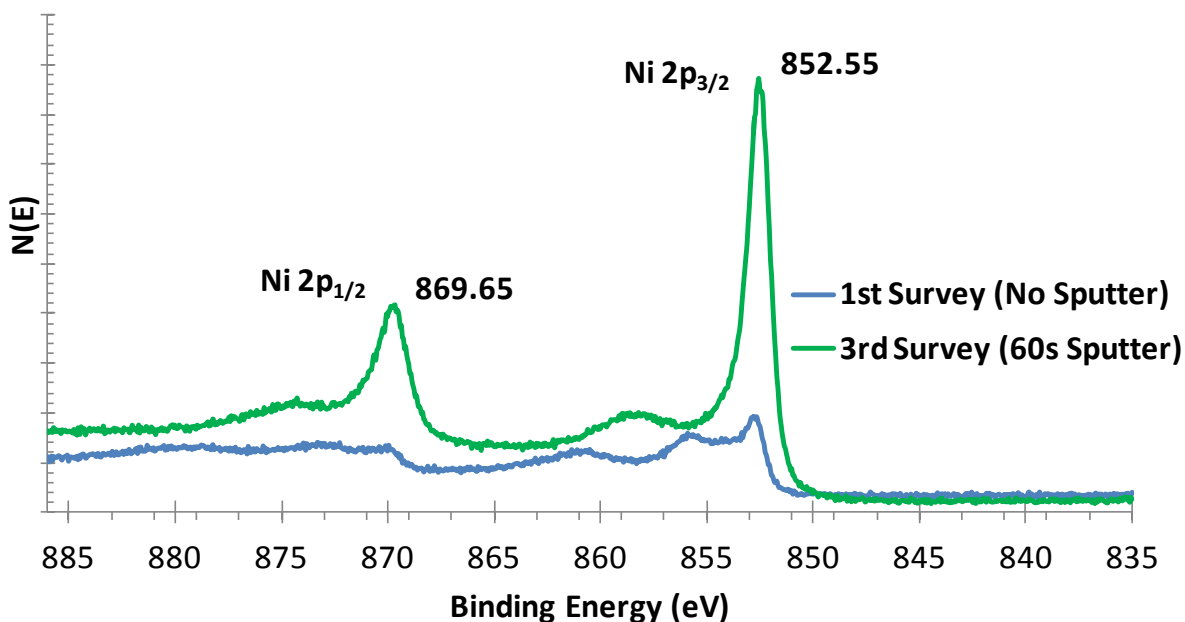
Figure 32. High Resolution XPS Multiplex of the Ni 2p Region of a 35 nm Thick Ni_xN Film Deposited at 150 °C Using the Three-Step Ni_xN ALD Process.

The surface morphology of the films was studied by atomic force microscopy (AFM). The root mean square (RMS) surface roughness of 35 nm thick films deposited at 120 °C was ~0.38 nm

indicating a very smooth surface (Figure 33). The RMS surface roughness of 35 nm thick films deposited at 180 °C was 4.4 nm indicating an average surface roughness (Figure 34).
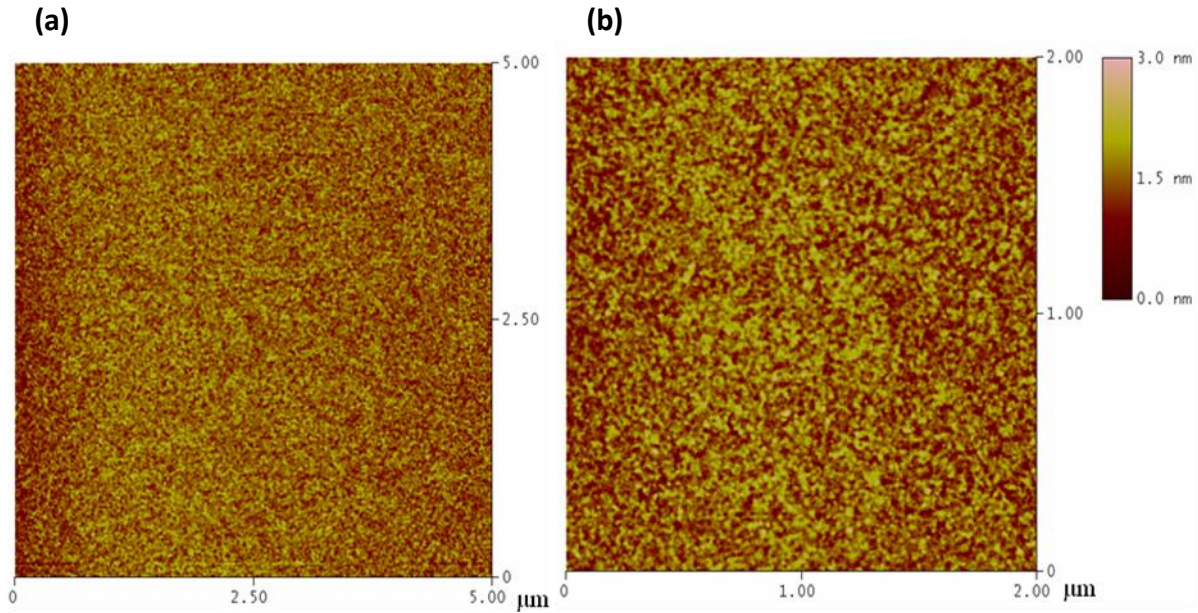

Figure 33. AFM Images of 35 nm Thick Films Deposited at 120 °C with RMS Surface Roughness Values of (a) 0.353 nm and (b) 0.387 nm.
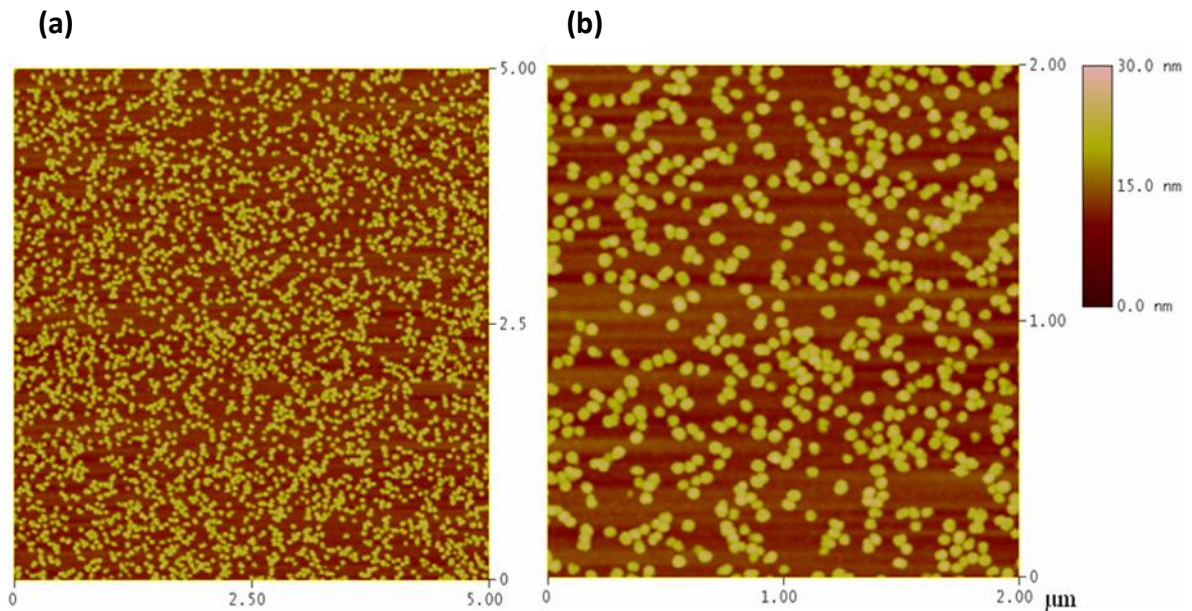

Figure 34. AFM Images of 35 nm Thick Films Deposited at 180 °C with RMS Surface Roughness Values of (a) 4.463 nm and (b) 4.349 nm.

The scanning electron micrograph images show that the film surfaces are uniform with no cracks or pinholes (Figure 35).
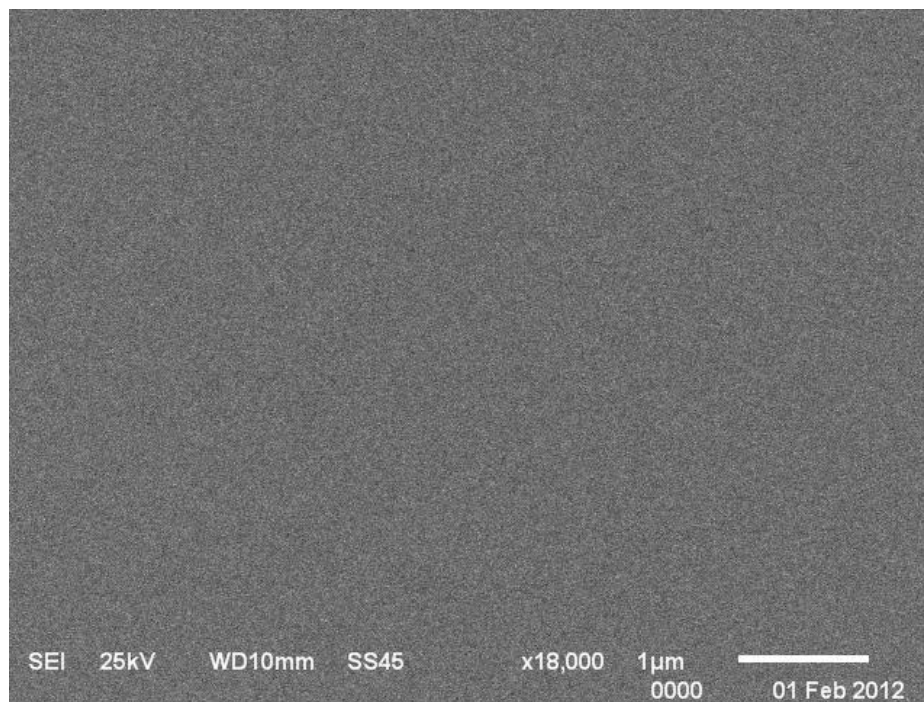

Figure 35. Top SEM View of a 35 nm Thick Ni_xN Film Deposited at 150 °C Using the Three-Step Ni_xN ALD Process.

Films deposited at all temperatures passed the scotch tape test. Therefore, the films show good adhesion.

7.2.2. New Low Temperature Ruthenium Substrate-Catalyzed Two-Step Ni$_x$N ALD Process

For the two-step process (Chart 8) precursor pulse lengths, substrate temperature, and number of deposition cycles were varied to evaluate the growth behavior.
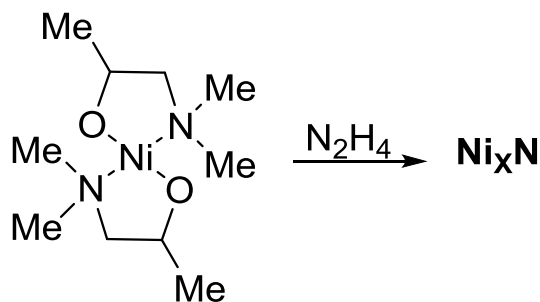

Chart 8. Scheme for the Growth of Ni$_x$N Thin Films by Two-Step Process.

The dependence of the film growth rate on the pulse length of **1** was examined at 150 °C (Figure 36). The number of deposition cycles, the hydrazine pulse length, and the purge lengths were held constant at 1000, 0.2 s, and 5.0 s, respectively. The growth rate was constant at about 0.25 Å/cycle with ≥ 2.0 s pulse lengths of **1**, which is consistent with the self-limited growth behavior.
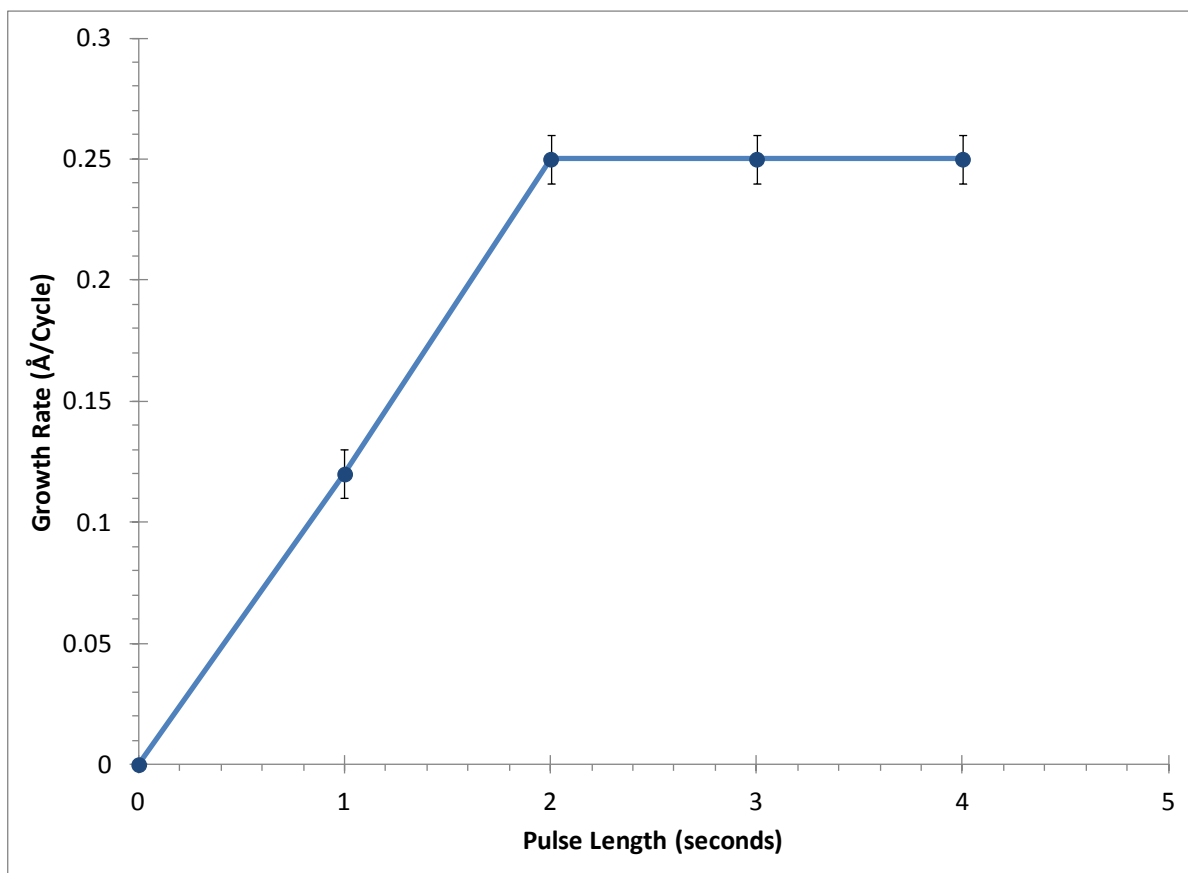
Figure 36. Plot of Growth Rate as a Function of Pulse Length of **1** at 150 °C for the Two-Step Ni$_x$N ALD Process.

The variation of the film growth rate as a function of pulse length of anhydrous hydrazine was investigated. Depositions were carried out at a substrate temperature of 150 °C (Figure 37). The number of deposition cycles, pulse length of **1**, and the purge lengths were held constant at 1000, 3.0 s, and 5.0 s, respectively. Saturative growth was observed for anhydrous hydrazine pulse lengths ≥ 0.1 s.
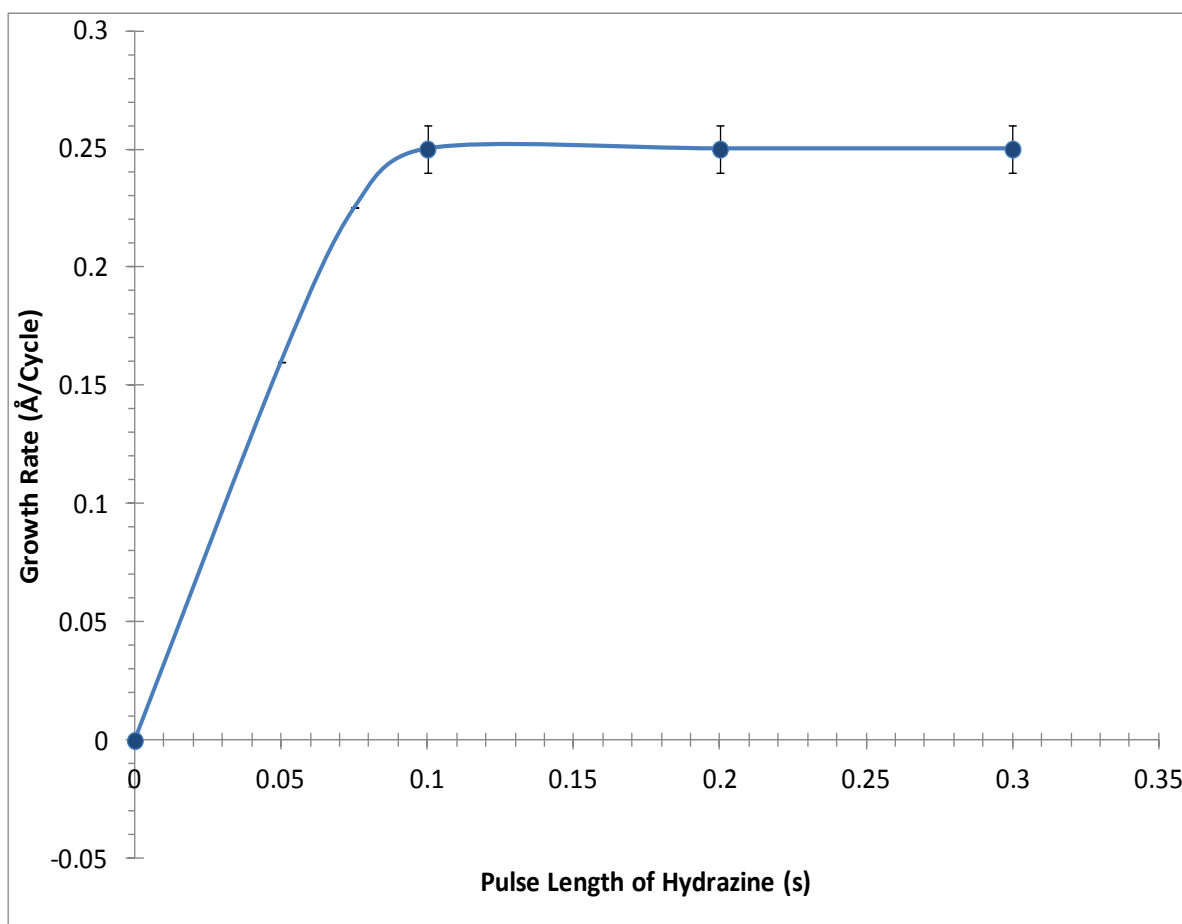
Figure 37. Plot of Growth Rate as a Function of Pulse Length of Hydrazine at 150 °C for the Two-Step Ni$_x$N ALD Process.

The film growth rate was investigated next, varying the deposition temperature (Figure 38). Depositions were carried out using 3.0 s and 0.2 s pulse lengths of **1** and anhydrous hydrazine pulse lengths, respectively, with a 5.0 s purge between pulses, and 1000 deposition cycles. The ALD window was observed between 140 and 180 °C where the growth rate was constant around 0.25 Å/cycle. Growth rates of 0.12, 0.18, and 0.33 Å/cycle were observed at 100, 120, and 200 °C, respectively. These temperatures are outside the ALD window. The lower growth rates could result from the low reactivity of precursors and the increased growth rate at

200 °C due to decomposition of the precursors and the accumulation of decomposition products on the film surface.
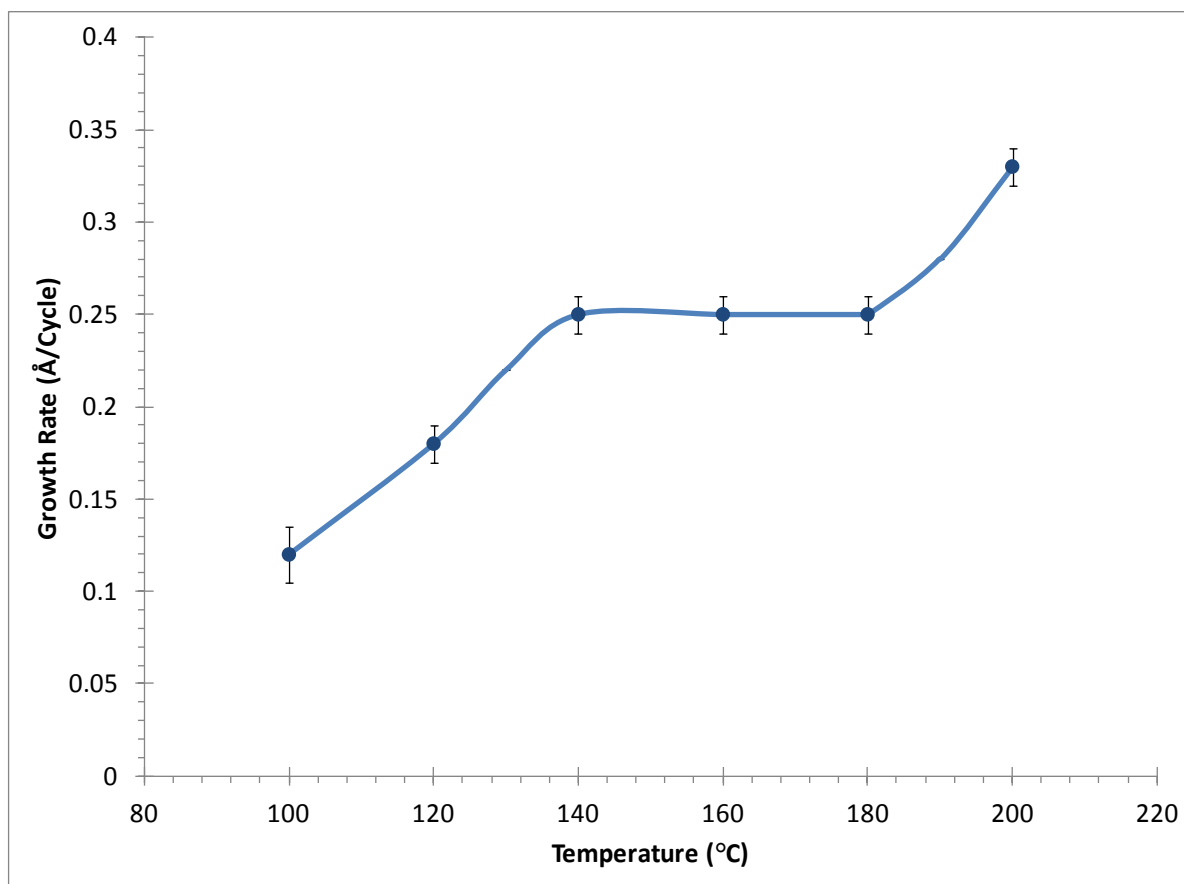

Figure 38. Plot of Growth Rate Versus Deposition Temperature for the Two-Step Ni_xN ALD Process.

The variations of film thickness with the number of deposition cycles was investigated. Depositions were carried out at 150 °C, using 2.0 s and 0.1 s pulse lengths of **1** and anhydrous hydrazine, respectively, with 5.0 s purge lengths between pulses. The film thickness varied linearly with the number of deposition cycles up to 1500 cycles (Figure 39). The slope of the line is 0.25 Å/cycle, which is equal to the saturative growth rate. Beyond 1500 deposition cycles film

thickness remained constant at ~32 nm, indicative of catalytic activation of hydrazine by ruthenium. Therefore, the film growth in this two-step process also proceeds by substrate-dependent catalysis of the precursors.
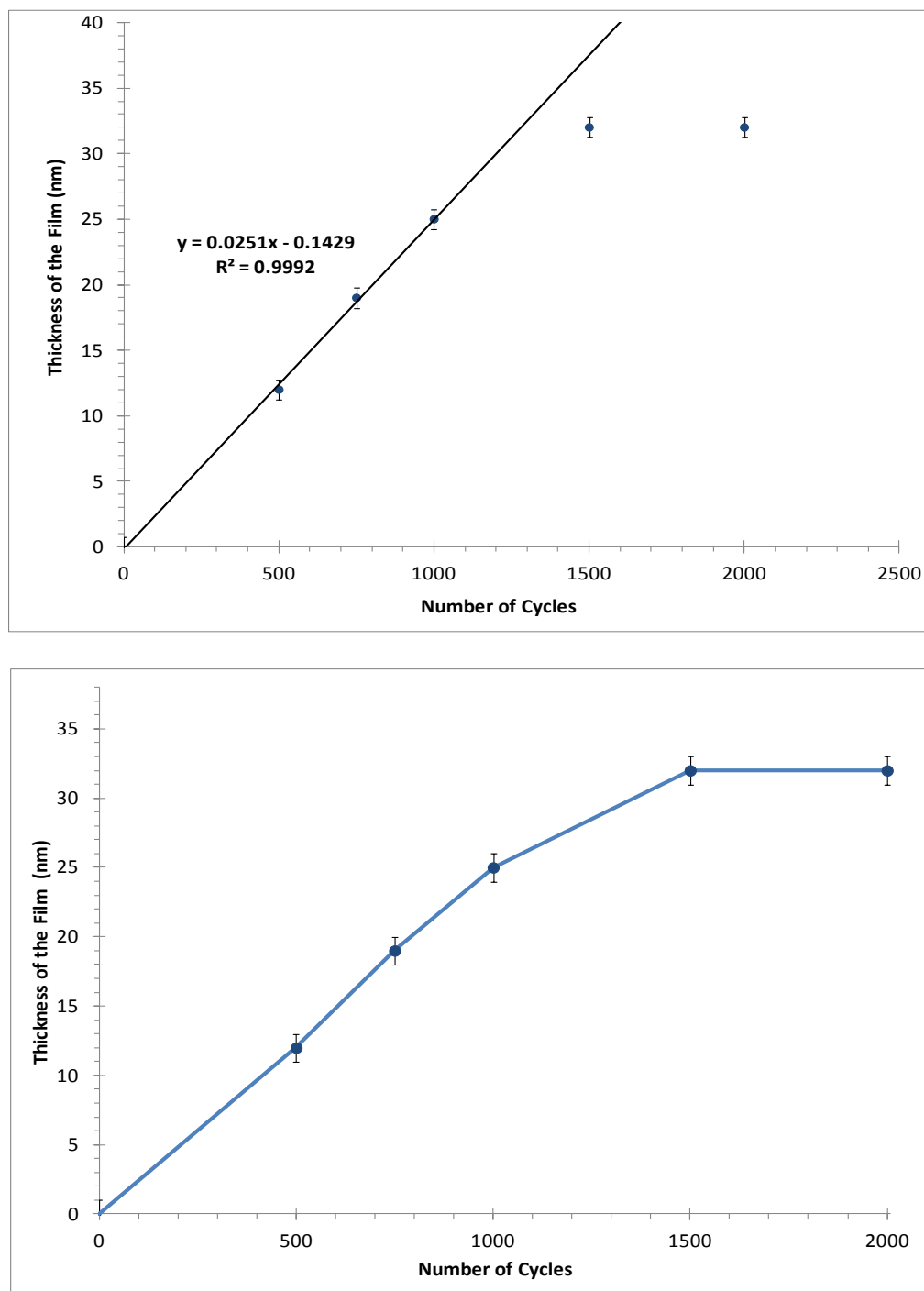

Figure 39. Plot of Thickness Versus Number of Cycles Graphs for the Two-Step Ni_xN Process.

Powder X-ray diffraction scans of 25 nm thick films deposited at various temperatures indicate that the films are amorphous as deposited (Figure 40).
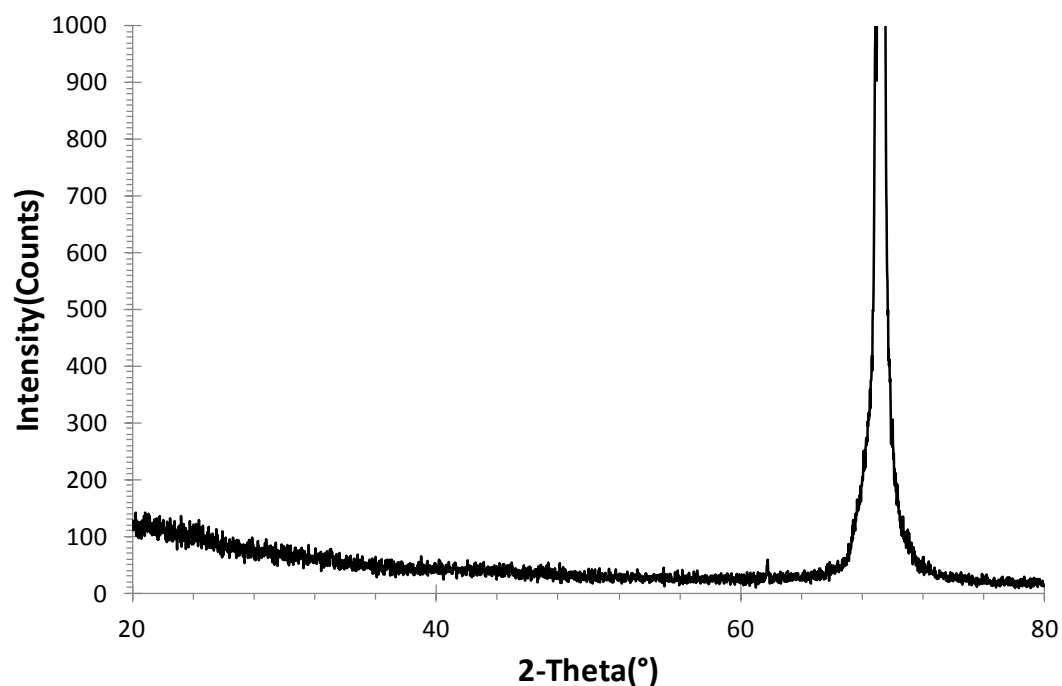

Figure 40. Powder X-Ray Diffraction Scan of a 25 nm Thick Ni_xN Film Deposited at 150 °C using the Two-Step Ni_xN ALD Process.

XPS was performed on 25 nm thick films deposited at 150 °C (Figure 41). The surface before argon ion sputtering revealed the expected ionizations for nickel and nitrogen. Ionizations arising from oxygen and carbon were also visible. After argon ion sputtering the composition of the films were 84.2 at % nickel, 8.9 at % nitrogen, 4.1 at % carbon, and 2.7 at % oxygen (Table 20). The Ni $2p^{1/2}$ and Ni $2p^{3/2}$ ionizations appeared at 869.9 and 852.5 eV for nickel metal (Figure 42).[160] The composition of the films are almost identical to the films obtained from the three-step process.
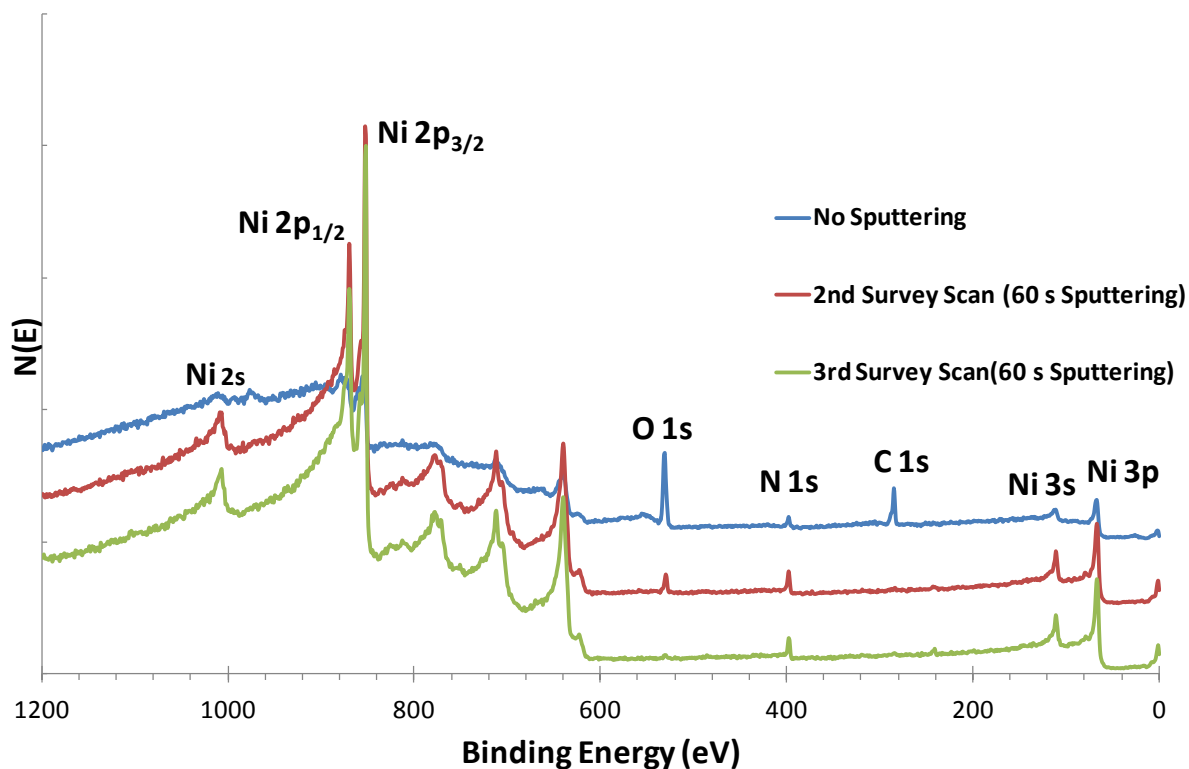
Figure 41. XPS Survey Spectrum for a 25 nm Thick Ni$_x$N Film Deposited at 150 °C Using the Three-Step Ni$_x$N ALD Process.

Table 20. Elemental Compositions of Ni, N, C, and O in 25 nm Thick Ni$_x$N Films Determined by XPS.

	Initial Survey	**Second Survey**	**Third Survey**
% Ni	30.8	80.1	84.2
% N	4.4	9.0	8.9
% C	32.0	4.5	4.1
% O	32.8	6.4	2.7
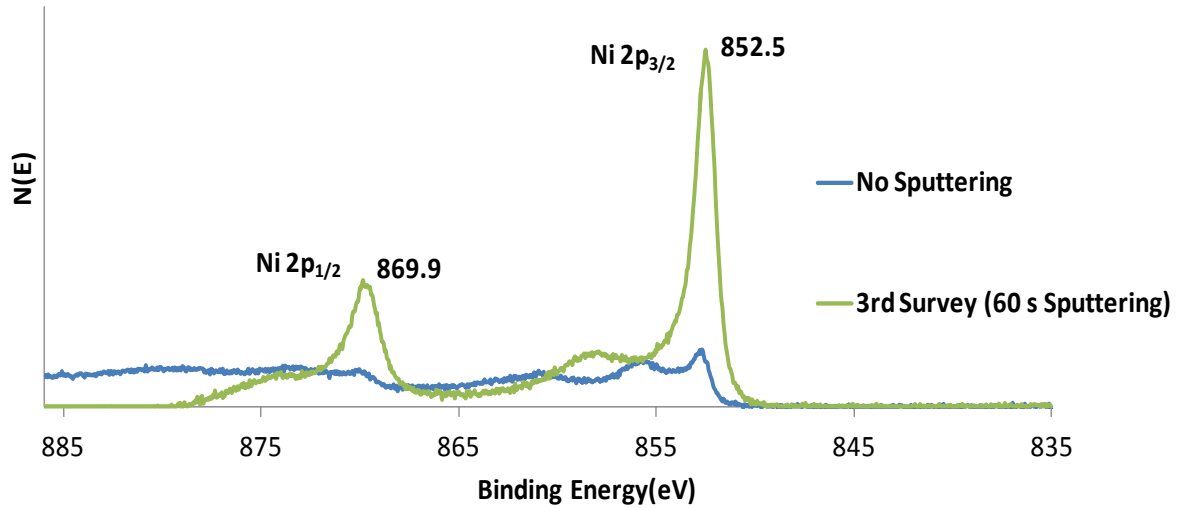
**Figure 42.** High Resolution XPS Multiplex of the Ni 2p Region of a 25 nm Thick Ni_xN Film Deposited at 150 °C Using the Two-Step Ni_xN ALD Process.

An AFM image of a 25 nm thick film deposited at 120 °C showed a RMS surface roughness of ~0.25 nm indicating a smooth film (Figure 43). The RMS surface roughness of 25 nm thick films deposited at 180 °C was also around 0.25 nm indicating a smooth surface (Figure 44).
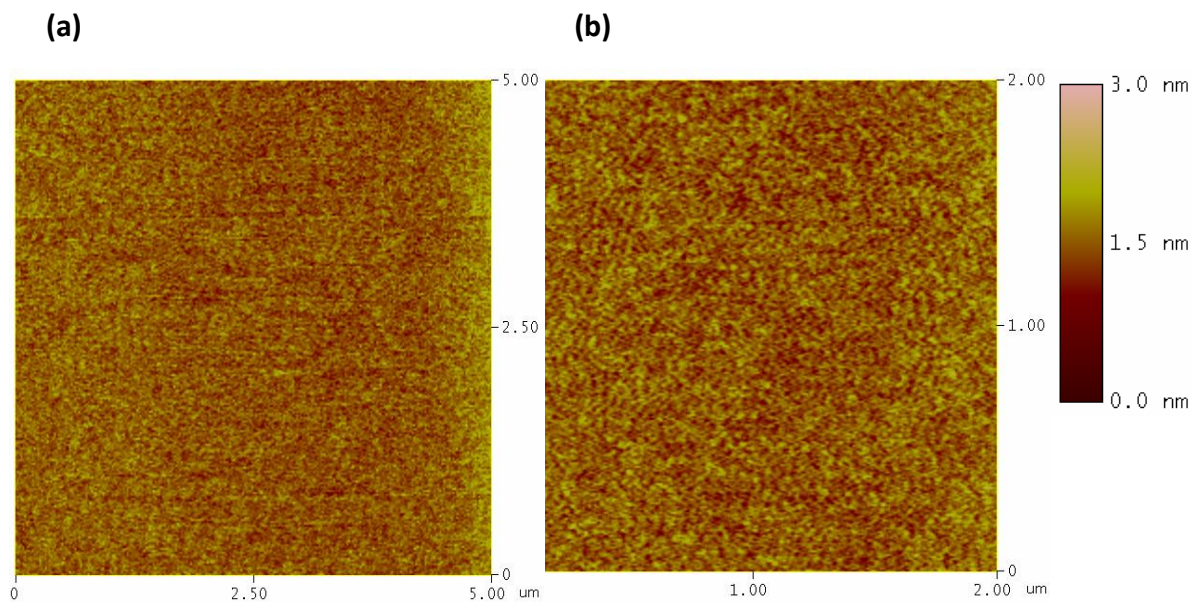
Figure 43. AFM Images of 25 nm Thick Films Deposited at 120 °C with RMS Surface Roughness Values of (a) 0.235 nm and (b) 0.254 nm.
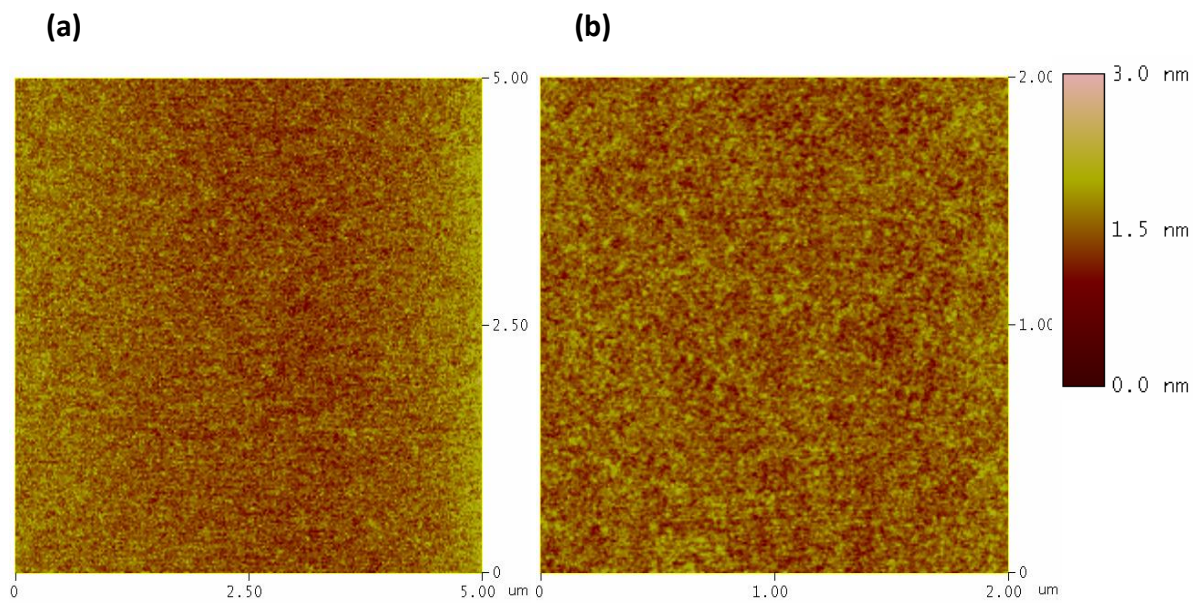
Figure 44. AFM Images of 25 nm Thick Films Deposited at 180 °C with RMS Surface Roughness Values of (a) 0.256 nm and (b) 0.236 nm.

The scanning electron micrograph images show a uniform surface which is free from cracks and pinholes (Figure 45).
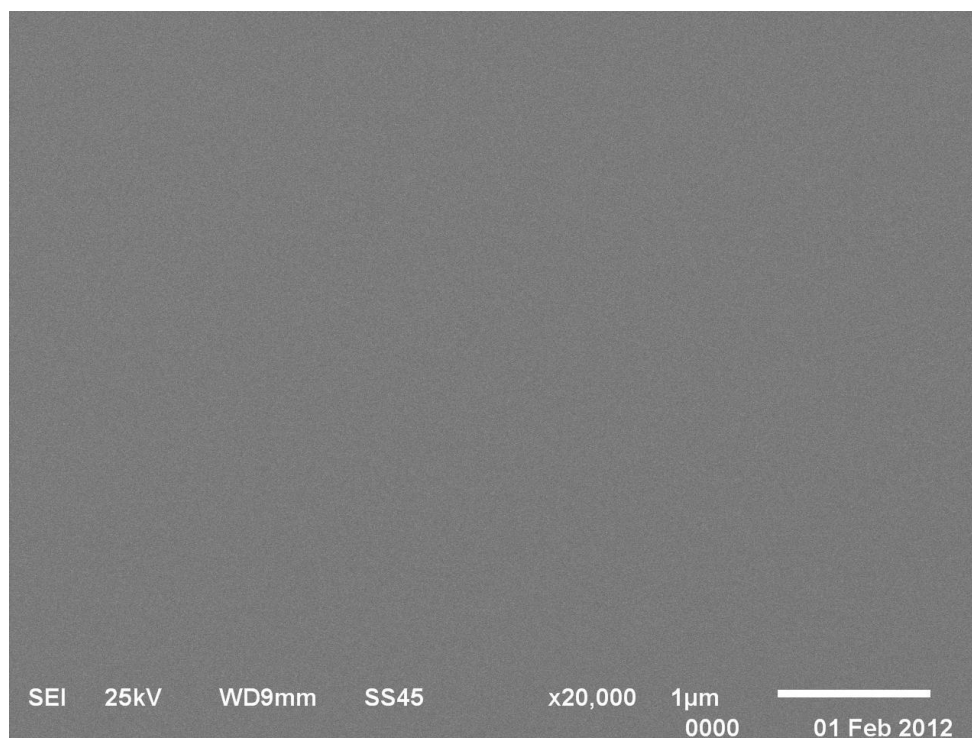
Figure 45. Top SEM View of a 25 nm Thick Ni$_x$N Film Deposited at 150 °C Using the Two-Step Ni$_x$N ALD Process.

Films deposited at all temperatures passed the scotch tape test demonstrating good adhesion.

7.2.3 Conclusions

The research work documented herein describes the first example of substrate-dependent catalytic thermal ALD film growth. Two new low temperature ruthenium substrate-catalyzed nickel nitride ALD processes were developed. For the three-step process the ALD window was observed between 120 and 180 °C where a constant growth rate of ~0.35 Å/cycle was obtained. For the two-step process an ALD window between 140 and 180 °C was observed with a constant

growth rate of ~0.25 Å/cycle. Both the two-step and three-step processes produced smooth thin films with RMS surface roughness values around 0.38-4.4 nm for the three-step process, and around 0.25 nm for the two step process. Crystalline films were obtained from the three-step process whereas amorphous films were produced from the two-step process. Amorphous films are desired for applications where the diffusion of materials through grain boundaries should be avoided. On the other hand, crystalline films are preferred in some applications where high purity films are needed with low resistivity values.

7.2.4 Future Work

Resistivity measurements will be performed at selected temperatures on films obtained from both the two-step and three-step ruthenium substrate-catalyzed low-temperature Ni_xN ALD processes. Due to the selective sputtering of nitrogen that can take place in XPS experiments, the composition of films deposited from both processes will be analyzed by Rutherford Backscattering measurements. A sufficient number of films for the measurements are prepared. Performance of the resistivity and Rutherford Backscattering measurements was assigned to Thomas J. Knisely by Prof. Charles H. Winter.

7.2.5 Experimental

Nickel Nitride Film Depositions. Thin film deposition experiments were carried out using an R-75BE ALD reactor manufactured by Picosun Oy. The reactor was operated under a flow of nitrogen (99.9995%) and the reactor pressure was kept at 8-12 m bar. Nitrogen was obtained by purification of air using a Texol GeniSys nitroGenerator. Nitrogen thus obtained was used as both carrier and purge gas. The deposition of Ni_xN thin films by ALD was studied using **1** as the nickel source, formic acid as a reducing agent, and anhydrous hydrazine (Sigma-Aldrich) as both a reducing agent and a source of nitrogen in the three-step process, and **1** as the nickel

source, anhydrous hydrazine as the reducing agent and nitrogen source in the two-step process. **1** was prepared according to a literature procedure.[154e] The optimum sublimation temperature for **1** at the reactor pressure was 100 °C from the initial growth trials. Depositions were carried out at substrate temperatures between 100 to 200 °C. To determine the extent of the surface saturation the pulse lengths of **1** and anhydrous hydrazine were varied in the two-step process and the pulse lengths of **1**, formic acid, and anhydrous hydrazine were varied in the three-step process. Films were deposited on 5 nm Ru/100 nm SiO_2/Si (5 x 5 cm) from Intel Corporation. The ruthenium oxide layer, which can be present on the surface, was not removed prior to depositions.

Film Characterization Methods. Film thickness measurements were performed using cross-sectional SEM micrographs collected on a JEOL-6510LV electron microscope. To determine the film growth rates, film thicknesses were divided by the number of deposition cycles. Five separate film thickness measurements were performed at different positions of the thin film and an average film thickness calculated. Powder X-ray diffraction spectra were collected with a Rigaku R200B 12 kW rotating anode diffractometer. The Cu Kα radiation (1.54056 Å) was used in the diffractometer at 40 kV and 150 mA. Atomic force micrograph images were obtained using a MultiMode nanoscope IIIa (Digital Instruments, VEECO). The samples were measured using the tapping mode in air. The measurements were taken using an E scanner with a maximum scanning size of 12 μm at a frequency of 1 or 2 Hz. A Tap150AI-G tip was employed with a resonance frequency of 150 kHz and a force constant of 5 N/m. Surface roughness was determined as root mean square values. X-ray photoelectron spectroscopy was performed using a PerkinElmer 5500 XPS system. Monochromatic Al Kα radiation was used in the XPS system. Surface sputtering was performed using an argon ion beam of 0.5 kV.

CHAPTER 8

CONCLUSIONS ON SUBSTRATE-CATALYZED ATOMIC LAYER DEPOSITION
RESEARCH PROJECT

A new substrate-dependent catalytic thermal ALD film growth process was developed. This substrate-dependent catalytic method addresses the problem of low reactivity of precursors for obtaining thin-film materials. Using the newly developed method, the low temperature growth of high purity, smooth, uniform, and conformal nickel nitride thin films was demonstrated.

In both nickel nitride ALD processes, hydrazine is activated by catalytic ruthenium sites on the substrate to afford nickel nitride thin films. The substrate dependent nature of the film growth is demonstrated by the growth plateau of thickness versus number of cycles graphs, caused by the cessation of film growth after reaching a certain film thickness. The present method can be used to carry out ALD reactions at low deposition temperatures by lowering the activation energy of the reaction. Achieving low deposition temperatures provides smooth films with low impurity incorporation and low resistivity values. Further, the method will enable the use of precursors which otherwise need high temperatures or may be unreactive due to a high activation energy barrier. Therefore, new material depositions which were not possible with conventional thermal ALD and plasma ALD will be possible using the substrate-dependent catalytic thermal ALD method reported herein.

The substrate-dependent catalytic process can be used with any catalytic substrate, including the noble metal substrates, and can be used with any co-reagent or precursor catalytically activated by the substrate material. Since the catalytic substrates can be easily manufactured by sputter coatings, the technique developed in this work can be used efficiently

for the production of large batches of thin-film materials. Because the new method addresses the low reactivity of precursors, it allows the deposition of films at low temperatures, and can be easily used in the production of thin film materials. The research work reported herein is a significant breakthrough in ALD process technology.

APPENDIX

Copyright Permissions for Reference 22.

License Number	3433090347165
License date	Jul 20, 2014
Licensed content publisher	John Wiley and Sons
Licensed content publication	Journal of Separation Science
Licensed content title	Totally organic biphasic solvent systems for extraction and descriptor determinations
Licensed copyright line	© 2012 WILEY-VCH Verlag GmbH & Co. KGaA, Weinheim
Licensed content author	Colin F. Poole,Thushara Karunasekara,Thiloka C. Ariyasena
Licensed content date	Nov 21, 2012
Start page	96
End page	109
Type of use	Dissertation/Thesis
Requestor type	Author of this Wiley article
Format	Print and electronic

Portion	Figure/table
Number of figures/tables	3
Original Wiley figure/table number(s)	Figure 3 Figure 4 Table 3
Will you be translating?	No

Title of your thesis / dissertation	(I)	Chromatographic Models for Solute Descriptor Determinations
	(II)	Ruthenium Substrate-Catalyzed Growth of Nickel Nitride Thin Films by Atomic Layer Deposition

Expected completion date	Oct 2014
Expected size (number of pages)	150
Total	0.00 USD

Copyright Permission for Reference 22 Continued.

License Number	3433890723509
License date	Jul 21, 2014
Licensed content publisher	John Wiley and Sons
Licensed content publication	Journal of Separation Science
Licensed content title	Totally organic biphasic solvent systems for extraction and descriptor determinations
Licensed copyright line	© 2012 WILEY-VCH Verlag GmbH & Co. KGaA, Weinheim
Licensed content author	Colin F. Poole,Thushara Karunasekara,Thiloka C. Ariyasena
Licensed content date	Nov 21, 2012
Start page	96
End page	109
Type of use	Dissertation/Thesis
Requestor type	Author of this Wiley article
Format	Print and electronic
Portion	Text extract

Number of Pages	2
Will you be translating?	No
Title of your thesis / dissertation	(I)Chromatographic Models for Solute Descriptor Determinations (II)Ruthenium Substrate-Catalyzed Growth of Nickel Nitride Thin Films by Atomic Layer Deposition
Expected completion date	Oct 2014
Expected size (number of pages)	150
Total	0.00 USD

Copyright Permission for Reference 23

Supplier	Elsevier Limited The Boulevard,Langford Lane Kidlington,Oxford,OX5 1GB,UK
Registered Company Number	1982084
Customer name	Thiloka C Ariyasena
Customer address	930 W Forest Ave Apt 5
	DETROIT, MI 48201
License number	3434750879982
License date	Jul 23, 2014
Licensed content publisher	Elsevier
Licensed content publication	Journal of Chromatography A
Licensed content title	Extension of the system constants database for open- tubular columns: System maps at low and intermediate temperatures for four new columns
Licensed content author	Sanka N. Atapattu,Kimberly Eggers,Colin F. Poole,Waruna Kiridena,Wladyslaw W. Koziol
Licensed content date	6 March 2009

Licensed content volume number	1216
Licensed content issue number	10
Number of pages	10
Start Page	1640
End Page	1649
Type of Use	reuse in a thesis/dissertation
Intended publisher of new work	other
Portion	figures/tables/illustrations
Number of figures/tables/illustrations	2
Format	both print and electronic
Are you the author of this Elsevier article?	No
Will you be translating?	No
Title of your thesis/dissertation	(I) Chromatographic Models for Solute Descriptor Determinations (II) Ruthenium Substrate-Catalyzed Growth of Nickel Nitride Thin Films by Atomic Layer Deposition
Expected completion date	Oct 2014
Estimated size (number of pages)	150
Elsevier VAT number	GB 494 6272 12
Permissions price	0.00 USD
VAT/Local Sales Tax	0.00 USD / 0.00 GBP

Copyright Permission for Reference 26.

Copyright Permission for Reference 34.

License Number	3433091274178
License date	Jul 20, 2014
Licensed content publisher	Springer
Licensed content publication	Chromatographia
Licensed content title	Models for Liquid–Liquid Partition in the System Ethanolamine-Organic Solvent and Their Use for Estimating Descriptors for Organic Compounds
Licensed content author	Thiloka C. Ariyasena
Licensed content date	Jan 1, 2013
Volume number	76
Issue number	3
Type of Use	Thesis/Dissertation
Portion	Full text
Number of copies	1
Author of this Springer article	Yes and you are the sole author of the new work

Order reference number	None
Title of your thesis / dissertation	(I)Chromatographic Models for Solute Descriptor Determinations (II)Ruthenium Substrate-Catalyzed Growth of Nickel Nitride Thin Films by Atomic Layer Deposition
Expected completion date	Oct 2014
Estimated size(pages)	150
Total	0.00 USD

Copyright Permission for Reference 34 Continued.

This is a License Agreement between Thiloka C Ariyasena ("You") and Springer ("Springer") provided by Copyright Clearance Center ("CCC"). The license consists of your order details, the terms and conditions provided by Springer, and the payment terms and conditions.

All payments must be made in full to CCC. For payment instructions, please see information listed at the bottom of this form.

License Number	3433920549022
License date	Jul 21, 2014
Licensed content publisher	Springer
Licensed content publication	Chromatographia
Licensed content title	Models for Liquid–Liquid Partition in the System Ethanolamine-Organic Solvent and Their Use for Estimating Descriptors for Organic Compounds
Licensed content author	Thiloka C. Ariyasena
Licensed content date	Jan 1, 2013
Volume number	76
Issue number	3
Type of Use	Book/Textbook
Requestor type	Publisher
Publisher	Not listed below
Portion	Full text
Format	Print and Electronic

Will you be translating?	No
Print run	6
Author of this Springer article	Yes and you are the sole author of the new work
Order reference number	None
Title of new book	(I) Chromatographic Models for Solute Descriptor Determinations (II) Ruthenium Substrate-Catalyzed Growth of Nickel Nitride Thin Films by Atomic Layer Deposition
Author of new book	Thiloka Chandima Ariyasena
Expected publication date of new book	Oct 2014
Estimated size of new book (pages)	150
Total	0.00 USD

Copyright Permission for Reference 49.

This is a License Agreement between Thiloka C Ariyasena ("You") and Springer ("Springer") provided by Copyright Clearance Center ("CCC"). The license consists of your order details, the terms and conditions provided by Springer, and the payment terms and conditions.

All payments must be made in full to CCC. For payment instructions, please see information listed at the bottom of this form.

License Number	3433100414469
License date	Jul 20, 2014
Licensed content publisher	Springer
Licensed content publication	Chromatographia
Licensed content title	Evaluation of Triethylamine as a Counter Solvent in Totally Organic Biphasic Liquid–Liquid Partition Systems
Licensed content author	Thiloka C. Ariyasena
Licensed content date	Jan 1, 2013
Volume number	76
Issue number	15
Type of Use	Thesis/Dissertation
Portion	Full text
Number of copies	1
Author of this Springer article	Yes and you are the sole author of the new work

Order reference number	None
Title of your thesis / dissertation	(I)Chromatographic Models for Solute Descriptor Determinations (II)Ruthenium Substrate-Catalyzed Growth of Nickel Nitride Thin Films by Atomic Layer Deposition
Expected completion date	Oct 2014
Estimated size(pages)	150
Total	0.00 USD

Copyright Permission for Reference 49 Continued.

<div align="center">

SPRINGER LICENSE
TERMS AND CONDITIONS

</div>

<div align="right">

Jul 21, 2014

</div>

This is a License Agreement between Thiloka C Ariyasena ("You") and Springer ("Springer") provided by Copyright Clearance Center ("CCC"). The license consists of your order details, the terms and conditions provided by Springer, and the payment terms and conditions.

All payments must be made in full to CCC. For payment instructions, please see information listed at the bottom of this form.

License Number	3433911447926
License date	Jul 21, 2014
Licensed content publisher	Springer
Licensed content publication	Chromatographia
Licensed content title	Evaluation of Triethylamine as a Counter Solvent in Totally Organic Biphasic Liquid–Liquid Partition Systems
Licensed content author	Thiloka C. Ariyasena
Licensed content date	Jan 1, 2013
Volume number	76
Issue number	15
Type of Use	Book/Textbook
Requestor type	Publisher
Publisher	Not listed below
Portion	Full text

Format	Print and Electronic
Will you be translating?	No
Print run	6
Author of this Springer article	Yes and you are the sole author of the new work
Order reference number	None
Title of new book	(I) Chromatographic Models for Solute Descriptor Determinations (II) Ruthenium Substrate-Catalyzed Growth of Nickel Nitride Thin Films by Atomic Layer Deposition
Author of new book	Thiloka Chandima Ariyasena
Expected publication date of new book	Oct 2014
Estimated size of new book (pages)	150
Total	0.00 USD

Copyright Permission for Reference 52.

Supplier	Elsevier Limited The Boulevard,Langford Lane Kidlington,Oxford,OX5 1GB,UK
Registered Company Number	1982084
Customer name	Thiloka C Ariyasena
Customer address	930 W Forest Ave Apt 5 DETROIT, MI 48201
License number	3464511435072
License date	Sep 08, 2014
Licensed content publisher	Elsevier
Licensed content publication	Journal of Chromatography A
Licensed content title	Determination of descriptors for polycyclic aromatic hydrocarbons and related compounds by chromatographic methods and liquid–liquid partition in totally organic biphasic systems
Licensed content author	Thiloka C. Ariyasena,Colin F. Poole
Licensed content date	26 September 2014

Licensed content volume number	1361
Licensed content issue number	n/a
Number of pages	15
Start Page	240
End Page	254
Type of Use	reuse in a thesis/dissertation
Portion	full article
Format	both print and electronic
Are you the author of this Elsevier article?	Yes
Will you be translating?	No
Title of your thesis/dissertation	(I)Chromatographic Models for Solute Descriptor Determinations (II)Ruthenium Substrate-Catalyzed Growth of Nickel Nitride Thin Films by Atomic Layer Deposition
Expected completion date	Oct 2014
Estimated size (number of pages)	150
Elsevier VAT number	GB 494 6272 12
Permissions price	0.00 USD
VAT/Local Sales Tax	0.00 USD / 0.00 GBP
Total	0.00 USD

REFERENCES

1. (a) EPA Risk Assessment: Risk Characterization. http://www.epa.gov/risk/risk-characterization.htm (accessed July 04, 2014); (b) U. S. Food and Drug Administration: Risk and Safety Assessment. http://www.fda.gov/Food/FoodScienceResearch/RiskSafetyAssessment/default.htm (accessed July 04, 2014); (c) Atapattu, S. N.; Poole, C. F., Determination of Descriptors for Semivolatile Organosilicon Compounds by Gas Chromatography and Non-aqueous Liquid-Liquid Partition. *J Chromatogr A* **2009,** *1216* (45), 7882-8; (d) Acree, W. E., Jr.; Grubbs, L. M.; Abraham, M. H., Prediction of Partition Coefficients and Permeability of Drug Molecules in Biological Systems with Abraham Model Solute Descriptors Derived from Measured Solubilities and Water-to-Organic Solvent Partition Coefficients, Toxicity and Drug Testing. InTech: 2012; pp 91-128; (e) Acree, W. E., Jr.; Grubbs, L. M.; Abraham, M. H. In *Prediction of Toxicity, Sensory Responses and Biological Responses with the Abraham Model, Toxicity and Drug Testing.*, InTech: 2012; pp 261-296.

2. Kan, A. T.; Tomson, M. B., UNIFAC Prediction of Aqueous and Nonaqueous Solubilities of Chemicals with Environmental Interest. *Environ. Sci. Technol.* **1996,** *30* (4), 1369-76.

3. Russom, C. L.; Breton, R. L.; Walker, J. D.; Bradbury, S. P., An Overview of the Use of Quantitative Structure-activity Relationships for Ranking and Prioritizing Large Chemical Inventories for Environmental Risk Assessments. *Environ. Toxicol. Chem.* **2003,** *22* (8), 1810-1821.

4. (a) Briggs, G. G., Theoretical and Experimental Relationships Between Soil Adsorption, Octanol-water Partition Coefficients, Water Solubilities, Bioconcentration Factors, and

the Parachor. *J. Agric. Food Chem.* **1981,** *29* (5), 1050-9; (b) Poole, S. K.; Poole, C. F., Chromatographic Models for the Sorption of Neutral Organic Compounds by Soil from Water and Air. *J. Chromatogr. A* **1999,** *845* (1 + 2), 381-399; (c) Hidalgo-Rodriguez, M.; Fuguet, E.; Rafols, C.; Roses, M., Performance of Chromatographic Systems to Model Soil-Water Sorption. *J. Chromatogr. A* **2012,** *1252*, 136-145; (d) Harner, T.; Mackay, D., Measurement of Octanol-Air Partition Coefficients for Chlorobenzenes, PCBs, and DDT. *Environ. Sci. Technol.* **1995,** *29* (6), 1599-606; (e) Sangster, J., Octanol-Water Partition Coefficients of Simple Organic Compounds. *J. Phys. Chem. Ref. Data* **1989,** *18* (3), 1111-1122; (f) Abraham, M. H.; Gil-Lostes, J.; Corr, S.; Acree, W. E., Determination of Partition Coefficients of Refrigerants by Gas Liquid Chromatographic Headspace Analysis. *J. Chromatogr. A* **2012,** *1265*, 144-148; (g) Abraham, M. H.; Acree, W. E., Jr.; Leo, A. J.; Hoekman, D., Partition of Compounds from Water and from Air into the Wet and Dry Monohalobenzenes. *New J. Chem.* **2009,** *33* (8), 1685-1692; (h) Sprunger, L. M.; Achi, S. S.; Acree, W. E.; Abraham, M. H.; Leo, A. J.; Hoekman, D., Correlation and Prediction of Solute Transfer to Chloroalkanes from Both Water and the Gas Phase. *Fluid Phase Equilib.* **2009,** *281* (2), 144-162; (i) Abraham, M. H.; Acree, W. E., Gas-Solvent and Water-Solvent Partition Coefficients of the Tetraphenyl Compounds of Group (IV). *New J. Chem.* **2012,** *36* (3), 626-631; (j) McElmurry, S. P.; Long, D. T.; Voice, T. C., Stormwater Dissolved Organic Matter: Influence of Land Cover and Environmental Factors. *Environ. Sci. Technol.* **2014,** *48* (1), 45-53.

5.   (a) Zhang, K.; Chen, M.; Scriba, G. K. E.; Abraham, M. H.; Fahr, A.; Liu, X., Human Skin Permeation of Neutral Species and Ionic Species: Extended Linear Free-Energy Relationship Analyses. *J. Pharm. Sci.* **2012,** *101* (6), 2034-2044; (b) Sprunger, L. M.;

Gibbs, J.; Acree, W. E., Jr.; Abraham, M. H., Correlation of Human and Animal Air-to-Blood Partition Coefficients with a Single Linear Free Energy Relationship Model. *QSAR Comb. Sci.* **2008,** *27* (9), 1130-1139; (c) Hoover, K. R.; Flanagan, K. B.; Acree, W. E., Jr.; Abraham, M. H., Chemical Toxicity Correlations for Several Protozoas, Bacteria, and Water Fleas Based on the Abraham Solvation Parameter Model. *J. Environ. Eng. Sci.* **2007,** *6* (2), 165-174; (d) Abraham, M. H.; Gil-Lostes, J.; Fatemi, M., Prediction of Milk/Plasma Concentration Ratios of Drugs and Environmental Pollutants. *Eur. J. Med. Chem.* **2009,** *44* (6), 2452-2458; (e) Abraham, M. H., The Permeation of Neutral Molecules, Ions, and Ionic Species Through Membranes: Brain Permeation as an Example. *J. Pharm. Sci.* **2011,** *100* (5), 1690-1701; (f) Bowen, K. R.; Flanagan, K. B.; Acree, W. E.; Abraham, M. H.; Rafols, C., Correlation of the Toxicity of Organic Compounds to Tadpoles Using the Abraham Model. *Sci. Total Environ.* **2006,** *371* (1-3), 99-109; (g) Mintz, C.; Acree, W. E., Jr.; Abraham, M. H., Correlation of Minimum Inhibitory Concentrations Toward oral Bacterial Growth Based on the Abraham Model. *QSAR Comb. Sci.* **2006,** *25* (10), 912-920; (h) Abraham, M. H., Human Intestinal Absorption-Neutral Molecules and Ionic Species. *J. Pharm. Sci.* **2014,** *103* (7), 1956-1966; (i) Abraham, M. H.; Gola, J. M. R.; Ibrahim, A.; Acree, W. E., Jr.; Liu, X., The Prediction of Blood-Tissue Partitions, Water-Skin Partitions and Skin Permeation for Agrochemicals. *Pest Manage. Sci.* **2014,** *70* (7), 1130-1137; (j) Ghafourian, T.; Samaras, E. G.; Brooks, J. D.; Riviere, J. E., Modelling the Effect of Mixture Components on Permeation Through Skin. *Int. J. Pharm.* **2010,** *398* (1-2), 28-32; (k) Sprunger, L.; Blake-Taylor, B. H.; Wairegi, A.; Acree, W. E.; Abraham, M. H., Characterization of the Retention Behavior of Organic and Pharmaceutical Drug Molecules on an Immobilized

Artificial Membrane Column with the Abraham Model. *J. Chromatogr. A* **2007,** *1160* (1-2), 235-245; (l) Abraham, M. H.; Ibrahim, A.; Acree, W. E., Air to Lung Partition Coefficients for Volatile Organic Compounds and Blood to Lung Partition Coefficients for Volatile Organic Compounds and Drugs. *Eur. J. Med. Chem.* **2008,** *43* (3), 478-485; (m) Hidalgo-Rodriguez, M.; Fuguet, E.; Rafols, C.; Roses, M., Modeling Nonspecific Toxicity of Organic Compounds to the Fathead Minnow Fish by Means of Chromatographic Systems. *Anal. Chem. (Washington, DC, U. S.)* **2012,** *84* (7), 3446-3452.

6.   (a) Poole, C. F.; Atapattu, S. N.; Poole, S. K.; Bell, A. K., Determination of Solute Descriptors by Chromatographic Methods. *Anal. Chim. Acta* **2009,** *652* (1-2), 32-53; (b) Dimitrov, S.; Pavlov, T.; Nedelcheva, D.; Reuschenbach, P.; Silvani, M.; Bias, R.; Comber, M.; Low, L.; Lee, C.; Parkerton, T.; Mekenyan, O., A Kinetic Model for Predicting Biodegradation. *SAR QSAR Environ. Res.* **2007,** *18* (5-6), 443-457; (c) Judson, R.; Houck, K.; Martin, M.; Knudsen, T.; Thomas, R. S.; Sipes, N.; Shah, I.; Wambaugh, J.; Crofton, K., In Vitro and Modelling Approaches to Risk Assessment from the U.S. Environmental Protection Agency ToxCast Programme. *Basic Clin. Pharmacol. Toxicol.* **2014,** *115* (1), 69-76.

7.   Kamlet, M. J.; Abboud, J. L.; Taft, R. W., The Solvatochromic Comparison Method. 6. The π* Scale of Solvent Polarities. *J. Am. Chem. Soc.* **1977,** *99* (18), 6027-6038.

8.   (a) Abboud, J. L. M.; Notario, R., Critical Compilation of Scales of Solvent Parameters. Part I. Pure, Non-Hydrogen Bond Donor Solvents. *Pure Appl. Chem.* **1999,** *71* (4), 645-718; (b) Laurence, C.; Nicolet, P.; Dalati, M. T.; Abboud, J.-L. M.; Notario, R., The

Empirical Treatment of Solvent-Solute Interactions: 15 Years of π*. *J. Phys. Chem.* **1994,** *98* (23), 5807-5816.

9.   Vitha, M.; Carr, P. W., The Chemical Interpretation and Practice of Linear Solvation Energy Relationships in Chromatography. *J. Chromatogr. A* **2006,** *1126* (1-2), 143-194.

10.   Poole, C. F.; Ariyasena, T. C.; Lenca, N., Estimation of the Environmental Properties of Compounds from Chromatographic Measurements and the Solvation Parameter Model. *J. Chromatogr. A* **2013,** *1317*, 85-104.

11.   Goss, K.-U., Predicting the Equilibrium Partitioning of Organic Compounds Using Just One Linear Solvation Energy Relationship (LSER). *Fluid Phase Equilib.* **2005,** *233* (1), 19-22.

12.   Mintz, C.; Acree, W. E., Jr., Comments on 'an Improved Characteristic Molecular Volume Parameter for Linear Solvation Energy Relationships of Acyclic Alkanes'. *J. Phys. Org. Chem.* **2007,** *20* (5), 365-367.

13.   Abraham, M. H.; Grellier, P. L.; McGill, R. A., Determination of Olive Oil-Gas and Hexadecane-Gas Partition Coefficients, and Calculation of the Corresponding Olive Oil-Water and Hexadecane-Water Partition Coefficients. *J. Chem. Soc., Perkin Trans. 2* **1987,** (6), 797-803.

14.   Abraham, M. H., Hydrogen bonding. 31. Construction of a Scale of Solute Effective or Summation Hydrogen-Bond Basicity. *J. Phys. Org. Chem.* **1993,** *6* (12), 660-84.

15.   (a) Abraham, M. H.; Grellier, P. L.; Prior, D. V.; Duce, P. P.; Morris, J. J.; Taylor, P. J., Hydrogen Bonding. Part 7. A scale of Solute Hydrogen-Bond Acidity Bsed on log K Values for Complexation in Tetrachloromethane. *J. Chem. Soc., Perkin Trans. 2* **1989,** (6), 699-711; (b) Abraham, M. H.; Berthelot, M.; Laurence, C.; Taylor, P. J., Analysis of

Hydrogen-Bond Complexation Constants in 1,1,1-Trichloroethane: the α2Hβ2H Relationship. *J. Chem. Soc., Perkin Trans. 2* **1998,** (1), 187-192; (c) Abraham, M. H.; Platts, J. A., Hydrogen Bond Structural Group Constants. *J. Org. Chem.* **2001,** *66* (10), 3484-3491; (d) Abraham, M. H.; Whiting, G. S., Hydrogen Bonding. XXI. Solvation Parameters for Alkylaromatic Hydrocarbons from Gas-Liquid Chromatographic Data. *J. Chromatogr.* **1992,** *594* (1-2), 229-41.

16.   Abraham, M. H., New Solute Descriptors for Linear Free Energy Relationships and Quantitative Structure-Activity Relationships. *Theor. Comput. Chem.* **1994,** *1* (Quantitative Treatments of Solute/Solvent Interactions), 83-134.

17.   Hidalgo-Rodriguez, M.; Fuguet, E.; Rafols, C.; Roses, M., Estimation of Biological Properties by Means of Chromatographic Systems: Evaluation of the Factors That Contribute to the Variance of Biological-Chromatographic Correlations. *Anal. Chem. (Washington, DC, U. S.)* **2010,** *82* (24), 10236-10245.

18.   (a) Li, J.; Carr, P. W., Measurement of Water-Hexadecane Partition Coefficients by Headspace Gas Chromatography and Calculation of Limiting Activity Coefficients in Water. *Analytical Chemistry* **1993,** *65* (10), 1443-1450; (b) Chaintreau, A.; Grade, A.; Munoz-Box, R., Determination of Partition Coefficients and Quantitation of Headspace Volatile Compounds. *Analytical Chemistry* **1995,** *67* (18), 3300-3304; (c) Atlan, S.; Trelea, I. C.; Saint-Eve, A.; Souchon, I.; Latrille, E., Processing Gas Chromatographic Data and Confidence Interval Calculation for Partition Coefficients Determined by the Phase Ratio Variation Method. *J. Chromatogr. A* **2006,** *1110* (1-2), 146-155.

19.   Abraham, M. H.; Ibrahim, A.; Zissimos, A. M., Determination of Sets of Solute

       Descriptors from Chromatographic Measurements. *J. Chromatogr. A* **2004,** *1037* (1-2),

       29-47.

20.   Abraham, M. H.; Chadha, H. S., Applications of a Solvation Equation to Drug Transport

       Properties. *Methods Princ. Med. Chem.* **1996,** *4* (Lipophilicity in Drug Action and

       Toxicology), 311-337.

21.   Abraham, M. H.; Smith, R. E.; Luchtefeld, R.; Boorem, A. J.; Luo, R.; Acree, W. E., Jr.,

       Prediction of Solubility of Drugs and Other Compounds in Organic Solvents. *J. Pharm.

       Sci.* **2010,** *99* (3), 1500-1515.

22.   Poole, C. F.; Karunasekara, T.; Ariyasena, T. C., Totally Organic Biphasic Solvent

       Systems for Extraction and Descriptor Determinations. *J. Sep. Sci.* **2013,** *36* (1), 96-109.

23.   Atapattu, S. N.; Eggers, K.; Poole, C. F.; Kiridena, W.; Koziol, W. W., Extension of the

       System Constants Database for Open-Tubular Columns: System Maps at Low and

       Intermediate Temperatures for Four New Columns. *J Chromatogr A* **2009,** *1216* (10),

       1640-9.

24.   Poole, C. F.; Poole, S. K., Separation Characteristics of Wall-Coated Open-Tubular

       Columns for Gas Chromatography. *J. Chromatogr. A* **2008,** *1184* (1-2), 254-280.

25.   Poole, C. F.; Poole, S. K., Foundations of Retention in Partition Chromatography. *J.

       Chromatogr. A* **2009,** *1216* (10), 1530-1550.

26.   Kiridena, W.; Atapattu, S. N.; Poole, C. F.; Koziol, W. W., System Maps for RP-LC on

       an Octadecylsiloxane-Bonded Silica Stationary Phase (SunFire C18). *Chromatographia*

       2008, *68* (1/2), 11-17.

27.   (a) Kiridena, W.; Atapattu, S. N.; Poole, C. F.; Koziol, W. W., Comparison of the Separation Characteristics of the Organic-Inorganic Hybrid Stationary Phases XBridge C8 and Phenyl and XTerra Phenyl in RP-LC. *Chromatographia* **2008,** *68* (7/8), 491-500; (b) Kiridena, W.; Poole, C. F.; Atapattu, S. N.; Qian, J.; Koziol, W. W., Comparison of the Separation Characteristics of the Organic-Inorganic Hybrid Octadecyl Stationary Phases XTerra MS C18 and XBridge C18 and Shield RP18 in RPLC. *Chromatographia* **2007,** *66* (7/8), 453-460.

28.   (a) Oumada, F. Z.; Roses, M.; Bosch, E.; Abraham, M. H., Solute-Solvent Interactions in Normal-Phase Liquid Chromatography: A Linear Free-Energy Relationships Study. *Anal. Chim. Acta* **1999,** *382* (3), 301-308; (b) Kiridena, W.; Poole, C. F., Influence of Solute Size and Site-Specific Surface Interactions on the Prediction of Retention in Liquid Chromatography Using the Solvation Parameter Model. *Analyst (Cambridge, U. K.)* **1998,** *123* (6), 1265-1270; (c) Tulp, H. C.; Goss, K.-U.; Schwarzenbach, R. P.; Fenner, K., Experimental Determination of LSER Parameters for a Set of 76 Diverse Pesticides and Pharmaceuticals. *Environ Sci Technol* **2008,** *42* (6), 2034-40.

29.   Poole, C. F., *The Essence of Chromatography*. Elsevier: Amsterdam, 2003.

30.   (a) Snyder, L. R.; Dolan, J. W.; Carr, P. W., The Hydrophobic-Subtraction Model of Reversed-Phase Column Selectivity. *J. Chromatogr. A* **2004,** *1060* (1-2), 77-116; (b) Marchand, D. H.; Snyder, L. R.; Dolan, J. W., Characterization and Applications of Reversed-Phase Column Selectivity Based on the Hydrophobic-Subtraction Model. *J. Chromatogr. A* **2008,** *1191* (1-2), 2-20.

31.   (a) Poole, C. F.; Ahmed, H.; Kiridena, W.; DeKay, C.; Koziol, W. W., Insights into the Retention Mechanisms on Perfluorohexylpropylsiloxane-Bonded (Fluophase-RP) and

Octadecylsiloxane-Bonded (Betasil C18) Stationary Phases Based on the Same Silica

Substrate in RP-LC. *Chromatographia* **2007,** *65* (3/4), 127-139; (b) Poole, C. F.; Ahmed,

H.; Kiridena, W.; DeKay, C.; Koziol, W. W., Contribution of Steric Repulsion to

Retention on an Octadecylsiloxane-Bonded Silica Stationary Phase in Reversed-Phase

Liquid Chromatography. *Chromatographia* **2005,** *62* (11-12), 553-561.

32.   (a) Abraham, M. H.; Al-Hussaini, A. J. M., Solvation Descriptors for the

Polychloronaphthalenes: Estimation of Some Physicochemical Properties. *J. Environ.*

Monit. **2001,** *3* (4), 377-381; (b) Hoover, K. R.; Coaxum, R.; Pustejovsky, E.; Stovall, D.

M.; Acree, W. E.; Abraham, M. H., Thermochemical Behavior of Dissolved Carboxylic

Acid Solutes: Part 4 - Mathematical Correlation of 4-Nitrobenzoic Acid Solubilities with

the Abraham Solvation Parameter Model. *Phys. Chem. Liq.* **2004,** *42* (4), 339-347; (c)

Flanagan, K. B.; Hoover, K. R.; Acree, W. E.; Abraham, M. H., Mathematical

Correlation of 1,2,4,5-Tetramethylbenzene Solubilities in Organic Solvents with the

Abraham Solvation Parameter Model. *Phys. Chem. Liq.* **2006,** *44* (2), 173-182.

33.   (a) Poole, S. K.; Poole, C. F., Quantitative Structure-Retention (Property) Relationships

in Micellar Electrokinetic Chromatography. *J. Chromatogr. A* **2008,** *1182* (1), 1-24; (b)

Fuguet, E.; Rafols, C.; Bosch, E.; Abraham, M. H.; Roses, M., Selectivity of Single,

Mixed, and Modified Pseudostationary Phases in Electrokinetic Chromatography.

Electrophoresis **2006,** *27* (10), 1900-1914; (c) Fu, C.; Khaledi, M. G., Micellar

Selectivity Triangle for Classification of Chemical Selectivity in Electrokinetic

Chromatography. *J. Chromatogr. A* **2009,** *1216* (10), 1891-1900; (d) Poole, C. F.; Poole,

S. K.; Abraham, M. H., Recommendations for the Determination of Selectivity in

Micellar Electrokinetic chromatography. *J. Chromatogr. A* **1998,** *798* (1 + 2), 207-222;

(e) Trone, M. D.; Khaledi, M. G., Statistical Evaluation of Linear Solvation Energy Relationship Models used to Characterize Chemical Selectivity in Micellar Electrokinetic Chromatography. *J. Chromatogr. A* **2000,** *886* (1+2), 245-257.

34.   Ariyasena, T. C.; Poole, C. F., Models for Liquid-Liquid Partition in the System Ethanolamine-Organic Solvent and Their Use for Estimating Descriptors for Organic Compounds. *Chromatographia* **2013,** *76* (3-4), 157-164.

35.   (a) Sarafraz-Yazdi, A.; Amiri, A., Liquid-Phase Microextraction. *TrAC, Trends Anal. Chem.* **2010,** *29* (1), 1-14; (b) Jeannot, M. A.; Przyjazny, A.; Kokosa, J. M., Single Drop Microextraction - Development, Applications and Future Trends. *J. Chromatogr. A* **2010,** *1217* (16), 2326-2336; (c) Poole, S. K.; Dean, T. A.; Oudsema, J. W.; Poole, C. F., Sample Preparation for Chromatographic Separations: An Overview. *Anal. Chim. Acta* **1990,** *236* (1), 3-42.

36.   Poole, C. F., New Trends in Solid-Phase Extraction. *TrAC, Trends Anal. Chem.* **2003,** *22* (6), 362-373.

37.   Ahmed, H.; Poole, C. F.; Kozerski, G. E., Determination of Descriptors for Organosilicon Compounds by Gas Chromatography and Non-Aueous Liquid-Liquid Partitioning. *J. Chromatogr. A* **2007,** *1169* (1-2), 179-192.

38.   Karunasekara, T.; Poole, C. F., Determination of Descriptors for Fragrance Compounds by Gas Chromatography and Liquid-Liquid Partition. *J. Chromatogr. A* **2012,** *1235*, 159-165.

39.   Karunasekara, T.; Atapattu, S. N.; Poole, C. F., Determination of Descriptors for Plasticizers by Chromatography and Liquid-Liquid Partition. *Chromatographia* **2012,** *75* (19-20), 1135-1146.

40.   Karunasekara, T.; Poole, C. F., Compounds for Expanding the Descriptor Space for

        Characterizing Separation Systems. *J. Chromatogr. A* **2012,** *1266*, 124-130.

41.   Karunasekara, T.; Poole, C. F., Models for Liquid-Liquid Partition in the System

        Ethylene Glycol-Organic Solvent and Their Use for Estimating Descriptors for Organic

        Compounds. *Chromatographia* **2011,** *73* (9-10), 941-951.

42.   (a) Jimenez, L.; Angulo, V.; Caparros, S.; Ariza, J., Comparison of Polynomial and

        Neural Fuzzy Models as Applied to the Ethanolamine Pulping of Vine Shoots. *Bioresour.*

        Technol. **2007,** *98* (18), 3440-3448; (b) Antoniou, E.; Buitrago, C. F.; Tsianou, M.;

        Alexandridis, P., Solvent Effects on Polysaccharide Conformation. *Carbohydr. Polym.*

        2010, *79* (2), 380-390; (c) Iida, K.; Sato, H., Proton Transfer Step in the Carbon Dioxide

        Capture by Monoethanol Amine: A Theoretical Study at the Molecular Level. *The*

        Journal of Physical Chemistry B **2012,** *116* (7), 2244-2248.

43.   Labban, A. S.; Marcus, Y., Solvatochromic Parameters of Ethanolamines. *J. Chem. Soc.,*

        Faraday Trans. **1997,** *93* (1), 77-79.

44.   (a) Gubskaya, A. V.; Kusalik, P. G., Molecular Dynamics Simulation Study of Ethylene

        Glycol, Ethylenediamine, and 2-Aminoethanol. 1. The Local Structure in Pure Liquids. *J.*

        Phys. Chem. A **2004,** *108* (35), 7151-7164; (b) Haufa, K. Z.; Czarnecki, M. A., Molecular

        Structure and Hydrogen Bonding of 2-Aminoethanol, 1-Amino-2-propanol, 3-Amino-1-

        propanol, and Binary Mixtures with Water Studied by Fourier Transform Near-Infrared

        Spectroscopy and Density Functional Theory Calculations. *Appl. Spectrosc.* **2010,** *64* (3),

        351-358.

45.   (a) Vorobyov, I.; Yappert, M. C.; DuPre, D. B., Hydrogen Bonding in Monomers and

        Dimers of 2-Aminoethanol. *J. Phys. Chem. A* **2002,** *106* (4), 668-679; (b) Sengwa, R. J.;

Sankhla, S.; Khatri, V.; Choudhary, S., Static Permittivity and Molecular Interactions in Binary Mixtures of Ethanolamine with Alcohols and Amides. *Fluid Phase Equilib.* **2010,** *293* (2), 137-140.

46.   Kennard, R. W. S., L. A., *Technometrics* **1969,** *11*, 137-148.

47.   (a) Poole, C. F.; Karunasekara, T., Solvent Classification for Chromatography and Extraction. *J. Planar Chromatogr.--Mod. TLC* **2012,** *25* (3), 190-199; (b) Karunasekara, T.; Poole, C. F., Models for Liquid-Liquid Partition in the System Formamide-Organic Solvent and Their Use for Estimating Descriptors for Organic Compounds. *Talanta* **2011,** *83* (4), 1118-1125.

48.   Baliah, V.; Ramakrishnan, V., Cryoscopic Behavior of Phenols in Ethanolamine. *Recl. Trav. Chim. Pays-Bas* **1963,** *82* (7), 709-12.

49.   Ariyasena, T. C.; Poole, C. F., Evaluation of Triethylamine as a Counter Solvent in Totally Organic Biphasic Liquid-Liquid Partition Systems. *Chromatographia* **2013,** *76* (15-16), 1031-1039.

50.   De Juan, A.; Fonrodona, G.; Casassas, E., Solvent Classification Based on Solvatochromic Parameters: A Comparison with the Snyder Approach. *TrAC, Trends Anal. Chem.* **1997,** *16* (1), 52-62.

51.   Karunasekara, T.; Poole, C. F., Models for Liquid-Liquid Partition in the System Dimethyl Sulfoxide-Organic Solvent and Their Use for Estimating Descriptors for Organic Compounds. *J. Chromatogr. A* **2011,** *1218* (28), 4525-4536.

52.   Ariyasena, T. C.; Poole, C. F., Determination of Descriptors for Polycyclic Aromatic Hydrocarbons and Related Compounds by Chromatographic Methods and Liquid-Liquid Partition in Totally Organic Biphasic Systems. *J Chromatogr A* **2014,** *1361*, 240-254.

53.   (a) Purcaro, G.; Moret, S.; Conte, L. S., Overview on Polycyclic Aromatic Hydrocarbons: Occurrence, Legislation and Innovative Determination in Foods. *Talanta* **2013,** *105*, 292-305; (b) Kim, K.-H. J., S. A.; Kabir, E.; Brown, R. J. C. , A Review of Airborne Polycyclic Aromatic Hydrocarbons (PAHs) and Their Human Health Effects. *Environ. Int.* **2013,** *60*, 71-80; (c) Ravindra, K.; Sokhi, R.; Van Grieken, R., Atmospheric Polycyclic Aromatic Hydrocarbons: Source Attribution, Emission Factors and Regulation. *Atmos. Environ.* **2008,** *42* (13), 2895-2921; (d) *Air Emissions Models for Waste and Waste Water*; US Environmental Protection Agency: Research Triangle Park, North Carolina, 27711., 1994; pp 1-532.

54.   (a) Lee, M. L.; Novotny, M. V.; Bartle, K. D., *Analytical Chemistry of Polycyclic Aromatic Compounds*. Academic Press: 1981; p 462 pp; (b) Marizetti, S. *Polycyclic Aromatic Hydrocarbons in the Environment: Environmental Fate and Transformation. Polycyclic Aromatic Compounds*; 2013; pp 311-330; (c) Plaza-Bolanos, P.; Frenich, A. G.; Vidal, J. L. M., Polycyclic Aromatic Hydrocarbons in Food and Beverages. Analytical Methods and Trends. *J. Chromatogr. A* **2010,** *1217* (41), 6303-6326.

55.   (a) Mackay, D. S., W. Y.; Ma, K. C.; Lee, S. C., *Handbook of Physical-Chemical Properties and Environmental Fate for Organic Compounds*. Taylor and Francis: Boca Raton, 2006; Vol. Vol. II; (b) Schroder, B.; Santos, L. M. N. B. F.; Rocha, M. A. A.; Oliveira, M. B.; Marrucho, I. M.; Coutinho, J. A. P., Prediction of Environmental Parameters of Polycyclic Aromatic Hydrocarbons with COSMO-RS. *Chemosphere* **2010,** *79* (8), 821-9.

56.   (a) Lu, G.-N.; Dang, Z.; Tao, X.-Q.; Yang, C.; Yi, X.-Y., Estimation of Water Solubility of Polycyclic Aromatic Hydrocarbons Using Quantum Chemical Descriptors and Partial

Least Squares. *QSAR Comb. Sci.* **2008,** *27* (5), 618-626; (b) Ma, Y.-G.; Lei, Y.-D.; Xiao, H.; Wania, F.; Wang, W.-H., Critical Review and Recommended Values for the Physical-Chemical Property Data of 15 Polycyclic Aromatic Hydrocarbons at 25°C. *J. Chem. Eng. Data* **2010,** *55* (2), 819-825; (c) Ha, Y.; Kwon, J.-H., Determination of 1-Octanol-Air Partition Coefficient Using Gaseous Diffusion in the Air Boundary Layer. *Environ. Sci. Technol.* **2010,** *44* (8), 3041-3046; (d) Altschuh, J.; Bruggemann, R.; Santl, H.; Eichinger, G.; Piringer, O. G., Henry's Law Constants for a Diverse Set of Organic Chemicals: Experimental Determination and Comparison of Estimation Methods. *Chemosphere* **1999,** *39* (11), 1871-1887.

57.   Ahmed, H.; Poole, C. F.; Kozerski, G. E., Determination of descriptors for organosilicon compounds by gas chromatography and non-aqueous liquid-liquid partitioning. *J. Chromatogr. A* **2007,** *1169* (1-2), 179-192.

58.   Acree, W. E., Jr.; Abraham, M. H., Solubility Predictions for Crystalline Nonelectrolyte Solutes Dissolved in Organic Solvents Based Upon the Abraham General Solvation Model. *Can. J. Chem.* **2001,** *79* (10), 1466-1476.

59.   Acree, W. E.; Abraham, M. H., Solubility Predictions for Crystalline Polycyclic Aromatic Hydrocarbons (PAHs) Dissolved in Organic Solvents Based Upon the Abraham General Solvation Model. *Fluid Phase Equilib.* **2002,** *201* (2), 245-258.

60.   (a) Monarrez, C. I.; Acree, W. E., Jr.; Abraham, M. H., Prediction and Mathematical Correlation of the Solubility of Fluorene in Alcohol Solvents Based Upon the Abraham General Solvation Model. *Phys. Chem. Liq.* **2002,** *40* (5), 581-591; (b) Stovall, D.; Hoover, K.; Acree, W.; Abraham, M., Solubility Behavior of Crystalline Polycyclic Aromatic Hydrocarbons (PAHs): Prediction of Fluorene Solubilities in Organic Solvents

with the Abraham Solvation Parameter Model. *Polycyclic Aromat. Compd.* **2005,** *25* (4), 313-326.

61.   Hoover, K. R.; Acree, W. E., Jr.; Abraham, M. H., Correlation of the Solubility Behavior of Crystalline 1-Nitronaphthalene in Organic Solvents with the Abraham Solvation Parameter Model. *J. Solution Chem.* **2005,** *34* (10), 1121-1133.

62.   (a) Qian, J.; Poole, C. F., Distribution of Neutral Organic Compounds Between n-Heptane and Fluorine-Containing Alcohols. *J. Chromatogr. A* **2007,** *1143* (1-2), 276-283; (b) Ahmed, H.; Poole, C. F., Distribution of Neutral Organic Compounds Between n-Heptane and Methanol or N,N-Dimethylformamide. *J. Sep. Sci.* **2006,** *29* (14), 2158-2165; (c) Karunasekara, T.; Poole, C. F., Models for Liquid-Liquid Partition in the System Propylene Carbonate-Organic Solvent and Their Use for Estimating Descriptors for Organic Compounds. *J. Chromatogr. A* **2011,** *1218* (6), 809-816; (d) Ahmed, H.; Poole, C. F., Model for the Distribution of Neutral Organic Compounds Between n-Hexane and Acetonitrile. *J. Chromatogr. A* **2006,** *1104* (1-2), 82-90.

63.   Abraham, M. H.; McGowan, J. C., The Use of Characteristic Volumes to Measure Cavity Terms in Reversed Phase Liquid Chromatography. *Chromatographia* **1987,** *23* (4), 243-6.

64.   Abraham, M. H.; Whiting, G. S.; Doherty, R. M.; Shuely, W. J., Hydrogen bonding. Part 13. A New Method for the Characterization of GLC Stationary Phases-the Laffort Data Set. *J. Chem. Soc., Perkin Trans. 2* **1990,** (8), 1451-60.

65.   Atapattu, S. N.; Eggers, K.; Poole, C. F.; Kiridena, W.; Koziol, W. W., Extension of the System Constants Database for Open-Tubular Columns: System Maps at Low and Intermediate Temperatures for Four New Columns. *J. Chromatogr. A* **2009,** *1216* (10), 1640-1649.

66.   Atapattu, S. N.; Poole, C. F., Solute Descriptors for Characterizing Retention Properties of Open-Tubular Columns of Different Selectivity in Gas Chromatography at Intermediate Temperatures. *J. Chromatogr. A* **2008,** *1195* (1-2), 136-145.

67.   Platts, J. A.; Abraham, M. H.; Butina, D.; Hersey, A., Estimation of Molecular Linear Free Energy Relationship Descriptors by a Group Contribution Approach. 2. Prediction of Partition Coefficients. *J. Chem. Inf. Comput. Sci.* **2000,** *40* (1), 71-80.

68.   Platts, J. A.; Butina, D.; Abraham, M. H.; Hersey, A., Estimation of Molecular Linear Free Energy Relation Descriptors Using a Group Contribution Approach. *J. Chem. Inf. Comput. Sci.* **1999,** *39* (5), 835-845.

69.   (a) Stenzel, A.; Endo, S.; Goss, K.-U., Measurements and Predictions of Hexadecane/Air Partition Coefficients for 387 Environmentally Relevant Compounds. *J. Chromatogr. A* **2012,** *1220*, 132-142; (b) Abraham, M. H.; Gil-Lostes, J.; Enrique Cometto-Muniz, J.; Cain, W. S.; Poole, C. F.; Atapattu, S. N.; Abraham, R. J.; Leonard, P., The Hydrogen Bond Acidity and Other Descriptors for Oximes. *New J. Chem.* **2009,** *33* (1), 76-81.

70.   (a) Abraham, M. H., Hydrogen bonding. XXVII. Solvation Parameters for Functionally Substituted Aromatic Compounds and Heterocyclic Compounds, from Gas-Liquid Chromatographic Data. *J. Chromatogr.* **1993,** *644* (1), 95-139; (b) Sprunger, L.; Proctor, A.; Acree, W. E.; Abraham, M. H., Characterization of the Sorption of Gaseous and Organic Solutes onto Polydimethyl Siloxane Solid-Phase Microextraction Surfaces Using the Abraham Model. *J. Chromatogr. A* **2007,** *1175* (2), 162-173; (c) Mutelet, F.; Rogalski, M.; Jones, J.; Horsten, R.; Floter, E., Using Temperature Gradient Gas Chromatography to Determine or Predict Vapor Pressures and Linear Solvation Energy Relationship Parameters of Highly Boiling Organic Compounds. *J. Chromatogr., A* **2003,**

988 (1), 117-132; (d) Mutelet, F.; Rogalski, M., Experimental Determination and Prediction of the Gas-Liquid n-Hexadecane Partition Coefficients. *J. Chromatogr. A* **2001,** *923* (1-2), 153-163; (e) Abraham, M. H.; Autenrieth, R.; Dimitriou-Christidis, P., The Estimation of Physicochemical Properties of Methyl and Other Alkyl Naphthalenes. *J. Environ. Monit.* **2005,** *7* (5), 445-449; (f) Sprunger, L. M.; Proctor, A.; Acree, W. E., Jr.; Abraham, M. H.; Benjelloun-Dakhama, N., Correlation and Prediction of Partition Coefficient Between the Gas Phase and Water, and the Solvents Dry Methyl Acetate, Dry and Wet Ethyl Acetate, and Dry and Wet Butyl Acetate. *Fluid Phase Equilib.* **2008,** *270* (1-2), 30-44.

71.   (a) Dabestani, R.; Ivanov, I. N., A Compilation of Physical, Spectroscopic and Photophysical Properties of Polycyclic Aromatic Hydrocarbons. *Photochem. Photobiol.* **1999,** *70* (1), 10-34; (b) Chu, W.; Chan, K. H., The Prediction of Partitioning Coefficients for Chemicals Causing Environmental Concern. *Sci. Total Environ.* **2000,** *248* (1), 1-10; (c) *Estimation Program Interface Suite for Microsoft Windows*, v.4.11; US EPA: Washington, DC, USA, 2012; (d) De Voogt, P.; Van Zijl, G. A.; Govers, H.; Brinkman, U. A. T., Reversed-Phase TLC and Structure-Activity Relationships of Polycyclic (Hetero) Aromatic Hydrocarbons. *J. Planar Chromatogr.--Mod. TLC* **1990,** *3* (1-2), 24-33; (e) Livinstone, D. J., Exploring QSAR Hydrophobic, Electronic, and Steric Constants, edited C. Hansch, A. Leo, and D. Hoekman. *Pestic. Biochem. Physiol.* **1996,** *56* (1), 78.

72.   (a) Odabasi, M.; Cetin, B.; Sofuoglu, A., Henry's Law Constant, Octanol-Air Partition Coefficient and Supercooled Liquid Vapor Pressure of Carbazole as a Function of Temperature: Application to Gas/Particle Partitioning in the Atmosphere. *Chemosphere* **2006,** *62* (7), 1087-1096; (b) Abraham, M. H.; Acree, W. E., Jr., Comparison of

Solubility of Gases and Vapours in Wet and Dry Alcohols, Especially Octan-1-ol. *J. Phys. Org. Chem.* **2008,** *21* (10), 823-832.

73.   Harner, T.; Bidleman, T. F., Measurement of Octanol-Air Partition Coefficients for Polycyclic Aromatic Hydrocarbons and Polychlorinated Naphthalenes. *J. Chem. Eng. Data* **1998,** *43* (1), 40-46.

74.   (a) Brennan, R. A.; Nirmalakhandan, N.; Speece, R. E., Comparison of predictive methods for Henrys law coefficients of organic chemicals. *Water Res.* **1998,** *32* (6), 1901-1911; (b) Raventos-Duran, T.; Camredon, M.; Valorso, R.; Mouchel-Vallon, C.; Aumont, B., Structure-Activity Relationships to Estimate the Effective Henry's Law Constants of Organics of Atmospheric Interest. *Atmos. Chem. Phys.* **2010,** *10* (16), 7643-7654.

75.   Abraham, M. H.; Andonian-Haftvan, J.; Whiting, G. S.; Leo, A.; Taft, R. S., Hydrogen Bonding. Part 34. The Factors that Influence the Solubility of Gases and Vapors in Water at 298 K, and a New Method for its Determination. *J. Chem. Soc., Perkin Trans. 2* **1994,** (8), 1777-91.

76.   (a) Abraham, M. H.; Acree, W. E., The Hydrogen Bond Properties of Water from 273 K to 573 K; Equations for the Prediction of Gas-Water Partition Coefficients. *Phys. Chem. Chem. Phys.* **2012,** *14* (20), 7433-7440; (b) Abraham, M. H.; Acree, W. E., Jr., Prediction of Gas to Water Partition Coefficients from 273 to 373 K Using Predicted Enthalpies and Heat Capacities of Hydration. *Fluid Phase Equilib.* **2007,** *262* (1-2), 97-110; (c) Abraham, M. H.; Ibrahim, A.; Acree, W. E., Partition of Compounds from Gas to Water and from Gas to Physiological Saline at 310 K: Linear Free Energy Relationships. *Fluid Phase Equilib.* **2007,** *251* (2), 93-109.

77.   Abraham, M. H.; Le, J., The Correlation and Prediction of the Solubility of Compounds in Water Using an Amended Solvation Energy Relationship. *J. Pharm. Sci.* **1999,** *88* (9), 868-880.

78.   (a) van Noort, P. C. M., Compound-Class Specific Estimation of Solid Organic Compound Vapor Pressure and Aqueous Solubility from Simple Molecular Structure Descriptors and the Temperature of Melting. *Chemosphere* **2009,** *77* (6), 838-841; (b) Yu, G.; Xu, X., Investigation of Aqueous Solubilities of Nitro-PAH (Polycyclic Aromatic Hydrocarbons) by Dynamic Couple-Column HPLC. *Chemosphere* **1992,** *24* (12), 1699-705.

79.   (a) Lei, Y. D.; Chankalal, R.; Chan, A.; Wania, F., Supercooled Liquid Vapor Pressures of the Polycyclic Aromatic Hydrocarbons. *J. Chem. Eng. Data* **2002,** *47* (4), 801-806; (b) Haftka, J. J. H.; Parsons, J. R.; Govers, H. A. J., Supercooled Liquid Vapour Pressures and Related Thermodynamic Properties of Polycyclic Aromatic Hydrocarbons Determined by Gas Chromatography. *J. Chromatogr. A* **2006,** *1135* (1), 91-100; (c) Odabasi, M.; Cetin, E.; Sofuoglu, A., Determination of Octanol-Air Partition Coefficients and Supercooled Liquid Vapor Pressures of PAHs as a Function of Temperature: Application to Gas-Particle Partitioning in an Urban Atmosphere. *Atmos. Environ.* **2006,** *40* (34), 6615-6625; (d) van Noort, P. C. M., QSPRs for the Estimation of Subcooled Liquid Vapor Pressures of Polycyclic Aromatic Hydrocarbons, and of Polychlorinated Benzenes, Biphenyls, Dibenzo-p-dioxins, and Dibenzofurans at Environmentally Relevant Temperatures. *Chemosphere* **2009,** *77* (6), 848-853.

80.   Quina, F. H.; Carroll, F. A.; Cheuy, D. M., A Linear Solvation Energy Relationship to Predict Vapor Pressure from Molecular Structure. *J. Braz. Chem. Soc.* **2005,** *16* (5), 1010-1016.

81.   (a) Hwang, C. S. In *Atomic Layer Deposition for Microelectronic Applications*, Wiley-VCH Verlag GmbH & Co. KGaA: 2012; pp 161-192; (b) Iwai, H., Roadmap for 22 nm and Beyond (Invited Paper). *Microelectron. Eng.* **2009,** *86* (7-9), 1520-1528; (c) Peercy, P. S., The Drive to Miniaturization. *Nature (London)* **2000,** *406* (6799), 1023-1026.

82.   Arden, W., Future Semiconductor Material Requirements and Innovations as Projected in the ITRS 2005 Roadmap. *Mater. Sci. Eng., B* **2006,** *134* (2-3), 104-108.

83.   International technology Roadmap for Semiconductors, 2013 Edition; Semiconsuctor Industry Association. http://www.itrs.net/Links/2013ITRS/Summary2013.htm (accessed August 17, 2014).

84.   (a) Ruhl, G.; Lehnert, W.; Lukosius, M.; Wenger, C.; Baristiran Kaynak, C.; Blomberg, T.; Haukka, S.; Baumann, P. K.; Besling, W.; Roest, A.; Riou, B.; Lhostis, S.; Halimaou, A.; Roozeboom, F.; Langereis, E.; Kessels, W. M. M.; Zauner, A.; Rushworth, S., Dielectric Material Options for Integrated Capacitors. *ECS J. Solid State Sci. Technol.* **2014,** *3* (8), N120-N125; (b) Arden, W., Future Roadblocks and Solutions in Silicon Technology as Outlined by the ITRS Roadmap. *Mater. Sci. Semicond. Process.* **2003,** *5* (4-5), 313-319; (c) Kingon, A. I.; Maria, J.-P.; Streiffer, S. K., Alternative Dielectrics to Silicon Dioxide for Memory and Logic Devices. *Nature (London)* **2000,** *406* (6799), 1032-1038.

85.   (a) Rickerby, J.; Steinke, J. H. G., Current Trends in Patterning with Copper. *Chem. Rev. (Washington, D. C.)* **2002,** *102* (5), 1525-1549; (b) Merchant, S. M.; Kang, S. H.;

Sanganeria, M.; Van Schravendijk, B.; Mountsier, T., Copper Interconnects for Semiconductor Devices. *JOM* **2001,** *53* (6), 43-48; (c) Rossnagel, S. M.; Wisnieff, R.; Edelstein, D.; Kuan, T. S., Interconnect Issues Post 45nm. *Tech. Dig. - Int. Electron Devices Meet.* **2005**, 95-97; (d) Kim, H., The Application of Atomic Layer Deposition for Metallization of 65 nm and Beyond. *Surf. Coat. Technol.* **2006,** *200* (10), 3104-3111; (e) Roule, A.; Amuntencei, M.; Deronzier, E.; Haumesser, P. H.; Da Silva, S.; Avale, X.; Pollet, O.; Baskaran, R.; Passemard, G., Seed Layer Enhancement by Electrochemical Deposition: The Copper Seed Solution for Beyond 45nm. *Microelectron. Eng.* **2007,** *84* (11), 2610-2614; (f) Whitman, C.; Moslehi, M. M.; Paranjpe, A.; Velo, L.; Omstead, T., Ultralarge Scale Integrated Metallization and Interconnects. *J. Vac. Sci. Technol., A* **1999,** *17* (4, Pt. 2), 1893-1897.

86.   Clark, R., Emerging Applications for High K Materials in VLSI Technology. *Materials* **2014,** *7* (4), 2913-2944.

87.   Ritala, M.; Niinisto, J., Industrial Applications of Atomic Layer Deposition. *ECS Trans.* **2009,** *25* (8, EuroCVD 17/CVD 17), 641-652.

88.   (a) Wu, F.; Wu, J.; Banerjee, S.; Blank, O.; Banerjee, P., Frontiers in Applied Atomic Layer Deposition (ALD) Research. *Mater. Sci. Forum* **2013,** *736* (Advances in Materials Development), 147-182, 37 pp; (b) Mackus, A. J. M.; Bol, A. A.; Kessels, E., The Use of Atomic Layer Deposition in Advanced Nanopatterning. *Nanoscale* **2014**, Ahead of Print; (c) Cheng, J.-H.; Seghete, D.; Lee, M.; Schlager, J. B.; Bertness, K. A.; Sanford, N. A.; Yang, R.; George, S. M.; Lee, Y. C., Atomic Layer Deposition Enabled Interconnect Technology for Vertical Nanowire Arrays. *Sens. Actuators, A* **2011,** *165* (1), 107-114; (d) Leskelae, M.; Kemell, M.; Kukli, K.; Pore, V.; Santala, E.; Ritala, M.; Lu, J., Exploitation

of Atomic Layer Deposition for Nanostructured Materials. *Mater. Sci. Eng., C* **2007,** *27* (5-8), 1504-1508; (e) Knoops, H. C. M.; Donders, M. E.; Baggetto, L.; van de Sanden, M. C. M.; Notten, P. H. L.; Kessels, W. M. M., Atomic Layer Deposition for All-Solid-State 3D-Integrated Batteries. *ECS Trans.* **2009,** *25* (4, Atomic Layer Deposition Applications 5), 333-344; (f) Kim, H.; Lee, H.-B.-R.; Maeng, W. J., Applications of Atomic Layer Deposition to Nanofabrication and Emerging Nanodevices. *Thin Solid Films* **2009,** *517* (8), 2563-2580; (g) Eisenbraun, E. T.; Carpenter, M.; Siddique, R.; Naczas, S.; Zeng, W.; Luo, F.; Kaloyeros, A. E., Atomic Layer Deposition: Emerging Materials, Processes, and Nanoscale Technical Applications. *ECS Trans.* **2006,** *1* (10, Atomic Layer Deposition), 29-36.

89.   (a) Rossnagel, S. M., Thin Film Deposition with Physical Vapor Deposition and Related Technologies. *Journal of Vacuum Science & Technology A: Vacuum, Surfaces, and Films* **2003,** *21* (5), S74; (b) Rumaiz, A. K.; Franklin, S.; Buzby, S.; Shah, S. I. In *Thin Film Formation Techniques*, John Wiley & Sons, Inc.: 2007; pp 721-753; (c) Erkens, G. V., J.; auf dem Brinke, T.; Fromme, M.; Mohnfeld, A., *Plasma_Assisted Surface Coating*. Suddeutscher Verlag onpact GmbH: Munich, Germany., 2011; p 6-18.

90.   Mahan, J. E., *Physical Vapor Deposition of Thin Films.* John Wiley & Sons, Inc.: New York, USA., 2000; p 115-119.

91.   Doll, G. L.; Mensah, B. A.; Mohseni, H.; Scharf, T. W., Chemical Vapor Deposition and Atomic Layer Deposition of Coatings for Mechanical Applications. *J. Therm. Spray Technol.* **2010,** *19* (1-2), 510-516.

92.   Doppelt, P., Why is Coordination Chemistry Stretching the Limits of Micro-Electronics Technology? *Coord. Chem. Rev.* **1998,** *178-180* (Pt. 2), 1785-1809.

93. Pierson, H. O.; Editor, *Handbook of Chemical Vapor Deposition: Principles, Technology and Applications, 2nd Edition*. William Andrew Publishing: 2000; p 482 pp.

94. Gates, S. M., Surface Chemistry in the Chemical Vapor Deposition of Electronic Materials. *Chem. Rev. (Washington, D. C.)* **1996,** *96* (4), 1519-1532.

95. Gladfelter, W. L., Selective Metalization by Chemical Vapor Deposition. *Chem. Mater.* **1993,** *5* (10), 1372-88.

96. Parsons, G. N.; George, S. M.; Knez, M., Progress and Future Direction for Atomic Layer Deposition and ALD-Based Chemistry. *MRS Bull.* **2011,** *36* (11), 865-871.

97. Parsons, G. N.; Elam, J. W.; George, S. M.; Haukka, S.; Jeon, H.; Kessels, W. M. M.; Leskela, M.; Poodt, P.; Ritala, M.; Rossnagel, S. M., History of Atomic Layer Deposition and Its Relationship with the American Vacuum Society. *J. Vac. Sci. Technol., A* **2013,** *31* (5), 050818/1-050818/11.

98. Ritala, M.; Niinisto, J., Chapter 4 Atomic Layer Deposition. In *Chemical Vapour Deposition: Precursors, Processes, and Applications*, The Royal Society of Chemistry: 2009; pp 158-206.

99. Puurunen, R. L., Surface Chemistry of Atomic Layer Deposition: A Case Study for the Trimethylaluminum/Water Process. *J. Appl. Phys.* **2005,** *97* (12), 121301/1-121301/52.

100. Musgrave, C. B. G., R. G, Precursors for Atomic Layer Deposition of High-κ Dielectrics. *Future Fab International,Process Gases, Chemicals and Materials* **2005,** *18*, 126-128.

101. (a) Pakkala, A.; Putkonen, M., Chapter 8 - Atomic Layer Deposition. In *Handbook of Deposition Technologies for Films and Coatings (Third Edition)*, Martin, P. M., Ed. William Andrew Publishing: Boston, 2010; pp 364-391; (b) Leskela, M.; Ritala, M., Atomic Layer Deposition Chemistry: Recent Developments and Future Challenges.

Angew. Chem., Int. Ed. **2003,** *42* (45), 5548-5554; (c) Niinisto, L.; Nieminen, M.; Paivasaari, J.; Niinisto, J.; Putkonen, M.; Nieminen, M., Advanced Electronic and Optoelectronic Materials by Atomic Layer Deposition: An Overview with Special Emphasis on Recent Progress in Processing of High-k Dielectrics and Other Oxide Materials. *physica status solidi (a)* **2004,** *201* (7), 1443-1452; (d) Ritala, M.; Leskela, M., Atomic Layer Epitaxy-A Valuable Tool for Nanotechnology? *Nanotechnology* **1999,** *10* (1), 19-24.

102.   Elers, K.-E.; Blomberg, T.; Peussa, M.; Aitchison, B.; Haukka, S.; Marcus, S., Film Uniformity in Atomic Layer Deposition. *Chem. Vap. Deposition* **2006,** *12* (1), 13-24.

103.   Lim, B. S.; Rahtu, A.; Gordon, R. G., Atomic Layer Deposition of Transition Metals. *Nat. Mater.* **2003,** *2* (11), 749-754.

104.   Kucheyev, S. O.; Biener, J.; Baumann, T. F.; Wang, Y. M.; Hamza, A. V.; Li, Z.; Lee, D. K.; Gordon, R. G., Mechanisms of Atomic Layer Deposition on Substrates with Ultrahigh Aspect Ratios. *Langmuir* **2008,** *24* (3), 943-948.

105.   (a) Poodt, P.; Cameron, D. C.; Dickey, E.; George, S. M.; Kuznetsov, V.; Parsons, G. N.; Roozeboom, F.; Sundaram, G.; Vermeer, A., Spatial Atomic Layer Deposition: A Route Towards Further Industrialization of Atomic Layer Deposition. *J. Vac. Sci. Technol., A* **2012,** *30* (1), 010802/1-010802/11; (b) Levy, D. H.; Nelson, S. F.; Freeman, D., Oxide Electronics by Spatial Atomic Layer Deposition. *J. Disp. Technol.* **2009,** *5* (12), 484-494; (c) Poodt, P.; van Lieshout, J.; Illiberi, A.; Knaapen, R.; Roozeboom, F.; van Asten, A., On the Kinetics of Spatial Atomic Layer Deposition. *J. Vac. Sci. Technol., A* **2013,** *31* (1), 01A108/1-01A108/7; (d) Levy, D. H.; Freeman, D.; Nelson, S. F.; Cowdery-Corvan, P.

J.; Irving, L. M., Stable ZnO Thin Film Transistors by Fast Open Air Atomic Layer Deposition. *Appl. Phys. Lett.* **2008,** *92* (19), 192101/1-192101/3.

106.   (a) Ritala, M.; Leskelae, M.; Nykaenen, E.; Soininen, P.; Niinistoe, L., Growth of Titanium Dioxide Thin Films by Atomic Layer Epitaxy. *Thin Solid Films* **1993,** *225* (1-2), 288-95; (b) Tiznado, H.; Zaera, F., Surface Chemistry in the Atomic Layer Deposition of TiN Films from TiCl4 and Ammonia. *J. Phys. Chem. B* **2006,** *110* (27), 13491-13498; (c) Kubala, N. G.; Rowlette, P. C.; Wolden, C. A., Plasma-Enhanced Atomic Layer Deposition of Anatase TiO2 Using TiCl4. *J. Phys. Chem. C* **2009,** *113* (37), 16307-16310; (d) Ritala, M.; Leskelae, M., Zirconium Dioxide Thin Films Deposited by ALE Using Zirconium Tetrachloride as Precursor. *Appl. Surf. Sci.* **1994,** *75* (1-4), 333-40; (e) Niinisto, J.; Kukli, K.; Heikkila, M.; Ritala, M.; Leskela, M., Atomic Layer Deposition of High-k Oxides of the Group 4 Metals for Memory Applications. *Adv. Eng. Mater.* **2009,** *11* (4), 223-234; (f) Ritala, M.; Leskelae, M.; Niinistoe, L.; Prohaska, T.; Friedbacher, G.; Grasserbauer, M., Development of Crystallinity and Morphology in Hafnium Dioxide Thin Films Grown by Atomic Layer Epitaxy. *Thin Solid Films* **1994,** *250* (1-2), 72-80; (g) Delabie, A.; Pourtois, G.; Caymax, M.; De Gendt, S.; Ragnarsson, L.-A.; Heyns, M.; Fedorenko, Y.; Swerts, J.; Maes, J. W., Atomic Layer Deposition of Hafnium Silicate Gate Dielectric Layers. *J. Vac. Sci. Technol., A* **2007,** *25* (4), 1302-1308; (h) Nyns, L.; Delabie, A.; Pourtois, G.; Van Elshocht, S.; Vinckier, C.; De Gendt, S., Study of the Surface Reactions in ALD Hafnium Aluminates. *J. Electrochem. Soc.* **2010,** *157* (1), G7-G12; (i) Scharf, T. W.; Prasad, S. V.; Dugger, M. T.; Kotula, P. G.; Goeke, R. S.; Grubbs, R. K., Growth, Structure, and Tribological Behavior of Atomic Layer-Deposited Tungsten Disulphide Solid Lubricant Coatings with Applications to MEMS. *Acta Mater.*

2006, *54* (18), 4731-4743; (j) Putkonen, M.; Niinistoe, L., Atomic Layer Deposition of B2O3 Thin Films at Room Temperature. *Thin Solid Films* **2006,** *514* (1-2), 145-149.

107.   (a) Hatanpaa, T.; Vehkamaki, M.; Ritala, M.; Leskela, M., Study of Bismuth Alkoxides as Possible Precursors for ALD. *Dalton Trans* **2010,** *39* (13), 3219-26; (b) Bachmann, J.; Jing, J.; Knez, M.; Barth, S.; Shen, H.; Mathur, S.; Goesele, U.; Nielsch, K., Ordered Iron Oxide Nanotube Arrays of Controlled Geometry and Tunable Magnetism by Atomic Layer Deposition. *J. Am. Chem. Soc.* **2007,** *129* (31), 9554-9555; (c) Putkonen, M.; Aaltonen, T.; Alnes, M.; Sajavaara, T.; Nilsen, O.; Fjellvaag, H., Atomic Layer Deposition of Lithium Containing Thin Films. *J. Mater. Chem.* **2009,** *19* (46), 8767-8771; (d) Jones, A. C.; Aspinall, H. C.; Chalker, P. R.; Potter, R. J.; Manning, T. D.; Loo, Y. F.; O'Kane, R.; Gaskell, J. M.; Smith, L. M., MOCVD and ALD of High-κ Dielectric Oxides Using Alkoxide Precursors. *Chem. Vap. Deposition* **2006,** *12* (2-3), 83-98; (e) Yang, T. S.; Cho, W.; Kim, M.; An, K.-S.; Chung, T.-M.; Kim, C. G.; Kim, Y., Atomic Layer Deposition of Nickel Oxide Films Using Ni(dmamp)2 and Water. *J. Vac. Sci. Technol., A* **2005,** *23* (4), 1238-1243; (f) Lee, J. P.; Park, M. H.; Chung, T.-M.; Kim, Y.; Sung, M. M., Atomic Layer Deposition of TiO2 Thin Films from Ti(OiPr)2(dmae)2 and H2O. *Bull. Korean Chem. Soc.* **2004,** *25* (4), 475-479; (g) Lee, B. H.; Hwang, J. K.; Nam, J. W.; Lee, S. U.; Kim, J. T.; Koo, S.-M.; Baunemann, A.; Fischer, R. A.; Sung, M. M., Low-Temperature Atomic Layer Deposition of Copper Metal Thin Films: Self-Limiting Surface Reaction of Copper Dimethylamino-2-propoxide with Diethylzinc. *Angew. Chem., Int. Ed.* **2009,** *48* (25), 4536-4539.

108.   (a) Aarik, J.; Aidla, A.; Jaek, A.; Leskelae, M.; Niinistoe, L., Precursor Properties of Calcium β-Diketonate in Vapor Phase Atomic Layer Epitaxy. *Appl. Surf. Sci.* **1994,** *75*

(1-4), 33-8; (b) Hamalainen, J.; Puukilainen, E.; Kemell, M.; Costelle, L.; Ritala, M.; Leskela, M., Atomic Layer Deposition of Iridium Thin Films by Consecutive Oxidation and Reduction Steps. *Chem. Mater.* **2009,** *21* (20), 4868-4872; (c) Niskanen, A.; Rahtu, A.; Sajavaara, T.; Arstila, K.; Ritala, M.; Leskela, M., Radical-Enhanced Atomic Layer Deposition of Metallic Copper Thin Films. *J. Electrochem. Soc.* **2005,** *152* (1), G25-G28; (d) Kim, S. K.; Hoffmann-Eifert, S.; Waser, R., Growth of Noble Metal Ru Thin Films by Liquid Injection Atomic Layer Deposition. *J. Phys. Chem. C* **2009,** *113* (26), 11329-11335; (e) Torndahl, T.; Ottosson, M.; Carlsson, J.-O., Growth of Copper(I) Nitride by ALD Using Copper(II) Hexafluoroacetylacetonate, Water, and Ammonia as Precursors. *J. Electrochem. Soc.* **2006,** *153* (3), C146-C151; (f) Dasgupta, N. P.; Lee, W.; Prinz, F. B., Atomic Layer Deposition of Lead Sulfide Thin Films for Quantum Confinement. *Chem. Mater.* **2009,** *21* (17), 3973-3978; (g) Sarkar, S. K.; Kim, J. Y.; Goldstein, D. N.; Neale, N. R.; Zhu, K.; Elliott, C. M.; Frank, A. J.; George, S. M., In2S3 Atomic Layer Deposition and Its Application as a Sensitizer on TiO2 Nanotube Arrays for Solar Energy Conversion. *J. Phys. Chem. C* **2010,** *114* (17), 8032-8039; (h) Putkonen, M.; Szeghalmi, A.; Pippel, E.; Knez, M., Atomic Layer Deposition of Metal Fluorides Through Oxide Chemistry. *J. Mater. Chem.* **2011,** *21* (38), 14461-14465.

109.   (a) Simko, J. P.; Meguro, T.; Iwai, S.; Ozasa, K.; Aoyagi, Y.; Sugano, T., Surface Photo-Absorption Study of the Laser-Assisted Atomic Layer Epitaxial Growth Process of Gallium Arsenide. *Thin Solid Films* **1993,** *225* (1-2), 40-6; (b) Jeong, W. G.; Menu, E. P.; Dapkus, P. D., Steric Hindrance Effects in Atomic Layer Epitaxy of Indium Arsenide. *Appl. Phys. Lett.* **1989,** *55* (3), 244-6; (c) Ott, A. W.; Johnson, J. M.; Klaus, J. W.; George, S. M., Surface Chemistry of In2O3 Deposition Using In(CH3)3 and H2O in a

Binary Reaction Sequence. *Appl. Surf. Sci.* **1997,** *112*, 205-215; (d) Ishii, M.; Iwai, S.; Ueki, T.; Aoyagi, Y., Surface Reaction Mechanism and Morphology Control in AlP Atomic Layer Epitaxy. *Thin Solid Films* **1998,** *318* (1,2), 6-10; (e) Lee, Y. J.; Kang, S.-W., Growth of Aluminum Nitride Thin Films Prepared by Plasma-Enhanced Atomic Layer Deposition. *Thin Solid Films* **2004,** *446* (2), 227-231; (f) Kukli, K.; Ritala, M.; Leskela, M.; Jokinen, J., Atomic Layer Epitaxy Growth of Aluminum Oxide Thin Films From a Novel Al(CH3)2Cl Precursor and H2O. *J. Vac. Sci. Technol., A* **1997,** *15* (4), 2214-2218; (g) Fan, J. F.; Toyoda, K., Self-Llimiting Behavior of the Growth of Alumina Using Sequential Vapor Pulses of TMA and Hydrogen Peroxide. *Appl. Surf. Sci.* **1992,** *60-61*, 765-9; (h) Kumagai, H.; Toyoda, K.; Matsumoto, M.; Obara, M., Comparative Study of Al2O3 Optical Crystalline Thin Films Grown by Vapor Combinations of Al(CH3)3/N2O and Al(CH3)3/H2O2. *Jpn. J. Appl. Phys., Part 1* **1993,** *32* (12B), 6137-40; (i) Jeong, C.-W.; Lee, J.-S.; Joo, S.-K., Plasma-Assisted Atomic Layer Growth of High-Quality Aluminum Oxide Thin Films. *Jpn. J. Appl. Phys., Part 1* **2001,** *40* (1), 285-289; (j) Wang, W. S.; Ehsani, H.; Bhat, I., Improved Cadmium Telluride Layers on Gallium Arsenide and Silicon Using Atomic Layer Epitaxy. *J. Electron. Mater.* **1993,** *22* (8), 873-8; (k) Sang, B.; Yamada, A.; Konagai, M., Growth of Boron-Doped ZnO Thin Films by Atomic Layer Deposition. *Sol. Energy Mater. Sol. Cells* **1997,** *49* (1-4), 19-26; (l) Yun, S. J.; Kim, Y. S.; Park, S.-H. K., Fabrication of CaS:Pb Blue Phosphor by Incorporating Dimeric Pb2+ Luminescent Centers. *Appl. Phys. Lett.* **2001,** *78* (6), 721-723.

110.   (a) Putkonen, M.; Sajavaara, T.; Niinisto, L., Enhanced Growth Rate in Atomic Layer Epitaxy Deposition of Magnesium Oxide Thin Films. *J. Mater. Chem.* **2000,** *10* (8),

1857-1861; (b) Huang, R.; Kitai, A. H., Temperature-Dependence of the Growth Orientation of Atomic Layer Growth Magnesia. *Appl. Phys. Lett.* **1992,** *61* (12), 1450-2; (c) Vehkamaki, M.; Hanninen, T.; Ritala, M.; Leskela, M.; Sajavaara, T.; Rauhala, E.; Keinonen, J., Atomic Layer Deposition of SrTiO3 Thin Films From a Novel Strontium Precursor - Strontium bis(tri-isopropylcyclopentadienyl). *Chem. Vap. Deposition* **2001,** *7* (2), 75-80; (d) Ihanus, J.; Haenninen, T.; Hatanpaeae, T.; Aaltonen, T.; Mutikainen, I.; Sajavaara, T.; Keinonen, J.; Ritala, M.; Leskelae, M., Atomic Layer Deposition of SrS and BaS Thin Films Using Cyclopentadienyl Precursors. *Chem. Mater.* **2002,** *14* (5), 1937-1944; (e) Putkonen, M.; Nieminen, M.; Niinistoe, J.; Niinistoe, L.; Sajavaara, T., Surface-Controlled Deposition of Sc2O3 Thin Films by Atomic Layer Epitaxy Using β-Diketonate and Organometallic Precursors. *Chem. Mater.* **2001,** *13* (12), 4701-4707; (f) Kim, W.-S.; Park, S.-K.; Moon, D.-Y.; Kang, B.-W.; Kim, H.-D.; Park, J.-W., Characteristics of La2O3 Thin Films Deposited Using the ECR Atomic Layer Deposition Method. *J. Korean Phys. Soc.* **2009,** *55* (2), 590-593; (g) Katamreddy, R.; Stafford, N. A.; Guerin, L.; Feist, B.; Dussarrat, C.; Pallem, V.; Weiland, C.; Opila, R., Atomic Layer Deposition of Rare-Earth Oxide Thin Films for High- κ Dielectric Applications. *ECS Trans.* **2009,** *19* (2, Silicon Nitride, Silicon Dioxide, and Emerging Dielectrics 10), 525-536; (h) Rose, M.; Niinisto, J.; Michalowski, P.; Gerlich, L.; Wilde, L.; Endler, I.; Bartha, J. W., Atomic Layer Deposition of Titanium Dioxide Thin Films from Cp*Ti(OMe)3 and Ozone. *J. Phys. Chem. C* **2009,** *113* (52), 21825-21830; (i) Katamreddy, R.; Wang, Z.; Omarjee, V.; Rao, P. V.; Dussarrat, C.; Blasco, N., Advanced Precursor Development for Sr and Ti Based Oxide Thin Film Applications. *ECS Trans.* **2009,** *25* (4, Atomic Layer Deposition Applications 5), 217-230; (j) Burton, B. B.; Fabreguette, F. H.; George, S. M.,

Atomic Layer Deposition of MnO using Bis(ethylcyclopentadienyl)Manganese and H2O. *Thin Solid Films* **2009,** *517* (19), 5658-5665; (k) Rooth, M.; Johansson, A.; Kukli, K.; Aarik, J.; Boman, M.; Haarsta, A., Atomic Layer Deposition of Iron Oxide Thin Films and Nanotubes Using Ferrocene and Oxygen as Precursors. *Chem. Vap. Deposition* **2008,** *14* (3-4), 67-70; (l) Elam, J. W.; Martinson, A. B. F.; Pellin, M. J.; Hupp, J. T., Atomic Layer Deposition of In2O3 Using Cyclopentadienyl Indium: A New Synthetic Route to Transparent Conducting Oxide Films. *Chem. Mater.* **2006,** *18* (15), 3571-3578.

111. (a) Becker, J. S.; Kim, E.; Gordon, R. G., Atomic Layer Deposition of Insulating Hafnium and Zirconium Nitrides. *Chem. Mater.* **2004,** *16* (18), 3497-3501; (b) Kwon, J.; Dai, M.; Halls, M. D.; Langereis, E.; Chabal, Y. J.; Gordon, R. G., In Situ Infrared Characterization during Atomic Layer Deposition of Lanthanum Oxide. *J. Phys. Chem. C* **2009,** *113* (2), 654-660; (c) Yang, R. B.; Bachmann, J.; Reiche, M.; Gerlach, J. W.; Goesele, U.; Nielsch, K., Atomic Layer Deposition of Antimony Oxide and Antimony Sulfide. *Chem. Mater.* **2009,** *21* (13), 2586-2588; (d) Becker, J. S.; Gordon, R. G., Diffusion Barrier Properties of Tungsten Nitride Films Grown by Atomic Layer Deposition From Bis(tert-butylimido)bis(dimethylamido)tungsten and Ammonia. *Appl. Phys. Lett.* **2003,** *82* (14), 2239-2241; (e) Miikkulainen, V.; Suvanto, M.; Pakkanen, T. A.; Siitonen, S.; Karvinen, P.; Kuittinen, M.; Kisonen, H., Thin Films of MoN, WN, and Perfluorinated Silane Deposited from Dimethylamido Precursors as Contamination Resistant Coatings on Micro-Injection Mold Inserts. *Surf. Coat. Technol.* **2008,** *202* (21), 5103-5109; (f) Kamiyama, S.; Miura, T.; Nara, Y., Comparison between SiO2 Films Deposited by Atomic Layer Deposition with SiH2[N(CH3)2]2 and SiH[N(CH3)2]3 Precursors. *Thin Solid Films* **2006,** *515* (4), 1517-1521; (g) Burton, B. B.; Kang, S. W.;

Rhee, S. W.; George, S. M., SiO2 Atomic Layer Deposition Using Tris(dimethylamino)silane and Hydrogen Peroxide Studied by in Situ Transmission FTIR Spectroscopy. *J. Phys. Chem. C* **2009,** *113* (19), 8249-8257; (h) Suzuki, I.; Yanagita, K.; Dussarrat, C., Extra Low-Temperature SiO2 Deposition Using Aminosilanes. *ECS Trans.* **2007,** *3* (15, Atomic Layer Deposition Applications 2), 119-128.

112.   (a) Rees, W. S., Jr.; Just, O.; Van Derveer, D. S., Molecular Design of Dopant Precursors for Atomic Layer Epitaxy of SrS:Ce. *J. Mater. Chem.* **1999,** *9* (1), 249-252; (b) He, W.; Schuetz, S.; Solanki, R.; Belot, J.; McAndrew, J., Atomic Layer Deposition of Lanthanum Oxide Films for High-κ Gate Dielectrics. *Electrochem. Solid-State Lett.* **2004,** *7* (7), G131-G133.

113.   (a) Lim, B. S.; Rahtu, A.; Park, J.-S.; Gordon, R. G., Synthesis and Characterization of Volatile, Thermally Stable, Reactive Transition Metal Amidinates. *Inorg. Chem.* **2003,** *42* (24), 7951-7958; (b) Wang, H.; Gordon, R. G.; Alvis, R.; Ulfig, R. M., Atomic Layer Deposition of Ruthenium Thin Films from an Amidinate Precursor. *Chem. Vap. Deposition* **2009,** *15* (10-11-12), 312-319; (c) Milanov, A. P.; Xu, K.; Laha, A.; Bugiel, E.; Ranjith, R.; Schwendt, D.; Osten, H. J.; Parala, H.; Fischer, R. A.; Devi, A., Growth of Crystalline Gd2O3 Thin Films with a High-Quality Interface on Si(100) by Low-Temperature H2O-Assisted Atomic Layer Deposition. *J. Am. Chem. Soc.* **2010,** *132* (1), 36-37.

114.   Saly, M. J.; Munnik, F.; Baird, R. J.; Winter, C. H., Atomic Layer Deposition Growth of BaB2O4 Thin Films from an Exceptionally Thermally Stable Tris(pyrazolyl)borate-Based Precursor. *Chem. Mater.* **2009,** *21* (16), 3742-3744.

115. (a) Putkonen, M. In *Precursors for ALD processes*, Wiley-VCH Verlag GmbH & Co. KGaA: 2012; pp 41-60; (b) Hatanpaa, T.; Ritala, M.; Leskela, M., Precursors as Enablers of ALD Technology: Contributions from University of Helsinki. *Coord. Chem. Rev.* **2013,** *257* (23-24), 3297-3322; (c) Pore, V.; Hatanpaa, T.; Ritala, M.; Leskela, M., Atomic Layer Deposition of Metal Tellurides and Selenides Using Alkylsilyl Compounds of Tellurium and Selenium. *J. Am. Chem. Soc.* **2009,** *131* (10), 3478-3480.

116. Leskela, M.; Aaltonen, T.; Hamalainen, J.; Niskanen, A.; Ritala, M., Atomic Layer Deposition of Metal Thin Films. *Proc. - Electrochem. Soc.* **2005,** *2005-09* (EUROCVD-15), 545-554.

117. Potts, S. E.; Kessels, W. M. M., Energy-Enhanced Atomic Layer Deposition for More Process and Precursor Versatility. *Coord. Chem. Rev.* **2013,** *257* (23-24), 3254-3270.

118. Kim, H., Characteristics and Applications of Plasma Enhanced-Atomic Layer Deposition. *Thin Solid Films* **2011,** *519* (20), 6639-6644.

119. (a) Kessels, E. P., H.; Potts, S.; van de Sanden, R., Plasma Atomic Layer Deposition. In *Atomic Layer Deposition of Nanostructured Materials*, Wiley-VCH Verlag & Co. KGaA: Boschstr. 12, 69469, Weinheim, Germany., 2011; pp 131-157; (b) Profijt, H. B.; Potts, S. E.; van de Sanden, M. C. M.; Kessels, W. M. M., Plasma-Assisted Atomic Layer Deposition: Basics, Opportunities, and Challenges. *J. Vac. Sci. Technol., A* **2011,** *29* (5), 050801/1-050801/26.

120. (a) Meyer, J. R., T., Low-Temperature Atomic Layer Deposition. In *Atomic Layer Deposition of Nanostructured Materials* Pinna, N. K., M., Ed. Wiley-VCH Verlag GmbH & Co. KGaA.: Boschstr. 12, 69469, Weinheim, Germany., 2012; pp 109-130; (b) George,

S. M., Atomic Layer Deposition: An Overview. *Chem. Rev. (Washington, DC, U. S.)* **2010,** *110* (1), 111-131.

121.   Groner, M. D.; Fabreguette, F. H.; Elam, J. W.; George, S. M., Low-Temperature Al2O3 Atomic Layer Deposition. *Chem. Mater.* **2004,** *16* (4), 639-645.

122.   (a) Knez, M.; Nielsch, K.; Niinistö, L., Synthesis and Surface Engineering of Complex Nanostructures by Atomic Layer Deposition. *Advanced Materials* **2007,** *19* (21), 3425-3438; (b) King, J. S.; Graugnard, E.; Roche, O. M.; Sharp, D. N.; Scrimgeour, J.; Denning, R. G.; Turberfield, A. J.; Summers, C. J., Infiltration and Inversion of Holographically Defined Polymer Photonic Crystal Templates by Atomic Layer Deposition. *Adv. Mater. (Weinheim, Ger.)* **2006,** *18* (12), 1561-1565.

123.   Knez, M.; Kadri, A.; Wege, C.; Goesele, U.; Jeske, H.; Nielsch, K., Atomic Layer Deposition on Biological Macromolecules: Metal Oxide Coating of Tobacco Mosaic Virus and Ferritin. *Nano Lett.* **2006,** *6* (6), 1172-1177.

124.   Scharrer, M.; Wu, X.; Yamilov, A.; Cao, H.; Chang, R. P. H., Fabrication of Inverted Opal ZnO Photonic Crystals by Atomic Layer Deposition. *Appl. Phys. Lett.* **2005,** *86* (15), 151113/1-151113/3.

125.   (a) Meyer, J.; Goerrn, P.; Bertram, F.; Hamwi, S.; Winkler, T.; Johannes, H.-H.; Weimann, T.; Hinze, P.; Riedl, T.; Kowalsky, W., Al2O3/ZrO2 Nanolaminates as Ultrahigh Gas-Diffusion Barriers-A Strategy for Reliable Encapsulation of Organic Electronics. *Adv. Mater. (Weinheim, Ger.)* **2009,** *21* (18), 1845-1849; (b) Hausmann, D. M.; Kim, E.; Becker, J.; Gordon, R. G., Atomic Layer Deposition of Hafnium and Zirconium Oxides Using Metal Amide Precursors. *Chem. Mater.* **2002,** *14* (10), 4350-4358.

126. (a) Utriainen, M.; Kröger-Laukkanen, M.; Johansson, L.-S.; Niinistö, L., Studies of Metallic Thin Film Growth in an Atomic Layer Epitaxy Reactor Using M(acac)2 (M=Ni, Cu, Pt) Precursors. *Applied Surface Science* **2000,** *157* (3), 151-158; (b) Johansson, A.; Torndahl, T.; Ottosson, L. M.; Boman, M.; Carlsson, J. O., Copper Nanoparticles Deposited Inside the Pores of Anodized Aluminium Oxide Using Atomic Layer Deposition. *Mater. Sci. Eng., C* **2003,** *C23* (6-8), 823-826; (c) Daub, M.; Knez, M.; Goesele, U.; Nielsch, K., Ferromagnetic Nanotubes by Atomic Layer Deposition in Anodic Alumina Membranes. *J. Appl. Phys.* **2007,** *101* (9, Pt. 2), 09J111/1-09J111/3; (d) Li, Z.; Gordon, R. G., Thin, Continuous, and Conformal Copper Films by Reduction of Atomic Layer Deposited Copper Nitride. *Chemical Vapor Deposition* **2006,** *12* (7), 435-441.

127. Knisley, T. J.; Ariyasena, T. C.; Sajavaara, T.; Saly, M. J.; Winter, C. H., Low Temperature Growth of High Purity, Low Resistivity Copper Films by Atomic Layer Deposition. *Chem. Mater.* **2011,** *23* (20), 4417-4419.

128. (a) Klaus, J. W.; Sneh, O.; Ott, A. W.; George, S. M., Atomic Layer Deposition of SiO2 Using Catalyzed and Uncatalyzed Self-Limiting Surface Reactions. *Surf. Rev. Lett.* **1999,** *6* (3 & 4), 435-448; (b) Klaus, J. W.; George, S. M., Atomic Layer Deposition of SiO2 at Room Temperature Using NH3-Catalyzed Sequential Surface Reactions. *Surf. Sci.* **2000,** *447* (1-3), 81-90; (c) Fang, G.; Chen, S.; Li, A.; Ma, J., Surface Pseudorotation in Lewis-Base-Catalyzed Atomic Layer Deposition of SiO2: Static Transition State Search and Born-Oppenheimer Molecular Dynamics Simulation. *J. Phys. Chem. C* **2012,** *116* (50), 26436-26448; (d) Kang, S.-W.; Yun, J.-Y.; Chang, Y. H., Growth of Cu Metal Films at Room Temperature Using Catalyzed Reactions. *Chem. Mater.* **2010,** *22* (5), 1607-1609;

(e) Du, Y.; Du, X.; George, S. M., SiO2 Film Growth at Low Temperatures by Catalyzed Atomic Layer Deposition in a Viscous Flow Reactor. *Thin Solid Films* **2005,** *491* (1-2), 43-53; (f) Jackson, D. H. K.; Wang, D.; Gallo, J. M. R.; Crisci, A. J.; Scott, S. L.; Dumesic, J. A.; Kuech, T. F., Amine Catalyzed Atomic Layer Deposition of (3-Mercaptopropyl)trimethoxysilane for the Production of Heterogeneous Sulfonic Acid Catalysts. *Chem. Mater.* **2013,** *25* (19), 3844-3851; (g) Kim, H. S.; Kim, H. J.; Kim, H. S.; Jeong, Y. K.; Kim, S. H.; Lee, S. W.; Jeong, B. K.; Lee, H. h.; Choi, B. H., Improvement of Luminescent Properties of Phosphor Powders Coated with Nanoscaled SiO2 by Atomic Layer Deposition. *Diffus. Defect Data, Pt. B* **2007,** *124-126* (Pt. 1, Advances in Nanomaterials and Processing, Part 1), 375-378; (h) Koutsonikolas, D. E.; Kaldis, S. P.; Sakellaropoulos, G. P., Pore Size Reduction and Performance Upgrade of Silica Membranes with an Ambient Temperature C-ALD Post-Treatment Method. *Sep. Sci. Technol.* **2011,** *46* (9), 1414-1418; (i) McCool, B. A.; DeSisto, W. J., Self-Limited Pore Size Reduction of Mesoporous Silica Membranes via Pyridine-Catalyzed Silicon Dioxide ALD. *Chem. Vap. Deposition* **2004,** *10* (4), 190-194; (j) McCool, B. A.; DeSisto, W. J., Synthesis and Characterization of Silica Membranes Prepared by Pyridine-Catalyzed Atomic Layer Deposition. *Ind. Eng. Chem. Res.* **2004,** *43* (10), 2478-2484.

129.   Ferguson, J. D.; Smith, E. R.; Weimer, A. W.; George, S. M., ALD of SiO2 at Room Temperature Using TEOS and H2O with NH3 as the Catalyst. *J. Electrochem. Soc.* **2004,** *151* (8), G528-G535.

130.   (a) Bachmann, J.; Zierold, R.; Chong, Y. T.; Hauert, R.; Sturm, C.; Schmidt-Grund, R.; Rheinlander, B.; Grundmann, M.; Gosele, U.; Nielsch, K., A Practical, Self-Catalytic, Atomic Layer Deposition of Silicon Dioxide. *Angewandte Chemie* **2008,** *47* (33), 6177-9;

(b) Rai, V. R.; Agarwal, S., Mechanism of Self-catalytic Atomic Layer Deposition of Silicon Dioxide Using 3-Aminopropyl Triethoxysilane, Water, and Ozone. *Chem. Mater.* **2011,** *23* (9), 2312-2316.

131.   Hausmann, D.; Becker, J.; Wang, S.; Gordon, R. G., Rapid Vapor Deposition of Highly Conformal Silica Nanolaminates. *Science (Washington, DC, U. S.)* **2002,** *298* (5592), 402-406.

132.   (a) de Rouffignac, P.; Li, Z.; Gordon, R. G., Sealing Porous Low-k Dielectrics with Silica. *Electrochem. Solid-State Lett.* **2004,** *7* (12), G306-G308; (b) Miller, K. A.; John, C.; Zhang, K. Z.; Nicholson, K. T.; McFeely, F. R.; Banaszak Holl, M. M., Self-Limiting Chemical Vapor Deposition of an Ultra-Thin Silicon Oxide Film Using Tri-(tert-butoxy)silanol. *Thin Solid Films* **2001,** *397* (1,2), 78-82.

133.   Burton, B. B.; Boleslawski, M. P.; Desombre, A. T.; George, S. M., Rapid SiO2 Atomic Layer Deposition Using Tris(tert-pentoxy)silanol. *Chem. Mater.* **2008,** *20* (22), 7031-7043.

134.   (a) Zhong, L.; Daniel, W. L.; Zhang, Z.; Campbell, S. A.; Gladfelter, W. L., Atomic Layer Deposition, Characterization, and Dielectric Properties of HfO2/SiO2 Nanolaminates and Comparisons with Their Homogeneous Mixtures. *Chem. Vap. Deposition* **2006,** *12* (2-3), 143-150; (b) Zhong, L.; Zhang, Z.; Campbell, S. A.; Gladfelter, W. L., Combinatorial CVD of ZrO2 or HfO2 Compositional Spreads with SiO2 for High κ Dielectrics. *J. Mater. Chem.* **2004,** *14* (21), 3203-3209.

135.   Hamalainen, J.; Ritala, M.; Leskela, M., Atomic Layer Deposition of Noble Metals and Their Oxides. *Chem. Mater.* **2014,** *26* (1), 786-801.

136. (a) Aaltonen, T.; Alen, P.; Ritala, M.; Leskela, M., Ruthenium Thin Films Grown by Atomic Layer Deposition. *Chem. Vap. Deposition* **2003,** *9* (1), 45-49; (b) Aaltonen, T.; Ritala, M.; Leskela, M., ALD of Rhodium Thin Films from Rh(acac)3 and Oxygen. *Electrochem. Solid-State Lett.* **2005,** *8* (8), C99-C101; (c) Aaltonen, T.; Ritala, M.; Sammelselg, V.; Leskela, M., Atomic Layer Deposition of Iridium Thin Films. *J. Electrochem. Soc.* **2004,** *151* (8), G489-G492; (d) Knapas, K.; Ritala, M., In situ Reaction Mechanism Studies on Atomic Layer Deposition of Ir and IrO2 from Ir(acac)3. *Chem. Mater.* **2011,** *23* (11), 2766-2771; (e) Aaltonen, T.; Ritala, M.; Sajavaara, T.; Keinonen, J.; Leskelae, M., Atomic Layer Deposition of Platinum Thin Films. *Chem. Mater.* **2003,** *15* (9), 1924-1928; (f) Hamalainen, J.; Sajavaara, T.; Puukilainen, E.; Ritala, M.; Leskela, M., Atomic Layer Deposition of Osmium. *Chem. Mater.* **2012,** *24* (1), 55-60; (g) Aaltonen, T.; Ritala, M.; Leskelae, M. In *Atomic Layer Deposition of Noble Metals*, Materials Research Society: 2005; pp 663-667.

137. Aaltonen, T.; Ritala, M.; Arstila, K.; Keinonen, J.; Leskelae, M., Atomic Layer Deposition of Ruthenium Thin Films from Ru(thd)3 and Oxygen. *Chem. Vap. Deposition* **2004,** *10* (4), 215-219.

138. Aaltonen, T.; Rahtu, A.; Ritala, M.; Leskela, M., Reaction Mechanism Studies on Atomic Layer Deposition of Ruthenium and Platinum. *Electrochem. Solid-State Lett.* **2003,** *6* (9), C130-C133.

139. Mackus, A. J. M.; Leick, N.; Baker, L.; Kessels, W. M. M., Catalytic Combustion and Dehydrogenation Reactions during Atomic Layer Deposition of Platinum. *Chem. Mater.* **2012,** *24* (10), 1752-1761.

140. Aaltonen, T.; Ritala, M.; Tung, Y.-L.; Chi, Y.; Arstila, K.; Meinander, K.; Leskelae, M., Atomic Layer Deposition of Noble Metals: Exploration of the Low Limit of the Deposition Temperature. *J. Mater. Res.* **2004,** *19* (11), 3353-3358.

141. (a) Martensson, P.; Carlsson, J.-O., Atomic Layer Epitaxy of Copper Growth and Selectivity in the Cu(II)-2,2,6,6-tetramethyl-3,5-heptanedionate/H2 Process. *J. Electrochem. Soc.* **1998,** *145* (8), 2926-2931; (b) Engdahl, C.; Nielsen, U., Hydrogen Dissociation on Copper: Importance of Dimensionality in Calculations of the Sticking Coefficient. *J. Chem. Phys.* **1993,** *98* (5), 4223-33.

142. Senkevich, J. J.; Tang, F.; Rogers, D.; Drotar, J. T.; Jezewski, C.; Lanford, W. A.; Wang, G.-c.; Lu, T.-m., Substrate-Independent Palladium Atomic Layer Deposition. *Chem. Vap. Deposition* **2003,** *9* (5), 258-264.

143. Tallarida, M.; Kukli, K.; Michling, M.; Ritala, M.; Leskela, M.; Schmeisser, D., Substrate Reactivity Effects in the Atomic Layer Deposition of Aluminum Oxide from Trimethylaluminum on Ruthenium. *Chem. Mater.* **2011,** *23* (13), 3159-3168.

144. Vempaire, D.; Fettar, F.; Ortega, L.; Pierre, F.; Miraglia, S.; Sulpice, A.; Pelletier, J.; Hlil, E. K.; Fruchart, D., Nonmagnetic Thin Layers of Ni3N. *J. Appl. Phys.* **2009,** *106* (7), 073911/1-073911/11.

145. Cloud, A. N.; Davis, L. M.; Girolami, G. S.; Abelson, J. R., Low-Temperature CVD of Iron, Cobalt, and Nickel Nitride Thin Films from Bis[di(tert-butyl)amido]metal(II) Precursors and Ammonia. *Journal of Vacuum Science & Technology A: Vacuum, Surfaces, and Films* **2014,** *32* (2), 020606.

146. Li, Z.; Gordon, R. G.; Pallem, V.; Li, H.; Shenai, D. V., Direct-Liquid-Injection Chemical Vapor Deposition of Nickel Nitride Films and Their Reduction to Nickel Films. *Chem. Mater.* **2010,** *22* (10), 3060-3066.

147. (a) Li, Z.; Gordon, R. G.; Li, H.; Shenai, D. V.; Lavoie, C., Formation of Nickel Silicide from Direct-Liquid-Injection Chemical-Vapor-Deposited Nickel Nitride Films. *J. Electrochem. Soc.* **2010,** *157* (6), H679-H683; (b) Lindahl, E.; Ottosson, M.; Carlsson, J. O., In Situ Study of Nickel Formation During Decomposition of Chemical Vapor Deposition Ni3N Films. *J. Vac. Sci. Technol., A* **2010,** *28* (5), 1203-1209.

148. (a) Neklyudov, I. M.; Morozov, A. N., Formation and Decay Kinetics of Nickel Nitrides Resulting from Nitrogen Ion implantation. The Nickel-Nitrogen Phase Diagram. *Physica B (Amsterdam, Neth.)* **2004,** *350* (4), 325-337; (b) Vempaire, D.; Miraglia, S.; Sulpice, A.; Ortega, L.; Hlil, E. K.; Fruchart, D.; Pelletier, J., Structure and Magnetic Properties of Nickel Nitride Thin Film Synthesized by Plasma-Based Ion Implantation. *J. Magn. Magn. Mater.* **2004,** *272-276* (Suppl. 1), E843-E844.

149. (a) Dorman, G. J. W. R.; Sikkens, M., Structure of Reactively Sputtered Nickel Nitride Films. *Thin Solid Films* **1983,** *105* (3), 251-8; (b) Kuznetsov, D. L.; Ugodnikov, G. G.; Filatov, I. E., Nickel Nitride Synthesized by Nitrogen Ion Beam Sputtering of a Nickel Target. *Tech. Phys. Lett.* **2008,** *34* (1), 87-89; (c) Popovic, N.; Bogdanov, Z.; Goncic, B.; Strbac, S.; Rakocevic, Z., Reactively Sputtered Ni, Ni(N) and Ni3N films: Structural, Electrical and Magnetic Properties. *Appl. Surf. Sci.* **2009,** *255* (7), 4027-4032.

150. (a) Lindahl, E.; Ottosson, M.; Carlsson, J. O., Chemical Vapour Deposition of Metastable Ni3N. *ECS Trans.* **2009,** *25* (8, EuroCVD 17/CVD 17), 365-372; (b) Lindahl, E.;

Ottosson, M.; Carlsson, J.-O., Growth and Stability of CVD Ni3N and ALD NiO Dual Layers. *Surf. Coat. Technol.* **2010,** *205* (3), 710-716.

151.   Li, Z. Atomic Layer Deposition and Direct-Liquid-Injection Chemical Vapor Deposition of Nickel Nitride Films and Their Conversion to Nickel Silicide Films. Ph.D. Thesis, Harvard University,, Cambridge, Massachusetts, 2011.

152.   Knisely, T. J. New precursors and Chemistry for the Growth of Transition Metal Films by Atomic Layer Deposition. Ph.D. Thesis, Wayne State University, Detroit, Michigan, 2012.

153.   Haukka, S.; Tuominen, M.; Vainonen-ahlgren, E.; Tois, E.; Li, W.-m.; Maes, J. W., Effect of Starting Surface in Atomic Layer Deposition. *Proc. - Electrochem. Soc.* **2003,** *2003-14* (Advanced Short-Time Thermal Processing for Si-Based CMOS Devices), 405- 416.

154.   (a) Kim, W.-H.; Lee, H.-B.-R.; Heo, K.; Lee, Y. K.; Chung, T.-M.; Kim, C. G.; Hong, S.; Heo, J.; Kim, H., Atomic Layer Deposition of Ni Thin Films and Application to Area- Selective Deposition. *J. Electrochem. Soc.* **2010,** *158* (1), D1-D5; (b) Chung, T.-M.; Lee, S. S.; Cho, W.; Kim, M.; Lee, Y. K.; Hwang, J.-H.; An, K.-S.; Kim, C. G., Volatile Nickel Aminoalkoxide Complexes as Liquid Precursors for Non-Volatile Memory Device of NiO Films by ALD. *Bull. Korean Chem. Soc.* **2011,** *32* (3), 783-784; (c) So, B.-S.; You, Y.-H.; Kim, K.-H.; Hwang, J.; Cho, W.; Lee, S. S.; Chung, T.-M.; Lee, Y. K.; Kim, C. G.; An, K.-S.; Kim, Y.-C.; Lee, Y.-H.; Seo, W.-S., Crystallization of Amorphous Silicon Thin Films Using Self-Limiting ALD of Nickel Oxide. *Electrochem. Solid-State Lett.* **2007,** *10* (5), J61-J64; (d) Yoo, S. H.; Choi, H.; Kim, H.-S.; Park, B. K.; Lee, S. S.; An, K.-S.; Lee, Y. K.; Chung, T.-M.; Kim, C. G., Synthesis and Characterization of

Nickel(II) Aminoalkoxides: Application to Molecular Precursors for MOCVD of Ni Thin Films. *Eur. J. Inorg. Chem.* **2011,** (11), 1833-1839; (e) Hubert-Pfalzgraf, L. G.; Kessler, V. G.; Vaissermann, J., Soluble NiII Alkoxides Based on Dimethylaminoisopropoxide Ligands: Molecular Structure of [Li(PriOH)Ni(μ2-OR)2Cl]2 and of cis-NiCl2(ROH)2 (R = CHMeCH2NMe2). *Polyhedron* **1997,** *16* (24), 4197-4203.

155.   Burton, B. B.; Lavoie, A. R.; George, S. M., Tantalum Nitride Atomic Layer Deposition Using (tert-Butylimido)tris(diethylamido)tantalum and Hydrazine. *J. Electrochem. Soc.* **2008,** *155* (7), D508-D516.

156.   Adhikari, M.; Majumdar, M. K.; Pati, A. K., Thermal Decomposition of Nickel and Copper Formates. *Fert. Technol.* **1976,** *13* (4), 285-8.

157.   (a) Rauscher, H.; Kostov, K. L.; Menzel, D., Adsorption and Decomposition of Hydrazine on Ruthenium(001). *Chem. Phys.* **1993,** *177* (2), 473-96; (b) Rodriguez, J. A.; Truong, C. M.; Goodman, D. W., Synthesis of Boron Nitride Ultrathin Films: The Bonding and Chemistry of Ammonia and Hydrazine on Ruthenium (0001) and Boron/Ru(0001) Surfaces. *J. Vac. Sci. Technol., A* **1992,** *10* (4, Pt. 1), 955-9.

158.   Waechtler, T.; Ding, S.-F.; Hofmann, L.; Mothes, R.; Xie, Q.; Oswald, S.; Detavernier, C.; Schulz, S. E.; Qu, X.-P.; Lang, H.; Gessner, T., ALD-Grown Seed Layers for Electrochemical Copper Deposition Integrated with Different Diffusion Barrier Systems. *Microelectron. Eng.* **2011,** *88* (5), 684-689.

159.   (a) Columbia, M. R.; Thiel, P. A., The Interaction of Formic Acid with Transition Metal Surfaces, Studied in Ultrahigh Vacuum. *J. Electroanal. Chem.* **1994,** *369* (1-2), 1-14; (b) Fahrenfort, J.; Rijen, L. L. v.; Sachtler, W. M. H., Decomposition of HCO2H on Metal Catalysts. *Proc. Symp. Mech. Heterogeneous Catalysis, Amsterdam, Neth.* **1960**, 23-48.

160.   Wagner, C. D. R., W. M.; Davis, L. E.; Moulder, J. F.; Murlenburg, G. E., *Handbook of X-ray Photoelectron Spectroscopy*. Perkin-Elmer Corporation: Eden Prairie, Minnesota, 1979; p 80,81.

ABSTRACT

(I) CHROMATOGRAPHIC METHODS FOR SOLUTE DESCRIPTOR DETERMINATIONS
(II) RUTHENIUM SUBSTRATE-CATALYZED GROWTH OF NICKEL NITRIDE THIN FILMS BY ATOMIC LAYER DEPOSITION

by

THILOKA CHANDIMA ARIYASENA

May 2015

Advisor: Prof. Colin F. Poole

Major: Chemistry

Degree: Doctor of Philosophy

Determination of distribution levels of environmentally important compounds in various environmental compartments is a major procedure in many fields including environmental risk assessment, food and drug safety, and the perfumery industry. Models for direct estimation of environmental properties were developed using gas chromatography and liquid-liquid partitioning. The developed models were used to derive descriptor values for environmentally important organic compounds. The accuracy of the developed models and descriptor values were demonstrated by the application to the estimation of standard environmental properties and by comparison with experimental solute property values.

Quantitative structure property relationships were constructed for totally organic biphasic partition systems of different polarity containing ethanolamine as the base solvent. The models demonstrate high accuracy and are of good statistical quality. The descriptor space for the determination of the hydrogen bond acidity descriptor was enhanced by the characterization of ethanolamine based partition systems. Models with high statistical quality were also developed

for the totally organic biphasic partition systems containing triethylamine as a counter solvent. The triethylamine-formamide system was identified as a suitable system to supplement the currently available totally organic biphasic systems for the determination of the hydrogen bond basicity descriptor.

Descriptor values for polycyclic aromatic hydrocarbons were determined using totally organic biphasic systems and gas and liquid chromatography methods. These descriptors were validated using theoretical models, standard environmental models, and by comparison with experimentally determined values. The descriptor values are homogeneous and accurate as a group. Therefore, the research work reported herein will enable the accurate measurement of solute properties for the estimation of environmental properties.

A substrate-dependent catalytic thermal ALD process was developed to address the low reactivity of precursors in atomic layer deposition processes. The developed process can be used to obtain smooth, high purity thin films at low deposition temperatures, and also for the deposition of materials which were found challenging so far using thermal and energy enhanced atomic layer deposition methods. Substrate-dependent catalytic thermal ALD technique can be conveniently used for the commercial production of thin-film materials. The deposition of pure, uniform and conformal nickel nitride thin films were demonstrated using $Ni(OCHMeCH_2NMe_2)_2$ precursor, and anhydrous hydrazine in a two-step process, and $Ni(OCHMeCH_2NMe_2)_2$ precursor, formic acid, and anhydrous hydrazine in a three-step process on ruthenium substrates. Films were characterized by X-ray diffraction, X-ray photoelectron spectroscopy, scanning electron microscopy, and atomic force microscopy techniques. The ALD window for the two-step process was observed between 140 and 180 °C with a growth rate of 0.25 Å/cycle. The ALD window for the three-step process was observed between 120 and 180 °C with a growth rate of 0.35Å/cycle.

Atomic force microscopy measurements demonstrated smooth thin films for the two-step process which was ~0.25 nm for 25 nm thick films deposited between 120-180 °C. The surface roughness of films varied between 0.38-4.4 nm for 35 nm thick films deposited by three-step process between 120-180 °C.

AUTOBIOGRAPHICAL STATEMENT

THILOKA CHANDIMA ARIYASENA

Education

Ph.D. Wayne State University, Detroit, MI, USA
Research: Gas Chromatography, Liquid Chromatography, Atomic Layer Deposition
2009 August-2014 December GPA: 3.74/4.00, Major: Inorganic, Minor: Analytical and Organic
Advisor: Professor Colin F. Poole

M.Sc. Wayne State University, Detroit, MI, USA
Research: Synthetic Inorganic Chemistry
2005-2008

B.Sc. Chemistry Special Degree, University of Peradeniya, Sri Lanka
1999-2003, Minor: Computer Science

Publications

Ariyasena, T. C.; Poole, C. F. "Determination of Descriptors for Polycyclic Aromatic Hydrocarbons and Related Compounds by Chromatographic Methods and Liquid-Liquid Partition in Totally Organic Biphasic Systems." *J. Chromatogr. A* **2014**, *1361*, 240-254.

Ariyasena, T. C.; Poole, C. F. "Evaluation of Triethylamine as a Counter Solvent in Totally Organic Biphasic Liquid-Liquid Partition Systems." *Chromatographia* **2013**, *76*, 1031-1039.

Ariyasena, T. C.; Poole, C. F. "Models for Liquid-Liquid Partition in the System Ethanolamine-Organic Solvent and Their Use for Estimating Descriptors for Organic Compounds". *Chromatographia* **2013**, *76*, 157-164.

Poole, C. F.; Ariyasena, T. C.; Lenca, N. "Estimation of the Environmental Properties of Compounds from Chromatographic Measurements and the Solvation Parameter Model."
J. Chromatogr. A **2013**, *1317*, 85-104.

Poole, C. F.; Karunasekara, T.; Ariyasena, T. C. "Totally Organic Biphasic Solvent Systems for Extraction and Descriptor Determinations." *J. Sep. Sci.* **2013**, *36,* 96-109.

Knisely, T. J.; Ariyasena T. C.; Sajavaara, T.; Saly, M. J.; Winter, C. H. "Low Temperature Growth of High Purity, Low Resistivity Copper Films by Atomic Layer Deposition." *Chem. Mater*. **2011**, *33*, 4417-4419.

Ariyasena, T. C.; Lenca, N.; Poole, C. F. "Determination of Descriptors for Weak Hydrogen-Bond Acids (Anilines, Anilides, Amides, Carbamates, and Ureas) by Gas Chromatography and Liquid-Liquid Partition" (*In Preparation*)

Patents

Winter, C. H.; Knisely, T. J.; Ariyasena, T. Atomic Layer Deposition of Transition Metal Thin Films. WO 2013006242 A1, January 10, 2013. US Patent.